

**UNIVERSIDADE DE SÃO PAULO**

**INSTITUTO DE QUÍMICA**

**Programa de Pós-Graduação em Química**

**Raphael Bacil Prata**

**Characterization of the electrochemical behaviour of  
anti-inflammatory and antipsychotic drugs and their  
interaction with biomolecules within their respective  
pathways.**

Versão corrigida da Tese defendida

São Paulo

Data do Depósito na SPG:

18/11/2021

Raphael Bacil Prata

**Caracterização do comportamento eletroquímico de fármacos  
anti-inflamatórios e anti-psicóticos e suas respectivas  
interações com biomoléculas de suas vias de ação.**

*Tese apresentada ao Instituto de Química da Universidade de São  
Paulo para obtenção do Título de Doutor em Ciências com ênfase em  
Química.*

*Orientadora: Profa. Dra. Silvia Helena Pires Serrano*

São Paulo

2021

Autorizo a reprodução e divulgação total ou parcial deste trabalho, por qualquer meio convencional ou eletrônico, para fins de estudo e pesquisa, desde que citada a fonte.

Ficha Catalográfica elaborada eletronicamente pelo autor, utilizando o programa desenvolvido pela Seção Técnica de Informática do ICMC/USP e adaptado para a Divisão de Biblioteca e Documentação do Conjunto das Químicas da USP

Bibliotecária responsável pela orientação de catalogação da publicação:  
Marlene Aparecida Vieira - CRB - 8/5562

P912c	Prata, Raphael Bacil Characterization of the electrochemical behaviour of anti-inflammatory and antipsychotic drugs and their interaction with biomolecules within their respective pathways. / Raphael Bacil Prata. - São Paulo, 2021. 412 p.
	Tese (doutorado) - Instituto de Química da Universidade de São Paulo. Departamento de Química Fundamental. Orientador: Serrano, Silvia Helena Pires
	1. Eletroquímica. 2. Eletroanalítica. 3. Eletroquímica molecular. 4. Anti-inflamatórios não esteroidais. 5. Anti-psicóticos atípicos. I. T. II. Serrano, Silvia Helena Pires, orientador.

“I may not have been the best student from the Chemistry Institute, but I am the  
proudest.”

Adapted from Billy Martin

IV

## Acknowledgments

This thesis is dedicated to my ‘families’ whom without I would not be able to achieve half of it. First, I would like to thank my parents, Servulo Sacramento Prata and Sandra Maria Bacil, who dedicated themselves to teach me the principles that consolidate who I am. Also, would like to thank grandparents José do Sacramento, Maria Alice Prata and Roberto Bacil and Eunice Oliveira Bacil, who in many ways, made work possible. I would like to thank my brother Gabriel Bacil Prata for his friendship and all the help on the way. Finally, to my girlfriend Isabela Fernandes de Oliveira who was by my side in every moment, always being helpful, supportive, and motivating me to achieve my goals.

Secondly, to my other family provided by the Instituto de Química, as a former student of our group said, we spend more time with our second family than with our actual family. So, I would like to thank my supervisor and one of my best friends, Professor Dr. Silvia Helena Pires Serrano for all these years in her group. She was essential in my formation in both professional and personal ways. To my former lab colleagues and friends, I would like to thank Professor Dr. Robson Pinho da Silva and Professor Dr. Rafael Martos Buoro for their guidance and help along with my initial phase in the group. Dr. Caroline Sanz Gomes, who endured several years in my presence from elementary school to the Ph.D. Especially to Professor Dr. ‘PV’ Antonio William O. Lima (*in memoriam*), for all the teachings about practical aspects of “gambiarra”. To my nowadays colleagues, I would like to thank Adriana D’Alessio Rendelucci, Sara do Nascimento Ferreira and Fernanda Pedro Costa for all the moments, coffee requests and friendship. A great special thanks to my beloved undergrad students, Estênio Augusto de

Oliveira Marcondes Filho, Raphael Sanchez Nakaya, Pedro Henrique 'Breja' Martin Garcia and Jéssica Luíza Cappelletti Mendonça, my sincere gratitude for the help with several data treatments, talks, companions and friendship, this work would not be possible without you. At last, but not least, to Maria Cristina Machado, and Lucia Delfino for the technical support who aided me for years (besides all the sabotage).

To my friends from other labs, I would like to thank Msc Vanessa Neiva de Ataíde and Msc Letícia Francine Mendes for a long friendship, you both are sisters to me. To Professor Dr. Thiago Matheus and Msc Jessica Selva (ft. Alice) my gratitude for all these years of friendship. Also, would like to special thank my dear friend Professor Dr. William Reis de Araújo for all the companionship in the lab throughout the years and all the discussions (productive or not, especially the not...).

To my friend from organic chemistry, I would like to thank Kevin de Aquino Dias who besides being a brother to me, extracted and purified my samples. To my friends in inorganic chemistry, Marcelo 'Pai' Cecconi who walked this path for many years with me, and to Elaine Mattos who came as an aggregate and now is a nice friend. A special thanks to Victor Vendruscolo for all of our lovely '3:00 a.m. chats', friendship, and for believing in me.

To my friends from abroad, I would like to thank Professor Dr. Richard G. Compton for all the teachings and our chats that still occur even after my return to Brazil. To my lab friends, Dr. Alex Suherman, Dr. Lifu Chen, Dr. Jake Yang, Professor Dr. Bertold Rasche, Dr. Hatem Amin and Dr. Ruochen Xie for a great year and an enduring friendship.

I would like to thank some professors/ friends in our department, Professor Dr. Thiago Paixão and Professor Dr. Mauro Bertotti for inviting me to participate in some of the works of their group. To Professor Dr. Lucas Rodrigues for several years of friendship (2008- ) and the insights towards chemical kinetics and Professor Dr. Fabio Rodrigues for being a great friend and all the chats throughout the years (sorry for being too chatty).

Finally, to the funding agencies CNPq projects nº 140833/2016-1 and 310114/2016-0 and CAPES project 88881.187396/2018-01 for funding this project and FAPESP for funding all equipment in the laboratory of Professor Silvia Serrano.

## Abstract

Prata, R. B. Characterization of the electrochemical behaviour of anti-inflammatory and antipsychotic drugs and their interaction with biomolecules within their respective pathways. 2021. 393p. Ph.D. Thesis. Graduate Program

In this work, divided in two parts, at first, we studied the chemical interactions of non-steroidal anti-inflammatory drugs (NSAIDs) and their target, the *cicloxygenase* enzyme, and secondly, the interaction between antipsychotics drugs with the catecholamine neurotransmitters, using electrochemical techniques. To achieve the prior goal, the electrochemical behaviour of dipyrone and its derivatives were studied at glassy carbon electrode, and a oxidation mechanism was proposed. Following, a *cicloxygenase* enzyme biosensor was developed to evaluate the anti-inflammatory properties and the pharmacological mechanism of the NSAIDs, and the interaction of the enzyme with the most used NSAIDs, dipyrone, acetyl-salicylic and salicylic acid, ibuprofen, acetaminophen, and naproxen were evaluated using differential pulse voltammetry technique. The voltammetric results suggest the least and the most effective in inhibit the peroxidase active site are the acetaminophen and the ibuprofen, respectively. Whilst the electrons paramagnetic resonance suggests the enzyme oxygenase active site, are least and the most effective inhibited by the salicylic acid and the dipyrone, respectively. These results confirm the inactivation of the enzyme by a reducer, although the study with the active site and the tyrosyl radical indicate that not only the enzyme can be inactivated by a redox reaction, but also that the NSAIDs perform an allosteric regulation of the enzyme hindering its process, and consequently deactivating the arachidonic cascade. In sequence, the chemical



interaction between the highly used antipsychotic drugs olanzapine and quetiapine and the catecholamine neurotransmitters were studied.

**Keywords:** Electrochemistry, electroanalysis, molecular electrochemistry, non-steroidal anti-inflammatory drugs, atypical antipsychotics.

## Resumo

Prata, R. B., Caracterização do comportamento eletroquímico de fármacos anti-inflamatórios e anti-psicóticos e suas respectivas interações com biomoléculas de suas via de ação. 2021. 393p. Tese (Doutorado) – Programa de Pós Graduação em Química. Instituto de Química, Universidade de São Paulo, São Paulo.

Neste trabalho, dividido em duas partes, em um primeiro momento, estudou-se as interações químicas dos anti-inflamatórios não esteroidais (AINEs) e seu alvo, a enzima cicloxigenase. Em segundo momento, estudou-se a interação dos antipsicóticos atípicos com os neurotransmissores catecolaminas, utilizando técnicas eletroquímicas. Para que o estudo das interações fosse possível, o comportamento de cada uma das moléculas foi estudado individualmente. Portanto, o comportamento eletroquímico da dipirona e seus derivados foram estudados em eletrodo de carbono vítreo, e um mecanismo de oxidação foi proposto. Em seguida, um biossensor da enzima cicloxigenase foi desenvolvido para avaliar as propriedades antiinflamatórias e o mecanismo farmacológico dos AINEs, e a interação da enzima com os AINEs mais utilizados, dipirona, ácido acetilsalicílico e salicílico, ibuprofeno, acetaminofeno e naproxeno foram avaliados usando a técnica de voltametria de pulso diferencial. Os resultados voltamétricos sugerem que os menos e mais eficazes em inibir o sítio peroxidase são: o paracetamol e o ibuprofeno, respectivamente. Enquanto a ressonância paramagnética de elétrons sugere que os menos e mais eficazes em inibir o sítio oxigenase da enzima hematina são: o ácido salicílico e a dipirona, respectivamente. Esses resultados confirmam a inativação da enzima por um

reduzidor, embora o estudo com o sítio ativo e o radical tirosila indique que não só a enzima pode ser inativada por uma reação redox, mas também que os AINEs realizam uma regulação alostérica do impedimento enzimático seu processo e, conseqüentemente, desativando a cascata aracdônica. Na sequência, foi estudada a interação química entre os antipsicóticos altamente usados olanzapina e quetiapina e os neurotransmissores catecolaminas.

**Palavras chave:** Eletroquímica, eletroanalítica, eletroquímica molecular, anti-inflamatórios não esteroidais, anti-psicóticos atípicos

## Table of Contents

Acknowledgments .....	V
Abstract .....	VIII
Resumo .....	X
General Introduction .....	21
Non-Steroidal Anti-inflammatory Drugs .....	22
The cyclooxygenase enzyme .....	22
Atypical antipsychotics .....	23
Neurotransmitters .....	26
References .....	28
Experimental .....	32
Chemicals and reagents .....	32
General apparatus .....	33
Chapter 1 .....	34
Mechanism of Electro-Oxidation of Metamizole using Cyclic Voltammetry at a Glassy Carbon Electrode .....	34
Introduction .....	35
Results and discussions .....	38
Conclusions .....	44
References .....	44

Chapter 2.....	48
Electrochemical behaviour of dipyrone (metamizole) and others pyrazolones .....	48
Introduction .....	49
Results and discussion .....	56
Electrochemical Characterization of MTM and the Other Pyrazolones .....	56
Mechanism Evaluation.....	64
Analytical Application .....	69
Conclusions .....	72
Acknowledgements.....	73
References.....	73
Appendix 2 - Electrochemical behaviour of dipyrone (metamizole) and others pyrazolones.....	83
MAA Obtainment and characterization .....	83
High Performance Liquid Chromatography (HPLC).....	83
Nuclear Magnetic Resonance (NMR). .....	84
UV – Vis Spectroscopy. ....	87
Chapter 3.....	89
Electrochemical oxidation of dipyrone and pyrazolone derivatives complexes with Fe (III), and its EC' mechanism.....	89
Introduction .....	90

Material and methods.....	<b>Error! Bookmark not defined.</b>
UV-Vis procedures.....	<b>Error! Bookmark not defined.</b>
Results and discussions.....	93
Complexes characterization.....	95
UV-Vis structural analysis of the phenazones and their respective complexes.....	95
Raman structural analysis of the phenazones and their respective complexes.....	99
Cyclic voltammetry and electrochemical behaviour of the complexes .....	103
Randles Sevcik equations and the processes mechanism .....	106
Tafel analysis and a catalytical effect of the complexes and the hydrolysis. .....	109
Conclusions .....	116
Acknowledgments .....	117
References.....	117
Appendix 3 - Electrochemical oxidation of dipyrone and pyrazolone derivatives complexes with Fe (III), and its EC' catalytic mechanism.....	124
Complexes characterization.....	124
Visual complexations of MTM-Fe (III) at different pH. ....	124
Visual complexations of the antipyrines with Fe (III) in acidic media.....	125
Spectroscopic structural analysis of the phenazones and their respective complexes.....	126

Cyclic voltammetry and electrochemical behaviour of the complexes.....	137
Randles Sevcik equations and oxidation mechanism discrimination of processes $E_{ap0}$ , $E_{ap1}$ , $E_{ap3}$ .....	139
Tafel analysis and a catalytical effect generated by the Fe (III) complexes. kinetic difference between the antipyrine derivatives and the respective complexes.....	141
Chapter 4.....	144
Electrochemical Cyclooxygenase biosensor to evaluate target – drug viability and interactions.....	144
Introduction .....	145
Materials and methods.....	150
Blotting and Enzyme extraction .....	150
Electronic Paramagnetic Resonance (EPR) .....	151
Electrode Modification.....	151
Electrochemical Impedance Spectroscopy (EIS) .....	152
Results and Discussion.....	153
Electrochemical Evaluation of <i>Cyclooxygenase</i> .....	153
COX interaction with NSAIDs .....	158
EPR spectra.....	165
Conclusions .....	168
Acknowledgments .....	169
References.....	169

Appendix 4 – Electrochemical Cyclooxygenase biosensor to evaluate target – drug viability and interactions.....	177
Extraction characterization – Western blotting.....	177
Results and discussion.....	178
Electrochemical Evaluation of <i>Cyclooxygenase</i> .....	178
Tafel analysis.....	178
COX interaction with NSAIDs .....	179
GCE@COX electrode stability.....	179
Chapter 5.....	180
Mechanism and kinetics of olanzapine and quetiapine oxidations at glassy carbon electrode. ....	180
Introduction .....	181
Results and discussions.....	184
The electrochemical behaviour of OLZP and QTP .....	185
Electrochemical oxidation processes I and II of OLZP .....	187
Digital simulations .....	194
Electrochemical oxidation processes III and IV .....	198
Mechanism proposition .....	203
Conclusion .....	204
Acknowledgments.....	205
References.....	205



Appendix 5 - Olanzapine and quetiapine oxidation mechanism in glassy carbon electrode at physiological pH.....	215
The obtention of the diffusion coefficients of OLZP and QTP .....	215
Electrochemical oxidation processes I and II of OLZP .....	217
Tafel Plots and charge transfer coefficients ( $\beta$ ).....	217
Electrochemical oxidation processes III and IV .....	219
Chapter 6.....	223
Dopamine oxidation at gold electrodes: mechanism and kinetics near neutral pH .....	223
Introduction .....	223
Results and discussion .....	230
Cyclic Voltammetry .....	230
Randles-Sevcik equation and ECE mechanism analysis.....	231
An analysis of the DA oxidation as an EECEE process.....	233
Digisim simulations .....	235
Conclusions .....	241
Acknowledgments.....	242
References .....	242
Appendix 6 – Dopamine oxidation at gold electrodes: mechanism and kinetics near neutral pH. - Supplementary Information .....	248
Chapter 7.....	249

New insights on the electrochemical mechanism of epinephrine on glassy carbon electrode. ....	249
Introduction .....	<b>Error! Bookmark not defined.</b>
Electrochemical procedures.....	<b>Error! Bookmark not defined.</b>
Results and discussions.....	<b>Error! Bookmark not defined.</b>
Cyclic and Square Wave Voltammetry – the electrochemical behaviour of epinephrine .....	<b>Error! Bookmark not defined.</b>
Randles-Sevcik equation and oxidation mechanism discrimination .....	<b>Error! Bookmark not defined.</b>
The kinetics of the epinephrine cyclization....	<b>Error! Bookmark not defined.</b>
The influence of pH at the cyclization chemical step ..	<b>Error! Bookmark not defined.</b>
Digital simulations .....	<b>Error! Bookmark not defined.</b>
Tafel analysis and validation of the simulations .....	<b>Error! Bookmark not defined.</b>
Conclusions .....	<b>Error! Bookmark not defined.</b>
Acknowledgments .....	<b>Error! Bookmark not defined.</b>
References.....	<b>Error! Bookmark not defined.</b>
Appendix 7 - New insights on the electrochemical mechanism of epinephrine on glassy carbon electrode – Supplementary material.....	282
Randles-Sevcik equation and oxidation mechanism discrimination .....	283
Kinetic analysis of the Epinephrine cyclization chemical step .....	284

The number of effective electrons method.....	284
The influence of pH at the cyclization chemical step.....	285
Digital simulations.....	287
Tafel analysis and validation of the simulations.....	289
References.....	290
Chapter 8.....	292
The chemical interaction between the neurotransmitter dopamine and the antipsychotic drugs olanzapine and quetiapine.....	292
Introduction.....	293
Chemicals and reagents.....	<b>Error! Bookmark not defined.</b>
Results and discussion.....	301
Cyclic voltammetry and the electrochemical behaviour of the molecules involved.....	302
Differential pulse voltammetry and the chemical rate constants.....	311
Interaction between olanzapine and dopamine.....	311
Interaction between quetiapine and dopamine.....	313
The catechol-piperazine minimalist model.....	315
Conclusions.....	316
Acknowledgments.....	317
References.....	317

Appendix 8 - The chemical interaction between the neurotransmitter dopamine and the anti-psychotic drugs olanzapine and quetiapine .....	326
Olanzapine (OLZP) Extraction, Purification and <sup>1</sup> H-NMR Analysis .....	326
Quetiapine (QTP) Extraction, Purification and <sup>1</sup> H-NMR Analysis.....	327
Cyclic voltammetry and the electrochemical behaviour of the molecules involved.....	328
Electron Paramagnetic Resonance (EPR) analysis .....	330
Differential pulse voltammetry and the chemical rate constants .....	331
Dopamine stability .....	331
The catechol-piperazine minimalist model .....	332
References.....	333
Chapter 9.....	334
A reaction between neurotransmitter epinephrine and antipsychotics drugs olanzapine and quetiapine at physiological pH. ....	334
Abstract.....	334
Introduction .....	335
Results and discussions.....	339
Cyclic voltammetry, and the general behaviour of the system .....	340
Square wave voltammetry and the influence of the chemical reaction between the neurotransmitter and the drugs .....	347
Tafel analysis and electrode kinetics .....	350
UV-Vis analysis of the adducts .....	351

Mechanism proposition .....	353
Conclusions .....	354
References.....	355
General conclusions.....	366
Perspectives.....	366
Abbreviations used by chapter .....	367
Chapter 1 - Mechanism of Electro-Oxidation of Metamizole using Cyclic Voltammetry at a Glassy Carbon Electrode .....	367
Chapter 2 - Electrochemical behaviour of dipyrone (metamizole) and others pyrazolones.....	368
Chapter 3 - Electrochemical oxidation of dipyrone and pyrazolone derivatives complexes with Fe (III), and its EC' mechanism. ....	369
Chapter 4 - Electrochemical Cyclooxygenase biosensor to evaluate target – drug viability and interactions.....	370
Chapter 5 - Mechanism and kinetics of olanzapine and quetiapine oxidations at glassy carbon electrode. ....	371
Chapter 6 - Dopamine oxidation at gold electrodes: mechanism and kinetics near neutral pH .....	372
Chapter 7 - New insights on the electrochemical mechanism of epinephrine on glassy carbon electrode. ....	373
Chapter 8 - The chemical interaction between the neurotransmitter dopamine and the antipsychotic drugs olanzapine and quetiapine.....	374

Chapter 9 - A reaction between neurotransmitter epinephrine and antipsychotics drugs olanzapine and quetiapine at physiological pH. ....	375
List of figures and schemes captions by chapter.....	376
Chapter 1 - Mechanism of Electro-Oxidation of Metamizole using Cyclic Voltammetry at a Glassy Carbon Electrode .....	376
Chapter 2 - Electrochemical behaviour of dipyrone (metamizole) and others pyrazolones.....	378
Appendix 2 - Electrochemical behaviour of dipyrone (metamizole) and others pyrazolones – Supplementary material.....	379
Chapter 3 - Electrochemical oxidation of dipyrone and pyrazolone derivatives complexes with Fe (III), and its EC' mechanism. ....	381
Appendix 3 - Electrochemical oxidation of dipyrone and pyrazolone derivatives complexes with Fe (III), and its EC' catalytic mechanism – Supplementary material.....	382
Chapter 4 - Electrochemical Cyclooxygenase biosensor to evaluate target – drug viability and interactions.....	385
Appendix 4 – Electrochemical Cyclooxygenase biosensor to evaluate target – drug viability and interactions – Supplementary material.....	386
Chapter 5 - Mechanism and kinetics of olanzapine and quetiapine oxidations at glassy carbon electrode. ....	388
Appendix 5 - Olanzapine and quetiapine oxidation mechanism in glassy carbon electrode at physiological pH – Supplementary material. ....	389

Chapter 6 - Dopamine oxidation at gold electrodes: mechanism and kinetics near neutral pH .....	390
Chapter 7 - New insights on the electrochemical mechanism of epinephrine on glassy carbon electrode. ....	392
Appendix 7 - New insights on the electrochemical mechanism of epinephrine on glassy carbon electrode – Supplementary material.....	393
Chapter 8 - The chemical interaction between the neurotransmitter dopamine and the antipsychotic drugs olanzapine and quetiapine.....	394
Appendix 8 - The chemical interaction between the neurotransmitter dopamine and the anti-psychotic drugs olanzapine and quetiapine Supplementary material. ....	396
Chapter 9 - A reaction between neurotransmitter epinephrine and antipsychotics drugs olanzapine and quetiapine at physiological pH.....	397
Papers in collaboration during the Ph.D. program .....	399
Book chapters published in collaboration during the Ph.D. program.....	406
Summarized CV.....	408
Educação.....	408
Formação complementar .....	408
Ocupação .....	409
Publicações em periódicos .....	409
Publicações de capítulos de livro.....	412





## General Introduction

Remedies occupy a distinct position in society nowadays. Both life expectation and quality increased significantly when drugs started to be part of people's routine. Among the several different groups of pharmaceuticals that surround us every day, two can be highlighted for a different but similar reason, the income they generate. [1]

The Non-Steroidal Anti-Inflammatory Drugs (NSAIDs) are the most sold worldwide. They are sold indiscriminately in most countries in regular drugstores. Although, some of them are limited in quantity due to side effects. On the other hand, a very different class of drugs has been increasing their usage, the psychiatric drugs. [1] Mental illness incidence has sharply increased in the last decades due to a radical change in psychiatry, which nowadays instead of inhumanly treat the patients, now are able to not only properly diagnostic the conditions, but also medicate the patients. [2] As the historically and stigmatized people which had hallucinations caused by other diseases, like syphilis/neurosyphilis or schizophrenia. Nowadays are better diagnosed, which culminate in an escalation of diagnosis of syndromes such as anxiety and depression. [3] As a consequence, a boost in studies regarding mental illness in general occurred. Therefore, the emergence of better treatments with specific drugs for them all, including schizophrenia. As a result, the antipsychotic class of drugs was created to treat with dignity these people that have been outcasts throughout history.

These drug classes, the antipsychotics and NSAIDs are hepatically metabolized by the same enzyme known as *cyclooxygenase-2* (COX) before

being filtered by the kidneys and excreted in the urine. [4] This catalyst is the main target of NSAIDs since it is responsible for one of the inflammatory responses, the arachidonic acid cascade. On the other hand, the only COX function towards the antipsychotics is to form metabolites that will be more easily solvated by urine. [5]

### **Non-Steroidal Anti-inflammatory Drugs**

As previously discussed, NSAIDs are the most commercialized pharmaceuticals worldwide. Several drugs of this group are familiar to people such as acetylsalicylic acid (ASA) known as Aspirin<sup>®</sup>, acetaminophen (APAP) known as Paracetamol<sup>®</sup>, diclofenac as Cataflam<sup>®</sup> or Voltarem<sup>®</sup> and dipyrrone as Novalgine<sup>®</sup> or Dorflex<sup>®</sup>. These medicines are mainly used as painkillers due to their analgesic effect. This outcome occurs because these drugs inhibit the COX enzyme in the liver, hindering one of the inflammatory cascades, the one involving the arachidonic acid. [5]

Regarding the NSAIDs, in the present work, our group addressed mainly dipyrrone (MTM) since it is the most used NSAID in Brazil. Under its commercial names, MTM appears in 1<sup>st</sup> and 4<sup>th</sup> in the list of most sold pharmaceuticals in Brazil as Dorflex<sup>®</sup> and Neusalgina<sup>®</sup>, respectively. [6,7] Thus, been responsible for most of the US\$ 41bi expected industrial income with drug selling by 2023. Moreover, although MTM is one of the titans of industry, the scientific literature lacks information regarding its electrochemical mechanism and the precise knowledge of how it works as a NSAID. [8] Especially, due to its indiscriminate use in Brazil when compared to the several restrictions observed in other countries. E.g. in European Union and the United States. [9]

### **The cyclooxygenase enzyme**

As previously stated, the COX enzyme is the target of NSAIDs. The enzyme belongs to the peroxidase class. [5] Therefore, its active site consists of a heme group, a protoporphyrin IX which complexes an iron, that catalyzes the reduction of peroxides, details will be further discussed in chapter III. [5,10] The peroxidase function is used to reduce the arachidonic acid-generating important metabolites that give sequence to the inflammatory process. To perform this process, the enzyme must be in its oxidated form (Iron IV) and therefore, a previous activation is necessary, the generation of the tyrosyl radical. Biologically, the generation of the tyrosyl radical is performed by an endogenous peroxide in which the enzyme operation depends. [4,11]

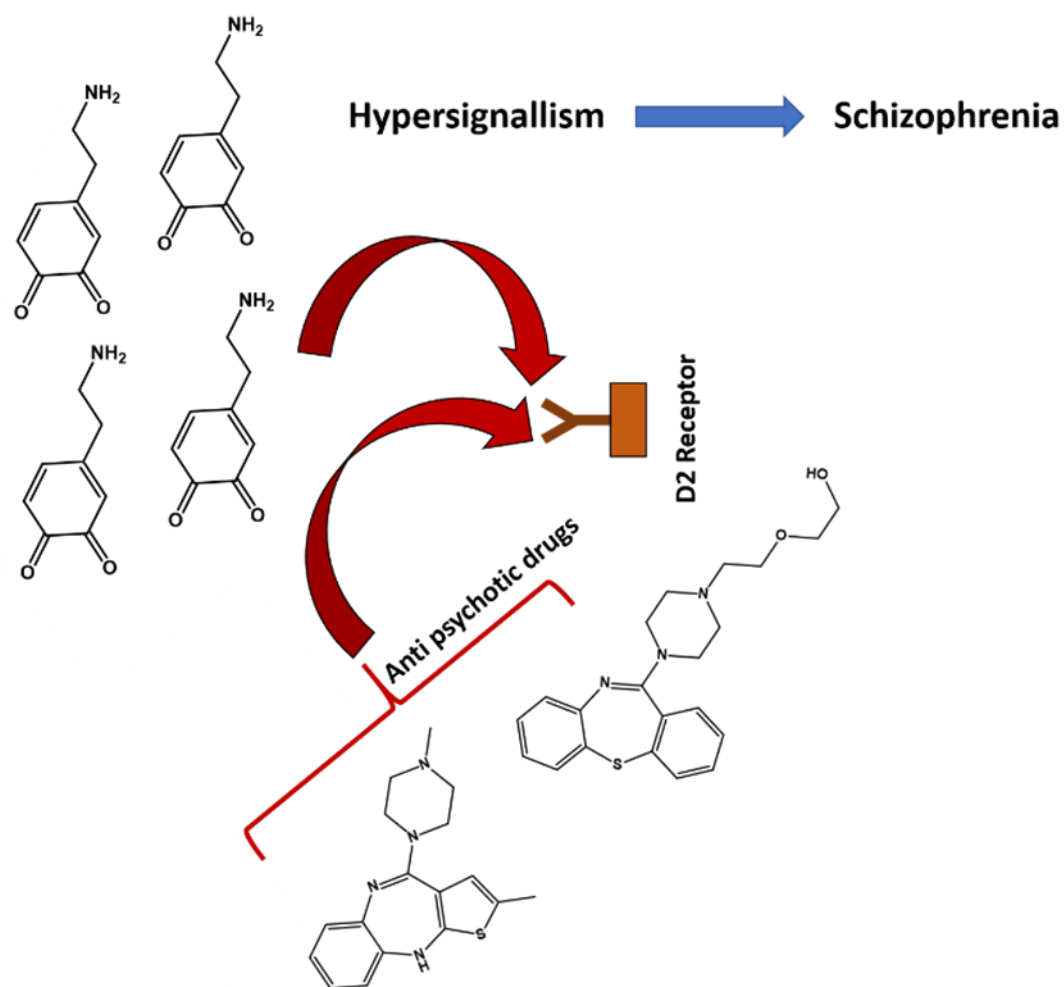
### **Atypical antipsychotics**

During the last years, mental disease occurrences have sharply increased. According to WHO (World Health Organization), they affect around 83 million people worldwide [12] Among these diseases schizophrenia and psychotic episodes are among the greatest increases, affecting about 0.7% of the world population. The antipsychotics were developed to better treat mental illness, mainly schizophrenia [13] although also used to treat bipolar disorders and major depressive disorder. [14] This class characterizes by its tendency to block the D2 receptors. This behaviour of the drugs is relevant since according to the biochemical hypothesis of schizophrenia, a malfunction in the mesolimbic pathway, which is known to be responsible for addiction and rewarding mechanisms, [15] generates high levels of dopamine, that saturates the receptors D2, resulting in psychosis and hallucinations. [16] Thus, this hypothesis

dictates that if a drug jeopardizes this saturation effect, the disease effects should decrease.

The first generation of antipsychotic drugs presented effectiveness against psychotic disorders. However, their utilization resulted in extrapyramidal effects in the patients such as paranoia, anxiety, tremors/ parkinsonism, spasms, akathisia, among others. [17–19] These harsh side effects resulted in a need for more new drugs that were at least as effective, and do not present such side effects. Therefore, a new class was developed, the atypical or second class of antipsychotics. [20]

The atypical antipsychotics, described as neuroleptics or major tranquilizers are the main treatment against schizophrenia. They are classified as serotonin-dopamine antagonists since, as their predecessors, they interact and block the receptors D2 and 5HT2. [2]



Scheme 1: Schematic representation of the competition between dopamine and the antipsychotics olanzapine and quetiapine.

Among the drugs, two are notorious for their high utilization in treatments, Olanzapine (OLZP) and Quetiapine (QTP). [21]

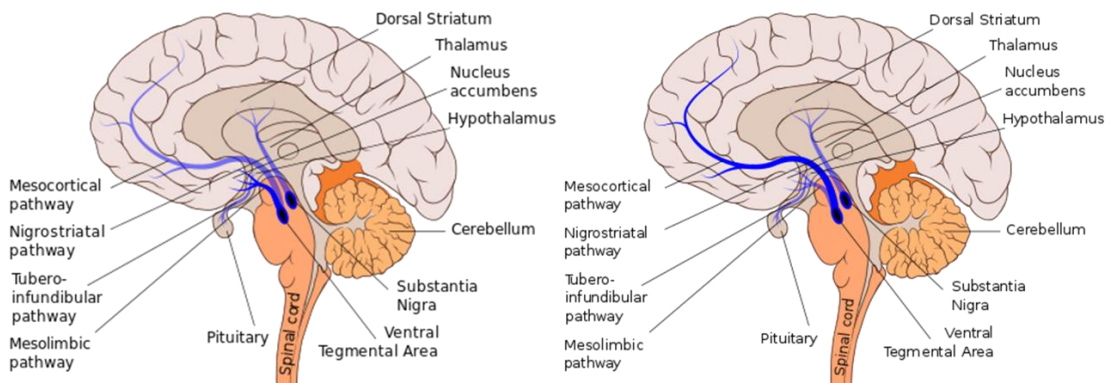
Although these drugs are relatively safe, their use may result in several side effects. Among them, the neuroleptic malignant syndrome, [22] which is a life-threatening complication, with high fever and weight gain being two of the main symptoms. [23] The weight gain has been used to treat anorexia nervosa and hypertension. [24] Besides, both drugs may cause problems during

pregnancy. [25] This continuous use could increase the oxidative stress in the patients, which aggravates their health problems. [26]

At last, the atypical antipsychotics are metabolized by hepatic cytochrome enzymes, known as CYP 450 [27,28], and their use may aggravate hepatic problems, such as cirrhosis.

### Neurotransmitters

As previously discussed, it is believed that mental illness strongly correlates with the malfunction of the mesolimbic pathway. [16]. However, the dopaminergic pathways are composed of six pathways: mesolimbic and mesocortical pathways, nigrostriatal pathway, tuberoinfundibular pathway, incertohypothalamic pathway, and hypothalamospinal projection. Among those, the mesolimbic and mesocortical pathways are believed to be linked with mental illnesses such as schizophrenia. [29]

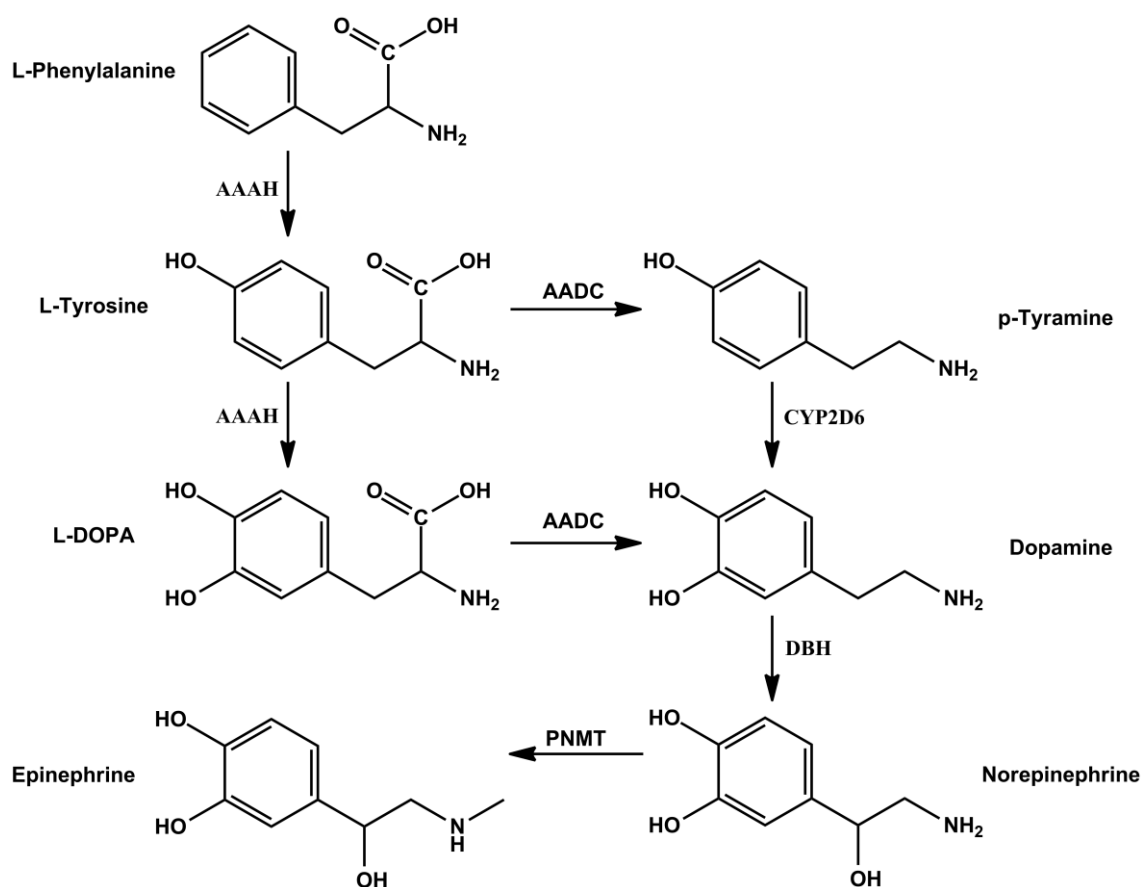


Scheme 2: Schematic representation of the mesolimbic (left) and mesocortical (right) pathways. Adapted from Wikipedia:

[https://en.wikipedia.org/wiki/Mesolimbic\\_pathway](https://en.wikipedia.org/wiki/Mesolimbic_pathway) and

[https://en.wikipedia.org/wiki/Mesocortical\\_pathway#cite\\_note-3](https://en.wikipedia.org/wiki/Mesocortical_pathway#cite_note-3)

In both of these pathways, the dopamine biosynthetic routes occur. A schematic representation is presented in scheme 2.



Scheme 3: Schematic representation of the biosynthetic pathway of the catecholamines. [30]

where AADC is the aromatic L-amino acid decarboxylase enzyme, PNMT is the Phenylethanolamine N-methyltransferase enzyme, AAAH is the Biopterin-dependent aromatic amino acid hydroxylase enzyme, DBH is the Dopamine beta-hydroxylase enzyme, COMT is the Catechol-O-methyltransferase enzyme and CYP2D6 is the Cytochrome P450 2D6 protein.

In summary, this work consists in studying the chemical interactions between the NSAIDs and their target, the COX enzyme, to provide a sensor which could aid phase 1 of drug development, as well as to study the chemical interactions

between the atypical antipsychotics olanzapine and quetiapine with neurotransmitters, which could trigger some side effects of this class of remedies.

## References

- [1] P. McGettigan, D. Henry, Use of Non-Steroidal Anti-Inflammatory Drugs That Elevate Cardiovascular Risk: An Examination of Sales and Essential Medicines Lists in Low-, Middle-, and High-Income Countries, *PLoS Med.* 10 (2013) e1001388. <https://doi.org/10.1371/journal.pmed.1001388>.
- [2] R.P. Bacil, E.A. de O. Marcondes Filho, K. de A. Dias, M.C. Portes, W.R. de Araujo, D. Oliveira-Silva, A.A. dos Santos, S.H.P. Serrano, The chemical interaction between the neurotransmitter dopamine and the antipsychotic drugs olanzapine and quetiapine, *J. Electroanal. Chem.* 881 (2021) 114946. <https://doi.org/10.1016/j.jelechem.2020.114946>.
- [3] R.P. Bacil, P.H.M. Garcia, W.R. de Araujo, S.H.P. Serrano, Mechanism and kinetics of olanzapine and quetiapine oxidations at glassy carbon electrode, *Electrochim. Acta.* 368 (2020) 137683. <https://doi.org/10.1016/j.electacta.2020.137683>.
- [4] A.L. Tsai, R.J. Kulmacz, Prostaglandin H synthase: Resolved and unresolved mechanistic issues, *Arch. Biochem. Biophys.* 493 (2010) 103–124. <https://doi.org/10.1016/j.abb.2009.08.019>.
- [5] S.S. Ayoub, R.J. Flower, M.P. Seed, *Cyclooxygenases Methods and Protocols*, 1st ed., Springer Science+Business Media, New York, NY, US, 2016.
- [6] S. Inc., Pharmaceutical sales by top 10 therapeutic areas worldwide in 2010, (n.d.). <https://www.statista.com/>.
- [7] S. Inc., Research and development expenditure of total U.S.



- pharmaceutical industry from 1995 to 2018 (in billion U.S. dollars), (2018).  
<https://www.statista.com/statistics/265085/research-and-development-expenditure-us-pharmaceutical-industry/>.
- [8] L. de A.A. Freitas, G. Radis-Baptista, Pharmaceutical Pollution and Disposal of Expired, Unused, and Unwanted Medicines in the Brazilian Context, *J. Xenobiotics*. 11 (2021) 61–76.  
<https://doi.org/10.3390/jox11020005>.
- [9] R.P. Bacil, R.M. Buoro, O.S. Campos, M.A. Ramos, C.G. Sanz, S.H.P. Serrano, Electrochemical behaviour of dipyrone (metamizole) and others pyrazolones, *Electrochim. Acta*. 273 (2018) 358–366.  
<https://doi.org/10.1016/j.electacta.2018.04.082>.
- [10] G.H. Rao, J.M. Gerrard, J.W. Eaton, J.G. White, The role of iron in prostaglandin synthesis: ferrous iron mediated oxidation of arachidonic acid., *Prostaglandins Med*. 1 (1978) 55–70.  
<http://www.ncbi.nlm.nih.gov/pubmed/715048>.
- [11] G. Wu, C.E. Rogge, J.-S. Wang, R.J. Kulmacz, G. Palmer, A.-L. Tsai, Oxyferryl Heme and Not Tyrosyl Radical Is the Likely Culprit in Prostaglandin H Synthase-1 Peroxidase Inactivation †, *Biochemistry*. 46 (2007) 534–542. <https://doi.org/10.1021/bi061859h>.
- [12] D. Riman, J. Rozsypal, V. Halouzka, J. Hrbac, D. Jirovsky, The use of micro carbon pencil lead electrode for sensitive HPLC-ED analysis of selected antipsychotic drugs, *Microchem. J*. 154 (2020) 104606.  
<https://doi.org/10.1016/j.microc.2020.104606>.
- [13] J. Lally, J.H. MacCabe, Antipsychotic medication in schizophrenia: a review, *Br. Med. Bull*. 114 (2015) 169–179.

<https://doi.org/10.1093/bmb/ldv017>.

- [14] K. Komossa, A.M. Depping, A. Gaudchau, W. Kissling, S. Leucht, Second-generation antipsychotics for major depressive disorder and dysthymia, *Cochrane Database Syst. Rev.* (2010). <https://doi.org/10.1002/14651858.CD008121.pub2>.
- [15] J.-L. Dreyer, New insights into the roles of microRNAs in drug addiction and neuroplasticity, *Genome Med.* 2 (2010) 92. <https://doi.org/10.1186/gm213>.
- [16] P. Seeman, Dopamine receptors and the dopamine hypothesis of schizophrenia, *Synapse.* 1 (1987) 133–152. <https://doi.org/10.1002/syn.890010203>.
- [17] H. Akagi, T. Manoj Kumar, Lesson of the week: Akathisia: Overlooked at a cost, *Br. Med. J.* 324 (2002) 1506–1507. <https://doi.org/10.1136/bmj.324.7352.1506>.
- [18] J.M. Pierre, Extrapyramidal Symptoms with Atypical Antipsychotics, *Drug Saf.* 28 (2005) 191–208. <https://doi.org/10.2165/00002018-200528030-00002>.
- [19] J.A. Lieberman, Effectiveness of Antipsychotic Drugs in Patients with Chronic Schizophrenia, *J. Clin. Psychiatry.* 68 (2007) e04. <https://doi.org/10.4088/JCP.0207e04>.
- [20] N.A. Crossley, M. Constante, P. McGuire, P. Power, Efficacy of atypical v. typical antipsychotics in the treatment of early psychosis: meta-analysis, *Br. J. Psychiatry.* 196 (2010) 434–439. <https://doi.org/10.1192/bjp.bp.109.066217>.
- [21] S. Leucht, C. Corves, D. Arbter, R.R. Engel, C. Li, J.M. Davis, Second-

- generation versus first-generation antipsychotic drugs for schizophrenia: a meta-analysis, *Lancet*. 373 (2009) 31–41. [https://doi.org/10.1016/S0140-6736\(08\)61764-X](https://doi.org/10.1016/S0140-6736(08)61764-X).
- [22] G. K. M. Nagraj, V. R, Olanzapine Induced Fever: A Case Report, *J. Neurobehav. Sci.* 2 (2015) 85. <https://doi.org/10.5455/JNBS.1443357705>.
- [23] L.K. Townsend, W.T. Pepler, N.D. Bush, D.C. Wright, Obesity exacerbates the acute metabolic side effects of olanzapine, *Psychoneuroendocrinology*. 88 (2018) 121–128. <https://doi.org/10.1016/j.psyneuen.2017.12.004>.
- [24] T.N. Peter Bosanac , Graham Burrows, Olanzapine in Anorexia Nervosa, *Aust. New Zeal. J. Psychiatry*. 37 (2003) 494. <https://doi.org/10.1046/j.1440-1614.2003.01221.x>.
- [25] A.A. Westin, M. Brekke, E. Molden, E. Skogvoll, I. Castberg, O. Spigset, Treatment With Antipsychotics in Pregnancy: Changes in Drug Disposition, *Clin. Pharmacol. Ther.* 103 (2018) 477–484. <https://doi.org/10.1002/cpt.770>.
- [26] C.J. Carter, Schizophrenia susceptibility genes converge on interlinked pathways related to glutamatergic transmission and long-term potentiation, oxidative stress and oligodendrocyte viability, *Schizophr. Res.* 86 (2006) 1–14. <https://doi.org/10.1016/j.schres.2006.05.023>.
- [27] B.K. Laurence Brunton, Bruce A. Chabner, Goodman and Gilman's *The Pharmacological Basis of Therapeutics*, Twelfth Ed, 2011. <https://doi.org/10.1213/00000539-198611000-00041>.
- [28] C. Hiemke, P. Baumann, N. Bergemann, A. Conca, O. Dietmaier, K. Egberts, M. Fric, M. Gerlach, C. Greiner, G. Gründer, E. Haen, U.

- Havemann-Reinecke, E. Jaquenoud Sirot, H. Kirchherr, G. Laux, U. Lutz, T. Messer, M. Müller, B. Pfuhlmann, B. Rambeck, P. Riederer, B. Schoppek, J. Stingl, M. Uhr, S. Ulrich, R. Waschgler, G. Zernig, AGNP Consensus Guidelines for Therapeutic Drug Monitoring in Psychiatry: Update 2011, *Pharmacopsychiatry*. 44 (2011) 195–235. <https://doi.org/10.1055/s-0031-1286287>.
- [29] F. Aricioglu, C.S. Ozkartal, G. Unal, S. Dursun, M. Cetin, N. Müller, Neuroinflammation in Schizophrenia: A Critical Review and The Future, *Klin. Psikofarmakol. Bülteni-Bulletin Clin. Psychopharmacol.* 26 (2016) 429–437. <https://doi.org/10.5455/bcp.20161123044657>.
- [30] X. Wang, J. Li, G. Dong, J. Yue, The endogenous substrates of brain CYP2D, *Eur. J. Pharmacol.* 724 (2014) 211–218. <https://doi.org/10.1016/j.ejphar.2013.12.025>.

## Experimental

### Chemicals and reagents

The buffer reagents were of analytical grade and used without any prior purification. The solutions were prepared using deionized water from a reverse osmosis device (Gehaka Co., model of ultra-pure OS10LX system, water resistivity 18 M $\Omega$  cm). 0.1 mol L<sup>-1</sup> phosphate buffer solutions (PBS) were prepared by solubilizing and diluting, respectively, the appropriate amount of NaH<sub>2</sub>PO<sub>4</sub> and H<sub>3</sub>PO<sub>4</sub> (Merck) in deionized water and the pH values were adjusted

by the addition of a 4.0 mol L<sup>-1</sup> NaOH (Merck) solution. The volumes were measured using EP-10 and EP-100 from Unipet-temicroliter Pipettes (Uniscience, Brazil). All experiments were performed at room temperature (25 ± 3 °C).

### **General apparatus**

All electrochemical experiments were performed in a potentiostat/galvanostat PGSTAT 101, Metrohm AUTOLAB, connected to an IME663 interface stirring device. Data processing was done by version 1.11.4 of NOVA software and the software Origin 2019. A Glassy Carbon Electrode (GCE) with a diameter of 3.0 mm was used as a working electrode, a Silver/ Silver Chloride (+ 0.222 V vs. SHE) in a saturated solution of potassium chloride and a platinum wire were used as a reference and auxiliary electrodes, respectively, in an electrochemical cell of 20 mL. Before every experiment, the electrochemical cell was degassed with industrial N<sub>2</sub>, and the GCE was polished using diamond spray suspensions with a decreasing particle size of 3.0, 1.0 and 0.1 μm from Kemet (Maidstone, UK) on a polishing pad from Buehler (Lake Bluff, Illinois, USA). The solutions were stirred before each electrochemical measurement. All pH measurements were performed using a model 654 pHmeter and a combined glass electrode, model 6.0203.100 (OE), both from Metrohm.

## Chapter 1

### **Mechanism of Electro-Oxidation of Metamizole using Cyclic Voltammetry at a Glassy Carbon Electrode**

In this chapter the initial electrochemical behaviour of the Non Steroidal Anti-Inflammatory Drug (NSAIDs) metamizole (MTM) also known as dipyrone will be discussed. This characterization was achieved by using cyclic voltammetry at glassy carbon electrode to study the electro-oxidation of metamizole, a pro-drug largely used in many countries as analgesic and anti-pyretic which the therapeutic properties are attributed to its hydrolyzed form, the 4-methyl-aminoantipyrine (MAA). Metamizole presents three oxidation processes in aqueous (Britton Robinson Buffer) and DMF media. The first process was characterized as reversible in the last medium. The differentiation between the process associated with the Metamizole and its respective hydrolyzed form the MAA, was investigated and allowed the proposition of a mechanism for the Metamizole oxidation.

This work has been published at the journal ECS Transactions (ECS Transactions 43 (1) 251-258, 2012) doi: 10.1149/1.4704966, and count with the help of Dr Rafael Buoro (from IQSC – USP), who participated in the interpretations of the experimental data, suggestions and revisions, to Dr Robson Pinho, who helped with experimental suggestions and discussions. Daniel Medina, who started this work with the preliminary data that was acquired. Dr

Antonio William O. Lima, who contributed with several experimental solution and data interpretation.

## **Introduction**

The metamizole (MTM) is pro-drug used as an analgesic, antipyretic and eventually as antispasmodic drug. [1] Its analgesic effect has been attributed to the inhibition of the Cyclooxygenase (COX) enzyme by the pharmacologically active metabolite (MAA), which reduces the oxidized states of the COX protein [2,3] and disables the prostaglandin synthesis, [4] which results in decreased of the inflammation and pain states, but not in the solution of the problem. It has been associated with severe adverse drug reactions as agranulocytosis and aplastic anemia.[1,5-7] Cases where the use of the MTM induced circumstantial allergic responses as rhinoconjunctivitis, [8,9] were reported, and therefore it was withdrawn from the market of some countries (Sweden, USA, Canada and others), restricted in others (Japan and Australia).[10] But despite this, it is still used in other countries (Brazil, Germany, Spain and France) [10,11] due its high analgesic potential and low cost. Several studies indicated that the incidence of agranulocytosis, a condition involving a severe reduction in the number of the white blood cells, inducted by the use of this pro-drug are between 0.2 and 2 cases per million, 7% of this cases result in the death of the patient.6,7 MTM is, structurally, a pyrazolone derivative with a metassulfonic group.[12] It is, in the organism, hydrolyzed to its pharmacologically active metabolite, the 4-methyl-amino-antipyrine (MAA), then it is enzymatically metabolized in the liver to 4-formyl-amino-antipyrine (FAA), a terminal metabolite, and 4-amino-antipyrine (4AA). The AA is acetylated to 4-acetyl-amino-antipyrine (AAA) by the enzyme *N-acetyl-transferase*. [1,10] Major of the reports in the literature refer to the MTM

determination and quantification using several techniques as HPLC [13] , Iodometry [14], FIA systems with Amperometric detection [15,16], Spectrophotometry, also associated with FIA systems by the addition of various reagents (Cerium IV, Iron III, Sodium Nitrite and 3-methyl-2-benzo-thiazolinone) [17,18] , Fluorimetry, Capillary Electrophoresis [19] and Voltammetry [20-25],but few knowledge about the electrochemical behavior of this pro-drug can be found and, therefore acquire this knowledge was the objective of this work.

### **Materials and Methods**

The experimental procedure was divided in two parts: the characterization of the electrochemical behavior in aqueous medium (Britton Robinson Buffer – BR) and in the organic solvent (Dimethylformamide – DMF) with Tetrabutylammonium Tetrafluorborate (Sigma-Aldrich) as a support electrolyte.

### **Reagents and Solutions**

All reagents were of analytical grade and the solutions were prepared using deionized water from a reverse osmosis device (Gehara Co., model OS10LX ultra-pure system, water resistivity  $\geq 18 \text{ M}\Omega \text{ cm}$ ). BR solutions, pH 2.0 – 10.0, were prepared neutralizing a mixed solution containing  $\text{H}_3\text{PO}_4$ ,  $\text{H}_3\text{CCOOH}$ ,  $\text{H}_3\text{BO}_3$ , all  $0.4 \text{ mol L}^{-1}$ , using  $4 \text{ mol L}^{-1}$  NaOH (Merck). The DMF solution was prepared solving the appropriated quantity of Tetrabutylammonium Tetrafluorborate (TT) (Sigma-Aldrich) in order to get a  $0.10 \text{ mol L}^{-1}$  solution.

### **Apparatus**

The voltammetric measurements were performed using a Potentiostat/ Galvanostat PGSTAT30 from Autolab Eco-Chemie and IME663 interface



coupled to the software NOVA version 1.6 or, alternatively, using the Potentiostat/Galvanostat Drop Sense, model  $\mu$ Stat 400 coupled to the software Drop View (version 2.0). The pH measurements were carried using a pH-meter model 654 and a Glass Electrode 6.0203.100(OE), both from Metrohm. Glassy Carbon Electrode (GCE) with 3 mm of diameter, Ag/AgCl, KCl<sub>(sat.)</sub> and Platinum Wire were used as working, reference and auxiliary electrodes, respectively, in a 20 cm<sup>3</sup> glass electrochemical cell.

### **Cyclic Voltammetry Measurements in aqueous media**

Several cyclic voltammograms were recorded in the supporting electrolyte, 9.0 mL of BR solution in the electrochemical cell, to get a stable baseline. After that, 1.0 mL of 0.01 mol L<sup>-1</sup> MTM solution was introduced into the cell, the mixture was homogenized and a new cyclic voltammogram was recorded. The experimental conditions were:  $v = 100 \text{ mV s}^{-1}$ ;  $E_i = + 0.1 \text{ V}$ ;  $E_\lambda = 1.4 \text{ V}$ ;  $E_f = + 0.1 \text{ V}$ . The potential window was eventually restricted in order to adequate the intentions of the experiment.

### **Cyclic Voltammetry Measurements in non aqueous media**

The procedure was the same as described before, but in this case, the supporting electrolyte was DMF containing 0.10 mol L<sup>-1</sup> of TT. The experimental conditions were:  $v = 100 \text{ mV s}^{-1}$ ;  $E_i = + 0.1 \text{ V}$ ;  $E_\lambda = 1.4 \text{ V}$ ;  $E_f = + 0.1 \text{ V}$ , but the potential window was eventually restricted in order to adequate the intentions of the experiment.

## Results and discussions

Cyclic voltammograms of MTM obtained in DMF medium shows three oxidation peaks,  $E_{ap1}$ ,  $E_{ap2}$  e  $E_{ap3}$ , and a reduction peak  $E_{cp}$  which, in close potential range, forms a reversible redox couple with  $E_{ap1}$ , Figures 1A and 1B. The reversibility criteria used for this classification were:  $E_p$  ( $E_{ap1} - E_{cp}$ ) = 63 mV and  $I_{a1p}/I_{cp}$  ratio of 0.94. Figure 1B confirms that  $E_{ap2}$  corresponds to the oxidation of the product formed in  $E_{ap1}$ .

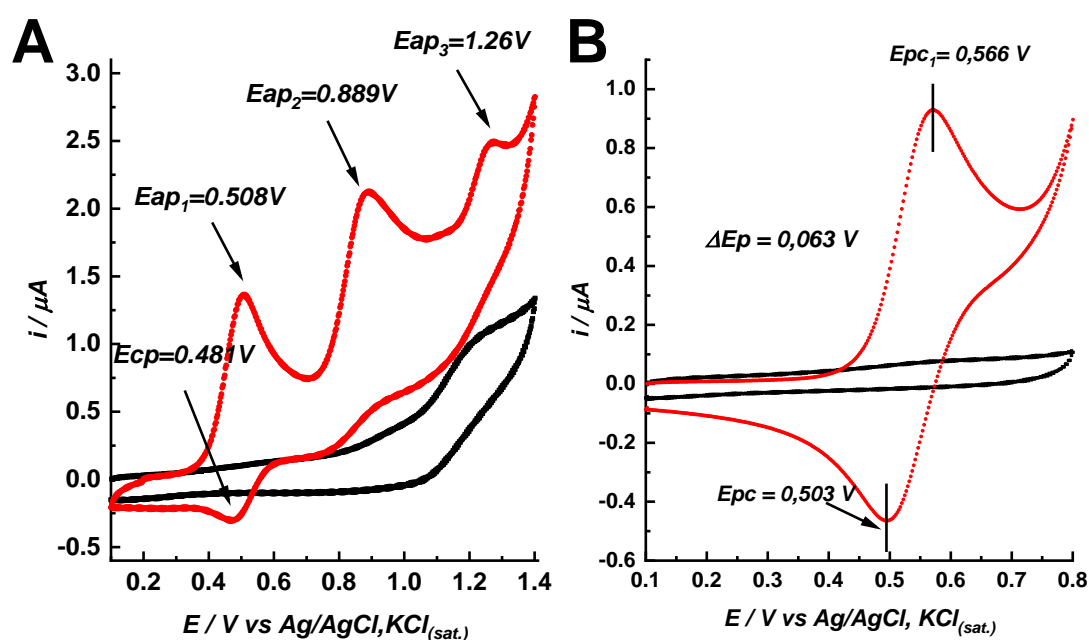


Figure 1. Cyclic Voltammograms obtained at GCE in solution  $1.0 \text{ mmol L}^{-1}$  of MTM in DMF with  $0.1 \text{ mol L}^{-1}$  of TT and  $100 \text{ mVs}^{-1}$ . Experimental Conditions: 1A.

$E_i = 0.1 V$ ;  $E_\lambda = 1.4 V$ ;  $E_f = 0.1 V$  and 1B.  $E_i = 0.1 V$ ;  $E_\lambda = 0.8 V$ ;  $E_f = 0.1 V$ .

Current Function - plots were used in order to elucidate whether the processes detected at  $E_{ap1-3}$  and  $E_{cp}$  correspond a simple electrochemical process or if

they have a coupled chemical reaction. As can be observed, the current function is approximately constant for the first and second electrochemical processes but decreased exponentially for the last 1 process showing that MTM is electrochemically oxidized following a EEEC or EECE [27] mechanism, Figure 2.

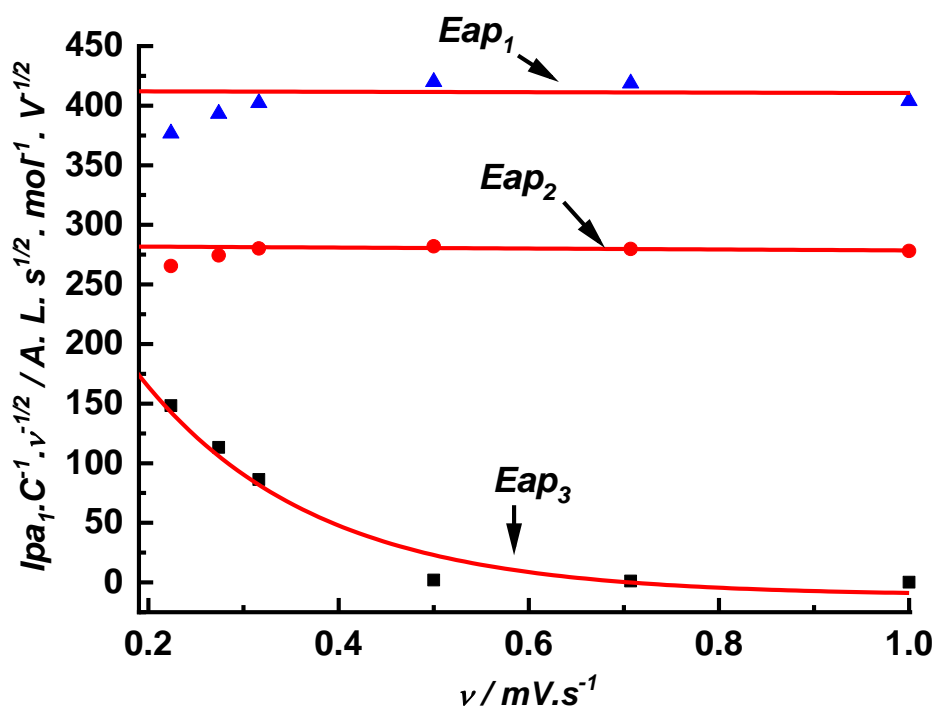


Figure 2. Current Function ( $I_p / C \times v^{1/2}$ ) versus. Plots obtained from cyclic voltammograms performed with a GCE in a DMF containing  $1.0 \text{ mmol L}^{-1}$  of MTM and  $0.10 \text{ mol L}^{-1}$  of TT. Curve Equations:  $I_{pa1} / C \times v^{1/2} = 413.5 - 4.79 v$ ;  $I_{pa2} / C \times v^{1/2} = 282.5 - 3.98 v$ ;  $I_{pa3} / C \times v^{1/2} = -11.7 \times 521.9 e^{(-x/0.184)} v$ .

Figure 3 shows that the same electrochemical processes obtained in DMF are detected in aqueous medium. The unique exception is the process detected at Ehp peak, attributed to the oxidation of the MAA product, which Ehp, shifted to less positive potential with increasing pH, Figure 3D. It is important to observe that in aqueous media, the voltammetric profile of the MTM at platinum electrodes

was different. [19] These results show that the hydrolysis process is favoured in alkaline medium and  $E_p$ / pH of 30 mV has been assigned a process involving two electrons and one proton [20, 24].

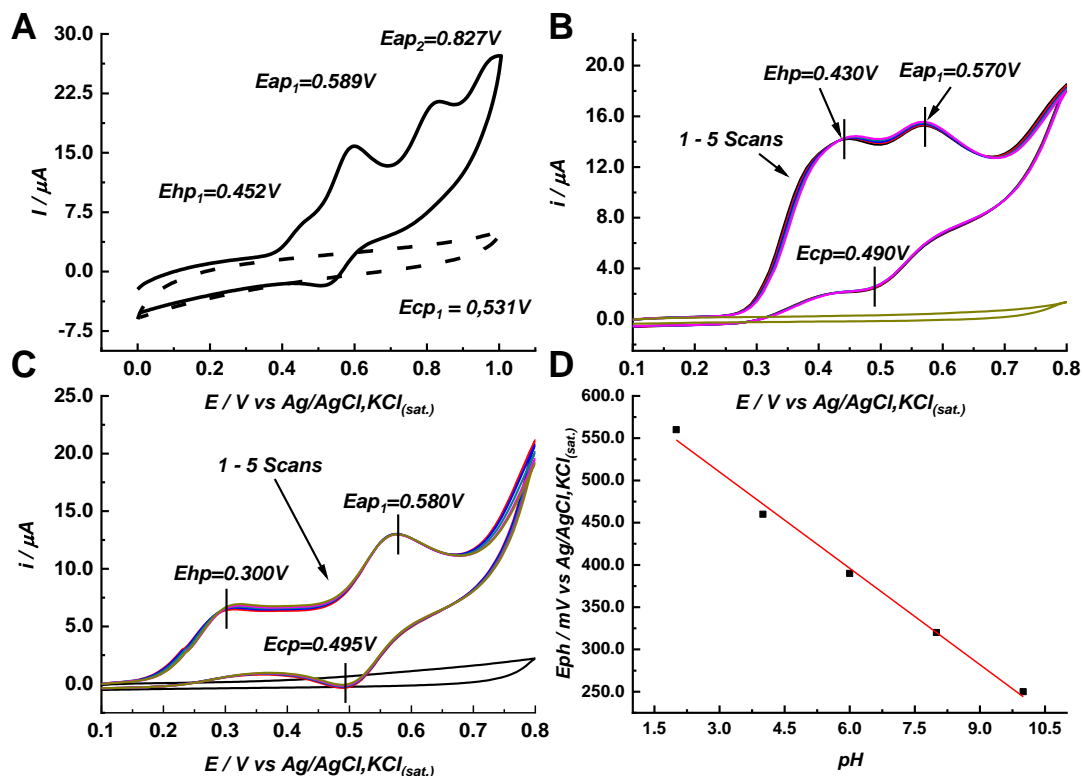


Figure 3. Cyclic voltammograms obtained in a solution of 1.0 mmol L<sup>-1</sup> of MTM in BR solution using GCE. Experimental conditions:  $v = 100 \text{ mV s}^{-1}$ . **3A.**  $E_i = 0.0 \text{ V}$ ;  $E_\lambda = 1.0 \text{ V}$ ;  $E_f = 0.0 \text{ V}$ , pH 4.0. **3B.**  $E_i = 0.1 \text{ V}$ ;  $E_\lambda = 0.8 \text{ V}$ ;  $E_f = 0.1 \text{ V}$ , pH 4.0; **3C.**  $E_i = 0.1 \text{ V}$ ;  $E_\lambda = 0.8 \text{ V}$ ;  $E_f = 0.1 \text{ V}$ , pH 8.0; **3D.**  $E_{hp}$  vs pH curve, constructed using the results obtained from cyclic voltammograms performed with a GCE in a solution containing 1.0 mmol L<sup>-1</sup> of MTM in BR solutions;  $E_{hp}$  vs pH plot ( $E_{hp} = 584 - 38\text{pH}$ ).

Cyclic voltammograms obtained using aqueous aged MTM solution show that the peak potential, attributed to the oxidation of MTM hydrolysis product

(MAA) was dismembered and a barely defined oxidation process was detected at 0.340 V, Figure 4a.

The same Figure also presented a peak at 0.890 V, denominated of  $E_{hp2}$ , which is near of 0.889 V, value observed at  $E_{ap2}$  in DMF medium. This fact indicated that MAA can present the same electroactive group presented by the product of the first oxidation stage of the MTM detected at  $E_{ap2}$  was of (Figures 1A, 3A and 4). Differential pulse voltammograms (DPV) obtained in MAA solution at pH 2.15; 4.0; 6.0 and 10 show that MAA oxidation process has a complex mechanism. The experimental results obtained using MAA (MTM solution prepared in deionized water and aged for 1 month), at pH 2.15 showed only one anodic peak correspondent to the oxidation of both MAA and MTM. Increasing pH to 4.0 no peak overlap was observed, illustrating three oxidation processes:  $E_{hdp1}$  at 0.30 V;  $E_{hdp2}$  at 0.37 V and  $E_{adp3}$  at 0.56 V.  $E_{adp3}$  was attributed to the oxidation of MTM and therefore, was pH independent, while  $E_{hdp1}$  and  $E_{hdp2}$ , attributed to the MAA oxidation, were pH dependent, Figure 4a.  $E_{hdp1}$  vs pH plot illustrated two linear regions (between 2.0 – 4.0 and 4.0 - 10, data not showed) indicating different oxidation mechanisms at the electrode surface. Applying the equation  $E_p/pH = 0.0592 p/n$  (where, p and n are, respectively, the proton and electron numbers), it is concluded that in 4.0 to 10 pH range, two electrons and one proton are involved in the oxidation of MAA at  $E_{hdp1}$ .

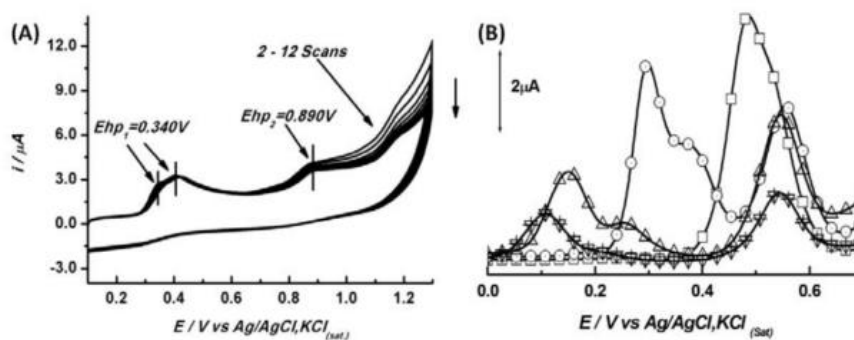
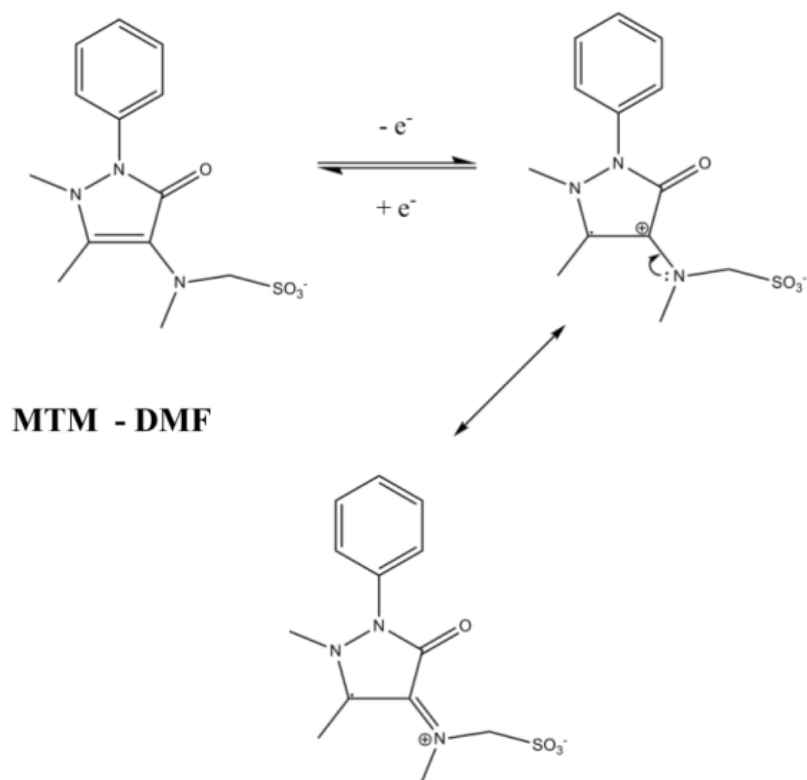
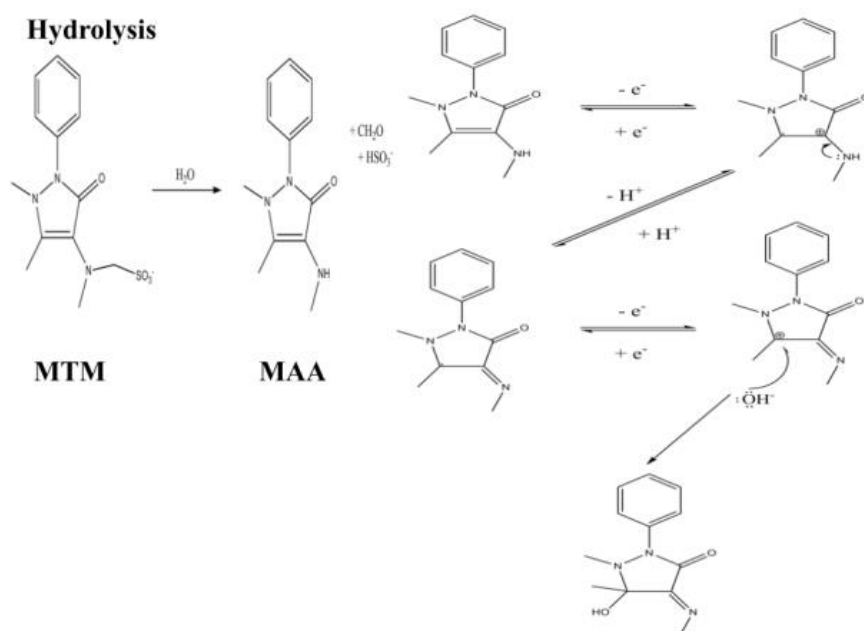


Figure 4. (a) Cyclic Voltammograms obtained in a solution  $1.0 \text{ mmol L}^{-1}$  of MTM in BR solution, pH 8.0 using GCE. (MTM solution aged for two weeks); Experimental Conditions:  $v = 100 \text{ mV s}^{-1}$ .  $E_i = 0.1 \text{ V}$ ;  $E_\lambda = 1.3 \text{ V}$ ;  $E_f = 0.1 \text{ V}$  and (b) Differential pulse voltammograms obtained in  $1.0 \text{ mmol L}^{-1}$  MAA (MTM solution aged for one month) at BR buffer pH 2.1 ( $-\square-$ ); 4.0 ( $--$ ); 8.0 ( $-\Delta-$ ); and 10 ( $-*-$ ). Experimental Conditions: potential range of  $0.0 \text{ V}$  to  $+0.7 \text{ V}$ ;  $v = 5.0 \text{ mV s}^{-1}$ , pulse amplitude =  $25 \text{ mV}$  and pulse width =  $50 \text{ ms}$ . Taking in account the presented results, an electro-oxidation mechanism, in which both products have the same electroactive groups, was proposed, Schemes 1a and 1b.



Scheme 1a. Proposition for MTM electro-oxidation mechanism in DMF. [26,27]



Scheme 1b. Proposition for MTM hydrolysis step to produce MAA and MAA electro-oxidation mechanism in BR buffer media. [26,27]

## Conclusions

Cyclic voltammograms of MTM obtained in DMF medium show three oxidation peaks,  $E_{ap1}$ ,  $E_{ap2}$  e  $E_{ap3}$ , and a reduction peak  $E_{cp}$  which, in close potential range, forms a reversible redox couple with  $E_{ap1}$ . The reversibility criteria used for this classification were:  $E_p$  ( $E_{ap1} - E_{cp}$ ) = 63 mV and  $I_{ap1}/I_{cp}$  ratio of 0.94. In this medium, only the last MTM oxidation process presented a coupled chemical reaction, but the MTM hydrolysis should be considered if BR buffer solutions are used. The same electrochemical processes obtained in DMF were detected in aqueous medium, except the process detected at  $E_{hp}$  peak, attributed to the oxidation of the MAA, product of the MTM hydrolysis, which the peak potential shifted to less positive potential with increasing pH. The MTM hydrolysis process is well known, [24] but not clearly correlation with electrochemical data was done before. The data obtained support the possibility that MAA can present the same electroactive group presented by the product of the first oxidation stage of the MTM. If the pharmacological analgesic effect has been attributed to the reduction of the COX by the oxidation of the MAA [2,3] and it has been clear that the MAA is a reducing agent, the proposed oxidation mechanism of MAA could represent a possible reaction, responsible by the Prostaglandin Synthesis inhibition, [4] giving the analgesic effect to the MAA and, consequently, to the MTM.

## References

[1]. M. Levy, E. Zylber-Katz and B. Rosenkranz, Clin. Pharmacokinet., 28, 216-234 (1995).



- [2]. M. Tubino, A. C. Biondo, M. M. D. C. Vila, L. Pezza and H. R. Pezza, *Eclet. Quim.*,35, 41 - 46 (2010).
- [3]. S. C. Pierre, R. Schimidt, C. Brenneis, M. Michaelis, G. Geisslinger and K. Scholich, *Bri. J. Pharmacol.*, 151, 494 - 503, (2007).
- [4]. R. Abbate, A. M. Gori, S. Pinto, M. Attanasio, R. Paniccia, M. Coppo, S. Castellani, B. Giusti, M. Boddi and G. G. N. Sernerri, *Prostag.Leukotr. Ess.*, 41,89 - 93 (1990).
- [5]. G. W. Basak, J. Drozd-Sokolowska and W. Wiktor-Jedrzejczak , *J. Intern. Med. Res.*, 38, 1374 - 1380 (2010).
- [6]. J. Wessel, M. Matya, M. Neugebauer, H. Kiefer, T. Daldrup, F. Torbah and H. Weber, *Eur. J. Pharm. Sci.*,28, 15 - 25 (2006).
- [7]. L. Pérez-Estrada, S. Malato, A. Aguera and A. Fernandez-Alba, *Catal. Today*,129, 207 - 214 (2007).
- [8]. E. Di Leo, E. Nettis, G. F. Calogiuri, A. Ferrarini and A. Vacca, *Allergy*, 65, 1070 -1071, (2010).
- [9]. S. Bellegrandi, R. Rosso, G. Mattiacci, A. Zaffiro, F. Di Sora and F. Menezella, *Allergy*, 54, 88 - 90 (1999).
- [10]. D. F. Feldmann, Z. Sebastian and T. Heberer, *Chemosphere*, 71, 1754 - 1764 (2008).
- [11]. I. M. Bensenor, *São Paulo Med. J.*, 119, 190 - 191 (2001).
- [12]. L. Loginova and O. Konovalova, *Talanta*,77, 915 - 923 (2008).
- [13]. K. Iwahara, T. Chizuo and M. Masato, *Clin. Chem.*, 52, 1829 - 1831 (2006).
- [14]. T. R. L. C. Paixão, R. C. Matos and M. Bertotti, *Talanta*, 61,725 - 732 (2003).

- [15]. A. C. Boni, A. Wong, R. A. F. Dutra and M. D. P. T. Sotomayor, *Talanta*, 85, 2067-2073 (2011).
- [16]. L. H. Marcolino-Junior, M. F. Bergamini, M. F. S. Teixeira, É. T. G. Cavaleiro and O. Fatibelo-Filho, *Il Farmaco*, 58, 999 - 1004 (2003).
- [17]. T. Pérez-Ruiz, C. M. Lozano and V. Tomás, *J. Pharm. Biomed.*, 12, 1109 - 1113 (1994).
- [18]. W. T. Suarez, O. D. Pessoa-Neto, F. C. Vicentini, B. C. Janegitz, R. C. Faria and O. Fatibelo-Filho, *Anal. Lett.*, 44, 340 - 348 (2011).
- [19]. L. Basáez, I. Peric, P. Jara, C. Sot, D. Contreras, C. Agui and P. Vanysek, *J. Chilean Chem. Soc.*, 53, 1572-1575 (2008).
- [20]. B. Muralidharan, G. Gopu, C. Vedhi and P. Manisankar, *J. Appl. Electrochem.*, 391177 - 1184 (2009).
- [21]. L. Li, L. Cheng, Z. Cai, S. Lan, X. Guo and Y. Li, *Chem. Res. Chinese U.*, 26, 537 -540 (2010).
- [22]. B. Muralidharan, G. Gopu, C. Vedhi and P. Manisankar, *App. Clay Sci.*, 42, 206 -213 (2008).
- [23]. I. Baranowska, P. Markowski, A. Gerle and J. Baranowski, *Bioelectrochem.*, 73, 5 -10 (2008).
- [24]. M. F. S. Teixeira, L. H. Marcolino-Junior, O. Fatibelo-Filho, E. R. Dockal and E. T. G. Cavaleiro, *J. Braz. Chem. Soc.*, 15, 803 - 808 (2004).
- [25]. R. Pauliukaite, M. E. Ghica, O. Fatibelo-Filho and C. M. A. Brett, *Com. Chem. Hight T. SCR.*, 13, 590 - 598 (2010).
- [26]. H. Lund and O. Hammerich, in *Organic Electrochemistry*, 4<sup>a</sup> Ed., p. 563 – 565, M. Dekker Inc., New York (1991).

[27]. J. M. Saveant, in Elements of molecular and biomolecular eletrochemistry, p. 152, John- Wiley-Interscience Inc. (2006).

## Chapter 2

### Electrochemical behaviour of dipyrone (metamizole) and others pyrazolones

This work has been published in the *Electrochimica Acta*. DOI: 10.1016/j.electacta.2018.04.082, and count with the help of Dr Rafael Buoro (from IQSC – USP), who participated in the interpretations of the experimental data, suggestions and revisions, to Dr Othon Campos (from UFES), who helped with experimental suggestions and discussions, Matesa Ramos, who aided in the data acquirement, Dr. Caroline Sanz, who also helped in the data acquirement, and revisions and my supervisor, Dr. Silvia Serrano, who was responsible for the project administration. The electrochemical oxidation of dipyrone (MTM) in aqueous medium was further studied using antipyrine derivatives such as the antipyrine (AA), 4-aminoantipyrine (4AA), 4-methyl-aminoantipyrine (MAA) and 4-dimethyl-aminoantipyrine (DMAA) as model molecules for the elucidation of all MTM voltammetric signals.

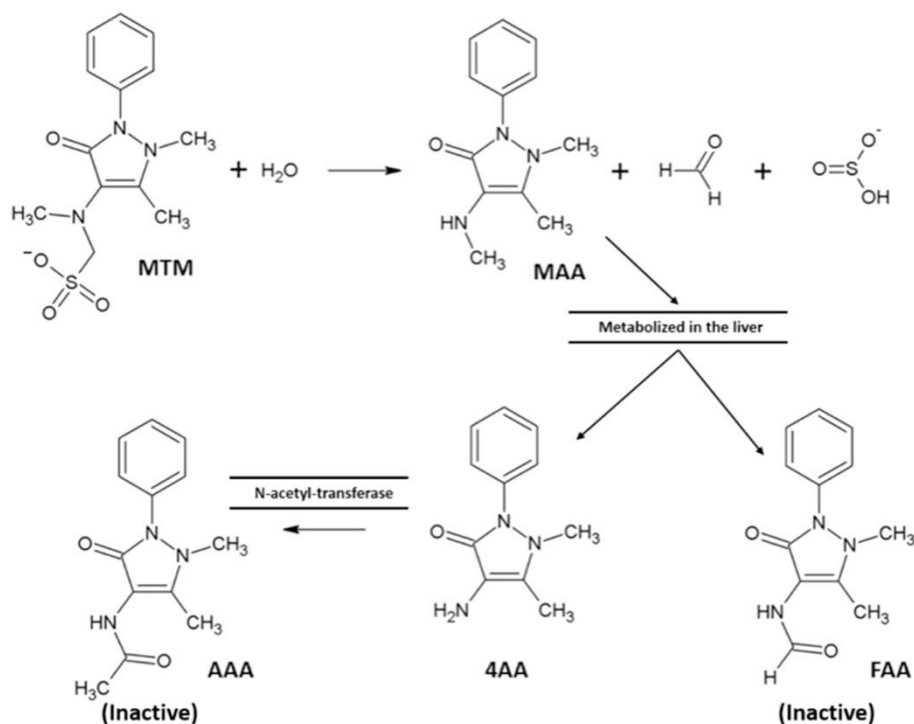
The MTM and the other pyrazolones show up to four oxidation electrochemical processes. The voltammograms obtained in AA solutions presented an irreversible electrochemical oxidation process involving one electron at  $E_{ap3}$ , which is common to all pyrazolone derivatives, while the amino pyrazolones present electrochemical oxidation processes at  $E_{ap0}$  or  $E_{ap1}$ . The stabilization of the oxidation products depends on different effects: the proton release added to the thermodynamic stability, in the case of the imine formation

at  $E_{ap0}$  (4AA and MAA) and the hyperconjugation ( $\sigma$ -stabilization) in the case of iminium formation (DMAA and MTM) at  $E_{ap1}$ . The process observed at  $E_{pa0}$  corresponds to the pH-dependent oxidation of the primary and secondary enamines, while the process observed at  $E_{ap1}$  occurs in the tertiary enamines, is pH independent. The oxidation peak potential follows the order: MAA < 4AA < DMAA < MTM and it was demonstrated that DMAA in an aqueous medium can simulate the MTM in an aprotic medium; therefore, the analytical MTM determination can be performed using the DMAA aqueous analytical curve. DMAA and MTM analytical curves, presented a linear range from 10  $\mu\text{mol L}^{-1}$  to 100  $\mu\text{mol L}^{-1}$  with a LOD of 1.94 and 2.97  $\mu\text{M}$  for DMAA and MTM, respectively, LOQ of 6.48 and 9.91  $\mu\text{M}$  ( $n = 10$ ) and, sensitivity of 0.96  $\mu\text{A}/\mu\text{M}$  for DMAA and 0.92  $\mu\text{A}/\mu\text{M}$ ; with recoveries of 95 to 105% for MTM.

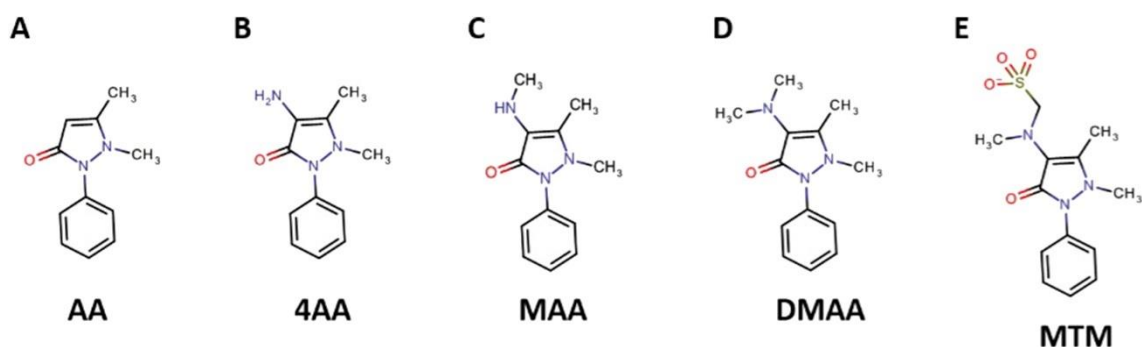
## Introduction

The antipyridines or pyrazolones are a group of the first synthesized pharmaceuticals to work as analgesics and antipyretics. The antipyrine (1,5-dimethyl-2-phenylpyrazol-3-one), AA, was the first one made by Knorr, thus, getting the group name. Some time after, other drugs were made, until they reached the aminoantipyrine (4-amino-1,5-dimethyl-2-phenylpyrazol-3-one), 4AA; the dimethylaminoantipyrine, a.k.a. pyramidon, (4-(dimethylamino)-1,5-dimethyl-2-phenylpyrazol-3-one), DMAA and finally, [(1,5-dimethyl-3-oxo-2-phenylpyrazol-4-yl)-ethylamino] methanesulfonic acid], known as metamizole or dipyrone, MTM, an injectable formulation with antipyretic and analgesic effects [1].

MTM undergoes a hydrolysis reaction and generates the 4-methylamino antipyrine, MAA [2–4], which is enzymatically metabolized in the liver producing other metabolites, such as 4-amino-2,3-dimethyl-1-phenyl-3-pyrazol-5-one, FAA and 4-dimethylamino-1,5-dimethyl-2-phenylpyrazol-3-one, AAA[4, 5], Schemes 1 and 2.



Scheme 1. The MTM hydrolysis and its generated products.



Scheme 2. Structure of the pyrazolones studied in this work.

The analgesic effect observed for MTM, as well as for other pyrazolones, is attributed to the inhibition of the cyclooxygenase enzyme (COX), in the liver, by the pharmacologically active metabolite, MAA [6, 7]; despite that, the inhibition mechanism of cyclooxygenase by the MTM is still unknown. Besides the COX hindering, the MTM and other pyrazolones can induce circumstantial allergic responses, such as Stevens–Johnson’s syndrome [8], rhinoconjunctivitis [9–11] and cause agranulocytosis [2, 8]. Still, MTM is in worldwide use [2, 3, 12–14].

Most studies dedicated to pyrazolones aim at their analytical detection. MTM gets more attention due to its high utilization, being determined and quantified by a variety of techniques, such as HPLC [15, 16], iodometry [17], FIA systems with amperometric detection [18–20], spectrophotometry, also associated with FIA systems by the addition of various reagents [21–23], capillary electrophoresis [24], NMR [16] and voltammetry [25–29]. **AA** is determined by HPLC [30–32], gas chromatography [33], NMR [34] and voltammetry [35–37]. Pyramidon also gets attention in some papers, such as HPLC with amperometric detection [30, 38], voltammetry [36], NMR [39] and a GC method utilized to detect DMAA in apprehended samples of cocaine, in which it is used as adulterant [40].

On an electrochemical overview, several studies were carried out with different types of electrodes, our group utilized a glassy carbon electrode in previous studies [2], Marcolino et al. [25] utilized carbon paste electrodes as working electrode, as well as, Teixeira et al. [35], which modifies the carbon paste with *N,N'*-ethylenebis(salicylideneaminato)oxovanadium(IV), and Cumba et al. [41], who utilized a carbon paste modified with a composite titanium phosphate/nickel hexacyanoferrate. Metallic electrodes were also utilized,

Basaez et al. [29] used platinum electrodes and Munoz et al. [42] disposable gold electrodes obtained from recordable CDs. The difference between carbon-based electrodes and metallic or metallic composites electrodes are the different potential windows and the electrochemical processes definitions. Therefore, carbon-based, such as glassy carbon electrodes, present a most adequate potential window to the electrochemical pyrazolones' oxidation mechanism study providing a constant surface for the electrochemical oxidation without surface passivation problems due to oxide formations in multiple scans, which can give an indirect response to the analyte through interactions with the formed oxide that are independent of the molecule itself, a problem in both platinum and gold electrodes.

The aim of this work was to study the electrochemical oxidation of MTM in an aqueous medium, using AA, 4AA, MAA and DMA as model molecules for the elucidation of all MTM voltammetric signals and to understand why the oxidation peak potentials are different although the oxidation sites are the same in all molecules, except AA. Using this strategy, it was possible not only to understand but also to describe the electrochemical oxidation mechanism and reactivity of MTM and other biologically active pyrazolones, as well as the probable inhibition mechanism of the COX enzyme.

## **Experimental**

### **Reagents and solutions**

All reagents were of analytical grade without any previous purification. The solutions were prepared using deionized water from a reverse osmosis device



(Gehara Co., model OS10LX ultra-pure (PBS),  $0.1 \text{ mol L}^{-1}$ , were prepared by mixing appropriate amounts of system, water resistivity  $> 18 \text{ M}\Omega \text{ cm}$ ). Phosphate buffer solutions  $\text{H}_3\text{PO}_4$  and  $\text{NaH}_2\text{PO}_4$  (Merck) in deionized water. Similar procedures were used to prepare the AA (Sigma Aldrich, code D-8890), 4AA (Sigma Aldrich, code A-4382), DMAA (Sigma Aldrich, code D8015) and MTM (Sigma Aldrich, code D-8890) solutions. The pH adjustments to the desired pH were performed by the addition of  $4.0 \text{ mol L}^{-1}$  NaOH solution. The supporting electrolyte used in the organic medium (DMF - Sigma Aldrich, code 227056) was  $0.1 \text{ mol L}^{-1}$  tetrabutylammonium tetrafluoroborate (TfBTBA e Merck code 8.18244.0025). All experiments were performed at room temperature ( $25 \pm 1 \text{ }^\circ\text{C}$ ) and micro volumes were measured using EP-10 and EP-100 Unipette microliter pipettes (Uniscience, Brazil).

### **Obtainment and characterization of MAA**

MAA was obtained by hydrolysis of  $10 \text{ mmol L}^{-1}$  MTM solutions at  $80 \text{ }^\circ\text{C}$  for 2 h under vigorous stirring. The MAA was extracted from the solution with chloroform and obtained in the solid form, after rotation evaporation of the solvent. It was resolubilized in  $\text{CDCl}_3$  to perform the NMR essays.

### **Apparatus**

All voltammograms were obtained using a PGSTAT 101 potentiostat/galvanostat, Metrohm AUTOLAB, connected to an IME663 interface stirrer device. The data treatment was performed with NOVA software version 1.10.4. and Origin 8.0. Glassy carbon electrode (GCE e 3 mm), Ag/AgCl,  $\text{KCl}_{(\text{sat})}$  and a platinum wire were used as working, reference and auxiliary electrodes,

respectively, in a 20 mL electrochemical cell. All pH measurements were performed using a pH meter model 654 and a combined glass electrode, model 6.0203.100 (OE), both from Metrohm. The spectrophotometric measurements were performed with an Agilent 8453 spectrophotometer with the Chem Station software from Agilent Technologies. The high-performance liquid chromatograms were obtained using a Shimadzu HPLC system LC 10 with UVevis detection and the data treatment performed with a software HPLC class LC 10. NMR spectra were obtained in a Bruker 500 MHz equipment with ACS labs software. All data were obtained at room temperature,  $25 \pm 3$  °C.

### **UV-vis spectra**

The UV and visible spectrophotometric measurements were performed using deuterium and tungsten lamps, respectively, and a quartz cuvette with 1.0 cm optical path. The blank spectra were performed in PBS, pH 7.4.

### **High-performance liquid chromatography (HPLC)**

The chromatograms were obtained with the Shimadzu Diode Array at 241 nm fixed wavelength using a reversed phase technique and analytical column of C18 (5.0 mm, 15 cm and 4.7 mm), previously coupled to a precolumn with a 1.0 mL loop. The mobile phase was methanol/PBS in a 55%/45% (V/V) proportion at pH 2.5 with a flow rate of  $1.0 \text{ mL min}^{-1}$ .

### **Nuclear magnetic resonance (NMR)**

The  $^1\text{H}$  and  $^{13}\text{C}$  NMR spectra (500 MHz frequency) were obtained using a Bruker equipment, <http://ca.iq.usp.br>. The samples were prepared in  $\text{CDCl}_3$ , a

sequence pulse zg30 was utilized in both spectra. To compare quantitatively the  $^1\text{H}$  and  $^{13}\text{C}$  NMR spectra, a computational simulation was obtained using the software ChemBioDraw 2010.

## **Electrochemical measurements**

### **Glassy carbon surface pretreatment.**

The GCE was polished using 1.0/0.1 mm size particle diamond spray (Buehler, US) in a metallographic felt (Buehler, US) to avoid superficial adsorption effects.

### **Cyclic voltammetry (CV).**

The voltammograms were performed using the following experimental conditions:  $E_{\text{initial}} = 0.0 \text{ V}$ ;  $E_{\text{I}} = 1.4 \text{ V}$ ,  $v = 100.0 \text{ mV s}^{-1}$ . The solutions were stirred before each measure.  $E_{\text{final}} = 0.0 \text{ V}$ , step potential = 2.0 mV. Distinct conditions in any assay are specified in the figure caption.

### **Square wave voltammetry (SWV).**

The SW voltammograms were obtained using the following experimental conditions:  $E_{\text{initial}} = 0.0 \text{ V}$ ;  $E_{\text{final}} = 1.4 \text{ V}$ ; step potential = 2.0 mV, pulse amplitude = 50.0 mV, frequency = 25.0 Hz, resulting in scan rate of  $v = 50.0 \text{ mV s}^{-1}$ . The solutions were stirred before each measurement.

### **Differential pulse voltammetry (DPV).**

The experimental conditions for DPV experiments were:  $E_{\text{initial}} = 0.0 \text{ V}$ ,  $E_{\text{final}} = 1.4 \text{ V}$ ; pulse amplitude = 50 mV; pulse width = 100.0 ms; step potential = 2.5 V;

interval time = 0.5s resulting in a scan rate of 5 mV s<sup>-1</sup>. The solutions were stirred before each measurement.

## Results and discussion

### Electrochemical Characterization of MTM and the Other Pyrazolones

Cyclic voltammograms obtained in the antipyrine solutions show up to four oxidation processes ( $E_{ap0}/E_{ap1}$ ,  $E_{ap2}$ ,  $E_{ap2'}$  and  $E_{ap3}$ ), Figure 1. The voltammograms obtained in AA solutions presented only  $E_{ap3}$  process because this molecule has no substituents on the pyrazolone ring; therefore, the most plausible oxidation possibility is in the nitrogen atom, adjacent to the aromatic ring, in a similar mechanism observed for acetaminophen [43], **Figure 1A**. The other molecules (4-AA, MAA, DMA and MTM) have an enamine moiety (group – C=C–N–) as a substituent of the pyrazolone ring, **Scheme 1**. The comparison between the voltammograms presented in **Figure 1A** with those on **Figures 1B–1E** permit the conclusion that the oxidation processes in these molecules involve the enamine moiety.

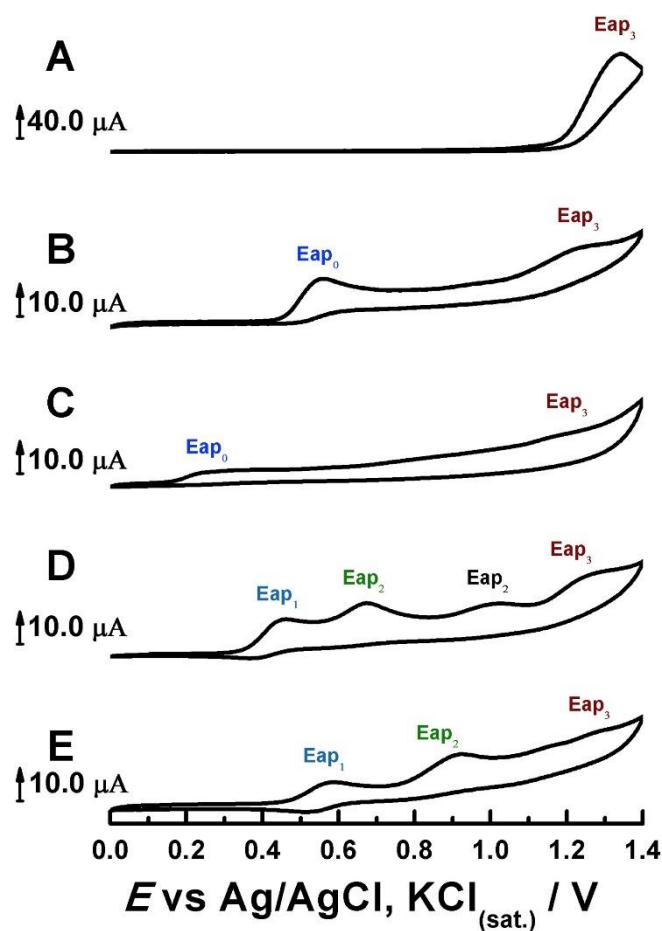


Figure 1. Cyclic voltammograms obtained with GCE in 0.1M PBS, pH = 7.4, containing 1mM of each of the compounds: AA (A); 4AA (B); MAA (C); DMAA (D); MTM (E).

Probably, the oxidation processes  $E_{ap_0}$  (4AA and MAA) and  $E_{ap_1}$  (DMAA and MTM) occur in the enamine itself; however, the oxidation products obtained in  $E_{ap_0}$  and  $E_{ap_1}$  differ in stability and the more stable the product, the less positive is the oxidation peak potential, **Table 1**.

Table 1. Oxidation peak potentials obtained from the cyclic voltammograms presented in figure 1.

Process/ Molecule	$E_{ap0}/V$	$E_{ap1}/V$	$E_{ap2}/V$	$E_{ap3}/V$
AA	–	–	–	1.25
4AA	0.552	–	–	1.22
MAA	0.245	–	–	1.24
DMAA	–	0.444	0.67	1.25
MTM	–	0.578	0.903	1.27

**Table 1** shows that the oxidation peak potential follows the order MAA < 4AA < DMAA < MTM. The first oxidation processes of 4AA and MAA (at  $E_{ap0}$ ) are irreversible and pH dependent, **Figures 1 and 2**, while for DMAA and MTM, the first oxidation process at  $E_{ap1}$  is pH independent and shows a small cathodic component in the reverse scan, **Figure 1E**. According to the slope of the Pourbaix diagrams, 0.054 V/pH and 0.055 V/ pH for 4AA and MAA, respectively, both oxidation processes occur involving the same number of electrons and protons and, the experimental  $pK_a$  value for both molecules is 7.4, Fig. 2.

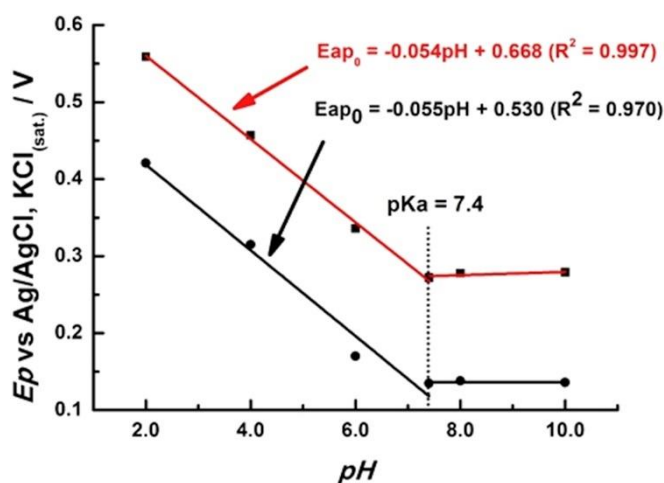


Figure 2. Pourbaix diagrams:  $E_{ap_0}$  from MAA (red line) and 4AA (black line).

To estimate the number of electrons involved in the oxidation processes, differential pulse voltammograms were obtained with GCE in aqueous and nonaqueous media and the data are presented in **Figures 3, 4** and **Table 2**. The  $E_{ap_0}$  peak obtained for 4AA (**Figure 3B**) and MAA (**Figure 3C**) can be mathematically deconvoluted to distinguish the involved processes. Two distinct peaks were obtained:  $E_{ap_0}$  the first one, which corresponds to the oxidation of the enamine (**red line, Figure 3B**) to the corresponding imine, which can undergo a hydrolysis, resulting in a product that can also be oxidized [44] (**green line, Figure 3B and red line on Figure 3C**).

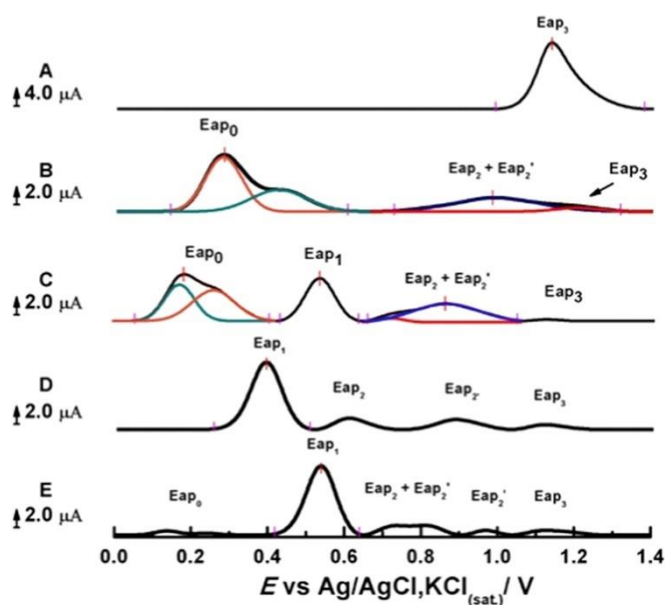


Figure 3. Differential pulse voltammograms obtained with GCE in  $0.1 \text{ mol L}^{-1}$  PBS, pH 7.4, containing  $1.0 \text{ mmol L}^{-1}$  of AA (**A**); 4AA (**B**); MAA (**C**); DMAA (**D**) and MTM (**E**). The peak width at half height values ( $w_{1/2}$ ) were obtained after the voltammogram deconvolution processes (colored lines).

To avoid water-dependent coupled chemical reactions, differential pulse voltammograms were also obtained in DMF containing  $0.1 \text{ mol L}^{-1}$  TFBTBA solution. It would have been expected that, in the absence of water, the pH-dependent oxidation peak potentials, which occur in the same moiety of the molecule, to have similar oxidation potentials, as in fact occurred for  $E_{ap0}$  and  $E_{ap1}$  peaks, Figure 4.

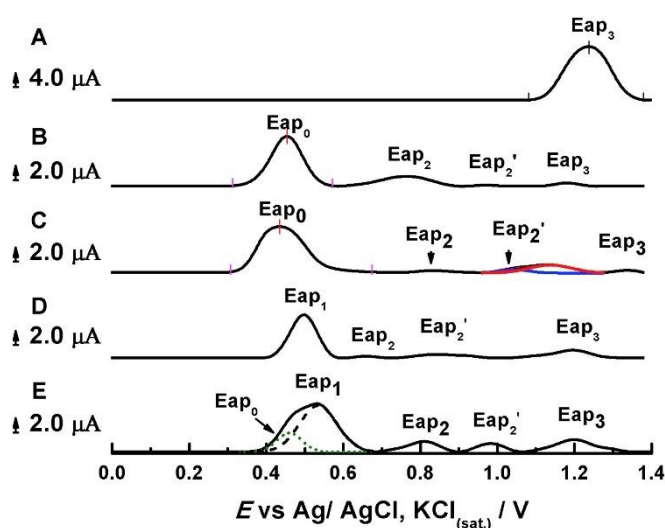


Figure 4. Differential pulse voltammograms obtained with GCE in DMF containing  $0.1 \text{ M}$  of TFBTBA and  $1.0 \text{ mmol L}^{-1}$  of A) AA; B) 4AA; C) MAA; D) DMAA; E) MTM. Deconvolution processes were performed, when necessary, to obtain the values of  $w_{1/2}$ . Experimental data are shown as black lines while deconvolutions are displayed as colored lines.

Table 2: Peak width at half height ( $w_{1/2}$ ) obtained from the differential pulse voltammograms presented in Figure 4.

$w_{1/2}$	$E_{ap0}$ / mV	$E_{ap1}$ / mV	$E_{ap2}$ / mV	$E_{ap3}$ / mV
AA	–	–	–	$96 \pm 6$



$w_{1/2}$	$E_{ap0}$ / mV	$E_{ap1}$ / mV	$E_{ap2}$ / mV	$E_{ap3}$ / mV
4AA	89 ± 3	–	99 ± 3	91 ± 5
MAA	107 ± 7	–	99 ± 6	110 ± 7
DMAA	–	91 ± 3	99 ± 4	102 ± 5
MTM	–	89 ± 4	99 ± 3	107 ± 6

Table 2 shows the peak width at half height ( $w_{1/2}$ ) values obtained in nonaqueous media for all oxidation processes and, according to these data,  $E_{ap0}$  (4AA and MAA) corresponds to a process involving one electron, given that the  $w_{1/2}$  values were 89 and 107 mV, respectively. In the same medium, the  $w_{1/2}$  values for DMAA and MTM at  $E_{ap1}$  were 91 and 89 mV, respectively, which are close to the theoretical value (90 mV) for a charge transfer reaction involving one electron, typical of processes in which the oxidized products are radical species.

It is important to note that the  $E_{ap0}$  value in **Figure 3E** is much less positive than the  $E_{ap0}$  value in **Figure 4E**; this great difference can be explained by the number of protic species in the reaction medium in which the measurements were taken.  $E_{ap0}$  in **Figure 3E** corresponds to the MAA oxidation from MTM hydrolysis; the oxidation process is proton-dependent and facilitated in an aqueous medium. DMF always contains a small amount of water and the MTM hydrolysis process is expected to occur, although to a small extent, but due to the low water content, the pH-dependent oxidation process will be difficult and observed at more positive potentials.

To evaluate the reversibility of the  $E_{ap_0}$  and  $E_{ap_1}$  processes, square wave voltammograms were obtained and data are presented in **Figure 5**.

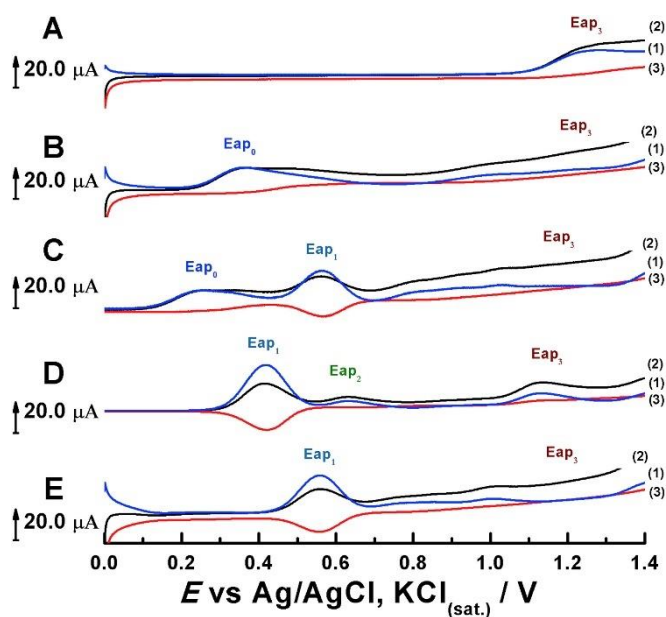


Figure 5: Square wave voltammograms (SWV) obtained with GCE in 0.1 M PBS, pH = 7.4, containing 1.0 mM of each of the compounds: **(A)** AA; **(B)** 4AA; **(C)** MAA; **(D)** DMAA; **(E)** MTM. (1) Total current; (2) forward current; (3) backward current.

As can be seen from Figure 5, only  $E_{ap_1}$  for DMAA has reversible character and this result can be associated with the difference in the substituents bonded to the pyrazolones ring: a tertiary enamine in the case of DMAA and a secondary enamine in the case of MAA.

In the first case, the iminium cation radical formed at  $E_{ap_1}$  can be stabilized by the hyperconjugation effect, improved by the hydrogens of two methyl groups ( $\sigma$ -stabilization) and therefore, can be reversibly reduced at  $E_{cp}$ . However, in the MAA, the electrochemical oxidation process is favored by the loss of one proton and enhanced by the thermodynamic stability of the product, which

confers a less positive oxidation peak potential to the MAA. The  $E_{ap0}$  oxidation process for MAA (**Figure 3C**), shows that the broad peak can be mathematically deconvoluted into two peaks:  $E_{ap0}$  the first one, corresponds to the oxidation of the enamine to the respective imine radical ( $\cdot\text{C}-\text{C}=\text{N}-\text{R}$ ), (**red line, Figure 3B**) [43], similarly to that observed during the formation of the Schiff's bases [45,46] and a small peak, corresponding to the oxidation of the hydrolysis imine radical product, formed in a coupled chemical reaction (**red line on Figure 3C**). This can be the main reason for the irreversibility of the process observed at  $E_{ap0}$  in the MAA molecule.

Note that a similar effect was observed for 4AA (**green line, Figure 3b**) and therefore, the product formed at  $E_{ap0}$  for 4AA suffers hydrolysis reaction and is subsequently oxidized, following a similar oxidation mechanism to MAA. The primary enamine in 4AA has no methyl substituent to stabilize the oxidation product, and then, the  $E_{ap0}$  has a more positive value than those observed for DMAA and MAA.

Finally, it is important to understand why the  $E_{ap1}$ , **Figure 3**, for the MTM has the most positive value of all molecules. This fact can be explained taking into account the presence of the sulfoxide group (an electronic acceptor) as a substituent in the enamine group, in relation to the other studied compounds, the stabilization of its oxidation product is difficult. The  $E_{ap0}$ , **Figure 4**, corresponds to the oxidation of MAA coming from the MTM hydrolysis process, while the  $E_{ap2}$  oxidation process corresponds to the oxidation of the product formed at  $E_{ap1}$ , as previously demonstrated for MTM [2].

## Mechanism Evaluation

The MTM first electrochemical oxidation occurs in the tertiary enamine without the presence of proton to produce an iminium cation radical, which can suffer a nucleophilic attack by water to produce another reactive intermediate. Thus, to evaluate the oxidation mechanism in the absence of a possible coupled reaction, cyclic voltammograms were obtained in DMF solutions containing TFBTBA as a supporting electrolyte, **Figure 6A** (full window) and **Figure 6B** (restricted window).

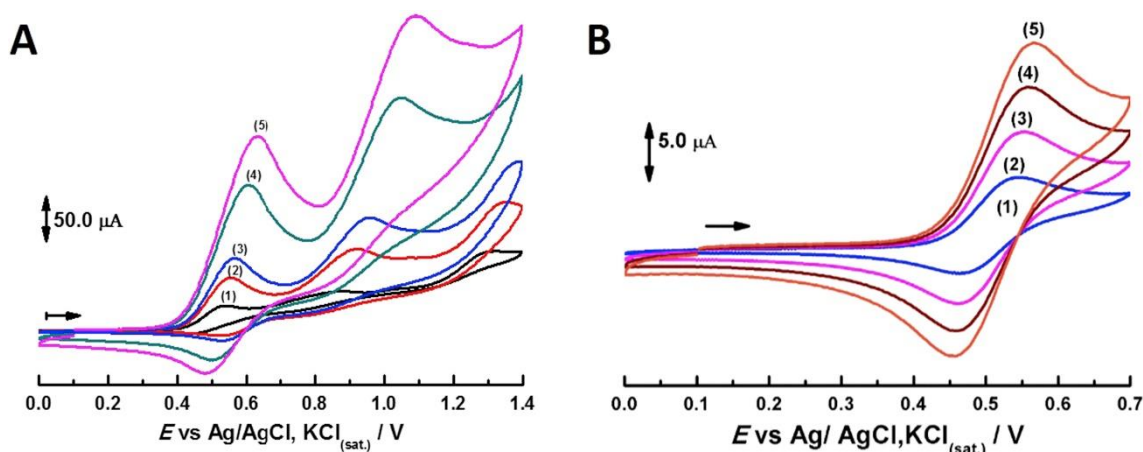


Figure 6: Cyclic voltammograms obtained with GCE in DMF containing  $0.1 \text{ mol L}^{-1}$  of TFBTBA and  $1.0 \text{ mmol L}^{-1}$  of MTM: **(A)**  $10 \text{ mV s}^{-1}$  (1);  $50 \text{ mV s}^{-1}$  (2);  $100 \text{ mV s}^{-1}$  (3);  $500 \text{ mV s}^{-1}$  (4) and  $1000 \text{ mV s}^{-1}$  (5); **(B)**  $E_0 = 0.0 \text{ V}$ ;  $E_\lambda = 1.4 \text{ V}$ ;  $E_f = 0.0 \text{ V}$  and  $10 \text{ mV s}^{-1}$  (1);  $50 \text{ mV s}^{-1}$  (2);  $100 \text{ mV s}^{-1}$  (3);  $500 \text{ mV s}^{-1}$  (4) and  $1000 \text{ mV s}^{-1}$  (5);  $E_0 = 0.0 \text{ V}$ ;  $E_\lambda = 0.7 \text{ V}$ ;  $E_f = 0.0 \text{ V}$ .

If the potential window is restricted to  $+0.7 \text{ V}$ , where the electrochemical process at  $E_{ap2}$  does not occur, it was observed that  $i_{pa1}/i_{pc}$  increases with increasing scan rate, reaching a stable value of 0.75 at  $100 \text{ mV s}^{-1}$ . These

results suggest that the product formed at  $E_{ap1}$  can, at high scan rate, be reduced at  $E_{pc}$  or be consumed, at low scan rates, by a coupled chemical reaction in an EC mechanism, Figure 7.

The process occurring at  $E_{pa1}$  is diffusion controlled throughout the scan range studied ( $\log i_{ap1} = 0.483 \log \nu + 0.730$ ,  $R^2 = 0.985$ ), while that occurring at  $E_{pa2}$  is diffusion controlled at higher scan rate [ $\log i_{ap2} = 0.443 \log \nu + 0.974$ ,  $R^2 = 0.982$  (for  $90 \text{ mV s}^{-1} \leq \nu \leq 1000 \text{ mV s}^{-1}$ )] and adsorption controlled at low scan rate [ $\log i_{ap2} = 0.893 \log \nu + 0.091$ ,  $R^2 = 0.947$  (for  $10 \text{ mV s}^{-1} \leq \nu \leq 90 \text{ mV s}^{-1}$ )], data not shown.

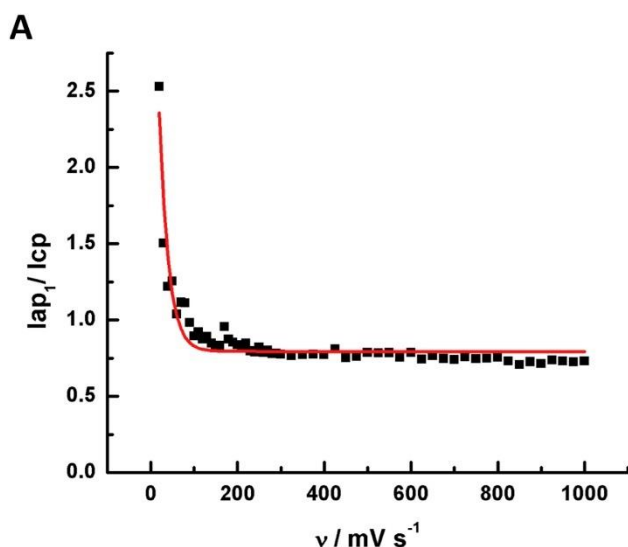


Figure 7:  $i_{ap1} / i_{cp}$  ratio as a function of scan rate ( $\nu$ ). Applied potential window restricted to the interval in which only the first electrochemical process occurs.

The diffusion regions, in both  $E_{ap1}$  and  $E_{ap2}$ , as well as the constant ratio  $i_{ap1}/i_{cp}$ , observed at high scan rates ( $>100 \text{ mV s}^{-1}$ ), indicate an electrochemical–electrochemical (EE) mechanism, which was previously studied [2]. The electrochemical mechanism at  $E_{ap1}$  changes as a function of

the scan rate, which is characteristic of electrochemical processes followed by a coupled chemical reaction.

**Figure 8** is a representation of the first MTM electrochemical process in nonaqueous medium.  $E_{ap1}$  increases linearly with increasing scan rate,  $v$ , from 10 to 100  $\text{mV s}^{-1}$  and the slope of the linear portion is 30  $\text{mV/decade } v$ , which is expected for an EC process involving one electron,  $E_{ap1}/E_{cp}$ . It is important to note that there is a region in the plot where  $E_{ap1}$  is constant and near of 0.56 V. Below this value, for low scan rates, the peak potential values are lower, showing that the chemical coupled reaction is facilitating the electrochemical process.

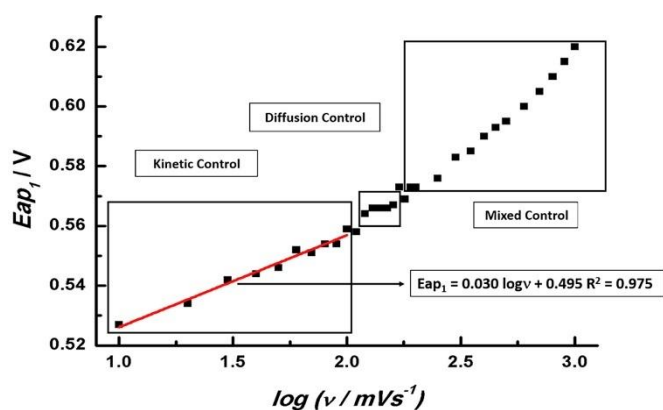


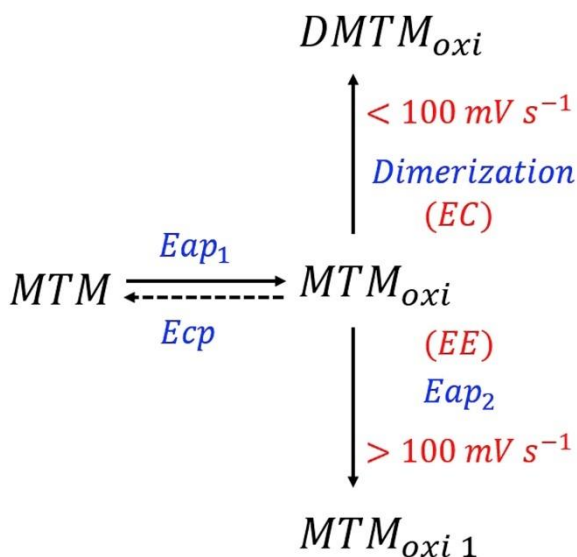
Figure 8:  $E_{ap1}$  vs  $\log v$  plot obtained in DMF containing  $0.1 \text{ mol L}^{-1}$  TFBTBA and  $1.0 \text{ mmol L}^{-1}$  MTM. ( $E_{p1} = 0.030 \log v + 0.495$ ,  $R^2 = 0.975$ ).

The chemical step after the electrochemical process is most likely a dimerization because a nucleophilic attack in an organic medium is highly unlikely to occur. In addition, the slope obtained in the  $E_{ap1}$  vs  $\log v$  plot is very close to the documented theoretical value, 29.9  $\text{mV}/\log v$  [47] as expected for a process involving a dimerization step. Thus, it is suggested that the coupled

chemical reaction is that represented by equation 1, where the oxidation product of the MTM formed in  $E_{ap1}$  undergoes a dimerization process and, apparently, this species is inactive.



The possible reaction pathways after the electrochemical oxidation of MTM are illustrated in **Scheme 3**.



Scheme 3. Schematic representation of the possible reaction pathways after the  $E_{ap1}$  process.

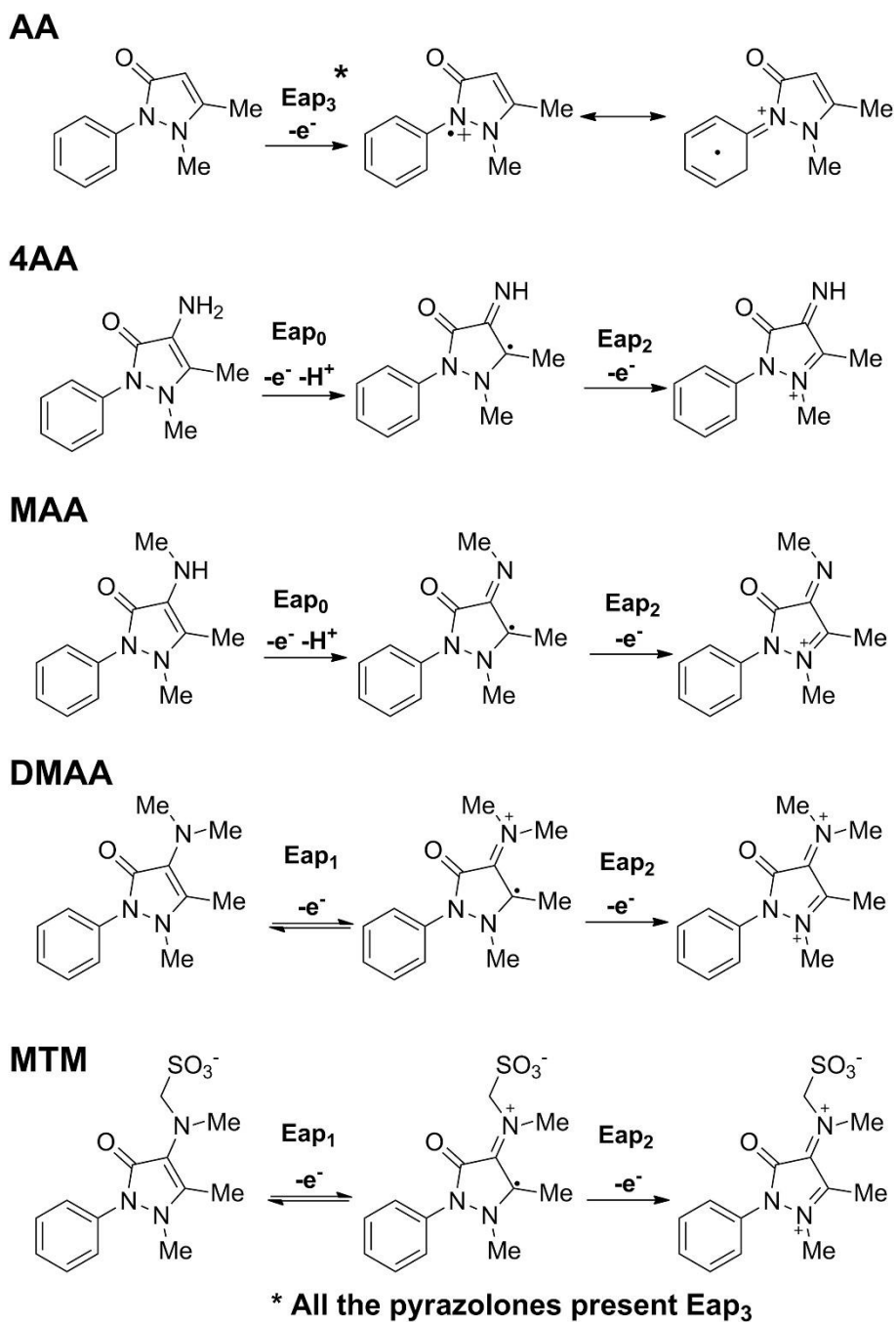
Table 3 compiles the voltammetric data for  $E_{ap0}$ ,  $E_{ap1}$ ,  $E_{ap2}$  and  $E_{ap3}$  in AA, 4AA, MAA, DMAA and MTM.

Table 3. Reversibility, number of the electrons and pH dependency of the electrochemical oxidation processes for the pyrazolone derivatives.

Process	Molecule	Reversibility	n° of electrons	pH dependency
Eap <sub>0</sub>	4AA, MAA	No	1	Yes
Eap <sub>1</sub>	DMAA, MTM	Yes	1	No
Eap <sub>2</sub>	AA, 4AA, MAA, MTM	No	1	No
Eap <sub>3</sub>	AA, 4AA, MAA, MTM	No	1	No

Based on the data presented in Table 3, an oxidation mechanism, Scheme 4, was proposed for the electrochemical oxidations of all pyrazolones studied.





Scheme 4. Electrochemical oxidation mechanism proposed for dipyrone and antipyrine molecules.

### Analytical Application

As observed in the S1 and S2 Figures, MTM's hydrolysis occurs with fast kinetics; thus, it is difficult to use MTM as a standard to obtain an analytical

curve. However, if the proposed mechanism is correct, it should be possible to use DMAA as a model molecule to substitute MTM, because both have the same  $E_{ap1}$  process.

To validate this hypothesis, an analytical curve was constructed utilizing DMAA in an aqueous medium and compared with another MTM curve in an organic medium. DMAA and MTM analytical curves, present a linear range from 10  $\mu\text{mol L}^{-1}$  to 100  $\mu\text{mol L}^{-1}$  with a limit of detection (LOD) of 1.94 and 2.97  $\mu\text{M}$  for DMAA and MTM, respectively, limit of quantitation (LOQ) of 6.48 and 9.91  $\mu\text{M}$  ( $n = 10$ ) [48] and a sensitivity of 0.96  $\mu\text{A}/\mu\text{M}$  for DMAA and 0.92  $\mu\text{A}/\mu\text{M}$  for MTM, Table 4 and **Figure 9**. Using this approach, MTM was quantified in commercial formulations with a recovery of 95 to 105%, **Table 4**.

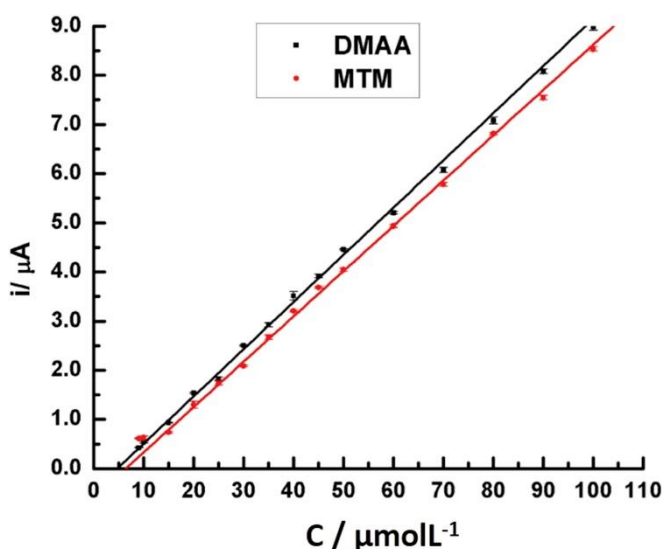


Figure 9: DMAA and MTM analytical curves obtained in PBS pH 7.4 (**black line**) and DMF containing 0.1  $\text{mol L}^{-1}$  of TFBTBA (**red line**), respectively. DMAA solutions in PB, pH = 7.4. Data obtained from square wave voltammograms in 10–100  $\mu\text{mol L}^{-1}$  range (average of five measurements).  $i_{p(\text{DMAA})}/\mu\text{A} = 0.96[\text{DMAA}]\mu\text{M} - 0.45$  ( $R^2 = 0.998$ ) and  $i_{p(\text{MTM})}/\mu\text{A} = 0.92[\text{MTM}]\mu\text{M} - 0.59$  ( $R^2 = 0.998$ ).

Table 4: Analytical parameters obtained for MTM Quantification in pharmaceutical samples using DMAA and MTM analytical curves.

Analytical Curve	Limit of detection ( $\mu\text{mol L}^{-1}$ )	Limit of quantification ( $\mu\text{mol L}^{-1}$ )
DMAA(PBS)	1.94	6.48
MTM (DMF)	2.97	9.91
Sample	Recovery - DMAA (%)	Recovery - MTM (%)
Novalgina <sup>TM</sup>	95.0	86.2
Dipyrone (Medley)	96.5	87.6
Dorflex <sup>TM</sup>	98.0	89.0
Neosaldina <sup>TM</sup>	105.0	95.2

The obtained recoveries are satisfactory, implying that the proposed mechanism is correct.

## Conclusions

The pyrazolones, depending on their structure, may exhibit up to four electrochemical processes,  $E_{ap0}$  or  $E_{ap1}$ ,  $E_{ap2}$ ,  $E_{ap2'}$  and  $E_{ap3}$ . The  $E_{ap3}$  process occurs in the pyrazolone ring. It involves an irreversible electron charge transfer and is common to all compounds of this class. The molecules with the enamine moiety present three electrochemical processes, in addition to  $E_{ap3}$ .

The processes  $E_{ap0}$  or  $E_{ap1}$ , both involving one electron, occur in the same electroactive moiety, the enaminoic nitrogen, substituent of the pyrazolone ring, and these processes depend on two different effects: the hyperconjugation ( $\sigma$ -stabilization) in the case of iminium cation radical formation (DMAA and MTM) at  $E_{ap1}$ , which electrochemical processes are pH independent and the proton release, added to the thermodynamic stability, in the case of the imine radical formation at  $E_{ap0}$  (4AA and MAA).

The  $E_{ap2}$  process, which occurs after the  $E_{ap0}$  or  $E_{ap1}$  processes, is irreversible, involves one electron and is not pH dependent. In MTM, the electrochemical oxidation at  $E_{ap2}$  competes with a chemical dimerization reaction, just after  $E_{ap1}$ . The electrochemical process is favored at high scan rates ( $>90 \text{ mV s}^{-1}$ ), when the chemical step is not favored, **Scheme 3**. The

complete electrochemical oxidation mechanism for several pyrazolones, which data were compiled in Table 3, is illustrated in **Scheme 4**.

Pharmaceutical samples of MTM were prepared in an organic medium and the drug was quantified using an aqueous DMAA analytical curve. Satisfying recoveries were obtained, which corroborates the proposed oxidation mechanism for these molecules.

The voltammetric study of the pyrazolone group allowed understanding the reactivity of the molecules and shows that at physiological pH, MAA (secondary enamine) is easily oxidized and can act as a good reducing agent, which is the probable reason for which the COX enzyme, with iron(III) in its peroxidase active site, is inhibited by the dipyrone.

### **Acknowledgements**

The authors would like to thank São Paulo Foundation Research (FAPESP), CNPq (Process 140833/2016-1), CAPES for the financial support and to Kevin Dias, PhD student, for the valuable discussions. This work is dedicated to Professor Dr. Antonio William Oliveira Lima (*in memoriam*).

### **References**

- [1] K. Brune, The early history of non-opioid analgesics, *Acute Pain*. 1 (1997) 33–40.

- [2] R.P. Bacil, R.M. Buoro, R.P. da Silva, D.B. Medinas, A.W.O. Lima, S.H.P. Serrano, Mechanism of Electro-Oxidation of Metamizole using Cyclic Voltammetry at a Glassy Carbon Electrode, *E C S Trans. Electrochem. Soc.* 43 (2012) 251–258.
- [3] L. Loginova, O. Konovalova, Test films for test-determinations on the base of reagents, immobilized in gelatinous gel, *Talanta*. 77 (2008) 915–923.  
doi:10.1016/j.talanta.2008.07.051.
- [4] H. Ergün, D. a C. Frattarelli, J. V. Aranda, Characterization of the role of physicochemical factors on the hydrolysis of dipyrone, *J. Pharm. Biomed. Anal.* 35 (2004) 479–487. doi:10.1016/j.jpba.2004.02.004.
- [5] M. Levy, E. Zylber-Katz, B. Rosenkranz, Clinical pharmacokinetics of dipyrone and its metabolites., *Clin. Pharmacokinet.* 28 (1995) 216–34.  
doi:10.2165/00003088-199528030-00004.
- [6] S.C. Pierre, R. Schmidt, C. Brenneis, M. Michaelis, G. Geisslinger, K. Scholich, Inhibition of cyclooxygenases by dipyrone., *Br. J. Pharmacol.* 151 (2007) 494–503. doi:10.1038/sj.bjp.0707239.
- [7] S. Bingham, P.J. Beswick, D.E. Blum, N.M. Gray, I.P. Chessell, The role of the cyclooxygenase pathway in nociception and pain, *Semin. Cell Dev. Biol.* 17 (2006) 544–554. doi:10.1016/j.semcdb.2006.09.001.
- [8] M. Levy, Hypersensitivity to pyrazolones, *Thorax*. 55 (2000) 72S–74.  
doi:10.1136/thorax.55.suppl\_2.S72.

- [9] J.C. Wessel, M. Matyja, M. Neugebauer, H. Kiefer, T. Daldrup, F.A. Tarbah, H. Weber, Characterization of oxalic acid derivatives as new metabolites of metamizol (dipyrone) in incubated hen's egg and human., *Eur. J. Pharm. Sci.* 28 (2006) 15–25. doi:10.1016/j.ejps.2005.11.010.
- [10] L.A. Pérez-Estrada, S. Malato, A. Agüera, A.R. Fernández-Alba, Degradation of dipyrone and its main intermediates by solar AOPs. Identification of intermediate products and toxicity assessment, *Catal. Today*. 129 (2007) 207–214. doi:10.1016/j.cattod.2007.08.008.
- [11] S. Bellegrandi, R. Rosso, G. Mattiacci, A. Zaffiro, F. Di Sora, F. Menzella, F. Aiuti, R. Paganelli, Combined immediate- and delayed-type hypersensitivity to metamizole., *Allergy*. 54 (1999) 88–90.  
<http://www.ncbi.nlm.nih.gov/pubmed/10195371> (accessed October 20, 2014).
- [12] E. Di Leo, E. Nettis, G.F. Calogiuri, A. Ferrannini, A. Vacca, Immediate rhinoconjunctivitis induced by metamiloze: an allergic reaction?, *Allergy*. 65 (2010) 1070–1071. doi:10.1111/j.1398-9995.2009.02299.x.
- [13] I.M. Benseñor, To use or not to use dipyrone ? Or maybe , Central Station versus ER ? That is the question ..., *São Paulo Med. J.* 119 (2001) 190–191.
- [14] D.F. Feldmann, S. Zuehlke, T. Heberer, Occurrence, fate and assessment of polar metamizole (dipyrone) residues in hospital and municipal wastewater, *Chemosphere*. 71 (2008) 1754–1764.  
doi:10.1016/j.chemosphere.2007.11.032.

- [15] K. Müssig, A. Pfäfflin, H.-U. Häring, E.D. Schleicher, Dipyrone (metamizole) metabolites interfere with HPLC analysis of plasma catecholamines but not with the determination of urinary catecholamines., *Clin. Chem.* 52 (2006) 1829–31. doi:10.1373/clinchem.2006.071662.
- [16] H.Z. Senyuva, I. Aksahin, S. Ozcan, B.V. Kabasakal, Rapid, simple and accurate liquid chromatography-diode array detection validated method for the determination of dipyrone in solid and liquid dosage forms, *Anal. Chim. Acta.* 547 (2005) 73–77. doi:10.1016/j.aca.2004.12.053.
- [17] T.R.L.C. Paixão, R.C. Matos, M. Bertotti, Diffusion layer titration of dipyrone in pharmaceuticals at a dual-band electrochemical cell, *Talanta.* 61 (2003) 725–732. doi:10.1016/S0039-9140(03)00334-5.
- [18] A.C. Boni, A. Wong, R.A.F. Dutra, M.D.P.T. Sotomayor, Cobalt phthalocyanine as a biomimetic catalyst in the amperometric quantification of dipyrone using FIA, *Talanta.* 85 (2011) 2067–2073. doi:10.1016/j.talanta.2011.07.038.
- [19] L.H. Marcolino-Júnior, M.F. Bergamini, M.F.S. Teixeira, É.T.G. Cavalheiro, O. Fatibello-Filho, Flow injection amperometric determination of dipyrone in pharmaceutical formulations using a carbon paste electrode, *Farm.* 58 (2003) 999–1004. doi:10.1016/S0014-827X(03)00182-4.
- [20] T. Pérez-Ruiz, C. Martínez Lozano, V. Tomás, Flow-injection determination of Novalgín using amperometric detection at a glassy carbon



electrode., *J. Pharm. Biomed. Anal.* 12 (1994) 1109–13.

<http://www.ncbi.nlm.nih.gov/pubmed/7803560> (accessed October 20, 2014).

[21] L.H. Marcolino, R.A. Sousa, O. Fatibello-Filho, F.C. Moraes, M.F.S. Teixeira, Flow-injection spectrophotometric determination of dipyrone in pharmaceutical formulations using ammonium molybdate as chromogenic reagent, *Anal. Lett.* 38 (2005) 2315–2326. doi:10.1080/15265160500316351.

[22] M. Tubino, A.C. Biondo, M.M.D.C. Vila, L. Pezza, H.R. Pezza, Spot-test identification and rapid quantitative sequential analysis of dipyrone, *Eclet. Quim.* 35 (2010) 41–46.

[23] W.T. Suarez, O.D. Pessoa-Neto, F.C. Vicentini, B.C. Janegitz, R.C. Faria, O. Fatibello-Filho, Flow Injection Spectrophotometric Determination of Dipyrone in Pharmaceutical Formulations Using Fe(III) as Reagent, *Anal. Lett.* 44 (2011) 340–348. doi:10.1080/00032719.2010.500777.

[24] L. Basáez, I.M. Peric, P. a Jara, C. a Soto, D.R. Contreras, C. Aguirre, P. Vanýsek, Electrochemical and Electrophoretic Study of Sodium Metamizole, *J. Chil. Chem. Soc.* 53 (2008) 3–6.

[25] I. Baranowska, P. Markowski, A. Gerle, J. Baranowski, Determination of selected drugs in human urine by differential pulse voltammetry technique, *Bioelectrochemistry.* 73 (2008) 5–10. doi:10.1016/j.bioelechem.2008.04.022.

[26] B. Muralidharan, G. Gopu, C. Vedhi, P. Manisankar, Determination of analgesics in pharmaceutical formulations and urine samples using nano

polypyrrole modified glassy carbon electrode, *J. Appl. Electrochem.* 39 (2009) 1177–1184. doi:10.1007/s10800-009-9782-9.

[27] L.J. Li, L.J. Cheng, Z. Cai, S.M. Lan, X.F. Guo, Y.Q. Li, Determination of Metamizole Sodium by Cyclic Voltammetry Under Microwave Activation, *Chem. Res. Chinese Univ.* 26 (2010) 537–540.

[28] B. Muralidharan, G. Gopu, C. Vedhi, P. Manisankar, Voltammetric determination of analgesics using a montmorillonite modified electrode, *Appl. Clay Sci.* 42 (2008) 206–213. doi:10.1016/j.clay.2007.11.005.

[29] M.F.S. Teixeira, L.H. Marcolino-júnior, O. Fatibello-filho, E.R. Dockal, Voltammetric Determination of Dipyrone Using a N,N'-ethylenebis(salicylideneaminato)oxovanadium(IV) Modified Carbon-paste Electrode, 15 (2004) 803–808.

[30] A. Burcinova, M. Tichi, V. Pacakova, K. Stulik, Application of amperometric detection to the high-performance liquid chromatographic determination of antipyrine and 4-aminoantipyrine in urine, *J. Chromatogr. B. V.* 455 (1988) 420–424.

[31] S. Zuehlke, U. Duennbier, T. Heberer, Determination of Polar Drug Residues in Sewage and Surface Water Applying Liquid Chromatography - Tandem Mass Spectrometry, 76 (2004) 6548–6554.

[32] E. Wang, J. Zhou, Simultaneous Determination of Aminopyrine and Antipyrine by Liquid Chromatography / Electrochemistry with a Parallel Dual Electrode, *Microchem. J.* 42 (1990) 259–266.

- [33] S. Lindgren, P. Collste, B. Norlander, F. Sjöqvist, Gas chromatographic assessment of the reproducibility of phenazone plasma half-life in young healthy volunteers., *Eur. J. Clin. Pharmacol.* 7 (1974) 381–385.  
doi:10.1007/BF00558211.
- [34] I. Wilson, J. Nicholson, M. Hofmann, Investigation of the human metabolism of antipyrine using coupled liquid chromatography and nuclear magnetic resonance spectroscopy of urine, *J. Chromatogr.* 617 (1993) 324–328. <http://www.sciencedirect.com/science/article/pii/037843479380507Z> (accessed October 21, 2014).
- [35] N. V Bashkatova, E.I. Korotkova, Y. a Karbainov, a Y. Yagovkin, a a Bakibaev, Electrochemical, quantum-chemical and antioxidant properties of antipyrine and its derivatives., *J. Pharm. Biomed. Anal.* 37 (2005) 1143–7.  
doi:10.1016/j.jpba.2004.11.046.
- [36] H. Yin, Y. Zhou, T. Liu, T. Tang, S. Ai, L. Zhu, Determination aminopyrine in pharmaceutical formulations based on APTS-Fe<sub>3</sub>O<sub>4</sub> nanoparticles modified glassy carbon electrode, *J. Solid State Electrochem.* 16 (2011) 731–738.  
doi:10.1007/s10008-011-1418-4.
- [37] H. Sayo, M. Masui, Anodic oxidation of amines. Part III. Cyclic voltammetry and controlled potential electrolysis of 4-dimethylaminoantipyrine (4-dimethylamino-2,3-dimethyl-1-phenyl- $\Delta^3$ -pyrazolin-5-one) in acetonitrile, *J. Chem. Soc., Perkin Trans. 2.* (1973) 1640–1645. doi:10.1039/P29730001640.

- [38] S. Zuehlke, U. Duennbier, T. Heberer, Determination of polar drug residues in sewage and surface water applying liquid chromatography-tandem mass spectrometry, *Anal. Chem.* 76 (2004) 6548–6554.  
doi:10.1021/ac049324m.
- [39] M.S. Caubet, A. Laplante, J. Caillé, J.L. Brazier, [ 13 C]Aminopyrine and [ 13 C]Caffeine Breath Test: Influence of Gender, Cigarette Smoking and Oral Contraceptives Intake, *Isotopes Environ. Health Stud.* 38 (2002) 71–77.  
doi:10.1080/10256010208033314.
- [40] S.F. Lapachinske, G.G. Okai, A. dos Santos, A.V. de Bairros, M. Yonamine, Analysis of cocaine and its adulterants in drugs for international trafficking seized by the Brazilian Federal Police, *Forensic Sci. Int.* 247 (2015) 48–53. doi:10.1016/j.forsciint.2014.11.028.
- [41] L.R. Cumba, U.D.O. Bicalho, D.R. Silvestrini, D.R. Do Carmo, Preparation and Voltammetric Study of a Composite Titanium Phosphate/Nickel Hexacyanoferrate and Its Application in Dipyrone Determination, *Int. J. Chem.* 4 (2012). doi:10.5539/ijc.v4n2p66.
- [42] R.A.A. Muñoz, R.C. Matos, L. Angnes, Amperometric determination of dipyrone in pharmaceutical formulations with a flow cell containing gold electrodes from recordable compact discs, *J. Pharm. Sci.* 90 (2001) 1972–1977.  
doi:10.1002/jps.1148.

- [43] D.J. Miner, J.R. Rice, R.M. Riggan, P.T. Kissinger, Voltammetry of acetaminophen and its metabolites, *Anal. Chem.* 53 (1981) 2258–2263. doi:10.1021/ac00237a029.
- [44] J.M. Savéant, *Elements of Molecular and Biomolecular Electrochemistry: An Electrochemical Approach to Electron Transfer Chemistry*, John Wiley & Sons, Inc., Hoboken, NJ, USA, 2006. doi:10.1002/0471758078.
- [45] J. Joseph, G.A.B. Rani, *Metal-Based Molecular Design Tuning Biochemical Behavior: Synthesis, Characterization, and Biochemical Studies of Mixed Ligand Complexes Derived From 4-Aminoantipyrine Derivatives*, *Spectrosc. Lett.* 47 (2014) 86–100. doi:10.1080/00387010.2013.776087.
- [46] N. Raman, A. Kulandaisamy, C. Thangaraja, P. Manisankar, S. Viswanathan, C. Vedhi, Synthesis, structural characterisation and electrochemical and antibacterial studies of Schiff base copper complexes, *Transit. Met. Chem.* 29 (2004) 129–135. doi:10.1023/B:TMCH.0000019409.50574.0a.
- [47] D. Pletcher, *Instrumental Methods in Electrochemistry*, 1st ed., Woodhead Publishing Limited, Southampton, 2001. <http://books.google.com/books?hl=en&lr=&id=Q6CjAgAAQBAJ&oi=fnd&pg=PP1&dq=Instrumental+Methods+in+Electrochemistry&ots=SjBuoNFS7W&sig=WTGL4H8jY8OCaPLMoulGimWeADY>.
- [48] J.N. Miller, J.C. Miller, *Statistics and Chemometrics for Analytical Chemistry*, 6th ed., Pearson, Gosport, 2010. doi:10.1198/tech.2004.s248.



## Appendix 2 - Electrochemical behaviour of dipyrone (metamizole) and others pyrazolones

### MAA Obtainment and characterization

HPLC, RMN and UV-Vis spectroscopy was employed in order to characterize the MAA which was obtained from MTM aging solutions.

### High Performance Liquid Chromatography (HPLC).

The hydrolysis reaction was expected to be quantitative. However, the HPLC essay results showed the formation of several other products and the establishment of an equilibrium between the MTM and MAA. The HPLC results are shown in figure S1, due to the structural similarity, the 4AA was used to estimate MAA elution time.

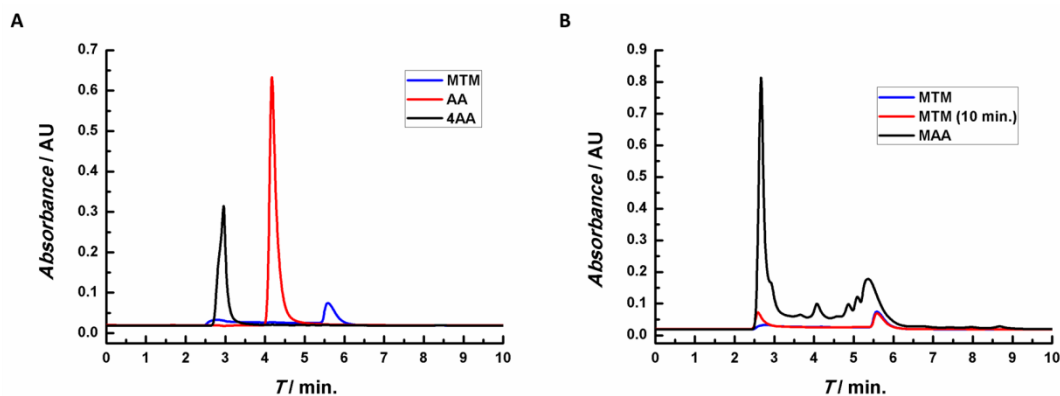


Figure S1. Chromatograms obtained in MeOH 55/ PB 45 (V/V),  $\text{pH}_{\text{apparent}} = 2.5$ , containing  $1.0 \text{ m mol L}^{-1}$  of: (-) MTM, (-) 4AA and (-) AA individual solutions (A) and (-) MTM, (-) MAA and (-) MTM, after 10 minutes (B).

The retention times in figure S1A for 4AA, AA and MTM are 2.5, 4.0 and 5.5 min, respectively. Since a C18 column was used, the most polar molecule, 4AA, presented the smallest retention time, being followed by the AA and the MTM, due to their molecular size. Neither molecules have liquid charges at pH = 2.5 and MTM presents a zwitterionic structure, which is protonated at the enamine, as estimated by the MarvinSketch 15.11.5 computational simulation software. Due to the fast MTM kinetic hydrolysis, the presence of MAA is already detectable in the newly prepared MTM solution and, as expected, the MAA presents a similar 4AA retention time, Figure S1B. Initially, it was believed that the MTM hydrolysis would have been complete, but the MTM peak is still visible at 5.5s (black line, Figure S1B). The presence of several other peaks was attributed to the phenazones sub products of the MTM hydrolysis as described in the literature, scheme 1.

Besides the equilibrium, the chromatograms confirm the presence of a significant amount of MAA in the MTM hydrolyzed solution, which is in accordance to an incomplete hydrolysis reaction.

### **Nuclear Magnetic Resonance (NMR).**

To confirm the MAA generation in the hydrolysis, the NMR spectra of aging MTM solutions were obtained, figures 2A and 2B.



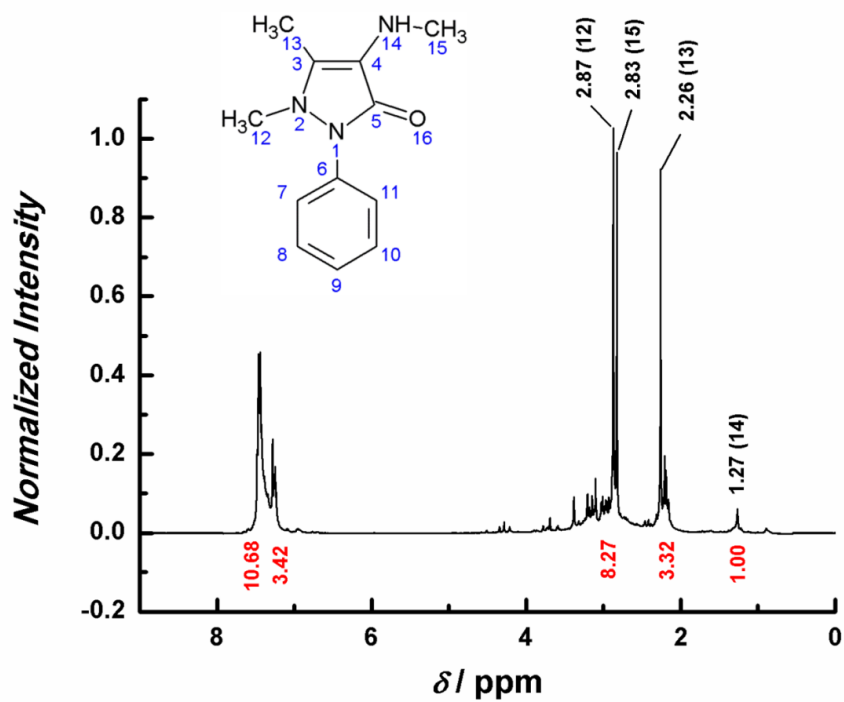


Figure S2A. <sup>1</sup>H NMR Spectrum vs CDCl<sub>3</sub> at 500 MHz, obtained in MAA, extracted with CHCl<sub>3</sub>, from 1.0 mM of MTM aging solutions.

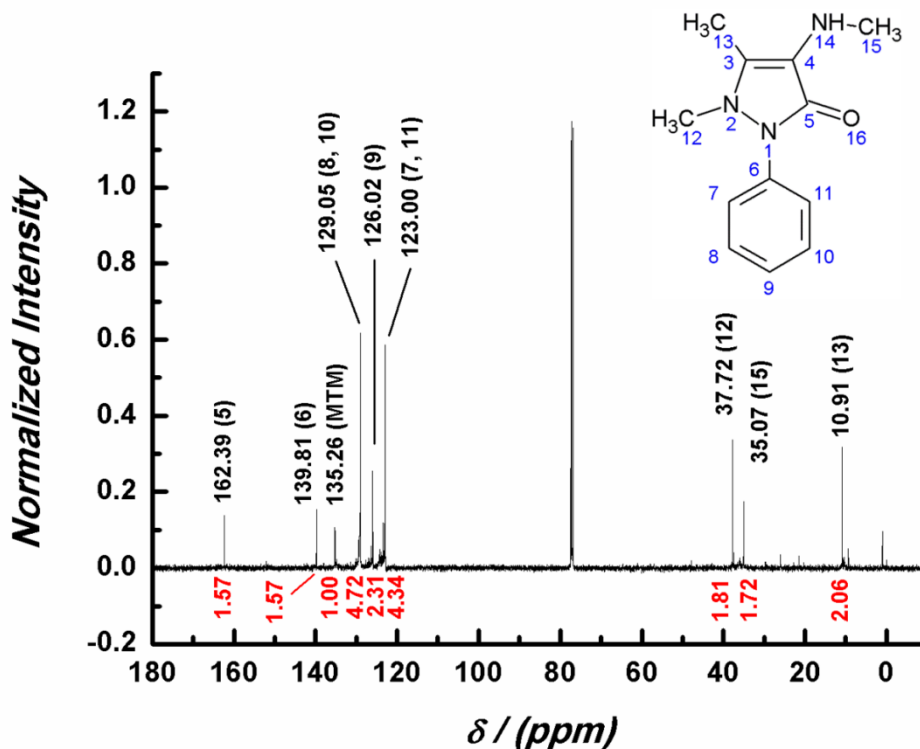


Figure S2B. <sup>13</sup>C NMR Spectrum vs CDCl<sub>3</sub> at 500 MHz, obtained in MAA, extracted with CHCl<sub>3</sub>, from 1.0 mM of MTM aging solutions.

Both obtained spectra of H1 and C13 are very similar to the theoretical ones previously foreseen to a MAA (in Chem Draw software). The exception is a peak of 135.26 ppm in C13 ascribed to the carbon adjacent to the sulfonate, suggesting the presence of MTM even after the extraction procedure. The values obtained by the peak integration between 7 and 8 ppm shows ten hydrogen nuclei in the aromatic hydrogen shift. Five nuclei were attributed to the MAA and five to the MTM, **Figure S2B**. This is in agreement with the HPLC data observed in figure 3A. Besides that, the most intense peaks show that the solution is mostly composed of MAA, as expected. The peaks-nuclei correspondence is shown in an inset on figures 2A and 2B.

In conclusion, the NMR data endorses that MTM hydrolysis leads to the establishment of a MTM/MAA equilibrium, as observed in the HPLC essays.

### UV – Vis Spectroscopy.

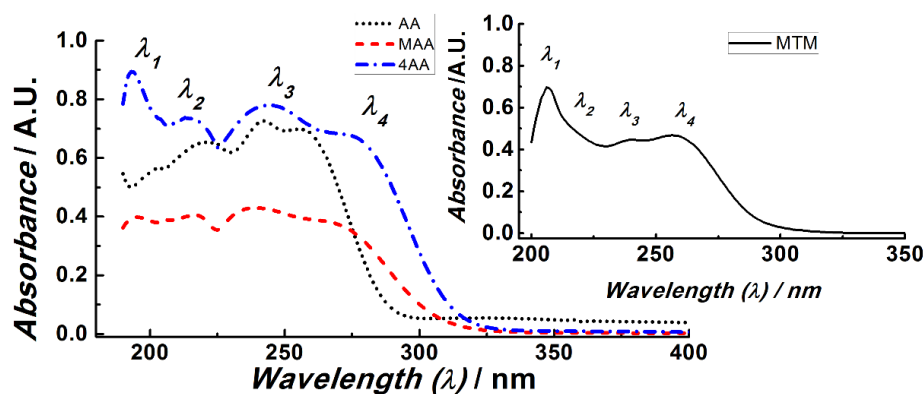


Figure S3: UV-VIS Spectra obtained from solutions containing 50.0  $\mu\text{mol L}^{-1}$  of MTM (Inset), MAA (-.-), 4AA, (- - -) and AA (...) in PBS pH = 7.4.

Table S1: Wavelengths of the bands in UV Spectra of Figure S3.

Wavelength	$\lambda_1$ (nm)	$\lambda_2$ (nm)	$\lambda_3$ (nm)	$\lambda_4$ (nm)
4AA	190	215	241	275
MAA	195	217	241	272
MTM	206	~220	241	257
AA	-	221	241	255

The AA spectrum presented three absorption bands, all due to  $\pi \rightarrow \pi^*$  transitions, Table s1, which are common to all phenazones. The absorption band,  $\lambda_2$ , was attributed to transition in  $\alpha, \beta$  unsaturation on the antipyrine ring. The adsorption band,  $\lambda_3$ , was ascribed to the transition of the aromatic ring. The adsorption band,  $\lambda_4$ , corresponds to the transition in the amide carbonyl.

Comparing the other three molecules with the AA, the adsorption band,  $\lambda_1$  in about 200 nm, was assigned to the  $n \rightarrow \sigma^*$  transition which corresponds to the non-ligand electrons in the nitrogens. Therefore, this transition is more significant in the amino phenazones (MTM, MAA and 4AA) due to the enamine group and almost not visible in the AA Spectra. The presence of three nitrogen atoms causes a stack of the  $n \rightarrow \sigma^*$  transition, this way it has a significant intensity besides the fact of being a transition forbidden by Laporte. The wavelength variation observed in  $\lambda_1$  in the MTM was due to the different substituents in the enamine group in each molecule that causes a bathochromic effect.

The absence of  $\lambda_2$  in the MTM was due to the electron withdrawing effect of the sulfonate group which changes the molecular electronic density and, therefore, increases the required energy to the occurrence of the transition, combining  $\lambda_1$  and  $\lambda_2$ .

The presence of the enamine increases the electronic density of the five-membered ring, observed in the  $\lambda_4$  shifts, promoting another bathochromic effect. In the molecules with the enamines (MAA and 4AA),  $\lambda_4$  is about 275 nm, without the enamine or sulfonated attached enamine,  $\lambda_4$  is about 255 nm.

## Chapter 3

### **Electrochemical oxidation of dipyrone and pyrazolone derivatives complexes with Fe (III), and its EC' mechanism.**

In this chapter, the complexation of Fe (III) with the antipyrines is discussed, this work counted with the collaboration of Pedro Garcia, Victor Vendruscolo, Elaine Mattos and Professor Lucas Rodrigues in data acquisition and data curation, and writing/ revision of the original draft, Professor William Reis helped with discussions, insights and with the revision of the original draft, as Professor Serrano administrated the project.

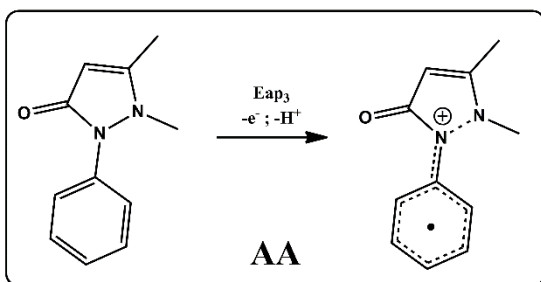
This study shows that iron III complexes with the antipyrines, as the phenazones can chelate the metal in a bidentated (AA) or tridentated (4AA, DMAA and MTM) way. The complexes involve one metal to two ligands and occur via the nitrogen of the enamine and nitrogens of the pyrazalone ring. The complexes formations change the nature of the oxidation processes occurring in the chelation points from irreversible to reversible, as can be seen in the Randles-Sevcik equations due to a  $\pi$ -backbonding effect from the metal to the ligands. When the complex of an antipyrine with a tertiary enamine, such as DMAA or MTM, is in the presence of a reducer, such as 4AA or MAA, they form a hybrid complexes  $[\text{Fe(III)}(4\text{AA})(\text{DMAA})]$  and  $[\text{Fe(III)}(\text{MAA})(\text{MTM})]$ , and their oxidation process occurring in the enamine is catalyzed by the reducer behaviour of 4AA and/ or MAA, forming a EC' mechanism. Therefore, presenting a sharp increase in the peak current values, until the concentration of the reducer diminishes.

## Introduction

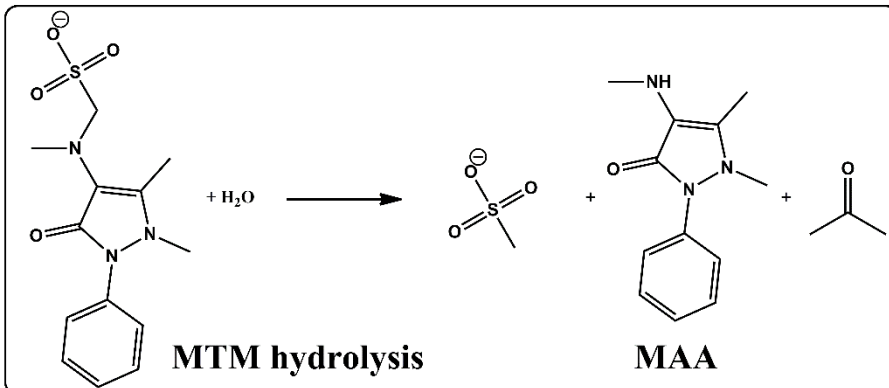
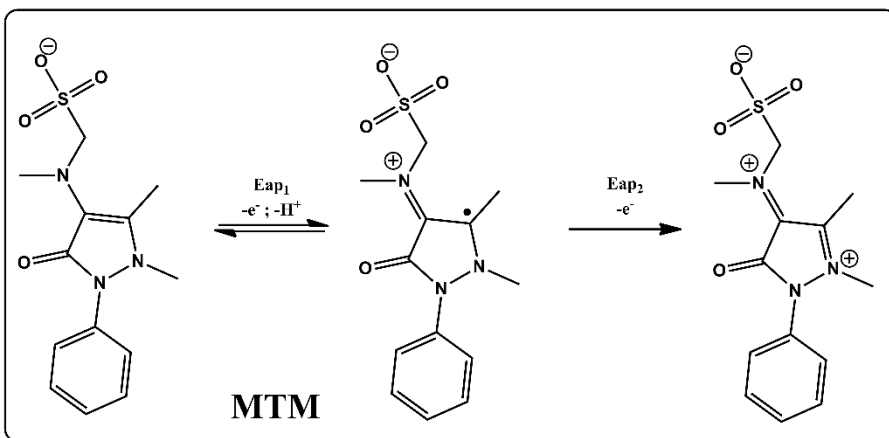
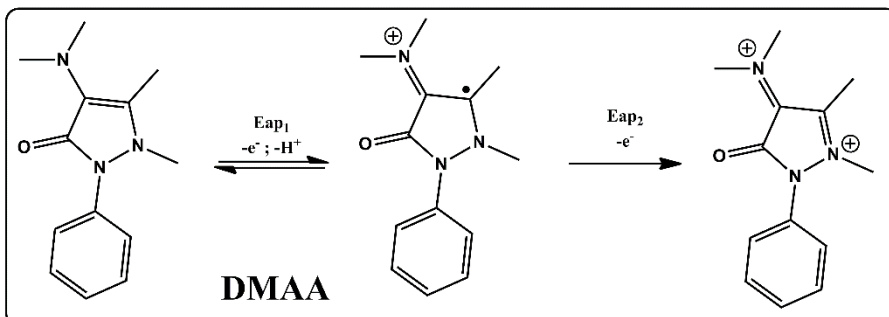
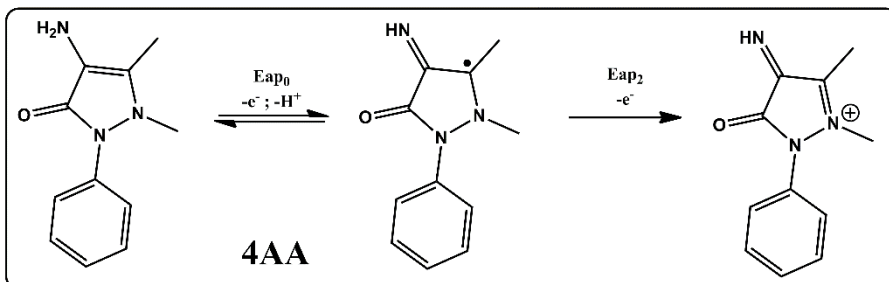
Sodium Metamizole (MTM) or Dipyrone is the most used analgesic worldwide. [1] Although its detailed mechanism of action remains unknown, it is believed that most of its analgesic effect are provided by the inhibition of the cyclooxygenase enzyme and TRPA1 channel by a derivative result from its hydrolysis. [2–4]

Historically, the MTM was a result of the evolution of the first synthetic analgesics made by Knorr, and the medical necessity of a strong analgesics for post-surgical procedures. However, the high dosages required to provide this effect results in a colloidal dispersion of the drug. A problem that was solved by making it a pro-drug. [5]

Recently our group addressed the reactivity of the MTM and the antipyrine group, their electrochemical oxidation mechanism in both aqueous e organic media were studied. Allowing the conclusion that these molecules oxidize in three processes,  $E_{ap0}/E_{ap1}$ ,  $E_{ap2}$  and  $E_{ap3}$ . The first oxidation ( $E_{ap0}$  and  $E_{ap1}$ ) generates a radical, it occurs in the enamine moiety in the antipyrine ring, forming an imine group. Involving one electron, and if possible (primary and secondary enamines), one proton. [6] The following process is an irreversible oxidation of the radical generated in the prior process. At last, a process which occurs in the pyrazolone ring, therefore, occurring to all phenazones. Specifically, in nitrogen vicinal to the aromatic moiety, involving one electron, thus, generating a radical that is, stabilized by the aromatic ring, and most likely resulting in the opening of the pyrazolone ring. These oxidations are illustrated bellow in, scheme 1.



**Eap<sub>3</sub> is common to all pyrazolones**



Scheme 1: Electrochemical oxidation mechanism of the antipyrines and MTM's hydrolysis reaction. [6]

Several studies indicate that a routine use of the MTM could result in the occurrence of agranulocytosis. That is a condition in which the number of the white blood cells (leucopenia) suffers a severe reduction. This disease affect approximately 2 cases per million, with a mortality of 7% of the patients. [7,8]. In addition, the use of the MTM induced circumstantial allergic responses, such as rhinoconjunctivitis. [8–10] As a consequence, MTM was withdrawn from regular market in some countries, such as Sweden, USA, Canada, among others or restricted in others, like the cases of Japan and Australia [2,4,11]. Despite that, other countries such as Brazil, Germany, Spain and France still allows its commercialization, due to its high analgesic potential and low cost. [2,6] Studies also suggest that the regular MTM utilization can lead to aplastic anemia. [12–14] However, the causes of this side effect remains unknown. [15]

Most works in the literature involving the MTM addresses to analytical methods of detection and quantification throughout a distinct variety of techniques, such as HPLC [16], Iodometry [17], FIA systems with amperometric detection [18,19], spectrophotometry, also associated with FIA systems via complex formation by adding iron III [20], capillary electrophoresis [21] and voltammetry [21–28].

Since the phenazones reactivity, and complexation with Fe (III) has not been the focus of the literature, the reactivity of the generated complexes remains unexplored in the literature besides the possible direct relation with the causes of aplastic anemia. Therefore, the aim of this paper is to describe the complexation



of Iron (III) by the antipyrines and their electrochemical oxidation in aqueous media.

## **Material and methods**

### **Apparatus**

All voltammograms were obtained using a PGSTAT 101 potentiostat/galvanostat, Metrohm AUTOLAB, connected to an IME663 interface stirrer device. The data treatment was performed with NOVA software version 1.11.4. and Origin 2019 pro. Glassy carbon electrode (GCE) with 3mm of diameter, Ag/AgCl, KCl<sub>(sat)</sub> (+222 vs SHE) and a platinum wire were used as working, reference and auxiliary electrodes, respectively, in a 10mL electrochemical cell. All pH measurements were performed using a pH meter model 654 and a combined glass electrode, model 6.0203.100 (OE), both from Metrohm. The spectrophotometric measurements were performed with an Agilent 8453 spectrophotometer with the Chem Station software from Agilent Technologies. All data were obtained at room temperature,  $25 \pm 1$  °C.

### **Chemical and reagents**

All reagents were of analytical grade without any previous purification. The solutions were prepared using deionized water from a reverse osmosis device (Gehara Co., model OS10LX ultra-pure, water resistivity of 18 MΩ cm). Phosphate buffer solutions (PBS), 0.1 mol L<sup>-1</sup>, were prepared by mixing appropriate amounts of H<sub>3</sub>PO<sub>4</sub> and NaH<sub>2</sub>PO<sub>4</sub> salts (Merck, São Paulo, Brazil) in deionized water. Similar procedures were used to prepare the AA (Sigma Aldrich, code D-8890), 4AA (Sigma Aldrich, code A-4382), DMAA (Sigma Aldrich, code D8015) and MTM (Sigma Aldrich, code D-8890) solutions. The pH adjustments to the desired pH were performed by the addition of 4.0 mol L<sup>-1</sup> NaOH solution.

All experiments were performed at room temperature ( $25 \pm 1$  °C) and micro volumes were measured using EP-10 and EP-100 Unipette microliter pipettes (Uniscience, Brazil).

### **UV-Vis procedures**

UV-vis spectra were performed using a Shimadzu UV-1601PC with both deuterium and tungsten lamps, and a quartz cuvette with 1.0 cm optical path. The blank spectra were performed in deionized water.

### **Electrochemical procedures**

#### **Cyclic voltammetry (CV)**

The voltammograms were performed by sweeping the potential from  $E_0 = 0.0$  V to a  $E_{\lambda} = 1.5$ , then from 1.5 V the potential was swept to a  $E_{\lambda 1} = -1.0$  V, and finally returning to a  $E_f = E_0 = 0.0$  V. The CV experiments were performed at voltage scan rates ( $v$ ) of 0.01, 0.02, 0.05, 0.10, 0.20, 0.50 and 1.00 V s<sup>-1</sup>. The solutions were stirred, and the working electrode was polished with diamond dispersions of 1.0 and 0.1  $\mu\text{m}$ , respectively, before each measurement.

### **Results and discussions**

In this section the complexations of the phenazones with iron III were systematically studied. At first, the visual complexation was used to study the stability of the complexes in distinct pHs. Following, the UV-Vis and Raman spectra were performed to obtain the stoichiometry and to observe which heteroatoms were chelating the metal. In possession of the respective structures of the complexes, their electrochemical behaviour was studied using cyclic voltammetry to obtain information regarding their reactivity. In sequence, the respective Randles-Sevcik equations were used to discriminate the oxidation processes of the ligands and the complexes. Finally, the Tafel analysis were

performed to both observe the kinetics, and to study the catalytical effect observed between MTM and iron III.

### **Complexes characterization**

#### **UV-Vis structural analysis of the phenazones and their respective complexes.**

To observe the chelating moieties of the ligands and the respective stoichiometry of the products formed, the UV-Vis spectra of the phenazones and their respective complexes were obtained.

Figure 1 shows that AA, 4AA, DMAA and MTM spectra presented three absorption bands, all due to  $\pi/n \rightarrow \pi^*$  transitions, as shown in Tables 1 and S1, which are common to all phenazones.

The first absorption band in 200 nm was attributed to  $\pi \rightarrow \pi^*$  transition of the aromatic moiety on the antipyrine ring. The second absorption band appears in 220 nm was ascribed to a transition  $n \rightarrow \pi^*$  related to the carbonyl moiety. The third and fourth adsorption band shows up in 240 and approximately 255/ 265 nm, both correspond to  $\pi \rightarrow \pi^*$  transitions in the  $\alpha$ ,  $\beta$  unsaturated moiety and to the enamine moieties, respectively. Figure S4 shows the  $\text{FeCl}_3$  spectrum, the absorption identified is in agreement with Loures et al. for Fe(III) [29]. It allows, to conclude that both Fe (III) aqua and  $[\text{Fe(III)(OH)}_2(\text{H}_2\text{O})_4]$  species were observed in solution.

The addition of Fe (III) (1 mL – 1 mM solutions) in the antipyrines, generates the formation of the complexes, as shown in figures S1 and S2. The apparition of a charge transfer (CT) band and the d-d bands were expected to occur to each of the Schiff's base. However, due to a degree of relaxation given

the strong field of the ligands, the latter were not observed as they are Laport forbidden.

Contrasting, to both AA and DMAA spectra; it can be observed that the Fe (III) addition on a 0,1 mmol L<sup>-1</sup> 4AA solution generates two different profiles. Firstly, a decrease on the intensity of the 240 e 255 nm bands related to the ligands, which can be more clearly observed in Figure S5. This occurs due to the oxidation of the Schiff base in which to 4AA generates a more stable product. In processes analogous to the oxidation processes Eap<sub>0</sub> and Eap<sub>2</sub>.

It was noticed a correlation between the increase in the 200 nm band intensity and the opening of the pyrazolone ring. Thus, confirming that to all phenazones, after Eap<sub>3</sub> oxidation process, the five membered ring tends to open. This occurs in the formation of iron complexes with all the ligands (AA, 4AA, DMAA, MTM) and was confirmed by the addition of oxidant, sodium persulfate, in the solutions only containing each Schiff base. With the addition of oxidant, the UV Vis absorption profile of AA remains the same, except for this significant increase in the UV region. It is also possible to observe that over time, this band decreases. Finally, as evidenced by the bands starting at 300 nm in figure S6 and figure S7, an excess of Fe (III) is necessary to the complex formation with AA.

Therefore, it can be concluded that it occurs in three steps. The first one is the oxidation process five membered ring, analogously to the electrochemical process Eap<sub>3</sub> Following, pyrazolone ring opens, and thirdly, the complex is formed. The complex formation results in a new absorption profile. It presents different bands, which includes a CT band at 285 nm and a couple of d-d bands such as 340 and 520 nm.

Commonly, in UV Vis spectra the formation of different species can be observed, as the ligand/ metal ratios are varied, due to an equilibrium in the coordination sphere. However, in all presented UV Vis spectra, and most notably in figure 1, the characteristic bands of only two species were noticed, the unbound Schiff base, and the formed complex. Thus, indicating a not only a fast kinetics, but also that its formation occurs in all the metal positions at once.

The identification of the transitions was possible due to the differences observed in the molar absorptivity ( $\epsilon$ ) values. For complexes without an inversion center, the d-d bands, which are prohibited by Laporte, present a  $\epsilon$  value between 100 and 1000, as for complexes with a high degree of symmetry, these values decrease to values between 1 and 100 [30]. These d-d and CT bands can be better identified in figures S8 and S9. Hereby, the presence of three bands in AA, with a characteristic  $\epsilon$  value, allow to conclude that two different complexes have been formed. The first one being more symmetric than the second, indicating that AA complexes present a stoichiometry of 1:2 metal/ ligand. As evidenced by the presence of two isomers, scheme 2. Given these results, it is possible to infer that, opposing to AA, the Schiff's bases such as 4AA, DMAA and MTM are all tridentate ligands. These complexes are stabilized by the  $\pi$ -backbonding of Schiff's base to unoccupied d orbitals of the metal ( $dy^2-x^2$  e  $dz^2$ ), that compensates the loss of resonance. Furthermore, the  $\pi$ -backbonding is more expressive in the DMAA complex, due to the donor behaviour of the methyl substituents.

Table 1: Absorption Bands of the studied Schiff Bases and their respective iron (III) complexes.

	$\pi \rightarrow \pi^*$	$n \rightarrow \pi^*$	$\pi \rightarrow \pi^*$	$\pi \rightarrow \pi^*$	$n \rightarrow \pi^*$	CT	d-d
	Aromatic	Carbonyl	$\alpha, \beta$ unsaturated	Enamine	NNBE		
AA	200 nm	220 nm	240 nm	265 nm	--	305 nm	365, 420, 470 nm
4AA	200 nm	227 nm	240 nm	255 nm	285 nm	335 nm	360-375; 520 nm
DMAA	200 nm	225 nm	229- 240 nm	255-265 nm	--	300-320;409 nm	370; 465; 560 nm
MTM	200 nm	230 nm	240 nm	270 nm	--	360 nm	480 nm; 415 nm

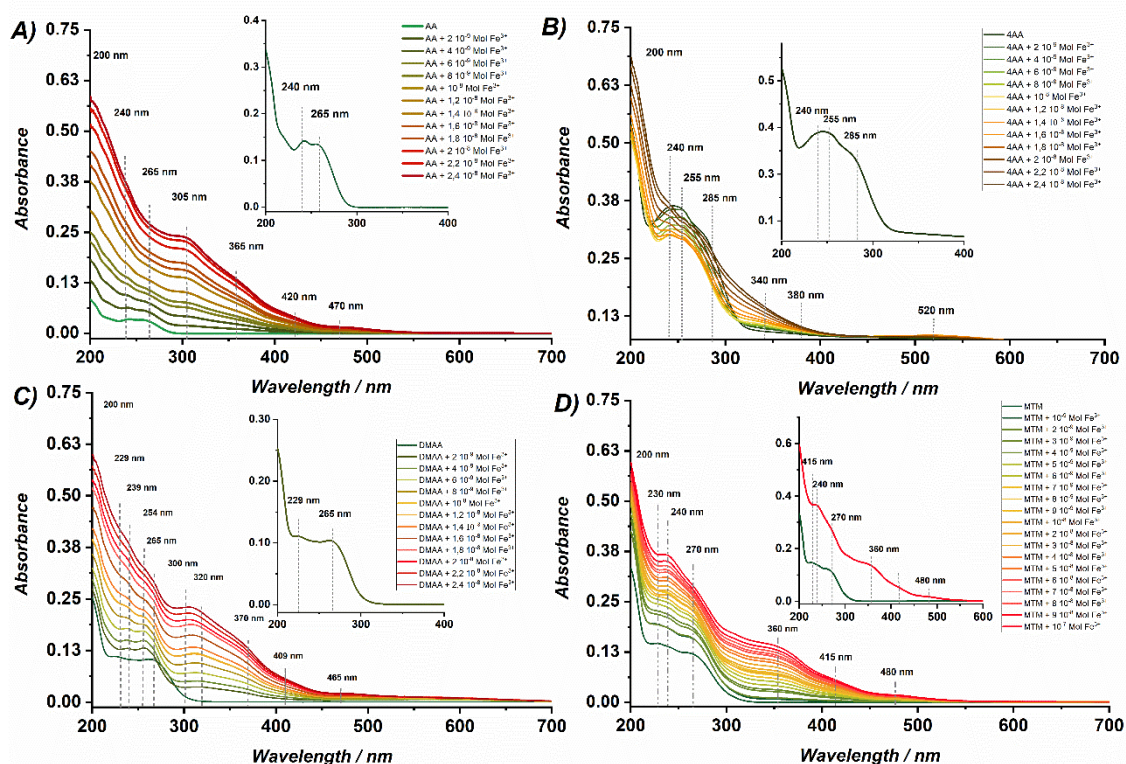


Figure 1: UV-Vis spectra as a function of the iron (III) addition for: A) AA, B) 4AA, C) DMAA and D) MTM

### Raman structural analysis of the phenazones and their respective complexes.

Figure 2 and S10 show the normalized Raman spectra of the phenazone complexes with iron through time, to both crystalized ligands and in solution.

Overall, figure 2 shows that the vibration mode can be attribute to three groups. The first one is the formation of the imine ligand site in the organic compounds: the bands ranging between  $1520$  and  $1580\text{ cm}^{-1}$ . Strong field imine coordination compounds show a C=N symmetric stretching modes between  $1500$  and  $1650\text{ cm}^{-1}$  [31] and Raman spectroscopy is sensitive for imine-mode vibrations in transition metal complexes because of the delocalization of the

electronic cloud around the bond, especially in complexes which presents a  $\pi$ -backbonding. [32,33] Hence, the appearance of imine modes not only shows the pyrazolone ring opens, as observed in UV-Vis spectra, but also corroborates the aforementioned chelation. The appearance of the C=N stretching is pronounced in all the complexes, as strong bands in 1567, in 1579 and 1576  $\text{cm}^{-1}$  can be observed to AA, DMAA and to MTM, respectively. Although the results suggest that these antipyrines can also reduce the metal, which could explain the fast disappearance of the Fe-MTM complex, as the MTM undergoes hydrolysis generating the MAA, a strong reducer. A result corroborated due to the Fe-MTM complex degradation kinetics in which after 5 s after the first spectrum no C=N bonding is detected. On the other hand, only the Fe-4AA complex shows weak vibration modes with respect to imine bonds, in 1522  $\text{cm}^{-1}$ , which is due to a poor Raman scattering signal and background luminescence. Additionally, a couple set of vibrations is shown around 1050, 1250 and 1410  $\text{cm}^{-1}$  are observed in the AA, 4AA and DMAA complexes, and due to their reducer behaviour, the disappearance of these bands can be assigned to other modes containing the imine group.

By comparing all the phenazone complexes, it can be established that among them, the complex with 4AA is the most favorable chelate by presenting a comparative major shift to lower energy. This is evidenced by weakening of the imine double bond which can be comprehended as a side effect of the metal back donation for the imine antibonding orbitals. [34] It is important to highlight, that two distinct events occur. The complexation and the homogeneous reduction processes can be associated with the electrochemical processes  $E_{ap0}$  and  $E_{ap1}$ , shown in the introduction. This association occurs because despite its stability,



the 4AA complex becomes labile after the 4AA oxidizes, and therefore, reducing the metal. An interpretation supported by the complete disappearance of the imine bond within 180 s of reaction and completely degrading before 600 s. Therefore, if not oxidized to the complex formation, the antipyrine derivative undergoes oxidation, consequently, acting as a reducer to either the metal or the complex.

The second set of vibrations are ascribed to the pyrazolone ring vibrations, especially the C=C and C=O stretching modes, in approximately  $1600\text{ cm}^{-1}$  and  $1660\text{ cm}^{-1}$ , respectively. [35] The carbonyl moiety vibrations are affected by the aqueous media, thus becoming a weak shoulder in the luminescence background when comparing to the crystal (Figure S10). All the C=C pyrazolones stretching modes gains intensity after Fe (III) complexation although the energy bond slightly varies depending on the complex. The bondings of both 4AA and DMAA complexes show a low energy shift compared to the ligand crystals. As the C=C of these pyrazolones bonds are suited to sever chain torsions to chelate in the three nitrogen sites, hence the energy bond weakening. However, at AA complex, the C=C mode slightly shifts to higher energy, which can be comprehended to aromatic ring contributions and minor torsion effects to chelation in two sites instead of three. As the MTM complex show no significant change in the vibration energy nor the intensity of these bands due to rapid hydrolysis kinetics and absence of the crystallized ligand. Overall, after the complex degradation no energy shift is observed for any of the compounds suggesting, the ligands retain their organic chain structure, instead of degrading.

Finally, the last group of vibration modes is assigned to aromatic ring. The aromatic C-H in-plane-bending occurs of around  $1000\text{ cm}^{-1}$  and despite of being

the most intense vibration in all complexes, it does not shift its energy after the complexation, which shows the integrity of the aromatic group to both before and after the chelation of the metal, although the carbonic chain vibration (C-C-C bending) shifts to higher energy, ca. 880  $\text{cm}^{-1}$ . [35] This is not only unaffected by the aqueous media in the non-polar moiety of the ligands but also the strengthening of the aromatic ring bond in all complexes, which can be related to iron  $\pi$ -backbonding to the ligand and the inductive effect caused by the Fe (III). [34]

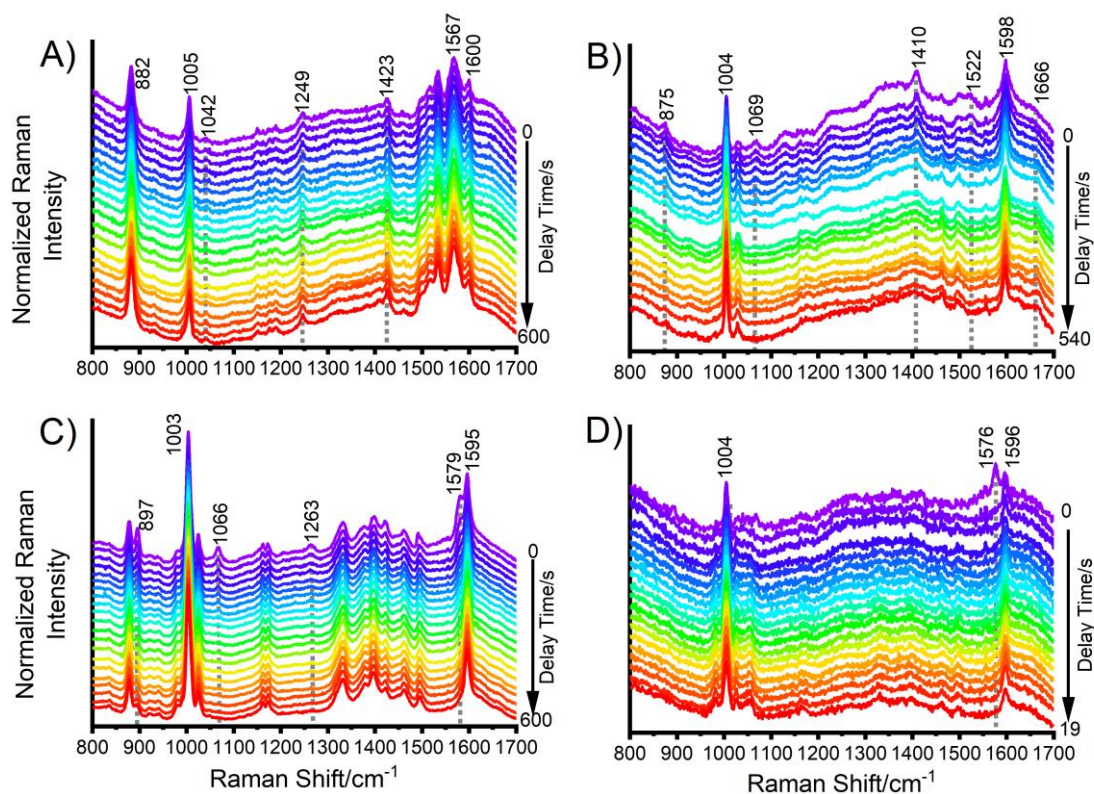
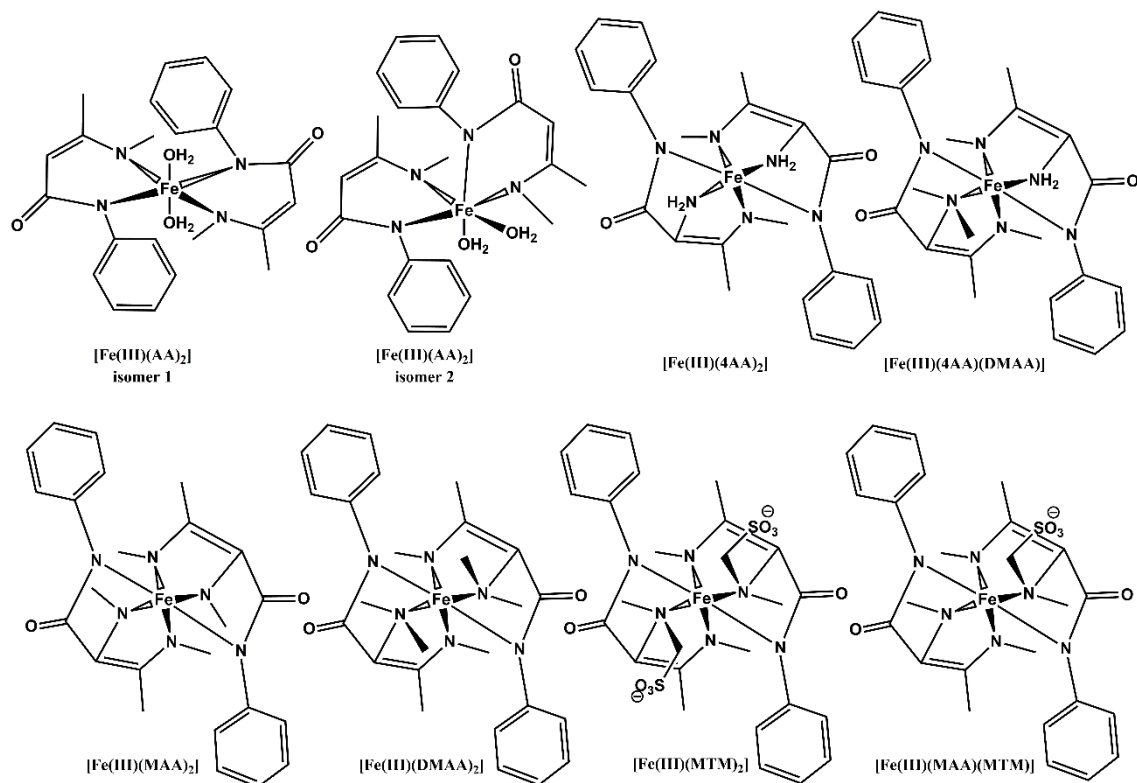


Figure 2: Raman spectra from crystal and solutions of A) AA and AA + Fe (III), B) 4AA and 4AA + Fe (III), C) DMAA and DMAA + Fe (III) and D) MTM and MTM + Fe (III).

Based on the UV-Vis and Raman spectra presented, the following structures were proposed to the complexes of the antipyridines with iron III, scheme 2.



Scheme 2: Proposition of the structures of the complexes formed between the phenazones and iron III.

To know how the complexation affects the pyrazolones reactivity, their electrochemical behaviour was observed using cyclic voltammetry

### Cyclic voltammetry and electrochemical behaviour of the complexes

As aforementioned, the electrochemical oxidation mechanism of the antipyridines was already discussed. However, both UV-Vis and Raman spectra allows to infer the complexes are being formed by the electroactive moieties. Thus, the CV experiments were performed to observe thermodynamic and kinetic differences in the heterogeneous processes of the phenazones.

Figure 3 show CVs obtained for each antipyrine and the respective complex. Figures 3A and 3B show the voltammograms of AA and  $[\text{Fe(III)(AA)}_2]$ . Both present the process  $\text{Eap}_3$ . Although, in the presence of Fe (III), the current scale observed significantly increases to scan rates above  $0.20 \text{ V s}^{-1}$ . Moreover, the peak potential slightly shifts to more positive values, indicating that after the opening of the pyrazolone ring and the formation of the complex, the energy required to oxidize this moiety is marginally the same. However, to high scan rates ( $>0.2 \text{ V s}^{-1}$ ), the peak current significantly increases, suggesting a fast heterogeneous kinetics to  $\text{Eap}_3$  of  $[\text{Fe(III)(AA)}_2]$  that is most likely hindered by some chemical step at slow scan rates.

Figures 3C show a typical CV of 4AA, with the processes,  $\text{Eap}_0$ ,  $\text{Eap}_2$  and  $\text{Eap}_3$ , as figure 3D shows these processes to the respective complex. The process  $\text{Eap}_0$  of  $[\text{Fe(4AA)}_2]$  present an increase in the peak currents values, although the peak potential values are significantly dislocated to more positive potentials, approximately of 150 mV, indicating the complex is more stable, hindering the oxidation process. A similar effect can also be observed to AA in the process  $\text{Eap}_3$ . These results strongly corroborate the spectra data, as both processes  $\text{Eap}_0$  and  $\text{Eap}_3$  occurring at the enamine, Schiff base, and the opened pyrazolone ring, present a shift in the potential values. Moreover,  $[\text{Fe(4AA)}_2]$  shows a great stability as  $\text{Eap}_0$  peak potential is increased. Nonetheless, the complexation increases the kinetics of the process  $\text{Eap}_0$ .

Figure 3E and 3F show a great difference into the peak potential values, the complex oxidation occurs in a much higher potential, although the current levels are maintained. This is most likely due to its tertiary enamine moiety, which oxidizes involving an electron, process  $\text{Eap}_1$ , and not a proton coupled electron

process, Eap<sub>0</sub>. This result in a more prominent action of backbonding effect into the stabilization of the non-ligand electrons, and consequently, a more difficult formation of its radical derivative. The Eap<sub>3</sub> process differently than previously observed shifts to less positive peak potential. Corroborating that the complexation of DMAA is tridentate, occurring via tertiary enamine and the nitrogen of the antipyrine ring.

Finally, figures 3G and 3H show the voltammograms of MTM and its complex. Comparing with figures 3E and 3G, the processes Eap<sub>1</sub>, Eap<sub>2</sub> and Eap<sub>3</sub> can be observed in both MTM and DMAA, as both molecules present a tertiary enamine. Therefore, these molecules present Eap<sub>1</sub> instead of Eap<sub>0</sub>. However, MTM undergoes a fast hydrolysis generating the MAA, which present the Eap<sub>0</sub>. Thus, a typical MTM voltammogram presents both process Eap<sub>0</sub> and Eap<sub>1</sub>. Because of the hydrolysis, when in the presence of Fe (III), three complexes can be formed [Fe(III)(MAA)<sub>2</sub>], [Fe(III)(MAA)(MTM)], and [Fe(III)(MTM)<sub>2</sub>]. The process Eap<sub>0</sub> sharply shifts its peak potential value as Eap<sub>1</sub> seems to slightly shift to less positive potential values. A result strongly suggests that all three complexes are formed. In addition, it also suggests that they interact each other. The peak potential values to all the derivatives with and without the presence of Fe (III) can be observed in table S2.

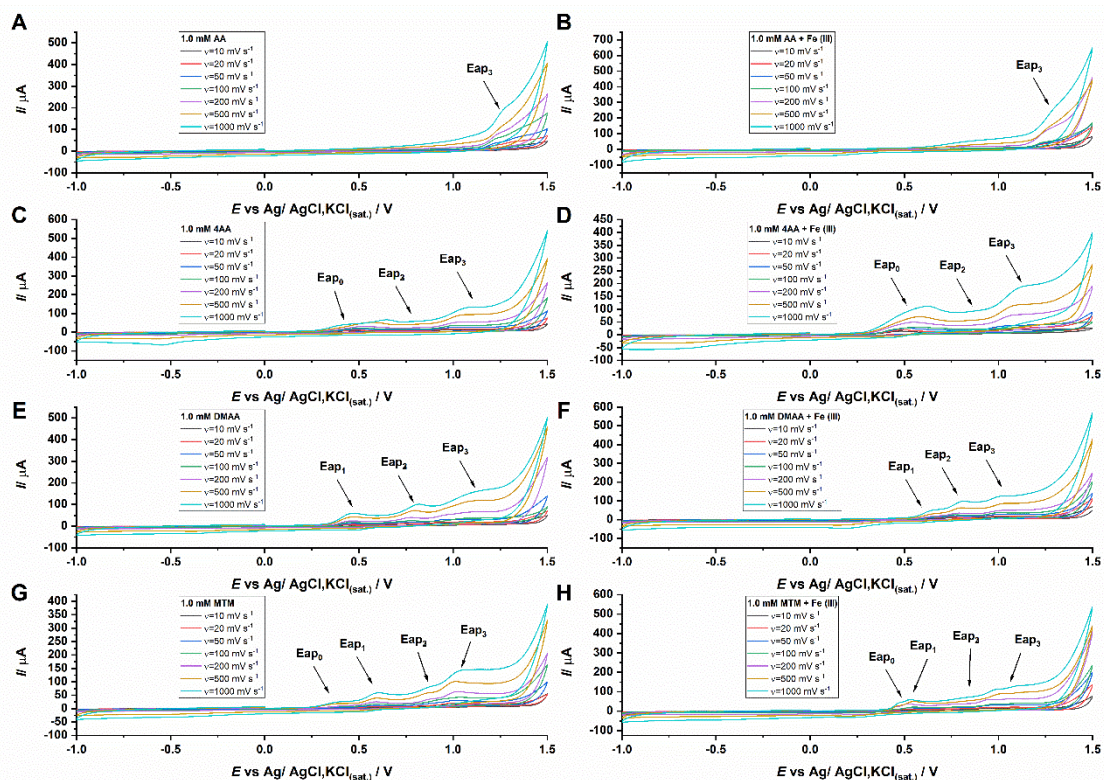


Figure 3: CV of A) 1.0 mM AA B) 1.0 mM AA + Fe (III) C) 1.0 mM 4AA D) 1.0 mM AA + Fe (III) E) 1.0 mM DMAA F) 1.0 mM AA + Fe (III) G) 1.0 mM MTM H) 1.0 mM AA + Fe (III) in solutions of 0.1 M HCl.

### Randles Sevcik equations and the processes mechanism

To better comprehend the changes that occur within the complexation, the Randles Sevcik theoretical predictions were obtained. These equations (1) and (2) [36], represent the reversible and multi-step irreversible cases, respectively, allows to predict the peak current results to distinct mechanisms.

$$I_p = 0.446 n F C A \sqrt{n F v D / R T} \quad (1)$$

$$I_p = 0.496 \sqrt{n' + \beta} F C A \sqrt{n F v D / R T} \quad (2)$$

where  $I_p$  is the peak current in A,  $n$  is the overall number of electrons transferred,  $n'$  is the number of electrons prior to the rate-determining step,  $\beta$  is the anodic

charge transfer coefficient,  $F$  is the Faraday Constant in Coulomb mol<sup>-1</sup>,  $C$  is the concentration in mol cm<sup>-3</sup>,  $A$  the electrode area in cm<sup>2</sup>,  $\nu$  is the scan rate in Vs<sup>-1</sup>,  $R$  is the Gas Constant in J K<sup>-1</sup> mol<sup>-1</sup> and  $T$  is the temperature in K. A diffusion coefficient ( $D$ ) of  $6.95 \times 10^{-6}$  cm s<sup>-1</sup> to AA,  $4.95 \times 10^{-6}$  cm s<sup>-1</sup> to 4AA,  $3.21 \times 10^{-6}$  cm s<sup>-1</sup> to DMAA, as presented in figures S9, S10 and S11, respectively.

Figure 4A shows a comparison between the Randles Sevcik predictions and the experimental peak current values obtained to both AA and [Fe(III)(AA)<sub>2</sub>]. It was observed that throughout the scan rate window observed (0.01 to 1.00 V s<sup>-1</sup>), AA's process Eap<sub>3</sub> fits the prediction of a multi-step irreversible process in which the rate determining step is the second step. On the other hand, to the isomer complexes [Fe(III)(AA)<sub>2</sub>], at scan rates below 0.20 V s<sup>-1</sup>, the peak current values suggest a similar multi-step irreversible process, as observed to the ligand, although with the first step as the rate determining one. Yet, to scan rates above 0.20 V s<sup>-1</sup> a mechanism shift can be seen, as the peak current values of the complexes sharply increases, suggesting that at high scan rates, the oxidation process behaves as a single step two electron reversible oxidation process. This effect can be explained due to a rearrangement resultant of the break of the N-N bond and the formation of two N-Fe bonds, providing a better heterogeneous kinetic to the Eap<sub>3</sub> process due to the  $\pi$ -backbonding effect of the metal.

A similar result can be observed in figure 4B. The oxidation process Eap<sub>0</sub> presents experimental peak current values which fits the theoretical predictions to a one electrons irreversible process. Despite that, the complex [Fe(III)(4AA)<sub>2</sub>], present an Eap<sub>0</sub> oxidation process as reversible single electron transfer to the whole scan rate window observed. This shift in the mechanism occurs due to the trident complex formed, which has the, already mentioned,  $\pi$ -backbonding effect

of the metal acting to stabilize the radical product. Resulting in a greater heterogeneous kinetic to the process  $E_{ap_0}$ .

Figure 4C shows that the peak current values to process  $E_{ap_1}$  behaves as a one electron irreversible process to both DMAA and to the complex  $[Fe(III)(DMAA)_2]$ . This result advocates that primary and secondary enamines heterogeneous kinetics are benefited from its ability to liberate the proton, thus reducing the energy of the molecule which stabilizes the formed product. However, tertiary enamines can only stabilize via hyperconjugation, which is not as effective the proton release. Therefore, jeopardizing the electrochemical kinetics of process  $E_{ap_1}$ .

Figure 4D displays the sum of the peak current values of both processes  $E_{ap_1}$ , from MTM, and  $E_{ap_0}$ , from its hydrolysis product, MAA. This sum is necessary because the hydrolysis hastily consumes the MTM generating MAA. Therefore, independently, the peak current values do not fit any of the theoretical predictions. On the other hand, the combined peak current values for the MTM alone behaves as a one electron irreversible electron transfer, which is expected, as  $E_{ap_1}$ , also presented an irreversible process, as, the combined results of the MTM/MAA complexes ( $[Fe(III)(MTM)_2]$  or  $[Fe(III)(MAA)(MTM)]$  or  $[Fe(III)(MAA)_2]$ ) behaves as a one electron reversible oxidation. This result is consistent with the ones observed in figures 4B and 4C for processes  $E_{ap_0}$  and  $E_{ap_1}$ , respectively. Indicating that the hydrolysis product oxidation,  $E_{ap_0}$  process, prevails over the MTM,  $E_{ap_1}$  process, hence shifting the behaviour of MTM from irreversible to reversible.



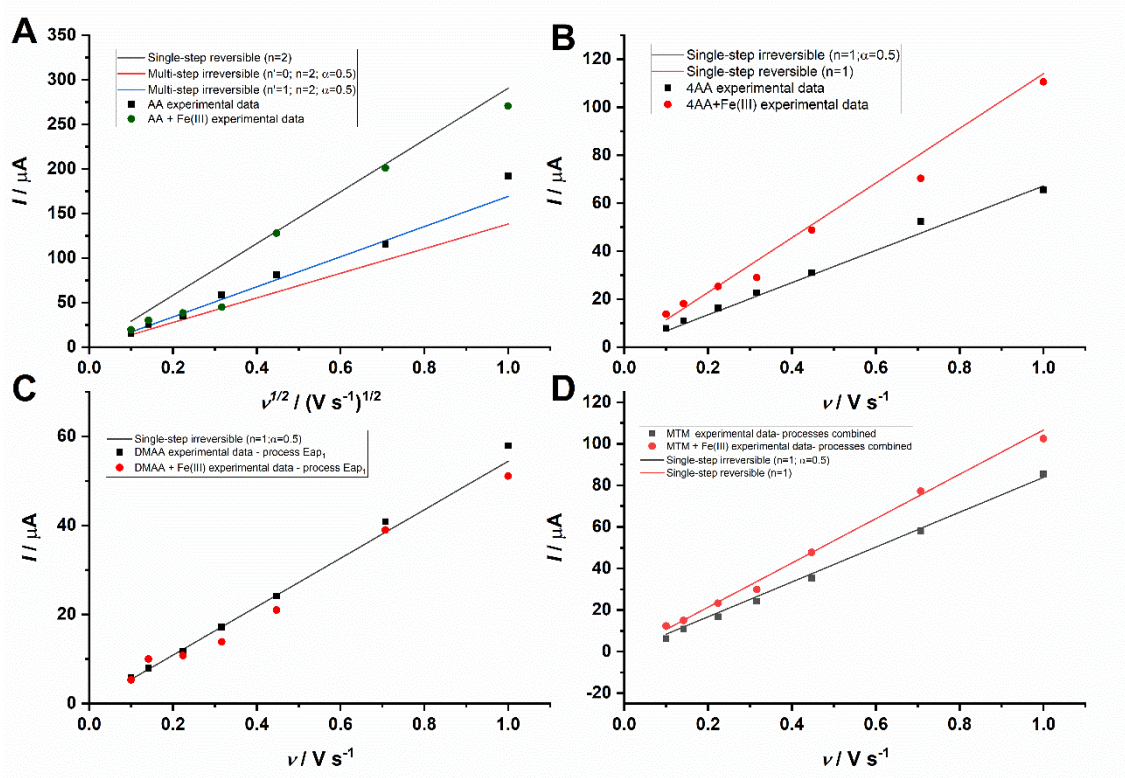


Figure 4: Randles Sevcik theoretical predictions compared to the experimental peak current values obtained to the processes A) Eap<sub>3</sub> of AA, B) Eap<sub>0</sub> of 4AA, C) Eap<sub>1</sub> of DMAA, D) combined values of Eap<sub>0</sub> and Eap<sub>1</sub> of MTM.

### Tafel analysis and a catalytical effect of the complexes and the hydrolysis.

In the previous section, the Randles Sevcik theoretical predictions show that with the complexation, both processes Eap<sub>0</sub> and Eap<sub>1</sub> undergoes a mechanism change from irreversible oxidation processes to reversible. To further comprehend this change, the Tafel analysis was conducted to observe the difference between the into the charge transfer coefficient ( $\beta$ ) heterogeneous of the complexes. This analysis provides the  $\beta$  values, according to equation 3 [37], which are directly correlated with the activation Gibbs energy involved in the oxidations, equation 4. [38]

$$\beta(E) = \frac{F}{RT} \frac{d \ln I}{dE} \quad (3)$$

$$\beta = \frac{1}{2} \left( 1 + \frac{\Delta G^\ddagger}{\lambda} \right) \quad (4)$$

where  $\beta$  is the charge transfer coefficient,  $\Delta G^\ddagger$  is the standard Gibbs energy of activation in  $\text{kJ mol}^{-1}$  and  $\lambda$  is the reorganization energy in  $\text{mol kJ}^{-1}$ . The respective Tafel analysis was performed according to Li et al. [39] and the results can be seen in figure 7.

Figure 5A shows the  $\beta$  values as a function of the potential values to both AA, and the complexes  $[\text{Fe(III)}(\text{AA})_2]$ . The charge transfer coefficients slightly shift to more positive values whilst the peak dislocates to more positive potential values. This result implies that  $E_{\text{ap}3}$  process has been mediated by the metal increasing the heterogeneous rate constant whilst the oxidation process remains similar to the original oxidation,  $E_{\text{ap}3}$ , whilst the oxidation process remains similar to the original oxidation,  $E_{\text{ap}3}$ .

Figure 5B shows a comparison between the charge transfer coefficients of 4AA and the  $[\text{Fe}(4\text{AA})_2]$ . The  $\beta$  values of the oxidation process  $E_{\text{ap}0}$  of the ligand is approximately of 0.4, and also presents a barely defined process which could be the indicative of side reaction, e.g. a following chemical step such as a Michael addition. In the complex  $[\text{Fe(III)}(4\text{AA})_2]$ , the oxidation process  $E_{\text{ap}0}$  becomes a reversible process. The  $\beta$  value of the process  $E_{\text{ap}0}$  significantly increases from 0.4 to 0.6, suggesting a greater faradaic current with a similar driving force. As formerly appointed, this result indicates a more prominent molecular orbital is formed, and it can not only stabilize the formed radical due to the  $\pi$ -backbonding effect, but also facilitate the electron transfer from the complex to the electrode, as a consequence of the Frank-Condon effect. Thus,

generating an increase in the electron transfer kinetics. It is also noteworthy that in the presence of the Fe (III), no barely defined process is displayed.

Figure 5C show the  $\beta$  values for a tertiary enamine oxidation in DMAA, with and without the metal in solution. The process  $E_{ap1}$  presents analogue charge transfer coefficient values to both DMAA and  $[Fe(DMAA)_2]$ . Although a significant dislocation in its peak potential can be noticed. This shift indicates the  $\pi$ -backbond effect stabilizes the complex by increasing its electron cloud. However, it does reflect in the increase the kinetic of the oxidation process. A consistent result with the Randles Sevcik predictions.

Figure 5D shows the  $\beta$  values to both MTM and the MTM with Fe (III). In the absence of the metal, the peaks of the processes  $E_{ap0}$  and  $E_{ap1}$  presents  $\beta$  values of approximately 0.3. When the Fe (III) is introduced, the  $\beta$  value of  $E_{ap0}$  from MAA sharply increases to approximately 1.0. Thus, with the formation of the complexes, the  $E_{ap0}$  becomes reversible, whist  $E_{ap1}$  from MTM remains in approximately 0.3. To evaluate if the kinetics change of process  $E_{ap0}$  was provided by the complexation, or the presence of both processes  $E_{ap0}$  and  $E_{ap1}$ , a study with both 4AA and DMAA was conducted.

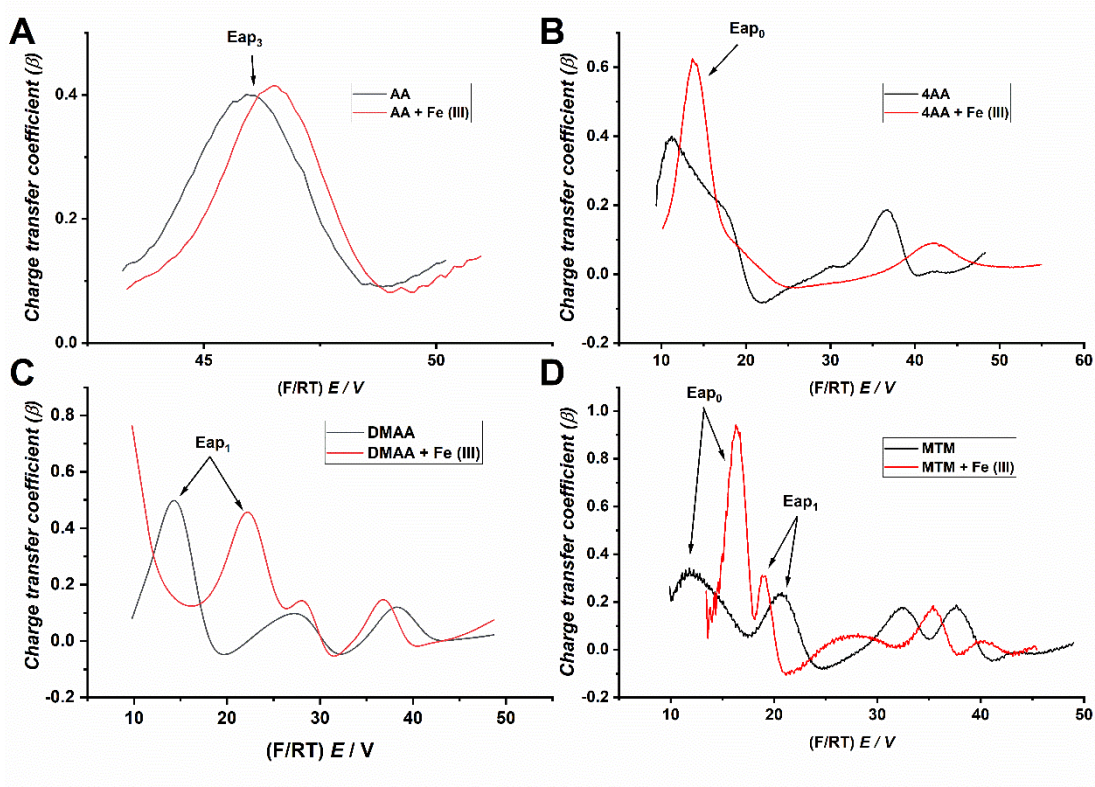


Figure 5: Plots of the charge transfer coefficient ( $\beta$ ) as a function of the applied potential.

Figures 6A and 6B show the CV of 1.0 mM 4AA and DMAA solutions in 0.1 M KCl, pH = 2.0, without and with 1.0 mM of Fe(III), respectively. Both figures show the presence of both oxidation processes  $E_{ap0}$  and  $E_{ap1}$  in an overlap of the processes in approximately 0.7 V and an increase of peak current values can be seen in figure 6B, the complexes solution. As the complexation induces a change in the heterogeneous processes, the Tafel analysis was conducted to obtain the charge transfer coefficients of the antipyridines and the respective complexes.

Initially, the CV of  $[Fe(4AA)_2]$  and  $[Fe(DMAA)_2]$  were obtained as a function of time. Figures 6C and 6D show CV of the complexes solution and the  $\beta$  values at different reaction times. Figure 8C shows a maximum of the peak current at t

= 0, and a decrease in the peak currents as a function of time, a result in agreement with the  $\beta$  values, observed in figure 6D, which present a maximum ( $\beta = 1$ ) at  $t = 0$ , and a decrease as function of time. Both results suggest the occurrence of a homogeneous catalysis involving the processes  $E_{ap0}$ ,  $E_{ap1}$ , and the Fe (III). Since the processes  $E_{ap0}$  and  $E_{ap1}$  together, already present a catalytic effect, the turnover frequency (TOF) to both processes were evaluated in both presence and absence of Fe (III).

Figures 6E and 6F show the catalytical Tafel plots, the turnover frequency (TOF) as a function of the applied potential and the Tafel lines, logarithm of TOF as a function of the applied potential. [40,41]

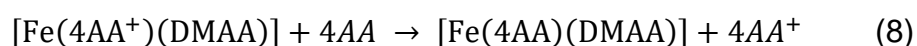
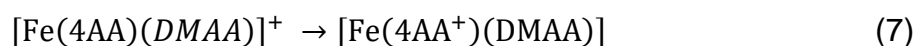
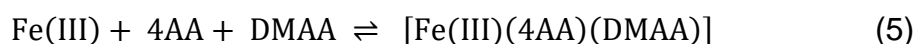
$$TOF = \frac{k^0 C^0}{1 + e^{[F/RT(E - E_f^0)]}} \quad (4)$$

where  $k^0$  is the standard rate constant of the process in  $\text{cm s}^{-1}$ ,  $C^0$  is the initial concentration of the catalyst in  $\text{mol L}^{-1}$ ,  $F$  is the Faraday constant in coulomb  $\text{mol}^{-1}$ ,  $R$  is the gas constant in  $\text{J K}^{-1} \text{mol}^{-1}$ ,  $E_f^0$  is the formal potential in Volts and  $E$  is the applied potential in Volts.

Figure 6E shows the catalytical Tafel plots of 1.0 mM 4AA and DMAA with 1.0 mM with and without Fe (III) solutions in 0.1 M KCl, pH = 2.0, at scan rates of 0.01, 0.1 and 1.0  $\text{V s}^{-1}$ . Comparatively, in each scan rate, the curves of the complexes formed presented a higher TOF than the ones of the without the metal in solution. A result that implies the Fe (III) actively participates of the catalytical process, increasing the rate of the reaction above the one observed for only the processes  $E_{ap0}$  and  $E_{ap1}$ . Figure 8F shows the Tafel lines to the experiment presented in figure 8E. The upper lines are the ones in which the complexes are formed, a result which corroborates the role in the reaction, most likely in the

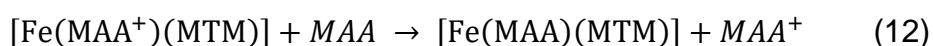
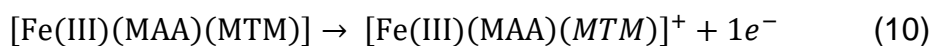
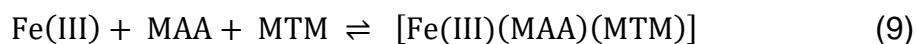
complex formation. The  $\pi$ -backbond effect increases the molecular orbitals of the complexes resulting in an increase of the overlap between the molecular and electrodic orbitals, thus enhancing the rate of the heterogeneous processes.

In overall, figure 6 indicates a homogeneous catalysis, which according the UV-Vis data could occur via a hybrid complex  $[\text{Fe}(4\text{AA})(\text{DMAA})]$ , or with 4AA/MAA acting as a reducer, generating an EC' mechanism. Moreover, the  $\beta$  values decrease with the time, showing that as the time passes, a chemical step occurs, as the Fe (III) is reduced to Fe (II), as observed in the Raman spectra, disforming the complexes and consequently, the  $\beta$  values observed after 30 min. decrease to a value of 0.4, coinciding with the values of the  $E_{ap1}$   $\beta$  value observed to the DMAA. The proposed steps of EC' catalytical process is presented in equations 5 to 8.



To evaluate the catalytical profile obtained with the combination of 4AA, DMAA and Fe (III), CV with the MTM complex were conducted to observe the catalysis involving the processes  $E_{ap0}$  of the MAA,  $E_{ap1}$  from MTM after their complexations. Figures 8G, 8H and 8I show CV of 1.0 mM MTM with 1.0 mM Fe (III) solutions in 0.1 M KCl, pH = 2.0. Figure 8G shows the CV of MTM complexes with Fe (III) in three different times, 0, 2.5 and 5 minutes. The CV at  $t = 0$  shows a oxidation profile of the complex  $[\text{Fe}(\text{MTM})_2]$ , the voltammograms at 2.5 and 5 minutes show the change in the profiles of the complex as a function of time,

presenting a sharp increase of the peak current of the overlapped processes  $E_{ap0}$  and  $E_{ap1}$ . Since the occurrence of the same catalytical process observed to MTM derivatives in the presence of Fe (III). To compare the processes of the derivatives and the MTM complexes, the Tafel analysis was conducted. [39] Figure 8H shows the Tafel plots of  $[Fe(MTM)_2]$  in each time. At  $t = 0$ , a value of the charge transfer coefficient of 1.08 can be observed, reinforcing the complexation results shifts the oxidation process to reversible, which agrees with the Randles Sevcik predictions. At 2.5 minutes, a charge transfer coefficient of 1.29, a super nernstian  $\beta$  value [42], corroborating the existence of catalytical process. Similarly to the results observed in figure 8D, at  $t = 5$  minutes, a decrease of the  $\beta$  value occurs with the progression of time, the catalysis is homogeneous and persists until the depletion of the reducer, MAA. The MTM EC' mechanism can be analogously illustrated by equations 9 to 12.



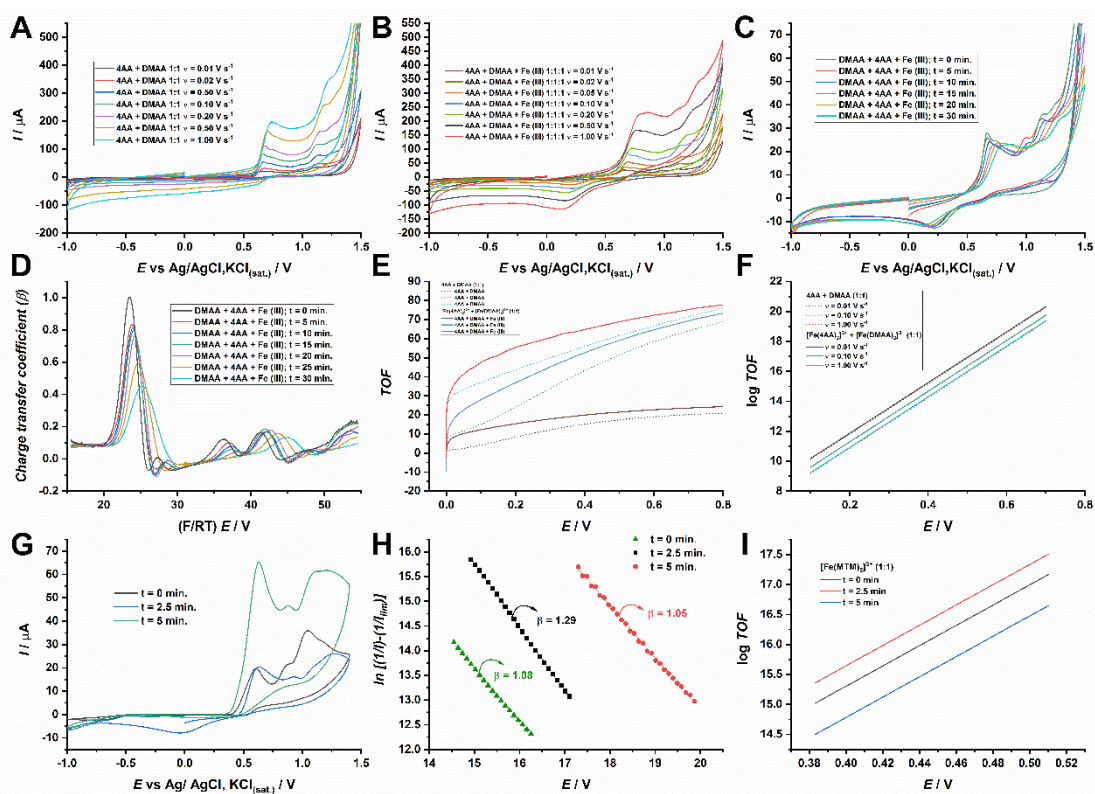


Figure 6: A) CV obtained in (1:1) 1.0 mM 4AA with DMAA solutions in 0.1 KCl, pH = 2.0 at different scan rates, B) CV obtained in (1:1:1) 1.0 mM 4AA, DMAA, and Fe (III) Ag/AgCl, KCl<sub>(sat.)</sub> / V in 0.1 KCl, pH = 2.0 at different scan rates C) CV obtained in (1:1) 1.0 mM 4AA with DMAA solutions in 0.1 KCl, pH = 2.0 at different times D) Charge transfer coefficients of the CVs presented in C, E) Turnover frequency as a function of the driving force for the systems presented in A and in B, F) Catalytic Tafel plots of the systems presented in A and B G) CV obtained in (1:1) 1.0 mM MTM with Fe (III) solutions in 0.1 KCl, pH = 2.0 at different times H) Tafel Plots from the voltammograms presented in F I) Catalytic Tafel plots of the system presented in G.

## Conclusions

The iron III complexes with the antipyridines, as the phenazones can chelate the metal in a bidentated (AA) or tridentated (4AA, DMAA and MTM) way. The



complexes involve one metal to two ligands and occur via the nitrogen of the enamine and nitrogens of the pyrazalone ring. The complexes formations change the nature of the oxidation processes occurring in the chelation points,  $E_{ap0}$  and  $E_{ap3}$ , from irreversible to reversible, as can be seen in the Randles-Sevcik equations due to a  $\pi$ -backbonding effect from the metal to the ligands. When the complex of an antipyrine with a tertiary enamine, such as DMAA or MTM, is in the presence of a reducer, such as 4AA or MAA, they form a hybrid complexes  $[Fe(III)(4AA)(DMAA)]$  and  $[Fe(III)(MAA)(MTM)]$ , and their oxidation process  $E_{ap1}$  is catalyzed by the reducer behaviour of 4AA and/ or MAA, forming a EC' mechanism. Therefore, presenting a sharp increase in the peak current values, until the concentration of the reducer diminishes.

### **Acknowledgments**

This work is dedicated to the memories of José Lopes do Sacramento, autodidactic, who dedicated his live to knowledge, charity, and his family and to the memories of Professor Jaim Lichtig, Professor from Institute of Chemistry from the University of São Paulo. The authors would like to acknowledge the Rectory of the University of São Paulo, CNPq projects n° 308787/2010-2 and 140833/2016-1, CAPES project 88881.187396/2018-01 and Fapesp for the grants and funding to this project.

### **References**

- [1] M. Lutz, Metamizole (Dipyrone) and the Liver: A Review of the Literature, *J. Clin. Pharmacol.* 59 (2019) 1433–1442. <https://doi.org/10.1002/jcph.1512>.
- [2] R.P. Bacil, R.M. Buoro, R.P. Da-Silva, D.B. Medinas, A.W. Lima, S.H. Serrano, Mechanism of Electro-Oxidation of Metamizole Using Cyclic

Voltammetry at a Glassy Carbon Electrode, *ECS Trans.* 43 (2012) 251–258.  
<https://doi.org/10.1149/1.4704966>.

[3] R. Nassini, C. Fusi, S. Materazzi, E. Coppi, T. Tuccinardi, I.M. Marone, F. De Logu, D. Preti, R. Tonello, A. Chiarugi, R. Patacchini, P. Geppetti, S. Benemei, The TRPA1 channel mediates the analgesic action of dipyron and pyrazolone derivatives, *Br. J. Pharmacol.* 172 (2015) 3397–3411.  
<https://doi.org/10.1111/bph.13129>.

[4] B. Hinz, O. Cheremina, J. Bachmakov, B. Renner, O. Zolk, M.F. Fromm, K. Brune, Dipyron elicits substantial inhibition of peripheral cyclooxygenases in humans: new insights into the pharmacology of an old analgesic, *FASEB J.* 21 (2007) 2343–2351. <https://doi.org/10.1096/fj.06-8061com>.

[5] K. Brune, The early history of non-opioid analgesics, *Acute Pain.* 1 (1997) 33–40.

[6] R.P. Bacil, R.M. Buoro, O.S. Campos, M.A. Ramos, C.G. Sanz, S.H.P. Serrano, Electrochemical behaviour of dipyron (metamizole) and others pyrazolones, *Electrochim. Acta.* 273 (2018) 358–366.  
<https://doi.org/10.1016/j.electacta.2018.04.082>.

[7] R. Abbate, A.M. Gori, S. Pinto, M. Attanasio, R. Paniccia, M. Coppo, S. Castellani, B. Giusti, M. Boddi, G.G. Neri Serner, Cyclooxygenase and lipoxygenase metabolite synthesis by polymorphonuclear neutrophils: in vitro effect of dipyron., *Prostaglandins. Leukot. Essent. Fatty Acids.* 41 (1990) 89–93. [https://doi.org/10.1016/0952-3278\(90\)90059-T](https://doi.org/10.1016/0952-3278(90)90059-T).

[8] J.C. Wessel, M. Matyja, M. Neugebauer, H. Kiefer, T. Daldrup, F.A. Tarbah, H. Weber, Characterization of oxalic acid derivatives as new metabolites

of metamizol (dipyrone) in incubated hen's egg and human., *Eur. J. Pharm. Sci.* 28 (2006) 15–25. <https://doi.org/10.1016/j.ejps.2005.11.010>.

[9] L.A. Pérez-Estrada, S. Malato, A. Agüera, A.R. Fernández-Alba, Degradation of dipyrone and its main intermediates by solar AOPs, *Catal. Today*. 129 (2007) 207–214. <https://doi.org/10.1016/j.cattod.2007.08.008>.

[10] E. Di Leo, E. Nettis, G.F. Calogiuri, A. Ferrannini, A. Vacca, Immediate rhinoconjunctivitis induced by metamiloze: an allergic reaction?, *Allergy*. 65 (2010) 1070–1071. <https://doi.org/10.1111/j.1398-9995.2009.02299.x>.

[11] L. Loginova, O. Konovalova, Test films for test-determinations on the base of reagents, immobilized in gelatinous gel, *Talanta*. 77 (2008) 915–923. <https://doi.org/10.1016/j.talanta.2008.07.051>.

[12] The International Agranulocytosis and Aplastic Anemia Study, Risk of agranulocytosis and aplastic anemia., *Jama*. 256 (1986) 1749–1757.

[13] S. Maj, P. Centkowski, A prospective study of the incidence of agranulocytosis and aplastic anemia associated with the oral use of metamizole sodium in Poland., *Med. Sci. Monit.* 10 (2004) 93–96. <http://www.ncbi.nlm.nih.gov/pubmed/15328493>.

[14] G.W. Basak, J. Drozd-Sokolowska, W. Wiktor-Jedrzejczak, J. Drozd-Sokolowska, W. Wiktor-Jedrzejczak, Update on the incidence of metamizole sodium-induced blood dyscrasias in Poland., *J. Int. Med. Res.* 38 (2010) 1374–1380. <http://www.ncbi.nlm.nih.gov/pubmed/20926010>.

[15] I.M. Benseñor, To use or not to use dipyrone ? Or maybe , Central Station versus ER ? That is the question ..., *São Paulo Med. J.* 119 (2001) 190–191.

[16] K. Iwahara, C. Tanabe, M. Maekawa, K. Müssig, A. Pfäfflin, H.-U. Häring, E.D. Schleicher, Dipyrone (metamizole) metabolites interfere with HPLC analysis

of plasma catecholamines but not with the determination of urinary catecholamines., Clin. Chem. 52 (2006) 1828–1829. <https://doi.org/10.1373/clinchem.2006.072272>.

[17] T.R.L.C. Paixão, R.C. Matos, M. Bertotti, Diffusion layer titration of dipyrone in pharmaceuticals at a dual-band electrochemical cell, Talanta. 61 (2003) 725–732. [https://doi.org/10.1016/S0039-9140\(03\)00334-5](https://doi.org/10.1016/S0039-9140(03)00334-5).

[18] A.C. Boni, A. Wong, R.A.F. Dutra, M.D.P.T. Sotomayor, Cobalt phthalocyanine as a biomimetic catalyst in the amperometric quantification of dipyrone using FIA, Talanta. 85 (2011) 2067–2073. <https://doi.org/10.1016/j.talanta.2011.07.038>.

[19] L.H. Marcolino-Júnior, M.F. Bergamini, M.F.S.S. Teixeira, E.T.G. Cavalheiro, O. Fatibello-Filho, É.T.G. Cavalheiro, O. Fatibello-Filho, Flow injection amperometric determination of dipyrone in pharmaceutical formulations using a carbon paste electrode., Farmaco. 58 (2003) 999–1004. [https://doi.org/10.1016/S0014-827X\(03\)00182-4](https://doi.org/10.1016/S0014-827X(03)00182-4).

[20] W.T. Suarez, O.D. Pessoa-Neto, F.C. Vicentini, B.C. Janegitz, R.C. Faria, O. Fatibello-Filho, Flow Injection Spectrophotometric Determination of Dipyrone in Pharmaceutical Formulations Using Fe(III) as Reagent, Anal. Lett. 44 (2011) 340–348. <https://doi.org/10.1080/00032719.2010.500777>.

[21] L. Basález, I.M. Peric, P. a Jara, C. a Soto, D.R. Contreras, C. Aguirre, P. Vanýsek, Electrochemical and Electrophoretic Study of Sodium Metamizole, J. Chil. Chem. Soc. 53 (2008) 3–6.

[22] B. Muralidharan, G. Gopu, C. Vedhi, P. Manisankar, Determination of analgesics in pharmaceutical formulations and urine samples using nano

polypyrrole modified glassy carbon electrode, *J. Appl. Electrochem.* 39 (2009) 1177–1184. <https://doi.org/10.1007/s10800-009-9782-9>.

[23] L.J. Li, L.J. Cheng, Z. Cai, S.M. Lan, X.F. Guo, Y.Q. Li, Determination of Metamizole Sodium by Cyclic Voltammetry Under Microwave Activation, *Chem. Res. Chinese Univ.* 26 (2010) 537–540.

[24] B. Muralidharan, G. Gopu, C. Vedhi, P. Manisankar, Voltammetric determination of analgesics using a montmorillonite modified electrode, *Appl. Clay Sci.* 42 (2008) 206–213. <https://doi.org/10.1016/j.clay.2007.11.005>.

[25] I. Baranowska, P. Markowski, A. Gerle, J. Baranowski, Determination of selected drugs in human urine by differential pulse voltammetry technique, *Bioelectrochemistry*. 73 (2008) 5–10. <https://doi.org/10.1016/j.bioelechem.2008.04.022>.

[26] M.F.S. Teixeira, L.H. Marcolino-júnior, O. Fatibello-filho, E.R. Dockal, Voltammetric Determination of Dipyrone Using a N,N'-ethylenebis(salicylideneaminato)oxovanadium(IV) Modified Carbon-paste Electrode, 15 (2004) 803–808.

[27] R. Pauliukaite, M.E. Ghica, O. Fatibello-Filho, C.M.A. Brett, Graphite-epoxy electrodes modified with functionalised carbon nanotubes and chitosan for the rapid electrochemical determination of dipyrone., *Comb. Chem. High Throughput Screen.* 13 (2010) 590–598. <http://www.ncbi.nlm.nih.gov/pubmed/20402639>.

[28] E.N. Naprienko, N.A. Skorik, N.N. Shaforostova, Investigation of iron(III) reactions with antipyrine and analgin, *Russ. J. Inorg. Chememistry.* 45 (2000) 1344–1349.

- [29] C.C.A. Loures, M.A.K. Alcântara, H.J.I. Filho, A.C.S.C. Teixeira, F.T. Silva, T.C.B. Paiva, G.R.L. Samanamud, *Advanced Oxidative Degradation Processes: Fundamentals and Applications*, *Int. Rev. Chem. Eng.* 5 (2013) 102. <https://doi.org/10.15866/ireche.v5i2.6909>.
- [30] D. Pavia, G. Lampman, G. Kriz, J. Vyvyan, *Introduction to spectroscopy*, 4th editio, BOOKS/ COLE CENGAGE Learning, Washington D.C., 2008. <http://books.google.com/books?hl=en&lr=&id=uX0GAAAAQBAJ&oi=fnd&pg=PR5&dq=Introduction+to+Spectroscopy&ots=loT7cSdq1R&sig=vF04fja6tJBBTB MGNnNI66jwiRM>.
- [31] P.W. Jensen, L.B. Jørgensen, Resonance raman spectra of some iron(II) imine complexes, *J. Mol. Struct.* 79 (1982) 87–92. [https://doi.org/10.1016/0022-2860\(82\)85035-7](https://doi.org/10.1016/0022-2860(82)85035-7).
- [32] Y. Ozaki, K. Iriyama, H. Ogoshi, T. Ochiai, T. Kitagawa, Resonance Raman characterization of iron-chlorin complexes in various spin, oxidation, and ligation states. 1. Comparative study with corresponding iron-porphyrin complexes, *J. Phys. Chem.* 90 (1986) 6105–6112. <https://doi.org/10.1021/j100281a011>.
- [33] K. Nakamoto, *Infrared and Raman Spectra of Inorganic and Coordination Compounds, Part A: Theory and Applications in Inorganic Chemistry*, 6th Editio, Wiley, 432AD.
- [34] R.W. Balk, D.J. Stufkens, A. Oskam, Influence of metal to di-imine  $\pi$ -backbonding on the resonance-Raman spectra of  $[M(CO)_4 L]$ ,  $fac-[Re(CO)_3 LCl]$ , and  $[Ru(CO)_3 L]$  complexes (M = Mo or W; L = di-imine), *J. Chem. Soc., Dalt. Trans.* 6 (1982) 275–282. <https://doi.org/10.1039/DT9820000275>.

- [35] J. Swaminathan, M. Ramalingam, V. Sethuraman, N. Sundaraganesan, S. Sebastian, Vibrational spectroscopic studies and DFT calculations of 4-aminoantipyrine, *Spectrochim. Acta Part A Mol. Biomol. Spectrosc.* 73 (2009) 593–600. <https://doi.org/10.1016/j.saa.2009.03.009>.
- [36] R.P. Bacil, L. Chen, S.H.P. Serrano, R.G. Compton, Dopamine oxidation at gold electrodes: Mechanism and kinetics near neutral pH, *Phys. Chem. Chem. Phys.* 22 (2020) 607–614. <https://doi.org/10.1039/c9cp05527d>.
- [37] R.P. Bacil, P.H.M. Garcia, W.R. de Araujo, S.H.P. Serrano, Mechanism and kinetics of olanzapine and quetiapine oxidations at glassy carbon electrode, *Electrochim. Acta.* 368 (2021) 137683. <https://doi.org/10.1016/j.electacta.2020.137683>.
- [38] R.P. Bacil, E.A. de O. Marcondes Filho, K. de A. Dias, M.C. Portes, W.R. de Araujo, D. Oliveira-Silva, A.A. dos Santos, S.H.P. Serrano, The chemical interaction between the neurotransmitter dopamine and the antipsychotic drugs olanzapine and quetiapine, *J. Electroanal. Chem.* 881 (2021) 114946. <https://doi.org/10.1016/j.jelechem.2020.114946>.
- [39] D. Li, C. Lin, C. Batchelor-McAuley, L. Chen, R.G. Compton, Tafel analysis in practice, *J. Electroanal. Chem.* 826 (2018) 117–124. <https://doi.org/10.1016/j.jelechem.2018.08.018>.
- [40] C. Costentin, S. Drouet, M. Robert, J.-M. Savéant, Turnover Numbers, Turnover Frequencies, and Overpotential in Molecular Catalysis of Electrochemical Reactions. Cyclic Voltammetry and Preparative-Scale Electrolysis, *J. Am. Chem. Soc.* 134 (2012) 11235–11242. <https://doi.org/10.1021/ja303560c>.

[41] J.-M. Savéant, C. Costentin, Elements of Molecular and Biomolecular Electrochemistry: An Electrochemical Approach to Electron Transfer Chemistry, 2nd editio, Wiley, 2019. <https://www.wiley.com/en-br/Elements+of+Molecular+and+Biomolecular+Electrochemistry%3A+An+Electrochemical+Approach+to+Electron+Transfer+Chemistry%2C+2nd+Edition-p-9781119292333>.

[42] H. Chen, R.G. Compton, Sub- and super-Nernstian Tafel slopes can result from reversible electron transfer coupled to either preceding or following chemical reaction, J. Electroanal. Chem. 880 (2021) 114942. <https://doi.org/10.1016/j.jelechem.2020.114942>.

### **Appendix 3 - Electrochemical oxidation of dipyrone and pyrazolone derivatives complexes with Fe (III), and its EC' catalytic mechanism.**

#### **Complexes characterization**

##### **Visual complexations of MTM-Fe (III) at different pH.**

To verify the complexation and observe which media provides the best stability and intensity to the complex, solutions of 1.0 mM MTM and Fe (III) were mixed (1:1) in aqueous media with different pH. Figure S1 shows that at room temperature, the chemical reaction between Iron III and MTM reaction generates a blue colored complex, which keeps the coloration for approximately 30 seconds (T = 1), that is followed by a light-yellow coloration, of about a minute (T = 2), and finally it turns to an uncolored solution (T = 3). Figure S1 shows not only a pH dependency of the intensity, but also dependency of its stability. No complexation was observed in basic media, which is expected due to the Fe (III) hydrolysis, forming its hydroxide derivative. Moreover, at T = 2, the complex in neutral media



is already discolored, as the one in acidic media still shows the blue coloration. Therefore, the formed complex persists for longer periods of time whilst it presents more intense coloration in acidic media. Thus, suggesting that its instability could be a result of the hydrolysis of the MTM and/or due to a reduction of the Fe(III), since the MTM derivatives present reducer properties. [6]

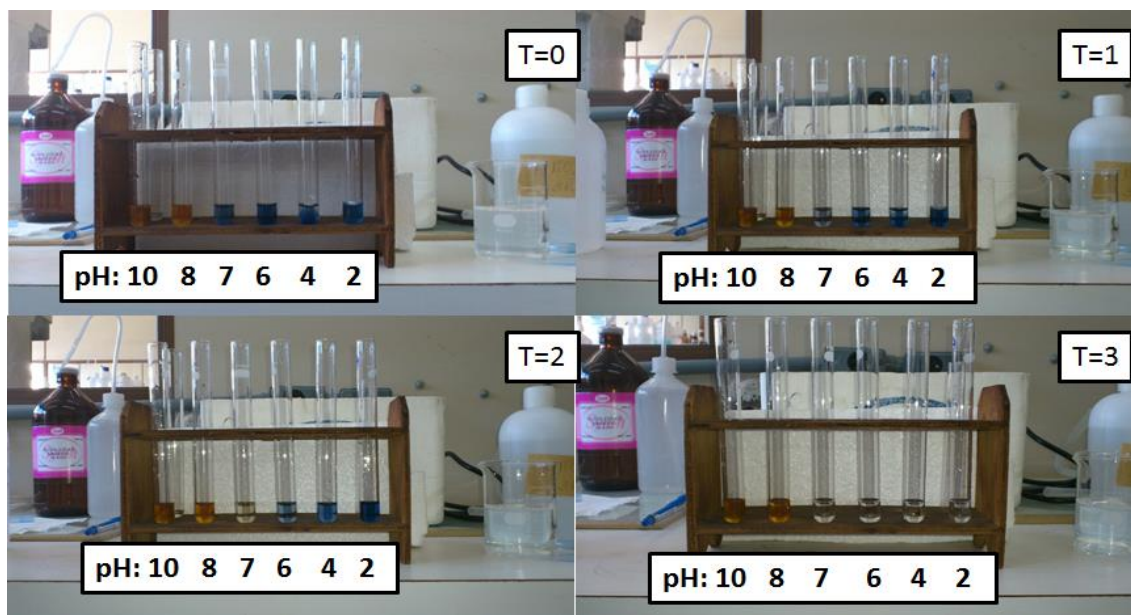


Figure S1: Complexation of MTM with Iron (III) 1.0 mM (1:1) at different pH values.

### Visual complexations of the antipyrines with Fe (III) in acidic media.

In the section above, the optimized conditions to the complexation were observed. Thus, the acidic conditions were used to observe the complex formation with the other antipyrines.

Figure S2 shows the respective complexations of the MTM derivatives with the metal. From left to right, the figure shows that AA complexes Fe (III), generating a strong charge transfer band that reflects a red color that persists for several days. The second one shows that 4AA also complex the metal, generating a band which results in a magenta coloration that is also persistent,

although not as much as the previous one with AA. The third one shows that as the previous derivatives, DMAA also complexes with Fe (III), but presenting a violet color, which is most likely due to the merge between the blue band generated by the tertiary enamine, as observed for the MTM, and the red one generated by the nitrogen of the antipyrine ring, as observed in the AA.

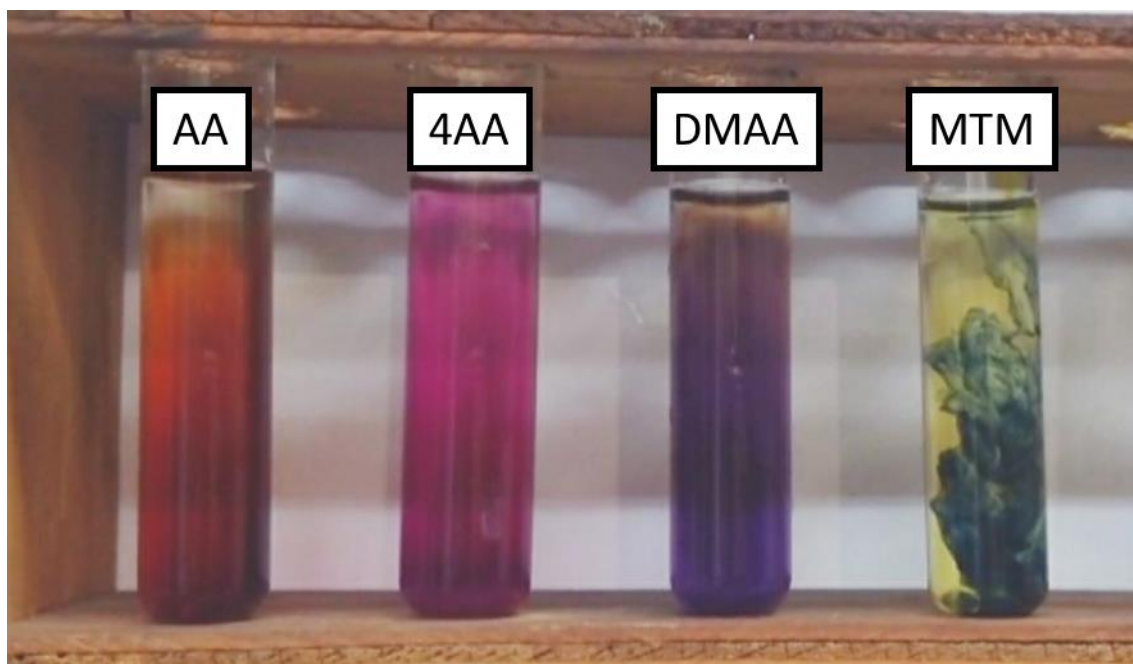


Figure S2: Complexation of A) AA; B) 4AA; C) DMAA; D) MTM with Iron (III) 1.0 mM (1:1) at acidic media (pH 2,0).

### **Spectroscopic structural analysis of the phenazones and their respective complexes.**

The study made in the present paper was better understood with the help of spectroscopic analysis. All of the pharmaceuticals used already have signature bands in the UV region, and more notably, all iron species have strong absorption bands within the visible light spectrum. Hence, we chose to

investigate the formation of chemical bonds and new species through UV-vis Spectroscopy.

The addition of Fe (III) (1 mL – 1 mM solutions) in the antipyrines, the formation of the complex was observed, as shown in the previous section. As can be seen by the appearance of charge transfer (CT) bands for all four Schiff bases, as well as, the d-d bands, which are Laporte forbidden. However, due to a degree of relaxation given the strong field ligands they were observed.

A rise of new bands as the redox reactions occurs and the displacement of other key bands, as the molecules are polarized, was expected. The results of this analysis can be found in Table S1. In this section the pharmaceuticals will be referred as Ligands, under the optic of coordination complexes. All observed bands in the UV-Vis part of the spectra for the free ligands and iron complexes are prescribed in Table S1.

The new absorption profile consists of several different bands that includes CT band at 285 and a couple d-d bands such as 340 and 520 related to Fe (III) complex. It is important to highlight that, usually, in UV Vis spectra the formation of complexes of different ligand/ metal ratios with the variation of the ligand concentration can be observed, due to an equilibrium in the coordination sphere. However, in all the presented UV Vis spectra, and most notably in Figure 3, the characteristic bands of only two species were noticed, the unbound Schiff base, and the formed complex. Thus, indicating that the complexes formation occurs with a fast kinetics or that its formation occurs in all the metal positions at once.

Table S1: Detailed attribution of the absorption Bands of the studied Schiff Bases and their respective iron (III) complexes.

	Wavelength	E (cm <sup>-1</sup> mol <sup>-1</sup> L)	Attribution
AA	200 nm	3310	$\pi \rightarrow \pi^*$ Aromatic
	220 nm	1420	$n \rightarrow \pi^*$ Carbonyl
	240 nm	1420	$\pi \rightarrow \pi^*$ $\alpha,\beta$ Unsaturated
	265 nm	1340	$\pi \rightarrow \pi^*$ Enamine
AA + Fe <sup>3+</sup>	305 nm	1493,3	CT
	365 nm	846,2	d-d
	420 nm	255,1	d-d
	470 nm	97,1	d-d
4AA	200 nm	5350	$\pi \rightarrow \pi^*$ Aromatic
	227 nm	2980	$n \rightarrow \pi^*$ Carbonyl
	240 nm	3660	$\pi \rightarrow \pi^*$ $\alpha,\beta$ Unsaturated
	255 nm	3630	$\pi \rightarrow \pi^*$ Enamine
	285 nm	2830	Nonbinding N electron
4AA + Fe <sup>3+</sup>	335 nm	933,3	CT

	360-375 nm	653,3	d-d
	520 nm	525,7	d-d
DMAA	200 nm	5990	$\pi \rightarrow \pi^*$ Aromatic
	225 nm	1100	$n \rightarrow \pi^*$ Carbonyl
	229-240 nm	260,7	$\pi \rightarrow \pi^*$ $\alpha,\beta$ Unsaturated
	254-265 nm	2040,9	$\pi \rightarrow \pi^*$ Enamine
DMAA + Fe <sup>3+</sup>	300-320 nm	1431,1	CT
	370 nm	852,4	d-d
	409 nm	3733,3	CT
	465 nm	151,8	d-d
	560 nm	336	d-d
MTM	200 nm	3170	$\pi \rightarrow \pi^*$ Aromatic
	230 nm	1480	$n \rightarrow \pi^*$ Carbonyl
	240 nm	1430	$\pi \rightarrow \pi^*$ $\alpha,\beta$ Unsaturated
	270 nm	1220	$\pi \rightarrow \pi^*$ Enamine
MTM + Fe <sup>3+</sup>	360 nm	852,4444	CT
	415 nm	354,6667	d-d
	480 nm	130,6667	d-d

4AA + DMAA	200	3340	$\pi \rightarrow \pi^*$ Aromatic
	230	1475	$n \rightarrow \pi^*$ Carbonyl
	238	1390	$\pi \rightarrow \pi^*$ $\alpha,\beta$ Unsaturated
	260	1340	$\pi \rightarrow \pi^*$ Enamine
	270	1290	-
	307	2299,11	CT
	360	1480,89	CT
	412	631,556	d-d
	477	227,111	d-d

Firstly, we can observe three main absorption bands in AA, all in the UV region, 200 nm, 220 nm, 240 nm and 265 nm, due to  $\pi \rightarrow \pi^*$  Aromatic,  $n \rightarrow \pi^*$  Carbonyl,  $\pi \rightarrow \pi^*$   $\alpha,\beta$  Unsaturated and  $\pi \rightarrow \pi^*$  Enamine, respectively. The Fe (III) solution was added in small volumes (20 mL) to observe the new spectra as the species formed. This experiment was designed so the Fe (III) was added in molar fractions of the AA in solution, so we could study the formation of complexes with one, two or three ligands. These results can be seen in Figure 1, in main text.

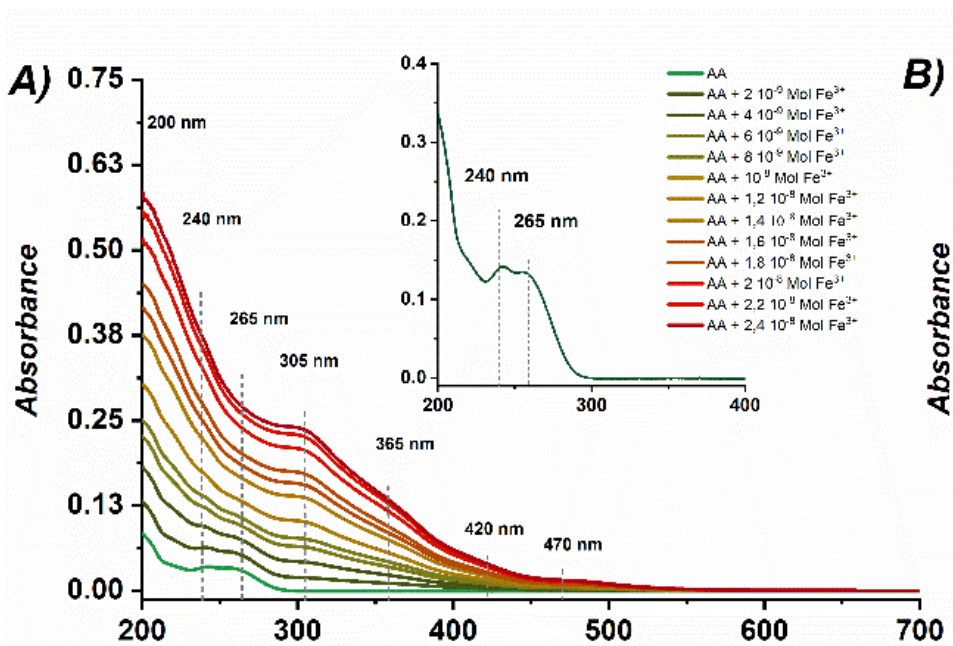


Figure S3: UV-Vis spectra of  $1.0 \mu \text{ mol L}^{-1}$  of AA in  $0.1 \text{ mol L}^{-1}$  KCl solutions,  $\text{pH} = 2.0$  and the subsequent additions of  $\text{Fe (III)}_{(\text{aq})}$

Oposely to expected, the UV-vis spectra of AA with the addition of Fe (III), did not show the presence of all three complexes, it was found that in with Fe(III) in excess, that there are only to species – The complex formed and  $\text{Fe(OH)}_2(\text{H}_2\text{O})_4$ . A similar teste was conducted, inverting the order o addition in other to see if this phenomenon was only because of the formation kinetic of the other two species,  $\text{Fe (AA)}_2\text{H}_2\text{O}$  and  $\text{Fe(AA)(H}_2\text{O)}_2$ . In Figure S3, similarly to what was seen before, only two stable species can be seen in solution: one complex and  $\text{Fe(OH)}_2(\text{H}_2\text{O})_4$ .

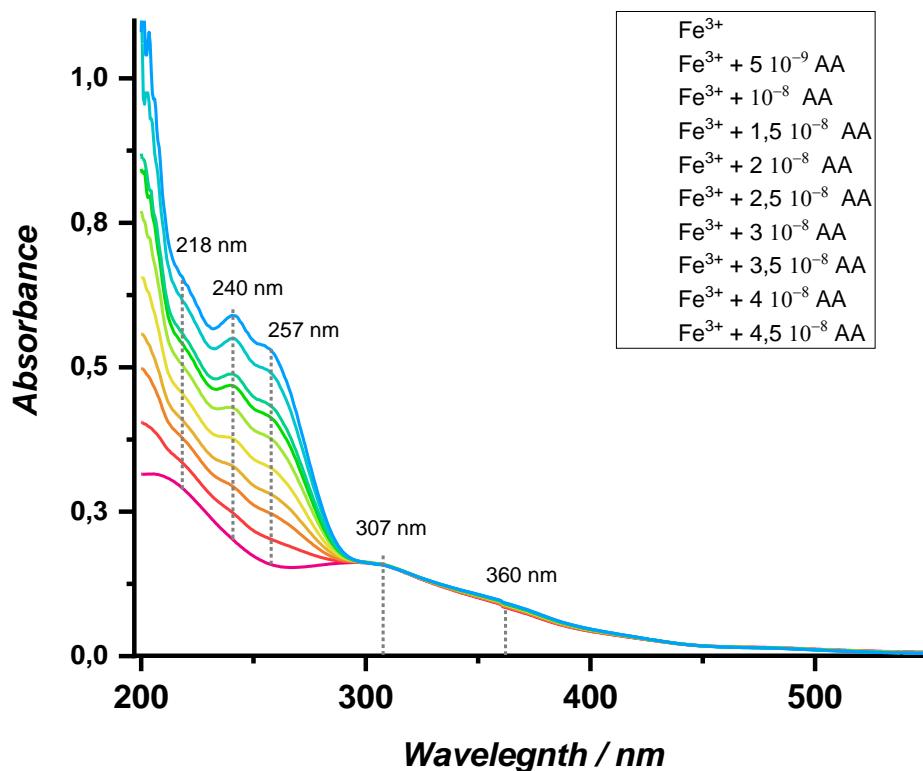


Figure S4: UV-Vis spectra of  $1.0 \mu\text{mol L}^{-1}$  of  $\text{Fe (III)}_{(\text{aq})}$  in  $0.1 \text{ mol L}^{-1}$  KCl solutions,  $\text{pH} = 2.0$  and the subsequent additions of AA

It was noticed a correlation between the increase in the 200 nm band intensity and the opening of the pyrazolone ring. Thus, confirming that to all phenazones, after Eap 3 oxidation process, the five membered ring tends to open. This occurs in the formation of iron complexes with all the ligands (AA, 4AA, DMAA, MTM) and was confirmed by the addition of oxidant, sodium persulfate, in the solutions only containing each Schiff base (Figure S5). With the addition of oxidant, the UV Vis absorption profile of AA remains the same, except for this significant increase in the UV region. It is also possible to observe that over time, this band decreases again to a certain point. Finally, as evidenced by the bands starting at 300 nm in figure S6 and figure S7, an excess of Fe (III) is



necessary to the complex formation with AA. Therefore, it occurs in three steps. The first one is the oxidation process Eap 3 by the Fe (III), which is then followed by the opening of the pyrazolone ring, and thirdly, the formation of the complex.

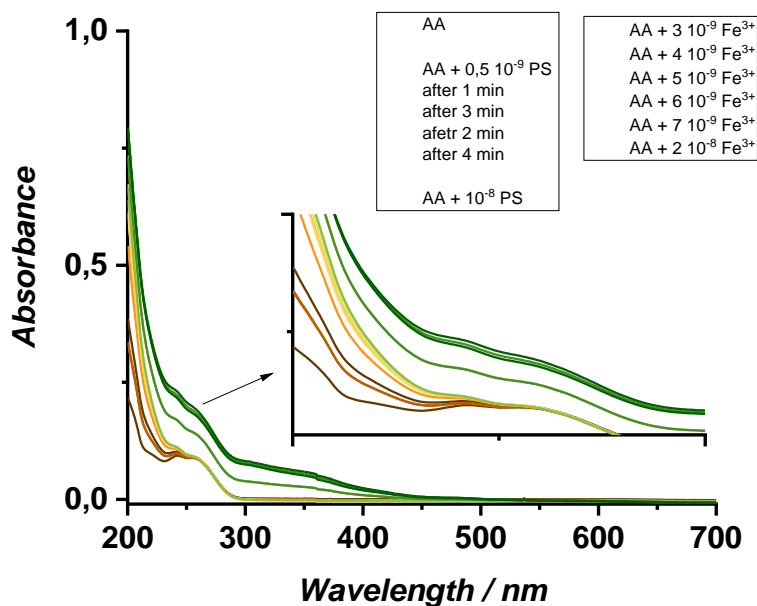


Figure S5: UV-Vis spectra of  $0.5 \cdot 10^{-9} \text{ mol L}^{-1}$  of AA in  $0.1 \text{ mol L}^{-1}$  KCl solutions,  $\text{pH} = 2.0$  at different times, and the subsequent additions of  $\text{Fe (III)}_{(\text{aq})}$

Contrasting, to both AA and DMAA spectra, it can be observed that the Fe (III) addition on a  $0,1 \text{ mmol L}^{-1}$  4AA solution generates two different profiles. Firstly, a decrease of the intensity in the 240 e 255 nm bands of the ligands, which can be more clearly observed in Figure S5. This occurs due to the oxidation of the Schiff base in which to 4AA generates a more stable product, as the proton coupled electrons transfer (PCET) allows the product to be a radical instead of a cation radical. Therefore, allowing the two main steps to be seen, the oxidation processes Eap<sub>0</sub> and Eap<sub>2</sub> .

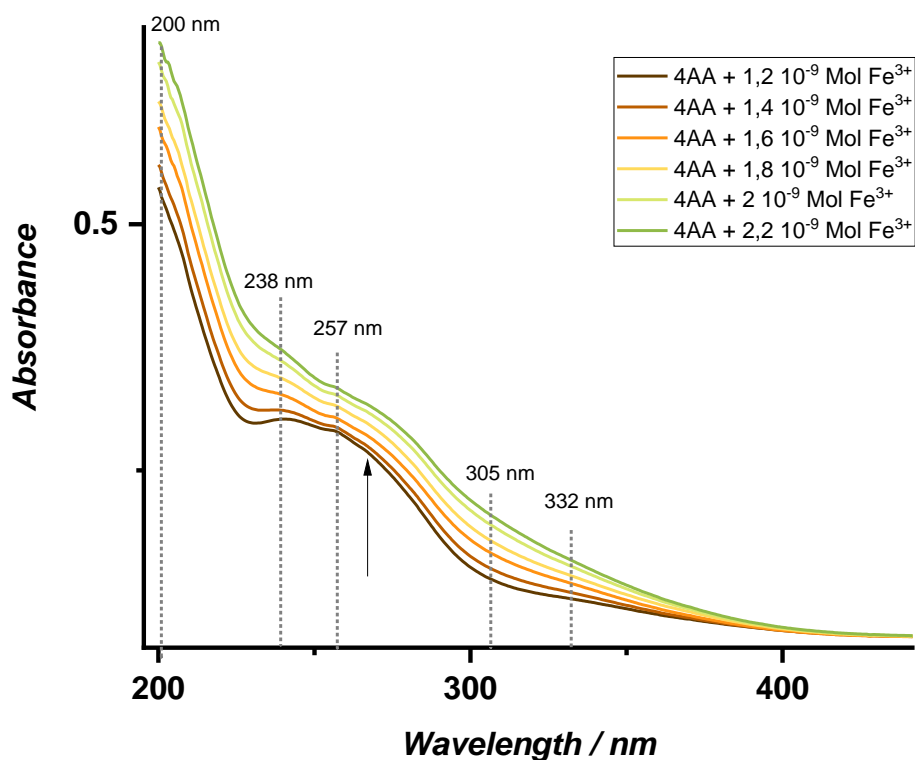


Figure S6: UV-Vis spectra of  $1.0 \mu\text{ mol L}^{-1}$  of 4AA in  $0.1 \text{ mol L}^{-1}$  KCl solutions,  $\text{pH} = 2.0$  and the subsequent additions of  $\text{Fe (III)}_{(\text{aq})}$

Figure S7 is a close up of absorption bands that occur in the visible spectrum. This analysis was made by using concentrated solutions of AA and  $\text{Fe(III)}$ ,  $5 \text{ mM}$  and  $1 \text{ mM}$ , respectively. This close up was relevant in order to understand the d-d transitions, and the symmetry of the complex – a key element in uncovering its structure and the mechanism studied. A similar procedure was made with 4AA as can be seen in Figure S8.

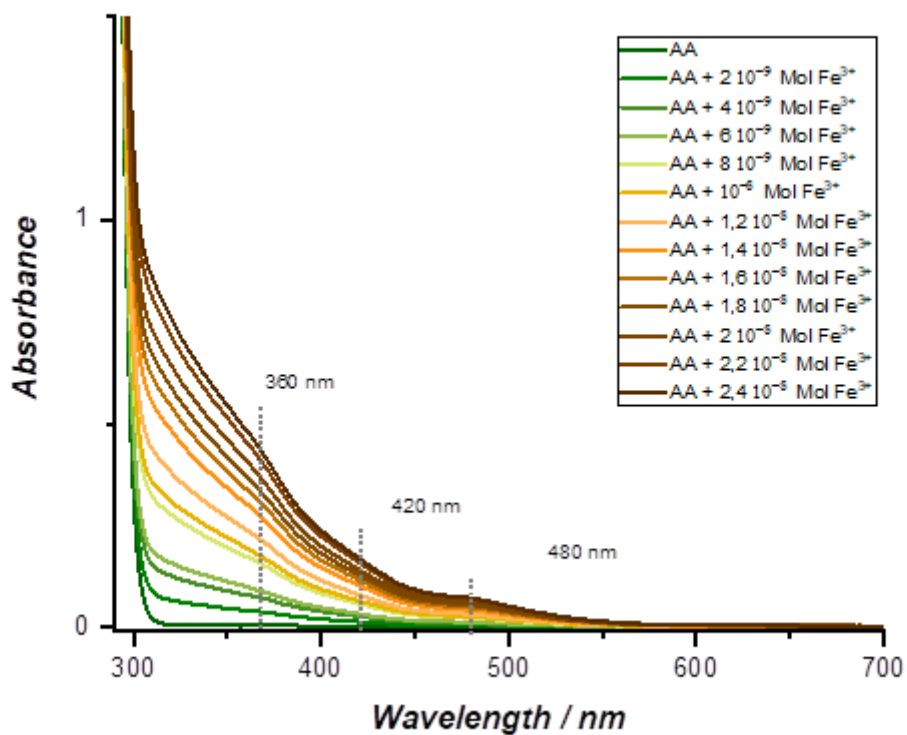


Figure S7: UV-Vis spectra of 1.0 μmol L<sup>-1</sup> of AA in 0.1 mol L<sup>-1</sup> KCl solutions, pH = 2.0 and the subsequent additions of Fe (III)<sub>(aq)</sub>

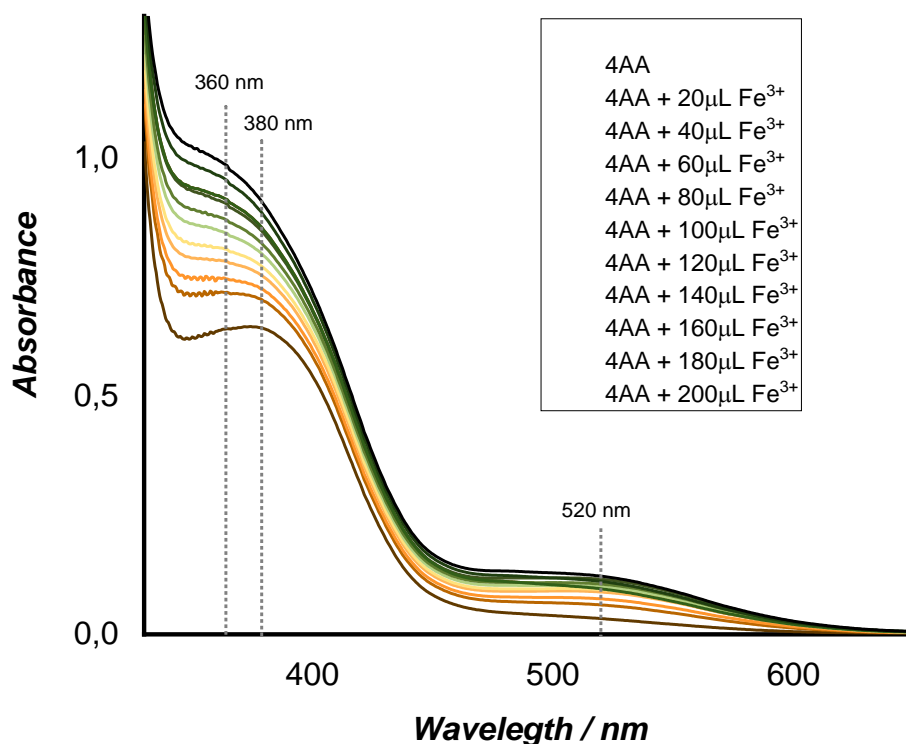


Figure S8: UV-Vis spectra of  $1.0 \mu\text{ mol L}^{-1}$  of 4AA in  $0.1 \text{ mol L}^{-1}$  KCl solutions,  $\text{pH} = 2.0$  and the subsequent additions of  $\text{Fe (III)}_{(\text{aq})}$

In Table S1, found values of absorption constants ( $\epsilon$ ) for all electronic transitions in all Ligands and their respective complexes can be found alongside their attributions. For complexes without an inversion center, the d-d bands, which are prohibited by Laporte, present a higher molar absorptivity,  $\epsilon$ , with values, between 100 and 1000. For complexes with a high degree of symmetry, these values tend to decrease to between 1 and 100 [30]. These d-d and CT bands can be better identified in figures S8 and S9. Hereby, the presence of three bands in AA, with a characteristic  $\epsilon$  value, allow to conclude that two different complexes

have been formed, the first one being more symmetric than the second, and indicating that the complexes stoichiometry is of 1:2 metal/ ligand.

As evidenced by the presence of two isomers, scheme 2. Given these results, it is possible to infer that, after the oxidation, the Schiff bases such as 4AA, DMAA and MTM are all tridentate ligands, opposing to AA, which is bidentate. These complexes are stabilized by the  $\pi$ -back bonding of Schiff base to unoccupied d orbitals of the metal ( $d_{xy}^2 - x^2 - y^2$  and  $d_{z^2}$ ), that compensates the loss of resonance. Furthermore, the  $\pi$ -back bonding is more expressive in the DMAA complex, due to the donor behavior of the methyl substituents.

### Cyclic voltammetry and electrochemical behaviour of the complexes

Table S2: Peak potential values of the antipyrine derivatives with and without the presence of Fe (III) as a function of the scan rate.

Process	MT							
$E_{ap0}$ and $E_{ap1}$	4AA	DMA	MTM/	M/	[Fe(III)(4	[Fe(III)(DM	[Fe(III)(MT	[Fe(III)(MT
	/ V	A/ V	V	V	AA)2]/ V	AA)2]/ V	M)2]*/ V	M)2]*/ V
	0.47			0.58				
0.01/ V s <sup>-1</sup>	0	0.452	0.358	7	0.479	0.630	0.500	0.593
	0.47			0.59				
0.02/ V s <sup>-1</sup>	6	0.459	0.437	7	0.496	0.640	0.438	0.515
	0.49			0.59				
0.05/ V s <sup>-1</sup>	7	0.464	0.421	0	0.517	0.646	0.430	0.512

	0.51			0.58				
0.10/ V s <sup>-1</sup>	39	0.460	0.404	6	0.569	0.637	0.453	0.548
	0.52			0.59				
0.20/ V s <sup>-1</sup>	8	0.464	0.419	7	0.548	0.643	0.453	0.516
	0.56			0.59				
0.50/ V s <sup>-1</sup>	96	0.465	0.388	3	0.577	0.646	0.464	0.552
	0.64			0.60				
1.00/ V s <sup>-1</sup>	3	0.466	0.404	2	0.621	0.658	0.472	0.530

---

MT

Process	AA/	4AA/	DMA	M/	[Fe(III)(A	[Fe(III)(4A	[Fe(III)(DM	[Fe(III)(MT
Eap <sub>3</sub>	V	V	A/ V	V	A) <sub>2</sub> ]/ V	A) <sub>2</sub> ]/ V	AA) <sub>2</sub> ]/ V	M) <sub>2</sub> ]*/ V
	1.21	0.966		1.09				
0.01/ V s <sup>-1</sup>	55	4	1.051	0	1.217	1.000	0.953	1.085
	1.22	0.973		1.12				
0.02/ V s <sup>-1</sup>	07	8	1.066	9	1.219	1.010	0.958	1.083
	1.21	0.986						
0.05/ V s <sup>-1</sup>	72	4	1.098		1.232	1.011	1.010	1.089
	1.22	1.002						
0.10/ V s <sup>-1</sup>	81	3	1.058		1.238	1.082	0.997	1.120
	1.23							
0.20/ V s <sup>-1</sup>	72	1.024	1.102		1.263	1.010	1.013	1.077
	1.26	1.043						
0.50/ V s <sup>-1</sup>	06	4	1.117		1.263	1.120	1.031	1.145

	1.26	1.082					
1.00/ V s <sup>-1</sup>	68	1	1.124	1.298	1.190	1.014	1.117

---

**Randles Sevcik equations and oxidation mechanism discrimination of processes Eap<sub>0</sub>, Eap<sub>1</sub>, Eap<sub>3</sub>**

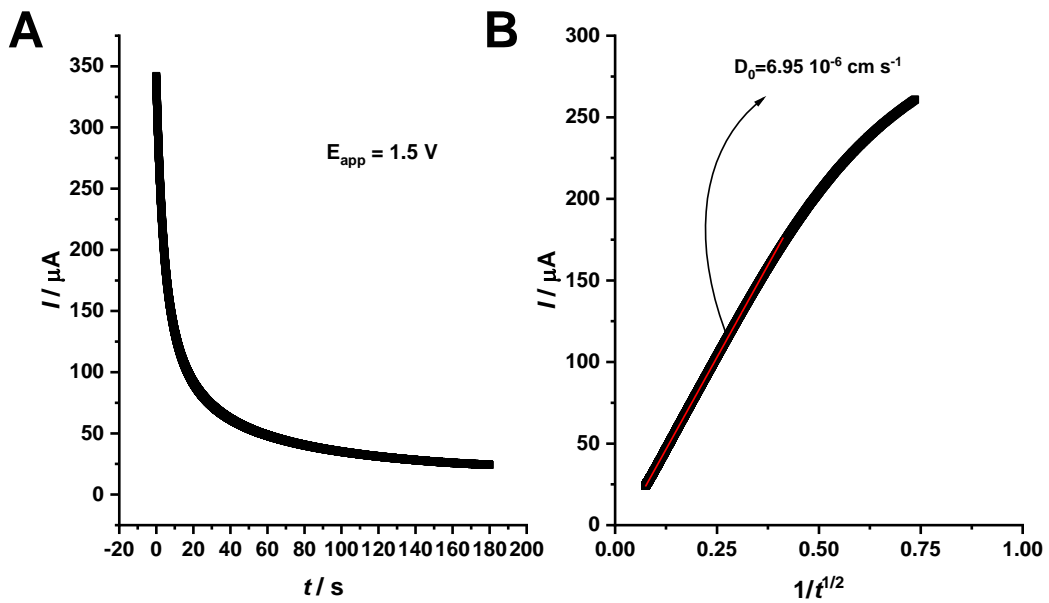


Figure S9: Chronoamperogram of a 1,0 mM AA solution in PBS, pH = 7,4.

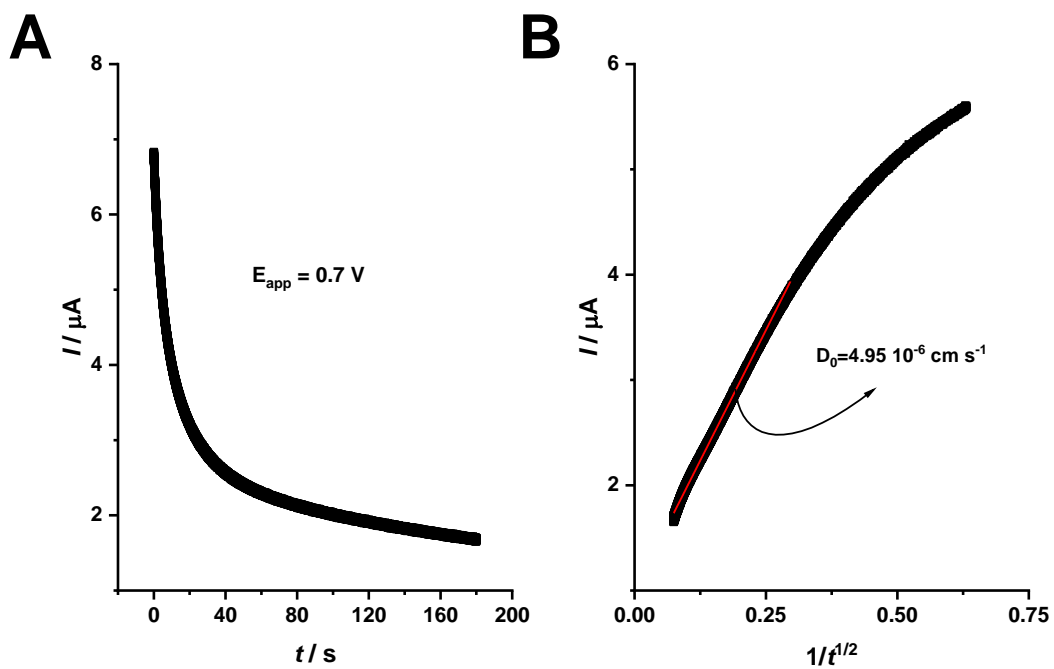


Figure S10: Cronoamperogram of a 1,0 mM 4AA solution in PBS, pH = 7,4.



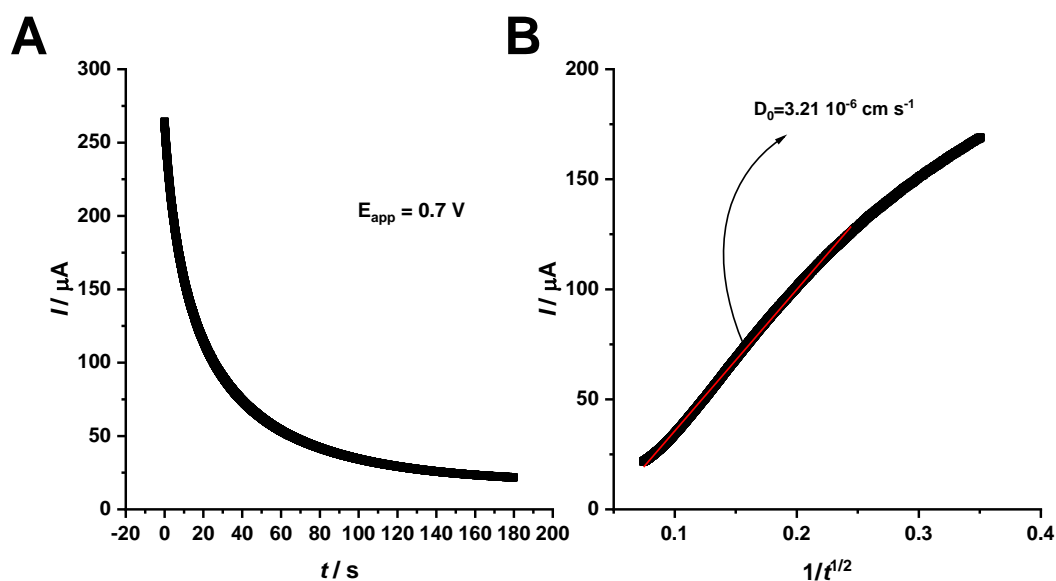


Figure S11: Cronoamperogram of a 1,0 mM DMAA solution in PBS, pH = 7,4.

**Tafel analysis and a catalytical effect generated by the Fe (III) complexes. kinetic difference between the antipyrine derivatives and the respective complexes**

To further understand of the observed catalysis between MTM and Fe (III), the process  $E_{ap_0}$  of the hydrolysis product MAA was studied by using the 4AA as a model. Similarly, the DMAA was used instead of the MTM, since it presents the  $E_{ap_1}$  process. Thus, by combining both 4AA and DMAA, allows to simulate the MTM system with its undergoing hydrolysis as it chelates the Fe (III).

Initially, the 4AA with DMAA combination was studied using UV-Vis to observe if any interaction occurs between them without the metal. Following the Fe (III) was added to observe possible shifts in the bands and similarities between the systems 4AA and DMAA with Fe (III), and the MTM in the presence of the Fe (III). As last, the electrochemical kinetics of the mimicking system was obtained to compare with the original MTM and Fe (III).

In figure 8, both bands previously observed to 4AA and DMAA can be observed. The phenazones 4AA and DMAA together presented a juxtaposition of the individual spectrum obtained for each molecule. After the addition of Fe (III), two CT bands can be spotted, the first one, in 307 nm, is comparable with a profile found in DMAA complex. The second one, in 360 nm was not priorly observed in the  $[\text{Fe(III)DMAA}_2]$  nor  $[\text{Fe(III)4AA}_2]$  spectra. Analogously, a d-d band in 412 nm has also no correspondence in the aforementioned complexes spectra. However, both CT and d-d complex band matches with the ones shown in the MTM complex spectrum. In light of those results, it can be concluded that the complex formed in the mimicking solution consists of one 4AA, and one DMAA, thus, forming  $[\text{Fe(III)(4AA)(DMAA)}]$ , that shows similar behavior to the  $[\text{Fe(MAA)(MTM)}]$  complex and is, therefore, a good mimetic for the dipyrone system.

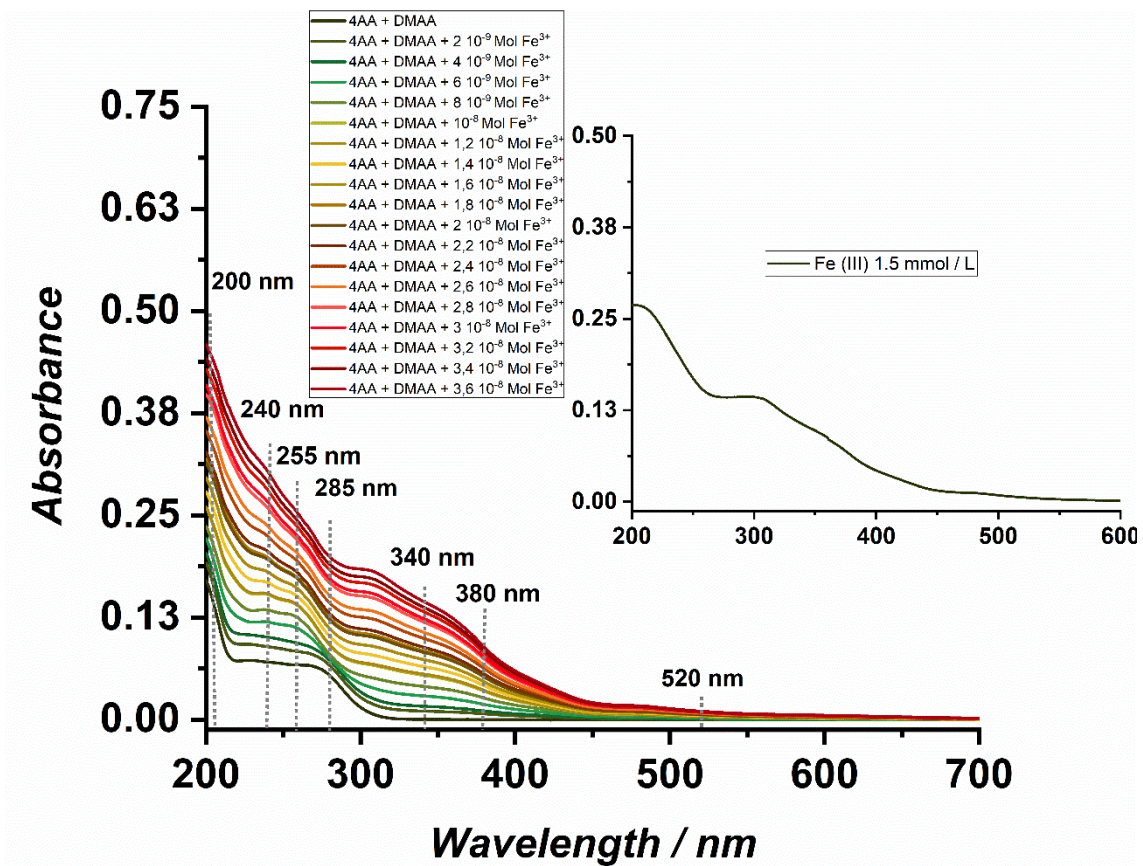


Figure S12: UV-Vis spectra as a function of the iron (III) addition for a 4AA and DMAA solution.

## Chapter 4

### **Electrochemical Cyclooxygenase biosensor to evaluate target – drug viability and interactions.**

In this chapter, we discuss a biosensor to analyze the anti-inflammatory properties of non-steroidal-anti-inflammatory drugs (NSAIDs). The chemical interaction between commercial NSAIDs and their target, *cyclooxygenase-2* enzyme (COX), was studied. This work counts with the help of many colleagues, Estenio helped with data acquirement and data curation, the same for Marcelo Portes, Gabriel Bacil, Guilherme Romualdo and Professor Barbizan performed the extraction and quantification of the biological sample, Professor William was responsible for data acquirement, discussions, data curation and revision, and Professor Serrano administrated the project.

The electrochemical behaviour of COX sensor presented two main reduction processes. We observed that one of them involves one electron and one proton related to tyrosyl radical reduction to tyrosine and the second relevant cathodic process comprises an one electron reduction from the Fe (IV) to Fe (III) species present in the enzyme's active site, which in the presence of hydrogen peroxide, results in a catalytical process. Based on these results, an electrochemical mechanism to the COX enzyme is proposed. Additionally, the quantitative inhibitory interaction mechanism of six commercial NSAIDs with the biosensor was studied. Acetylsalicylic acid, dipyron, and the ibuprofen presented the higher COX inhibitory percentual, being therefore, the most effective NSAIDs among the studied group. The salicylic acid also presented a significant inhibition capability in both electrochemical and EPR studies. The

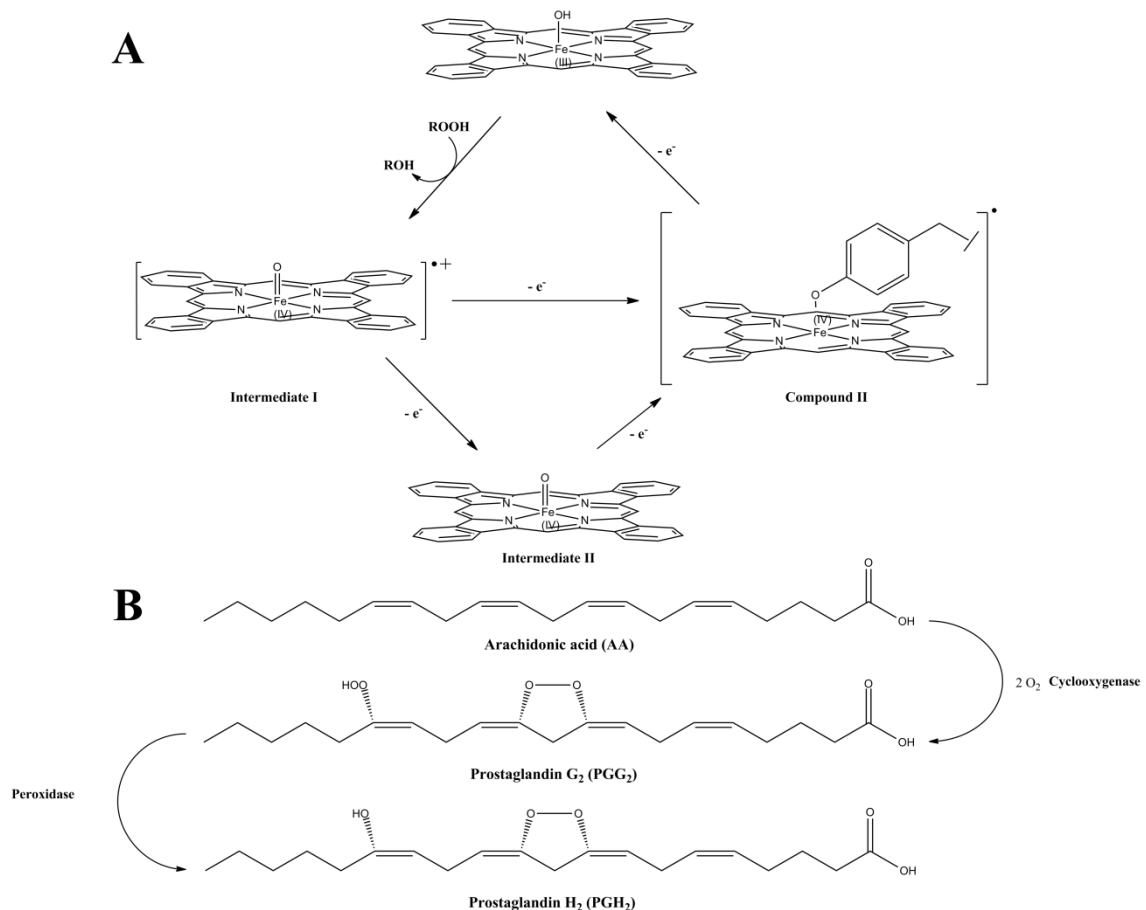
effect of some NSAIDs, like dipyron and acetaminophen, can be explained by the redox inhibition hypothesis and could be related to directly interaction and inactivation of iron present in the enzyme's active site. Ibuprofen and naproxen presented irreversible COX inhibition. Despite that, the EPR shows that these drugs have relatively weak interactions with the COX active site, suggesting they should interact with the external enzyme's structures resulting in the inhibition of its activity. Finally, the developed enzymatic sensor presented a high potential to study antinflammatory properties of well-known drugs, and can be a useful tool in the development of new NSAIDs, in a more efficient way. Therefore, this biosensor presents a high applicability in the drug development, pharmaceutical, and biomedical applications in both academia and industry.

## **Introduction**

The biosensors are devices, capable of providing specific quantitative or semi-quantitative analytical information using a biological recognition element using biomolecules to generate a physical or chemistry response. (Asal et al., 2018; Gaudin, 2017; Thevenot et al., 1999) The use of biomolecules such as proteins or DNA provides high specificity and sensibility, hence providing reliable sensors of a great variety of sizes, shapes, and analytical signals. (Asal et al., 2018; El Harrad et al., 2018; Prakash et al., 2009) Among the biomolecules, one of the most relevant from an economical point of view is the *Cyclooxygenase-2* enzyme (COX).

The COX or *Prostaglandin-Endoperoxide Synthase* ([EC 1.14.99.1](#)) is one of the three isoforms of the *Cyclooxygenase* enzyme, which is predominantly a hepatic enzyme, and responsible for triggering the inflammatory response by converting arachidonic acid (AA) into prostaglandins (PG). (Ayoub et al., 2010;

Hla and Neilson, 2006; Simmons et al., 2004; Smith and Marnett, 1991) To perform this conversion, the COX presents two different functions: Firstly, a cyclooxygenase function, responsible for the AA conversion of the fatty acid in an endoperoxide. Secondly, the peroxidase function, that reduces the peroxide into two alcohols. (Ayoub et al., 2010; Simmons et al., 2004; Smith and Marnett, 1991) The enzyme monomer presents two active sites. The peroxidase one is a heme (Htin) group, that consists of a protoporphyrin IX molecule with Iron (III) coordinated, figure 1. (Buoro et al., 2017, 2016) The second active site is provided by a Tyrosine (Tyr) amino acid in the 385 position, which is oxidized into a radical by the Htin, thus starting the reaction in the AA. (Bhattacharyya et al., 1996; Shimokawa et al., 1990) These joint steps result in substrate conversion into a PG in an orchestrated mechanism; first, the cyclooxygenase function is triggered, and then the peroxidase one is activated, figure 1. (Smith and Marnett, 1991)



Scheme 1: Schematic representation of the COX enzyme; 1A) the active site of the enzyme and its chemical steps. 1B) the cyclooxygenase and peroxidase reactions of the enzyme to convert the AA into PGH<sub>2</sub>. (Tsai et al., 1995; Tsai and Kulmacz, 2010)

The enzyme has a 'self-activation' mechanism, which consists of an endogenous peroxide, which activates the enzyme, by oxidizing the Iron (III) in the Htin center. Also, if the endoperoxide concentration drops below 10 nM, the enzyme will be inhibited. (Smith and Marnett, 1991) Thus, the hydroperoxide is essential to the generation of the Tyr radical, which is responsible for jumpstarting the enzymatic system, figure 1A.

In sequence, the AA is catalyzed to Prostaglandin G<sub>2</sub> (PGG<sub>2</sub>) with the addition of molecular oxygen, (Shimokawa et al., 1990) which will then undergo

a reduction in the Htin center. The now-activated Htin presents an oxyferryl moiety that executes the peroxidase function reducing intermediate to the PGH<sub>2</sub>, figure 1B. (Ayoub et al., 2010; Wu et al., 2007)

In their review, Smith and Marnett compile the principal modulation routes of the COX activity, numbering four reasons in which the enzyme can be deactivated. The reasons are: 1) *diminishing concentrations of either substrates of the enzyme*; 2) *diminishing concentrations of the hydroperoxide necessary to activate the COX (which is corroborated by Tsai and Kulmacz (Tsai et al., 1995; Tsai and Kulmacz, 2010)*; 3) *reduce the oxidized forms of the enzyme to the native or reduced form*; 4) *interfere with arachidonate binding in the active sites.* (Bhattacharyya et al., 1996; Smith and Marnett, 1991) With these ways of deactivating the COX in mind, we focused on the third and fourth reasons; in other words, the reducer capacity of the inhibitor drugs which target the COX and their allosteric regulation of the enzyme.

The most popular COX inhibitors are the NSAID (Non-Steroidal Anti-Inflammatory Drugs) which are the most used drugs in the world, the painkillers. (Hamberg, 1972; Smith et al., 1990; Smith and DeWitt, 1995) Smith and Marnett, say that in general, the NSAIDs compete with the AA for the cyclooxygenase active site (the 385 Tyr), but do not inhibit the peroxide activity of the enzyme. Therefore, resulting in the inactivation of the oxyferryl heme radical (peroxidase function) and not the tyrosyl radical (cyclooxygenase function). (Wu et al., 2007) In addition, some inhibitors cause secondary effects that can be covalent or non-covalent, as the Acetylsalicylic Acid (AAS) acetylation in the serine (Ser) amino acid and indomethacin, which works as an allosteric regulation, respectively. (Smith and Marnett, 1991) Besides that, Paik et al. suggest that the flufenamic



acid and some NSAIDs could inhibit the enzyme while inducing COX expression. Furthermore, their results indicate that the flufenamic acid's anti-inflammatory effects and some other NSAIDs occur due to their inhibitory action on the mitogen-induced expression of COX-2 and downstream markers of inflammation in addition to their inhibitory effect on COX enzyme activity. (Paik, 2000)

Several NSAID relates with the COX enzyme, the AAS as mentioned earlier, the Acetaminophen (Engström Ruud et al., 2013; Ghanem et al., 2016), the Ibuprofen. (Orlando et al., 2015), Dipyrrone. (Bacil et al., 2012, 2018) The only one which has the inhibition mechanism well known is the AAS, which was proposed by Vane and Botting (Vane and Botting, 2003). According to then, the AAS undergoes hydrolysis generating an acetyl group, which reacts with a Ser termination, shifting the COX structure and deactivating the enzyme, and the Salicylic Acid (AS), that is also related to the COX, as described by Mitchell et al. and McCarty et al., (McCarty and Block, 2006; Mitchell et al., 1997), but it is inhibition mechanism, as the others remain unclear.

In mechanistic studies of the COX, Landino et al. observed that nitric oxide and superoxide activate the enzyme biosynthesis of prostaglandins. (Landino et al., 1996). Furthermore, Deeb et al. observed that peroxynitrite interacts with the enzyme modulating the enzyme (Deeb et al., 2010), as Tsai (Tsai and Kulmacz, 2010), they concluded that the tyrosyl radical generated in the oxygenase step is crucial to enzyme activity. Extrapolating both conclusions, its interaction with radical-like species should hinder the COX processes.

In the electrochemical field, the COX utilization is rare (El Harrad et al., 2018). However, one paper describes a biosensor developed for analytical applications, Campanella et al. used a COX biosensor to determine NSAIDs in

milk and cheese. (Campanella et al., 2009) Noah et al. used an immunosensor to detect metals using the concept of metal-enhanced detection to monitor the COX-2 (Noah et al., 2011a) and Noah et al. also used the immunosensor to detect and quantify pain biomarkers (Noah et al., 2011b). Despite that, the enzymatical biosensors can be used in different applications such as evaluating how biomolecules interact with each other, e.g., a drug and its target enzyme. Moreover, these biosensors can evaluate if their interaction with any interest molecule is reversible, irreversible and if it enhances or inhibits the enzyme activity; besides that, it also allows some mechanism insights. (El Harrad et al., 2018)

Therefore, this work aims to evaluate the electrochemical behaviour of the enzyme, and then obtain a voltammetric biosensor that measures the enzyme inhibition by any molecule.

## **Materials and methods**

### **Blotting and Enzyme extraction**

Liver samples from the left lobe (~100 mg) were homogenized with phosphate buffered solution (PBS) (0.15M NaCl, 300  $\mu$ M KCl, 1.5  $\mu$ M KH<sub>2</sub>PO<sub>4</sub>, 8 mM NaH<sub>2</sub>PO<sub>4</sub>, and 10  $\mu$ l mL<sup>-1</sup> protease inhibitor cocktail [Sigma-Aldrich, USA]) in the proportion of 30 mg of tissue 100  $\mu$ L<sup>-1</sup> of buffer (4 °C, 2 h). In sequence, the extracted material was centrifuged (1500 $\times$ g, 4 °C, 20 min) and the supernatant was collected for protein quantification by Bradford's method. Aliquots of liver homogenates containing 7  $\mu$ g of total protein were heated (95 °C, 5 min) in Laemmli sample buffer (2.5 mM Tris, 2% SDS, 10% glycerol, 0.01% bromophenol blue, 5% 2-mercaptoethanol) and then electrophoretically separated in a 10% SDS-PAGE gel under reducing conditions, later being transferred to

nitrocellulose membranes (Bio-Rad Laboratories, USA). The membranes were blocked with non-fat milk in TBS-T (1 M Tris, 5 M NaCl, pH 7.2, 500  $\mu$ L Tween-20) (1 h) and incubated with rabbit polyclonal anti-COX-2 (ab15191, ~72kD, 1:1000 dilution, Abcam, UK) a primary antibody in 5% BSA solution for an overnight period. After this treatment, they were submitted to five wash steps with TBS-T and then incubated with specific horseradish conjugated secondary antibody, according to the primary antibody. Finally, after another five wash steps, the membranes were treated with immunoreactive protein, an Amersham ECL Select Western Blotting Detection Reagent (GE Healthcare Life Sciences, UK), which generate chemiluminescence that was measured by a G:BOX Chemi system (Syngene, UK) controlled by software Syngen.

### **Electronic Paramagnetic Resonance (EPR)**

The EPR spectra were obtained at room temperature  $20 \pm 2$  °C with a 15 G modulating amplitude and  $7.10 \cdot 10^2$  of gain, with a time constant of 20,48 ms. The data acquirement was made with the software 32Bit WinEPR Acquisition Version 4.33 Rev.12, and the spectra were treated with the software WinEPR System Version 2.22 Rev.12

### **Electrode Modification**

Before each modification, the glassy carbon electrode (GCE) was polished using a wet super fine sandpaper – P7000 from Riken Corundum Co. LTD from Japan. Then it was modified by drop-casting, first by applying 7.5  $\mu$ L of GLU in the GCE surface, and the electrode was left in a continuous air flux. Next, the enzyme was added to the surface, by applying 7.5  $\mu$ L of the homogenate in the GCE. The electrode was then left in a support until the homogenate was dry, the procedure was performed at room temperature ( $25 \pm 3$  °C).

After the modification, the electrode surface was rinsed thoroughly with deionized water and differential pulse voltammograms were recorded in supporting electrolyte to obtain a steady baseline.

## **Electrochemical Measurements**

### **Cyclic Voltammetry (CV) and Linear Sweep Voltammetry (LSV)**

The voltammograms were performed using the following experimental conditions:  $E_{\text{initial}} = 0.0 \text{ V}$ ;  $E_{\lambda 1} = + 0.2 \text{ V}$ ,  $E_{\lambda 2} = - 1.4 \text{ V}$   $E_{\text{final}} = 0.0 \text{ V}$ , step potential =  $2.0 \text{ mV}$  and  $v = 100.0 \text{ mV s}^{-1}$ . The solutions were stirred before each measurement. Distinct conditions in any essay were specified in the caption figure.

### **Differential Pulse Voltammetry (DPV)**

The experimental conditions for DPV experiments were:  $E_{\text{initial}} = + 0.4 \text{ V}$ ,  $E_{\text{final}} = - 1.4 \text{ V}$ ; pulse amplitude =  $50 \text{ mV}$ ; pulse width =  $100.0 \text{ ms}$ ; step potential =  $2.5 \text{ mV}$  and interval time =  $0.5 \text{ s}$  resulting in scan rate of  $5 \text{ mV s}^{-1}$ . The solutions were stirred before each measurement.

To perform the kinetic curve, 15 DPV were obtained in sequence, with a stirrer between each assay. The oxygen was removed from the solution by bubbling nitrogen gas into the solution before the beginning of each assay.

### **Electrochemical Impedance Spectroscopy (EIS)**

An Autolab PGSTAT128N (Eco Chemie, Utrecht, the Netherlands), linked with a NOVA 1.11 software, was used to record electrochemical impedance spectroscopy (EIS) in solutions with and without the atmospheric  $\text{O}_2$  and both in the presence and absence of a  $5.0 \text{ mmol L}^{-1}$  peroxide solution in  $0.1 \text{ PBS}$ ,  $\text{pH} =$

7.4 at frequencies between  $10^5$  and  $10^{-1}$  s<sup>-1</sup>. A potential of 0.0 V, -0.2 V, -0.7 V was applied to observe the electrochemical processes. The experiments were performed at room temperature ( $25 \pm 3$  °C).

## Results and Discussion

This section initially presents the electrochemical characterization of the electrode modification obtained through different voltammetry techniques (CV, DPV and SWV). Following, the interaction of the modified electrode with the NSAIDs was studied using DPV and EPR.

### Electrochemical Evaluation of *Cyclooxygenase*

The enzymatic modification was evaluated using CV, DPV, SWV, and impedance figures 1 and S1. The CVs, figure 1A, do not allow to distinguish clearly any electrochemical processes from the background current. Thus, DPV and SWV were obtained to better observe the enzymatic processes.

Figures 1B and C, show three reduction processes, Ecp<sub>1</sub>, Ecp<sub>2</sub>, and Ecp<sub>3</sub>. In Figure 1B the  $w_{1/2}$  values of each process were obtained to correlate with the number of electrons involved. The processes Ecp<sub>1</sub>, Ecp<sub>2</sub>, and Ecp<sub>3</sub> presented a  $w_{1/2}$  of  $125.3 \pm 6.1$ ,  $102.4 \pm 2.8$  and  $178.7 \pm 9.6$ , respectively. These values suggest reductions involving one electron to processes Ecp<sub>1</sub> and Ecp<sub>2</sub>, as Ecp<sub>3</sub> is inconclusive, according to Brett et al. (Brett et al., 1993). Figure 1C shows that neither of the three processes presented anodic components, thus being irreversible.

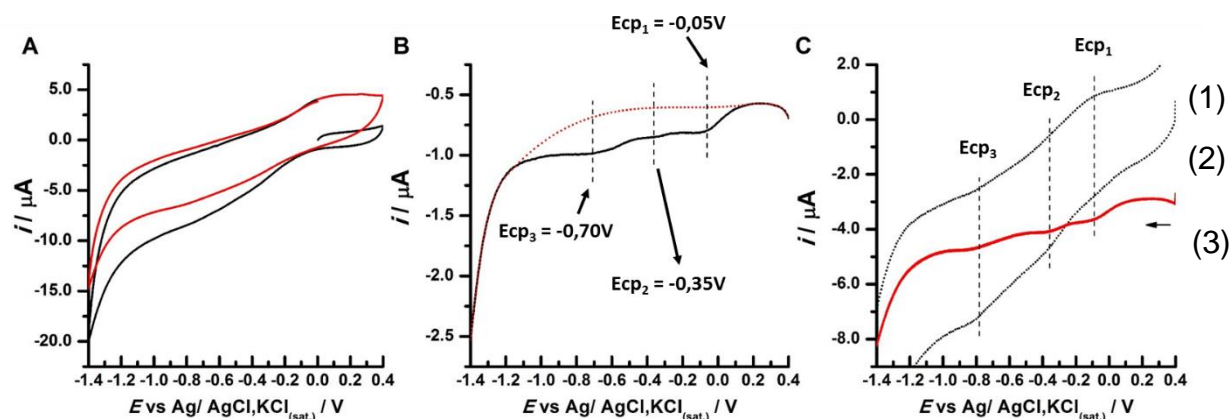


Figure 1: A) CV obtained in GCE-COX at PB 0.1 M, pH 7.4 (1<sup>st</sup> scan GCE-COX – Black, Blank scan – Red); B) DPV obtained in GCE-COX at PB 0.1 M, pH 7.4 (Scan GCE-COX – Black, Blank scan – Red); C) SWV obtained in GCE-COX at PB 0.1 M, pH 7.4 ((1) Backward Current, (2) Forward Current, (3) Total Current), the experimental conditions were presented in the previous section.

Due to the irreversible character of the three processes, the DPV technique was selected to evaluate the interaction in further experiments.

As aforementioned, the COX has two functions, oxygenase, and peroxidase. The modified electrode was evaluated in peroxide presence, which can mimic the enzyme's substrate, the arachidonic acid. (Smith and Marnett, 1991; Wu et al., 2007) Figure 2A shows that Eap<sub>3</sub> is catalyzed in the presence of the peroxide, as previously observed to Htin. (Buoro et al., 2017, 2016) Thus, Eap<sub>3</sub> was ascribed the reduction of iron in the enzyme active site, which is then chemically oxidized by the peroxide and following electrochemically reduced in the electrode, generating an electrocatalytic cycle, the Tafel plots (Figure S2) also corroborate the three processes that occur with the first electron transfer is the rate determining.

Since Eap<sub>3</sub> was ascribed to the peroxidase function, the initial hypothesis was that Ecp<sub>2</sub> could be associated with the oxygenase function, being then the reduction process of oxidized Tyr<sub>385</sub>. To better comprehend Ecp<sub>2</sub>, DPV with COX@GCE was performed in the presence of Tyr, with and without peroxide, figure 2.

Figure 2 shows that in the presence of peroxide, the current scale sharply rose in both processes and the addition of Tyr generated current increments in both processes Ecp<sub>2</sub> and Ecp<sub>3</sub>. This result suggests these processes are connected 'via peroxide'. Since the process Ecp<sub>2</sub> decreases in the presence of only the peroxide during the time, figure S1, it was concluded that Ecp<sub>2</sub> is most likely the reduction of the tyrosyl radical chemically formed by the peroxide that oxidizes the Tyr. It is also important to observe that ferryl radical formed in the enzymes' active site is also capable of oxidizing the Tyr, as aforementioned. Also, in figure 3A, endogenous peroxide of the homogenate oxidizes the Tyr, since its concentration is way smaller than the 5 mM peroxide addition, the current observed in both processes is diminutive when compared. In conclusion, the oxygenase and the peroxidase functions perform a concerted mechanism.

Figure 2A shows the DPV in the absence of peroxide with subsequent 10  $\mu$ L additions of 1.0mM tyrosine. When in the presence of the Tyr without peroxide, only the current observed in process Ecp<sub>2</sub> significantly increases, corroborating that Ecp<sub>2</sub> is the reduction of the tyrosyl radical. Figure 2B shows that the subsequent addition of 10  $\mu$ L a 1.0 mM peroxide solution in a solution already containing 10 mM of tyrosine results in an increase of the peak currents of both processes Eap<sub>2</sub> and Eap<sub>3</sub>. A result that reinforces a concerted mechanism of the enzyme.

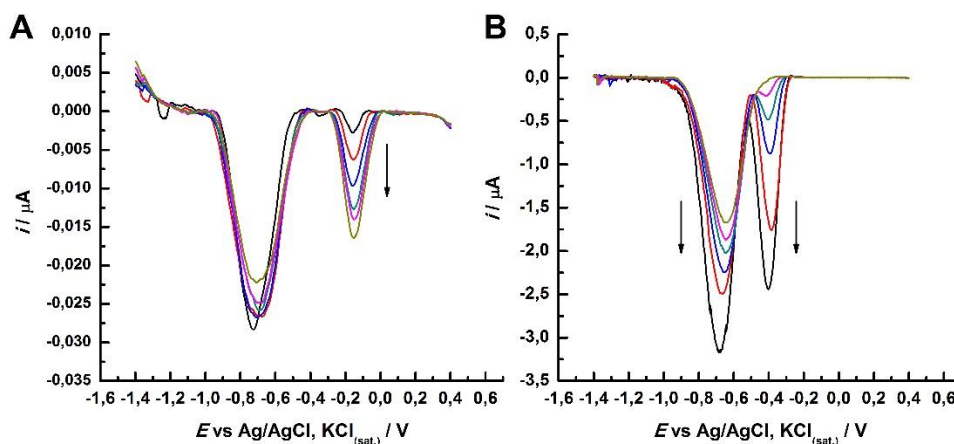


Figure 2: DPV obtained in GCE-COX 50 $\mu$ M Tyr solutions in PB 0.1 M, pH 7.4 A) Without the presence of 5mM H<sub>2</sub>O<sub>2</sub>; B) Within the presence of 5mM H<sub>2</sub>O<sub>2</sub>.

To complement the electrochemical characterization, the Tafel plots were obtained from Linear Sweep Voltammetry (LSV), figure S2. The plots strongly indicate that for both processes the first (only) electron reductions are the rate-determining step, due to their  $\alpha$  values between 0 and 1.

Since the process is mediated by the COX immobilized in the electrode's surface, the electrochemical process is submitted to the enzymes' turnover constant ( $k_{cat}$ ), and sequential addition of peroxide provides a Michaelis-Menten response, which results in enzymes kinetic curve, figure 3. The Michaelis-Menten plot provides the enzyme's constants such as  $K_m$  and  $V_m$ , the turnover constant,  $K_{cat}$ , also can be obtained. From figure 3, the obtained values were:  $K_m = 4.33 \cdot 10^{-6}$ ,  $k_{cat} = 5.69 \text{ s}^{-1}$ ,  $V_m = 40.2 \mu \text{ mol L}^{-1}$  these values were in accordance to the COX constants observed in the literature. (Liu and Roth, 2016; Mukherjee et al., 2007; Smith and Marnett, 1991)



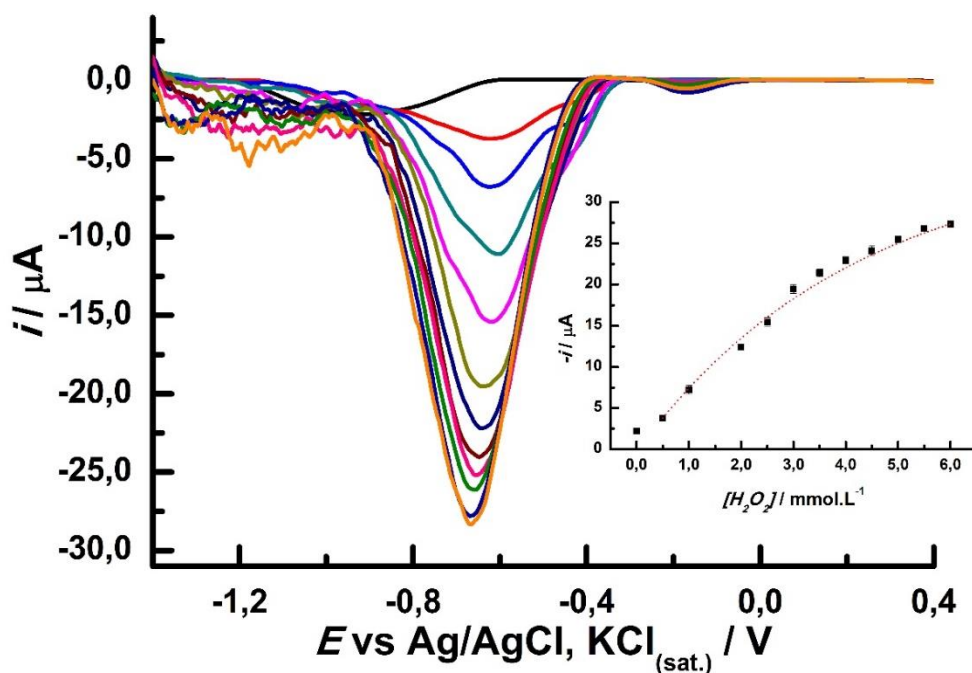
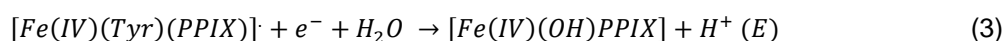
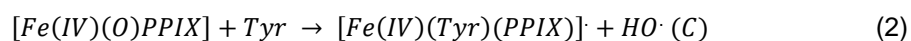
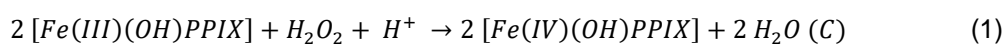
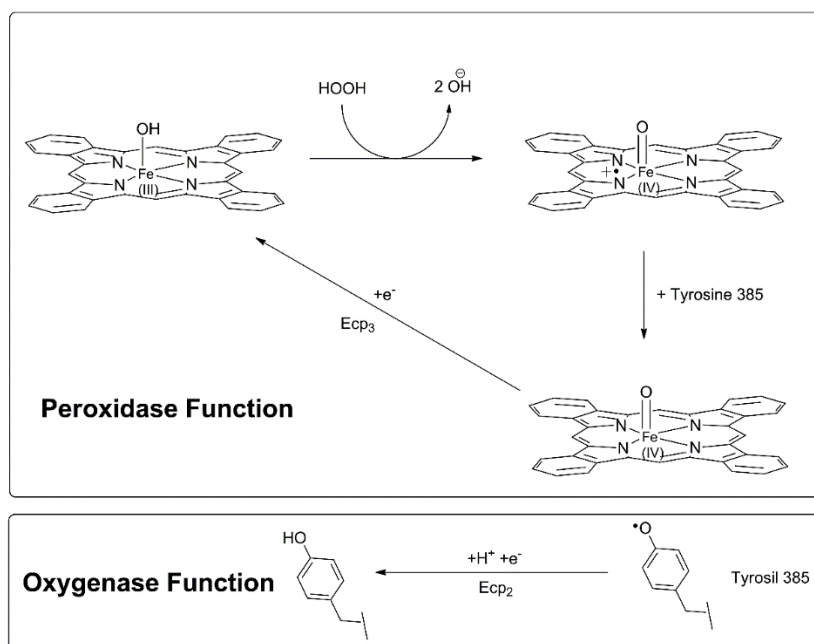


Figure 3: DPV obtained in GCE-COX at several different  $\text{H}_2\text{O}_2$  concentrations in PB 0.1 M, pH 7.4 solutions; Figure 3 Inset:  $i$  versus concentration curve obtained from 4 voltammograms.

Compiling the results, and with the literature information, it can be concluded that the results are in accord with the literature. (Ayoub et al., 2010; Bhattacharyya et al., 1996; Dorlet et al., 2002; Simmons et al., 2004; Smith and Marnett, 1991; Tsai and Kulmacz, 2000; Wu et al., 2007) Thus, the following steps and an electrochemical mechanism were proposed:





Scheme 2: Proposed catalytic electrochemical mechanism of COX.

### COX interaction with NSAIDs

Since the enzyme mechanism was well observed using voltammetry techniques, the same protocol was then used to evaluate the interactions between the NSAIDs and the enzyme in which the literature claims they inhibit.

Initially, a series of voltammograms, see figure S3, with the COX@GCE only in the presence of 5 mM peroxide solutions were recorded for 90 minutes to test the durability of the modified electrode and to compare with the initial peak current values obtained. The peak current values were stable through the test after an initial 9.89% drop of its initial signal. Therefore, the obtained values were normalized to measure the COX inhibition %, according to equation 4.

$$COX \text{ Inhibition } \% = \left[ 1 - \left( \frac{I_{COX+NSAIDs}}{I_{COX}} \right) \right] \times 100 \quad (4)$$

where  $I_{COX+NSAID}$  is the peak current of the process Ecp<sub>3</sub> in  $\mu A$  of COX@GCE in the presence of 5 mM of H<sub>2</sub>O<sub>2</sub> and 50  $\mu mol L^{-1}$  of a NSAID in 0,1 mol L<sup>-1</sup> of PBS,

pH = 7.4 and  $I_{COX}$  is the peak current of the process  $E_{cp3}$  in  $\mu A$  of COX@GCE in the presence of 5 mM of  $H_2O_2$ .

Figures 4A to 4F present DPV obtained in a time difference of 15 minutes to evaluate the changes of  $I_{COX + NSAID}$  as a function of time. Initially, a voltammogram was recorded with the COX@GCE in the peroxide solution without any NSAIDs to obtain the  $I_{COX}$ . Following,  $50 \mu mol L^{-1}$  of a NSAID was introduced into the solution, which was stirred, and then voltammograms were recorded. After 98 minutes, the electrode was removed from the solution, carefully washed and inserted into a new peroxide solution without the drug to evaluate the reversibility of the inhibition. The peak current obtained after the reinsertion of the COX@GCE in a 5mM  $H_2O_2$  solution without the NSAIDS is presented as a dashed line in figure 4 for each NSAID.

Regarding the chemical interaction between the enzyme and drugs, as expected, all drugs tested generated a sharp decrease of  $E_{cp3}$  peak current. Despite that, different inhibition profiles were observed. In voltammograms of SA, ASA, MAA, and IBU figures 4A, 4B, 4D and 4E, it was observed slight sequential decreases after the initial sharp decline. On the other hand, voltammograms of APAP and NPX did not present that sequence of decreases, figures 4C and 4F. In addition, after the reduction process  $E_{cp3}$ , a small process can be seen around -1.25 V for all the drugs, except the APAP. Suggesting the appearance of an electroactive structure of the enzyme after the inhibition with those remedies. Another highlight was the  $E_{cp2}$ , the reduction of the tyrosyl group into tyrosine, it can only be observed in the MAA and NPX interactions, especially into the MAA one, suggesting the other tested drugs also use this inhibition route.

The inset figures show an increase of current after the wash to SA and APAP, figures 4A and 4C, hardly change to ASA, IBU and NPX, figures 4B and 4F, and surprisingly, to the MAA a decrease was observed even after the electrode has been taken out from the solution containing the drug, as already reported to IBU. (Orlando et al., 2015)

### **Aspirin and Salicylic Acid**

Observing figures 4A and 5A to ASA and 4B and 5B to SA, in green, the obtained data show a more significant inhibition of ASA than observed for SA, which is expected since the ASA undergoes hydrolysis generating SA and acetate. The latter is well known to inhibit the COX by acetylation of the 530 serine. Thus, the result replicates the conclusions of Vane experiments. Moreover, after a gentle wash and the introduction of the electrode in a new solution of peroxide without the drug, to evaluate the reversibility of the inhibition, two different results were observed for ASA and SA. The latter presented an increase of the current, and the prior kept the same signal previously observed. Thus, allowing the conclusion that the SA inhibition is reversible and the ASA is irreversible, which is expected for ASA since the main inhibition mechanism of ASA is due to the acetylation of the serine 530, which block access to the active site. (Vane and Botting, 2003).

Regarding the inhibition caused by SA, little information regarding how the SA inhibits the COX enzyme can be found in the literature. Provided that the COX enzyme in its active form has a ferroxyl in the protoporphyrin IX, and as Smith and Marnett and Wu et al. observed, reducers inactivate the enzyme (Smith and Marnett, 1991; Wu et al., 2007), the SA should act as a reducer in the active site, reducing the ferroxyl to iron (II). This hypothesis is also observed in other NSAIDs

effects. Following, since it is believed that MAA (dipyrone) and acetaminophen are also reducers, the same experiment interaction experiment was performed.

### **Acetaminophen and 4-Methyl-Aminoantipyrine (Dipyrone)**

Two of the worldwide famous NSAIDs are the APAP and the MAA (dipyrone). Lately, our group studied the dipyrone and the antipyrine group, concluding that they are great reducers. (Bacil et al., 2018, 2012) With that said, comparing the figures 4C, 5C and the figures 4D and 5D, it is noticeable that both drugs APAP and MAA also interact with the enzyme, resulting in approximately 60 and 75 percent of inactivation of COX enzyme. Although, after 100 minutes of experiment and the wash, when the reversibility of the inhibition was studied, the difference was huge. APAP presented a slight decrease, being therefore reversible. Meanwhile, the MAA kept inhibiting until it almost completely inactivated the system.

Once again the redox inactivation is the most likely scenario. This hypothesis was already used to explain the analgesic effect of SA and APAP (paracetamol), according to Aronoff et al. and Anderson and Smith, the APAP's effect is due to its reducer capability, which reduces the cation radical state in the active site of the COX enzyme. (Anderson, 2008; Aronoff et al., 2006; Smith, 2009). Besides that, other works attributed its effects to interactions in the nervous system. (Courade et al., 2001b, 2001a; Engström Ruud et al., 2013). These results just like one developed by our group corroborate the redox hypothesis since we previously concluded that the MAA is a very strong reducer. (Bacil et al., 2018, 2012)

### **Ibuprofen and Naproxen**

Two other drugs present in the list of the most used NSAIDs (“NHS - NSAIDs,” n.d.) are the IBU and the NPX, figures 4E and 5E, and figures 4F and 5F. Like the ASA, these two drugs not only presented an inhibition above 50 percent, they also kept inhibiting the enzyme after the wash and the new solution therefore, their inhibition is irreversible. The literature presents few papers where these molecules have been studied with electrochemical techniques, since their elevated oxidation potential, which means they are bad reducers and thus, the redox inactivation seems unlikely. Once again, compared to the ASA inhibition, the acetyl interacts with the enzyme's structure resulting in allosteric regulation. This situation is the most likely scenario for the inhibitions of IBU and NPX. Although further studies should be realized to confirm this hypothesis.

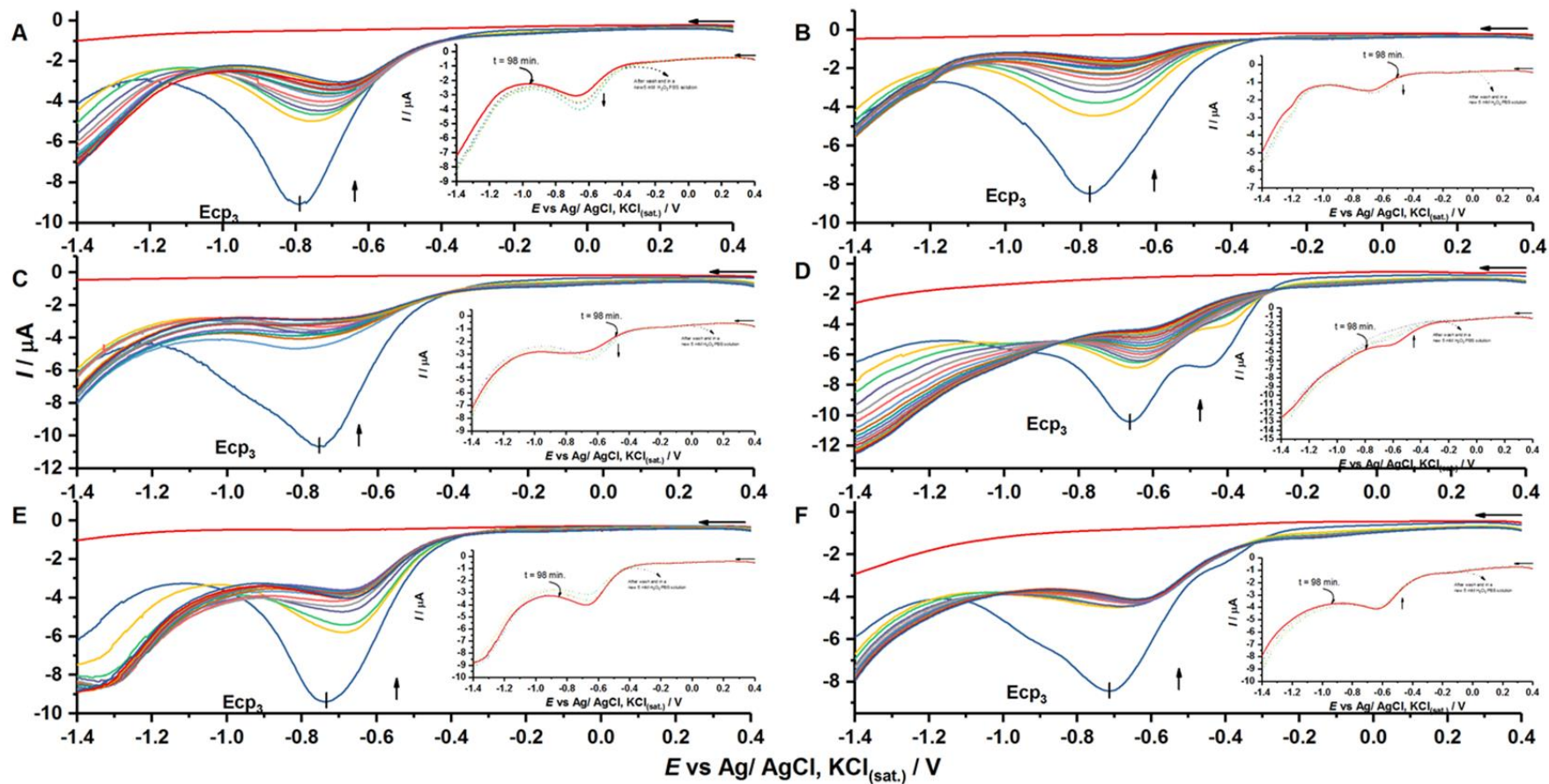


Figure 4: DPV in GCE-COX at 5.0 mM H<sub>2</sub>O<sub>2</sub> and 50 μmol L<sup>-1</sup> of A) SA, B) ASA, C) APAP, D) MAA, E) IBU, F) NPX, in PB 0.1 M solutions, pH 7.4;. Inset) DPV was obtained in GCE-COX after a gentle wash in a new 5.0 mM H<sub>2</sub>O<sub>2</sub> solution PB 0.1 M solution, pH 7.4 without the presence of the NSAID.

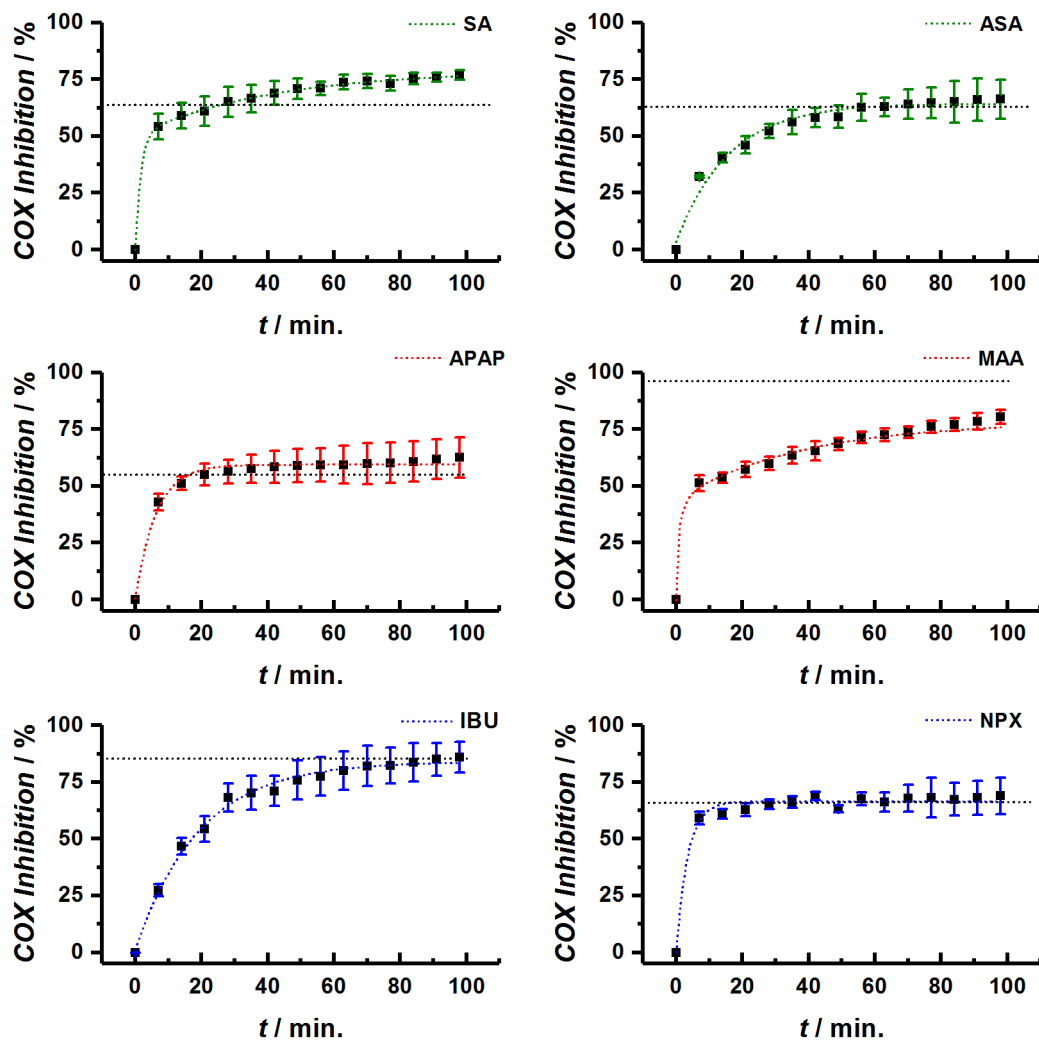


Figure 5: Plots of the inhibition percentage versus time for some NSAIDs; A) Salicylic Acid (SA); B) Acetyl Salicylic Acid (ASA); C) Acetaminophen (APAP); D) 4-Methyl-Aminoantipyrine (MAA); E) Ibuprofen (IBU); F) Naproxen (NPX)



Table 1: COX inhibition % observed each NSAID on COX@GCE .

Drug	COX Inhibition %	COX Inhibition % (after wash)
SA	77.2 ± 3.9	63.6 ± 4.2
ASA	66.4 ± 5.4	64.0 ± 6.3
APAP	62.3 ± 7.2	55.3 ± 7.1
MAA	79.8 ± 2.8	96.7 ± 3.4
IBU	85.3 ± 7.3	85.1 ± 5.5
NPX	68.4 ± 2.9	66.1 ± 3.5

### EPR spectra

To further explore the inhibitory effect from the NSAIDs, the EPR of Htin with tyrosine, which mimics the enzyme's active site, was performed to compare the inhibitions via cyclooxygenase and peroxidase functions.

EPRs spectra show that htin itself presents a silent EPR spectrum. However, in the presence of tyrosine, the tyrosyl radical is generated, such as previously reported by Tsai et al., a result that reinforces our proposed electrochemical mechanism involving the tyrosyl radical, figure 2 and scheme 2. Initially, the peroxide was used to form the radical, however, instead of forming the tyrosyl, it oxidized the htin, showing that without the complete structure of the enzyme, the htin is not robust enough to stabilize the Fe (IV) before the porphyrin structure oxidizes. Therefore, the EPR was performed only with htin in the presence of tyrosine.

Figure 6 shows that all NSAIDs interacted with the tyrosyl generated resulting in a decrease of the EPR signal, and therefore, all the studied NSAIDs

could inhibit the radical formation, which extrapolated to the COX enzyme should result in the oxygenase function inhibition.

Table 2 shows that SA interacted poorly with the system htin and tyrosyl, being the less effective NSAID with a performance of 48.3% of inhibition. The second worst was the IBU with about 58.8%, followed by the NPX with 68.2%. The other three drugs presented a significant performance as APAP presented a 76.8 % of inhibition, whilst ASA and MAA presented an inhibition % of 84.3% and 87.2%, respectively.

Comparing the voltammetric and the EPR spectra responses, figure 7, the SA presented the greatest divergence, a result that should suggest the SA most likely interacts as an allosteric regulator of the enzyme. However, after the wash and a reevaluation of the SA performance, it drops more than 13%, thus, suggesting that it probably blocks the enzyme's channel with a weak interaction. The second greatest divergence was the IBU which presents the last but one position with the Htin-tyrosine interaction, strongly indicating the IBU anti-inflammatory effect relies upon an allosteric regulation by interacting with the COX structure and not with its active sites. Following, NPX presented a similar result to IBU suggesting it also interacts with the external enzyme's structures resulting in allosteric regulation. The APAP that presents a poor 62,3% result in the voltammetric study being even worst after the washing experiment with 55% of inhibition, in the htin-tyrosine essay presents an inhibition of 76.8%. Therefore, the APAP results suggest it hinders the AA cascade by interacting with the cyclooxygenase site. The ASA differently from the SA presented a high inhibition in both essays, hence the acetyl moiety can not only interact with the serine, but it can also interact with both the tyrosyl and the htin. Finally, the MAA (dipyrone)

presents great results to both experiments, strongly suggesting this molecule can directly interact with the active sites, deactivating the enzyme.

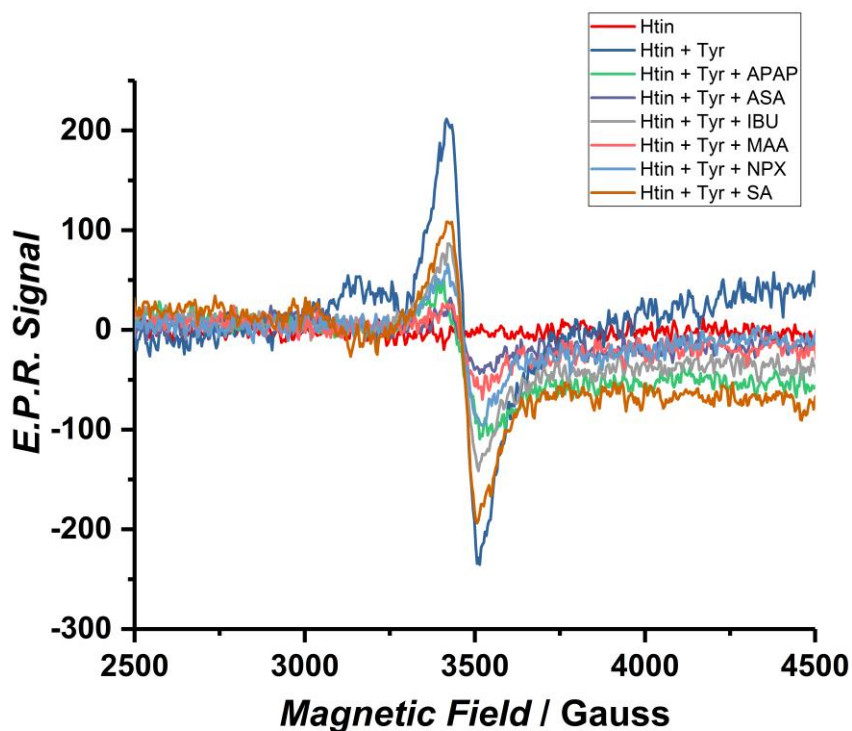


Figure 6: X-band EPR plots of hematin-induced tyrosyl radicals and their spectra in the presence of NSAIDs.

Table 2: Htin with tyrosine inhibition % from the EPR spectra

Drug	Htin with tyrosine inhibition %
SA	48.3
IBU	58.8
NPX	68.2
APAP	76.8
ASA	84.3

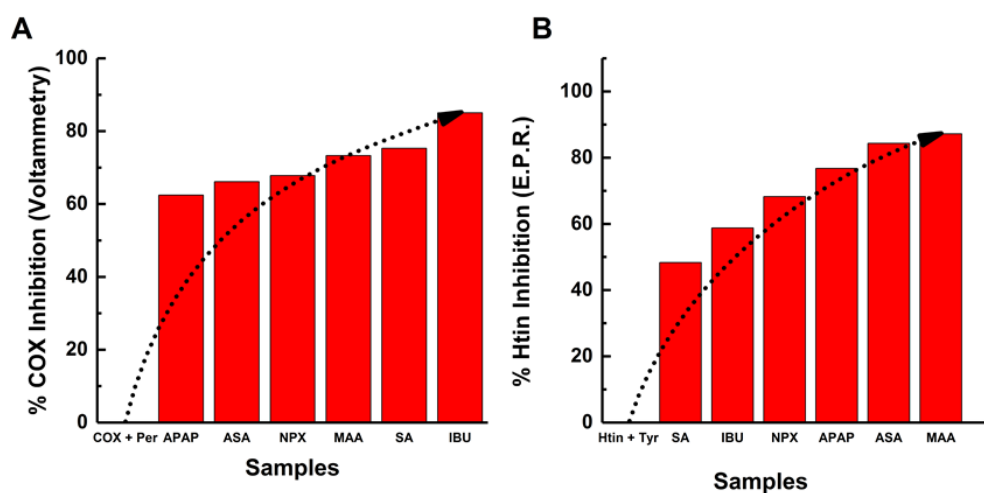


Figure 7: A) Bar graph of COX inhibitions in % observed for each NSAIDs at DPV, obtained at GCE-COX in 5mM H<sub>2</sub>O<sub>2</sub> at PBS, pH 7.4; B) Bar graph of Htin inhibitions in % observed for each NSAIDs at EPR, obtained at Htin 100  $\mu$ M and Tyr 100  $\mu$ M at H<sub>2</sub>O. 50 $\mu$ M and 5 $\mu$ M of drugs were used, respectively.

## Conclusions

In this paper, we develop a biosensor, which allows us to study the interaction between NSAIDs and their target, the COX enzyme. The COX@GCE electrochemical behavior has been characterized and it presented up to three reduction processes, two of which were related to the enzymes functions, oxygenase, and peroxidase. In addition, the electrode kinetics presented results in agreement with the one observed to the COX enzyme. Using the processes related to the enzyme's function, the interaction with the NSAID, salicylic and acetyl-salicylic acid, ibuprofen, naproxen, acetaminophen, and dipyron were evaluated. The combination of the voltammetric and EPR results allowed us to not only observe the % of inhibition of the enzyme but also to attribute

mechanistic insights to the enzyme's suppression. The salicylic acid appears to be an allosteric regulator, as the acetylsalicylic acid inhibits the enzyme thanks to its acetyl moiety. Both ibuprofen and naproxen are also allosteric regulators, however, they interact with external structures of the enzyme. The acetaminophen results suggest that its anti-inflammatory effect relies upon the inhibition of the oxygenase function, and the dipyron acts as a reducer deactivating both the ferroxyl in the peroxidase active site and the tyrosyl radical, therefore, hindering both active sites of the COX enzyme. Finally, this sensor has shown the potential not only to better comprehend the daily remedies but also to aid in the development of new ones. Since this biosensor allows us to observe and compare the lead molecules, their mechanism as well as comparing them with well-known, it could present high industrial applicability.

### **Acknowledgments**

The authors would like to thank National Council for Scientific and Technological Development (CNPq) (Process 140833/2016-1), São Paulo Foundation Research (FAPESP) (Process 2016/ 11985-6), Brazilian Federal Agency for Support and Evaluation of Graduate Education - CAPES (Process: PDSE - 88881.187396/2018-01) for the financial support.

### **References**

Anderson, B.J., 2008. Paracetamol (Acetaminophen): Mechanisms of action. *Paediatr. Anaesth.* 18, 915–921. <https://doi.org/10.1111/j.1460-9592.2008.02764.x>

- Aronoff, D.M., Oates, J.A., Boutaud, O., 2006. New insights into the mechanism of action of acetaminophen: Its clinical pharmacologic characteristics reflect its inhibition of the two prostaglandin H<sub>2</sub> synthases. *Clin. Pharmacol. Ther.* 79, 9–19. <https://doi.org/10.1016/j.clpt.2005.09.009>
- Asal, M., Özen, Ö., Şahinler, M., Polatoğlu, İ., 2018. Recent developments in enzyme, DNA and immuno-based biosensors. *Sensors*. <https://doi.org/10.3390/s18061924>
- Ayoub, S.S., Flower, R.J., Seed, M.P., 2010. Cyclooxygenases: Methods and Protocols, *Climate Change 2013 - The Physical Science Basis, Methods in Molecular Biology*. Humana Press, Totowa, NJ. <https://doi.org/10.1007/978-1-59745-364-6>
- Bacil, R.P., Buoro, R.M., Campos, O.S., Ramos, M.A., Sanz, C.G., Serrano, S.H.P., 2018. Electrochemical behaviour of dipyrone (metamizole) and others pyrazolones. *Electrochim. Acta* 273, 358–366. <https://doi.org/10.1016/j.electacta.2018.04.082>
- Bacil, R.P., Buoro, R.M., Da-Silva, R.P., Medinas, D.B., Lima, A.W., Serrano, S.H., 2012. Mechanism of Electro-Oxidation of Metamizole Using Cyclic Voltammetry at a Glassy Carbon Electrode. *ECS Trans.* 43, 251–258. <https://doi.org/10.1149/1.4704966>
- Bhattacharyya, D.K., Lecomte, M., Rieke, C.J., Garavito, R.M., Smith, W.L., 1996. Involvement of arginine 120, glutamate 524, and tyrosine 355 in the binding of arachidonate and 2-phenylpropionic acid inhibitors to the cyclooxygenase active site of ovine prostaglandin endoperoxide H synthase-

1. J. Biol. Chem. 271, 2179–2184. <https://doi.org/10.1074/jbc.271.4.2179>
- Brett, C.M.A., Maria, A.N.A., Brett, O., 1993. *Electrochemistry: Principles , Methods , and Applications*, 1 ed. ed. Oxford University Press, New York.
- Buoro, R.M., Bacil, R.P., Sanz, C.G., Campos, O.S., Serrano, S.H.P., 2017. Biomimetic behavior and nanomolar detection of hydrogen peroxide on an electrochemically pre-treated hematin modified glassy carbon electrode. *Sensors Actuators B Chem.* 250, 169–178. <https://doi.org/10.1016/j.snb.2017.03.176>
- Buoro, R.M., Campos, O.S., Bacil, R.P., Serrano, S.H.P., 2016. Insights toward the Electrochemical Behavior of Hematin Using a Hematin Modified Glassy Carbon Electrode. *J. Electrochem. Soc.* 163, G178–G185. <https://doi.org/10.1149/2.0021613jes>
- Campanella, L., Di Persio, G., Pintore, M., Tonnina, D., Caretto, N., Martini, E., Lelo, D., 2009. Determination of nonsteroidal anti-inflammatory drugs (NSAIDs) in milk and fresh cheese based on the inhibition of cyclooxygenase. *Food Technol. Biotechnol.* 47, 172–177.
- Courade, J.P., Besse, D., Delchambre, C., Hanoun, N., Hamon, M., Eschalier, A., Caussade, F., Cloarec, A., 2001a. Acetaminophen distribution in the rat central nervous system. *Life Sci.* 69, 1455–1464. [https://doi.org/10.1016/S0024-3205\(01\)01228-0](https://doi.org/10.1016/S0024-3205(01)01228-0)
- Courade, J.P., Caussade, F., Martin, K., Besse, D., Delchambre, C., Hanoun, N., Hamon, M., Eschalier, A., Cloarec, A., 2001b. Effects of acetaminophen on monoaminergic systems in the rat central nervous system. *Naunyn.*

Schmiedebergs. Arch. Pharmacol. 364, 534–537.  
<https://doi.org/10.1007/s002100100484>

Deeb, R.S., Cheung, C., Nuriel, T., Lamon, B.D., Upmacis, R.K., Gross, S.S., Hajjar, D.P., 2010. Physical evidence for substrate binding in preventing cyclooxygenase inactivation under nitrate stress. *J. Am. Chem. Soc.* 132, 3914–3922. <https://doi.org/10.1021/ja910578y>

Dorlet, P., Seibold, S.A., Babcock, G.T., Gerfen, G.J., Smith, W.L., Tsai, A.L., Un, S., 2002. High-field EPR study of tyrosyl radicals in prostaglandin H2 synthase-1. *Biochemistry* 41, 6107–6114. <https://doi.org/10.1021/bi015871f>

El Harrad, L., Bourais, I., Mohammadi, H., Amine, A., 2018. Recent Advances in Electrochemical Biosensors Based on Enzyme Inhibition for Clinical and Pharmaceutical Applications. *Sensors* 18, 164.  
<https://doi.org/10.3390/s18010164>

Engström Ruud, L., Wilhelms, D.B., Eskilsson, A., Vasilache, A.M., Elander, L., Engblom, D., Blomqvist, A., 2013. Acetaminophen reduces lipopolysaccharide-induced fever by inhibiting cyclooxygenase-2. *Neuropharmacology* 71, 124–129.  
<https://doi.org/10.1016/j.neuropharm.2013.03.012>

Gaudin, V., 2017. Advances in biosensor development for the screening of antibiotic residues in food products of animal origin – A comprehensive review. *Biosens. Bioelectron.* 90, 363–377.  
<https://doi.org/10.1016/j.bios.2016.12.005>

Ghanem, C.I., Pérez, M.J., Manautou, J.E., Mottino, A.D., 2016. Acetaminophen



- from liver to brain: New insights into drug pharmacological action and toxicity. *Pharmacol. Res.* 109, 119–131. <https://doi.org/10.1016/j.phrs.2016.02.020>
- Hamberg, M., 1972. Inhibition of prostaglandin synthesis in man. *Biochem. Biophys. Res. Commun.* 49, 720–726. [https://doi.org/10.1016/0006-291X\(72\)90470-6](https://doi.org/10.1016/0006-291X(72)90470-6)
- Hla, T., Neilson, K., 2006. Human cyclooxygenase-2 cDNA. *Proc. Natl. Acad. Sci.* 89, 7384–7388. <https://doi.org/10.1073/pnas.89.16.7384>
- Landino, L.M., Crews, B.C., Timmons, M.D., Morrow, J.D., Marnett, L.J., 1996. Peroxynitrite, the coupling product of nitric oxide and superoxide, activates prostaglandin biosynthesis. *Proc. Natl. Acad. Sci. U. S. A.* 93, 15069–15074. <https://doi.org/10.1073/pnas.93.26.15069>
- Liu, Y., Roth, J.P., 2016. A revised mechanism for human cyclooxygenase-2. *J. Biol. Chem.* 291, 948–958. <https://doi.org/10.1074/jbc.M115.668038>
- McCarty, M.F., Block, K.I., 2006. Preadministration of high-dose salicylates, suppressors of NF- $\kappa$ B activation, may increase the chemosensitivity of many cancers: An example of proapoptotic signal modulation therapy. *Integr. Cancer Ther.* 5, 252–268. <https://doi.org/10.1177/1534735406291499>
- Mitchell, J. a, Saunders, M., Barnes, P.J., Newton, R., Belvisi, M.G., 1997. Sodium salicylate inhibits cyclo-oxygenase-2 activity independently of transcription factor (nuclear factor kappaB) activation: role of arachidonic acid. *Mol. Pharmacol.* 51, 907–912. <https://doi.org/10.1124/mol.51.6.907>
- Mukherjee, A., Brinkley, D.W., Chang, K.M., Roth, J.P., 2007. Molecular oxygen dependent steps in fatty acid oxidation by cyclooxygenase-1. *Biochemistry* 173

46, 3975–3989. <https://doi.org/10.1021/bi602502j>

NHS - NSAIDs [WWW Document], n.d. URL <https://www.nhs.uk/conditions/nsaids/> (accessed 11.16.21).

Noah, N.M., Marcells, O., Almalletti, A., Lim, J., Sadik, O.A., 2011a. Metal Enhanced Electrochemical Cyclooxygenase-2 (COX-2) Sensor for Biological Applications. *Electroanalysis* 23, 2392–2399. <https://doi.org/10.1002/elan.201100241>

Noah, N.M., Mwilu, S.K., Sadik, O.A., Fatah, A.A., Arcilesi, R.D., 2011b. Immunosensors for quantifying cyclooxygenase 2 pain biomarkers. *Clin. Chim. Acta* 412, 1391–1398. <https://doi.org/10.1016/j.cca.2011.04.017>

Orlando, B.J., Lucido, M.J., Malkowski, M.G., 2015. The structure of ibuprofen bound to cyclooxygenase-2. *J. Struct. Biol.* 189, 62–66. <https://doi.org/10.1016/j.jsb.2014.11.005>

Paik, J.H., 2000. Two opposing effects of non-steroidal anti-inflammatory drugs on the expression of the inducible cyclooxygenase- mediation through different signaling pathways. *J. Biol. Chem.* 275, 28173–28179. <https://doi.org/10.1074/jbc.M002329200>

Prakash, P.A., Yogeswaran, U., Chen, S.M., 2009. A review on direct electrochemistry of catalase for electrochemical sensors. *Sensors* 9, 1821–1844. <https://doi.org/10.3390/s90301821>

Shimokawa, T., Kulmacz, R.J., DeWitt, D.L., Smith, W.L., 1990. Tyrosine 385 of prostaglandin endoperoxide synthase is required for cyclooxygenase catalysis. *J. Biol. Chem.* 265, 20073–20076.

- Simmons, D.L., Botting, R.M., HLA, T., 2004. Cyclooxygenase Isozymes: The Biology of Prostaglandin Synthesis and Inhibition. *Pharmacol. Rev.* 56, 387–437. <https://doi.org/10.1124/pr.56.3.3>
- Smith, H.S., 2009. Potential analgesic mechanisms of acetaminophen. *Pain Physician* 12, 269–280.
- Smith, W.L., DeWitt, D.L., 1995. Biochemistry of prostaglandin endoperoxide H synthase-1 and synthase-2 and their differential susceptibility to nonsteroidal anti-inflammatory drugs. *Semin. Nephrol.* 15, 179–194.
- Smith, W.L., DeWitt, D.L., Shimokawa, T., Kraemer, S.A., Meade, E.A., 1990. Molecular basis for the inhibition of prostanoid biosynthesis by nonsteroidal anti-inflammatory agents. *Stroke* 21, IV24--8.
- Smith, W.L., Marnett, L.J., 1991. Prostaglandin endoperoxide synthase: structure and catalysis. *Biochim. Biophys. Acta - Lipids Lipid Metab.* 1083, 1–17. [https://doi.org/10.1016/0005-2760\(91\)90119-3](https://doi.org/10.1016/0005-2760(91)90119-3)
- Thevenot, D.R., Tóth, K., Durst, R.A., Wilson, G.S., 1999. Electrochemical Biosensors: Recommended Definitions and Classification. *Pure Appl. Chem.* 71, 2333–2348. <https://doi.org/10.1351/pac199971122333>
- Tsai, A., Kulmacz, R.J., Palmer, G., 1995. Spectroscopic Evidence for Reaction of Prostaglandin H Synthase-1 Tyrosyl Radical with Arachidonic Acid. *J. Biol. Chem.* 270, 10503–10508. <https://doi.org/10.1074/jbc.270.18.10503>
- Tsai, A.L., Kulmacz, R.J., 2010. Prostaglandin H synthase: Resolved and unresolved mechanistic issues. *Arch. Biochem. Biophys.* 493, 103–124. <https://doi.org/10.1016/j.abb.2009.08.019>

- Tsai, A.L., Kulmacz, R.J., 2000. Tyrosyl radicals in prostaglandin H synthase-1 and -2. *Prostaglandins Other Lipid Mediat.* 62, 231–254. [https://doi.org/10.1016/S0090-6980\(00\)00083-6](https://doi.org/10.1016/S0090-6980(00)00083-6)
- Vane, J.R., Botting, R.M., 2003. The mechanism of action of aspirin. *Thromb. Res.* 110, 255–258. [https://doi.org/10.1016/S0049-3848\(03\)00379-7](https://doi.org/10.1016/S0049-3848(03)00379-7)
- Wu, G., Rogge, C.E., Wang, J.-S., Kulmacz, R.J., Palmer, G., Tsai, A.-L., 2007. Oxyferryl Heme and Not Tyrosyl Radical Is the Likely Culprit in Prostaglandin H Synthase-1 Peroxidase Inactivation †. *Biochemistry* 46, 534–542. <https://doi.org/10.1021/bi061859h>

**Appendix 4 – Electrochemical Cyclooxygenase biosensor to evaluate target – drug viability and interactions.**

**Extraction characterization – Western blotting**

Since the enzyme samples were not commercial ones, western blotting essays were performed to characterize the liver samples and confirm the presence of the enzyme. The presented bands indicate the COX-2 protein expression, figure S1. For endogenous control,  $\beta$ -actin bands were also obtained figure S1.

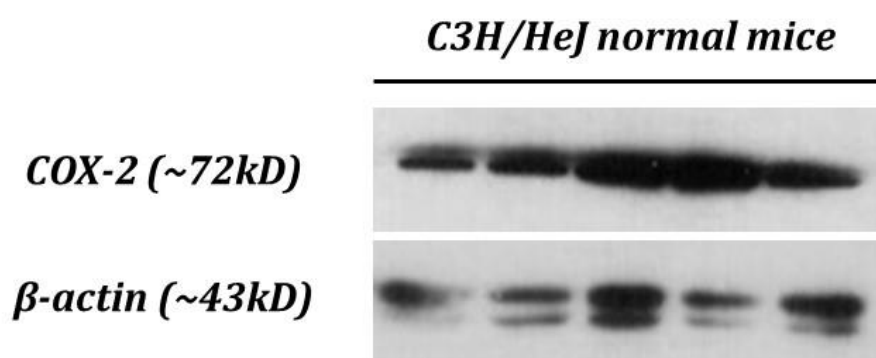


Figure S1. Detection of COX-2 protein expression by western blotting assay. The protein samples were obtained from C3H/HeJ mice's liver from a control group, whose animals were submitted to a fibrosis-associated hepatocarcinogenesis model.

To evaluate the stability of processes Ecp<sub>2</sub> and Ecp<sub>3</sub>, DPVs were performed during 98 minutes, figure S1A and B. During the experiment, Ecp<sub>2</sub> current drop about 84% while Ecp<sub>3</sub> current initially drops 8.76%, keeping steady after that, showing small variations about 1%, figure S1B. As highlighted by Smith et al.<sup>8</sup> reducers can inhibit the COX activity and according to Tsai et al.<sup>14</sup>

reducers in elevated concentration result in an auto-inactivation of the COX. Thus, interactions between the NSAIDs and the peroxidase function of COX can be evaluated by monitoring the process  $E_{ap3}$ . Moreover, NSAIDs might also hinder COX function by binding in allosteric sites.

## **Results and discussion**

This section presents the electrochemical characterization of the electrode modification obtained through different voltammetry techniques (CV, DPV and SWV).

### **Electrochemical Evaluation of *Cyclooxygenase***

#### **Tafel analysis**

To complement the electrochemical characterization, the Tafel plots were obtained from Linear Sweep Voltammetry (LSV), figure 3. The plots strongly indicate that for both processes the first (only) electron reductions are the rate-determining step, due to their slopes of approximately 0.5. The Tafel plots slopes corroborate that  $E_{cp2}$  is the tyrosyl reduction and more, that the  $E_{cp3}$  is the iron reduction from IV to III, which is catalyzed by the peroxide reaction.

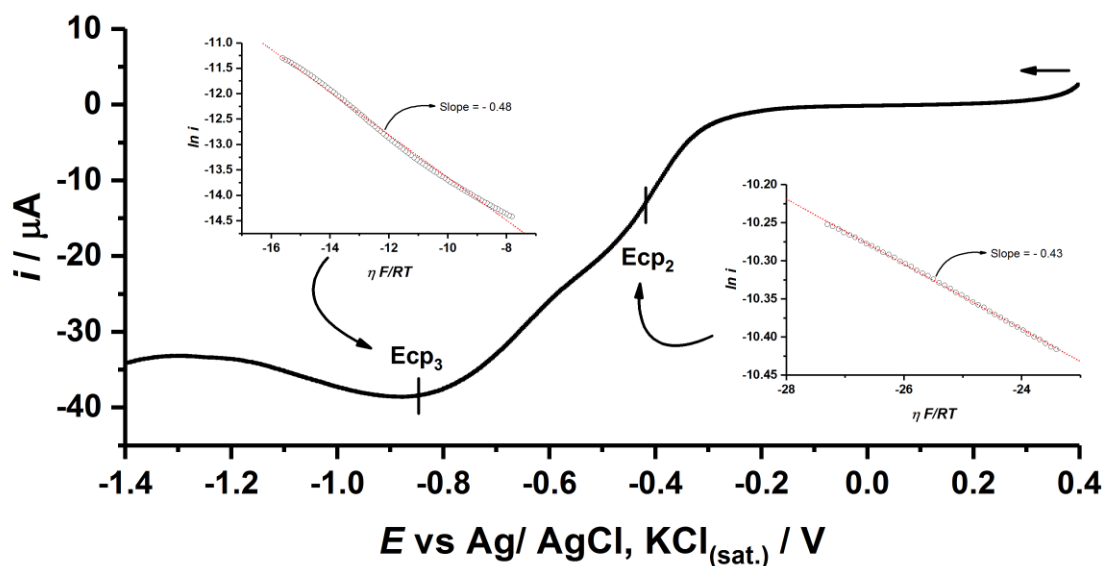
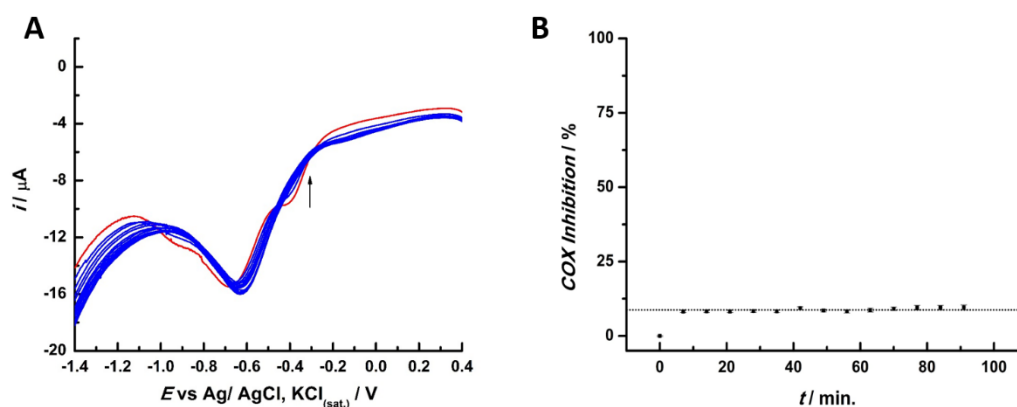


Figure S2: Linear Sweep Voltammetry and the Tafel plots of processes Ecp<sub>2</sub> and Ecp<sub>3</sub>.

### COX interaction with NSAIDs

### GCE@COX electrode stability



Figures S3: A) DPV obtained in GCE-COX at 5mM H<sub>2</sub>O<sub>2</sub> solutions in 0.1 M PB, pH 7.4; B)  $-i$  versus  $t$  plot of the Ecp<sub>3</sub> process from figure 4A.

## Chapter 5

### **Mechanism and kinetics of olanzapine and quetiapine oxidations at glassy carbon electrode.**

In this chapter the electrochemical mechanisms of the atypical antipsychotics olanzapine and quetiapine will be discussed. This work is published in *Electrochimica Acta*, DOI: 10.1016/j.electacta.2020.137683. This manuscript counts with the collaboration of Pedro Garcia in data curation and writing the original draft, and Professor William Reis in data acquisition, data curation, discussions and revision of the original draft, Professor Silvia Serrano administrated the project.

The electrochemical oxidation mechanisms of highly used anti-psychotic drugs olanzapine and quetiapine were systematically studied using cyclic voltammetry in 0.1 M phosphate buffer solutions, at different pH values to better understand their reactivity, effect and eventually its side effects. Olanzapine presents four redox processes: I, which forms a reversible redox process with a cathodic process; II, a proton coupled electron transfer, involving one proton and one electron that occurs at the outer nitrogen of the benzodiazepine ring and have two follow up chemical steps which compete against each other, a dimerization in an EC<sub>2</sub> and a nucleophilic addition in an EC mechanism. The EC mechanism was successfully simulated, and the kinetic parameters were obtained. The processes III and IV are present in both molecules and were ascribed to a sequential oxidation at the outer nitrogen of the piperazine ring,

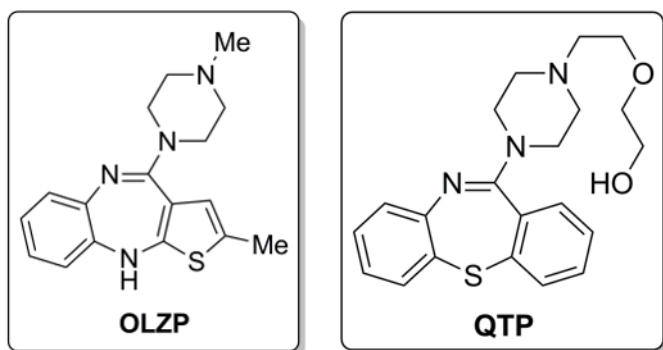


which initially forms an ammonium radical via a proton coupled electron transfer, process III, to later form an imine in process IV.

## **Introduction**

Recently our group addressed the chemical reaction which occurs between the neurotransmitter dopamine (DA) and the highly used anti-psychotic drugs, olanzapine (OLZP) and quetiapine (QTP). [1] During that work it was observed that both drugs react with DA and that the reaction occurs between the catechol moiety of DA and the piperazine moiety of the medicines. The literature partially describes the oxidation mechanism of OLZP, suggesting that it occurs at the nitrogen of the diazepine ring. [2,3] However, it lacks information regarding a more complete redox mechanism to better understand the redox properties of both molecules, mainly the reactivity of the piperazine moieties.

Nowadays, mental disease occurrences have significantly increased. According to WHO (World Health Organization), they affect around 83 million people worldwide [4] Among these diseases schizophrenia is increasing significantly, affecting about 0.7% of the world population. [5] The most common schizophrenia treatment consists of the use of drugs, typical and atypical anti-psychotic drugs, or a combination of both of them, in a treatment known as polypharmacy [6]. Among the drugs, two are notorious, Olanzapine (OLZP) and Quetiapine (QTP). [7]



Scheme 1: Molecular structure of the anti-psychotic drugs olanzapine (OLZP) and quetiapine (QTP).

Although these drugs are relatively safe, their use may result in several side effects. Among them, the neuroleptic malignant syndrome, [8] which is a life-threatening complication, with high fever and weight gain being two of the main symptoms. [9] The weight gain has been used to treat anorexia nervosa and hypertension. [10] Besides, both drugs may cause problems during pregnancy. [11] Therefore, the constant monitoring of their concentration levels and their metabolites in patient's samples is of the utmost importance. [12–14]

As a result, several studies address the detection of these molecules in the literature, most of them utilize HPLC separation techniques with different detectors to quantify OLZP [15–20] and QTP, [4,21] although, the use of different techniques was reported for analytical proposes towards OLZP, such as UV-Vis spectrophotometry, [22] mass spectrometry. [23] Electroanalytical techniques, like potentiometry [24,25], have also been used to analyze both drugs and polarography to detect QTP[26]. Among them, the most used are voltammetric sensors to detect OLZP [2,27–33] and QTP. [34–38] One particular problem is that since these drugs are the most reliable treatment for mental disorders, specially schizophrenia, their utilization has been indiscriminate. [39] This

continuous use could increase the oxidative stress in the patients, which aggravates their health problems. [40] Moreover, both drugs are metabolized by hepatic cytochrome enzymes, known as CYP 450 [41,42], and their use may aggravate hepatic problems, such as cirrhosis. Therefore, the comprehension of their electrochemical mechanism and reactivity could enlighten possible redox interactions.

This work aims to elucidate the electrochemical mechanisms of the highly used anti-psychotic drugs OLZP and QTP in phosphate buffer solutions (PBS) using cyclic voltammetry and digital simulations in aqueous media to better understand their reactivity, effect and eventually side effects.

## **Materials and methods**

### **General Apparatus**

All pH measurements were performed using a model 654 pH meter and a combined glass electrode, model 6.0203.100 (OE), both from Metrohm. All electrochemical experiments were performed in a potentiostat/galvanostat PGSTAT 101, Metrohm AUTOLAB, connected to an IME663 interface stirring device. Data processing was done by version 1.11.4 of NOVA software and the software Origin 2019. A Glassy Carbon Electrode (GCE) with a diameter of 3.0 mm was used as a working electrode, a Silver/ Silver Chloride (+0.222 V vs. SHE) in a saturated solution of potassium chloride and a platinum wire were used as a reference and auxiliary electrodes, respectively, in an electrochemical cell of 20 mL. Before every experiment, the electrochemical cell was degasseddegassed with industrial N<sub>2</sub>, and the GCE was polished using diamond spray suspensions with a decreasing particle size of 3.0, 1.0 and 0.1 μm from Kemet (Maidstone,

UK) on a polishing pad from Buehler (Lake Bluff, Illinois, USA). The solutions were stirred before each electrochemical measurement.

### **Chemicals and reagents**

The buffer reagents were of analytical grade and used without any prior purification, except for QTP and OLZP whose extraction, purification and  $^1\text{H-NMR}$  analysis have been performed according to Bacil et al [1]. The solutions were prepared using deionized water from a reverse osmosis device (Gehara Co., model of ultra-pure OS10LX system, water resistivity  $18\text{M}\Omega\text{cm}$ ).  $0.1\text{ mol L}^{-1}$  phosphate buffer solutions (PBS) were prepared by solubilizing and diluting, respectively, the appropriate amount of  $\text{NaH}_2\text{PO}_4$  and  $\text{H}_3\text{PO}_4$  (Merck) in deionized water and the pH values were adjusted by the addition of a  $4.0\text{ mol L}^{-1}$   $\text{NaOH}$  (Merck) solution. The volumes were measured using EP-10 and EP-100 from Unipettemicroliter Pipettes (Uniscience, Brazil). All experiments were performed at room temperature ( $25 \pm 3\text{ }^\circ\text{C}$ ).

### **Electrochemical procedures**

Cyclic voltammograms (CV) were performed by sweeping the potential ranging from  $-1.0\text{ V}$  to  $1.5\text{ V}$ , then from  $1.5$  and back to  $-1.0\text{ V}$  and in a restricted potential window from  $-0.1\text{ V}$  to  $0.6\text{ V}$ . The scan rates were varied between  $0.01$  and  $10.0\text{ V s}^{-1}$ . All simulations were performed using the EC-Lab software v. 10 40 from BioLogic (Seyssinet-Pariset, France).

### **Results and discussions**

In this section, the voltammetric behaviour of anti-psychotic drugs was studied using cyclic voltammetry. Initially, OLZP and QTP were observed in a wide potential window to observe the electrochemical processes from each

molecule. Secondly, the voltage scan rate was varied to show the nature of the processes and possible follow-up chemical steps. Thirdly, the potential window was restricted, to the first oxidation process of OLZP and it was studied independently and in sequence, digital simulations were obtained to simulate the respective steps experimentally observed. At last, the processes common to both molecules were studied.

### **The electrochemical behaviour of OLZP and QTP**

The experiments, performed, in a wide potential window show that OLZP presents four electrochemical processes. The first OLZP oxidation step occurs at approximately 0.2 (vs Ag/AgCl, KCl<sub>(sat.)</sub>) V, being a reversible process, the oxidation step was labelled as process I and the reduction, process II, figures 1A and 1B. Meanwhile, both OLZP and QTP present two oxidation processes around 0.85 V: process III, and a second one around 1.10 V, process IV, figure 1C. Although the processes III and IV of OLZP are barely defined, it can be observed in figure 1D that both molecules OLZP and QTP present a couple of peaks in the transfer coefficients,  $\beta$ , around the same potential value for both molecules, therefore, being ascribed as the same processes III and IV to both molecules. The transfer coefficients were obtained according to the equation 1. [43,44]

$$\beta = \frac{F}{RT} \frac{d \ln I}{dE} \quad (1)$$

where F is the Faraday constant in C mol<sup>-1</sup>, R is the gas constant in J (K mol)<sup>-1</sup> and T is the temperature in K.

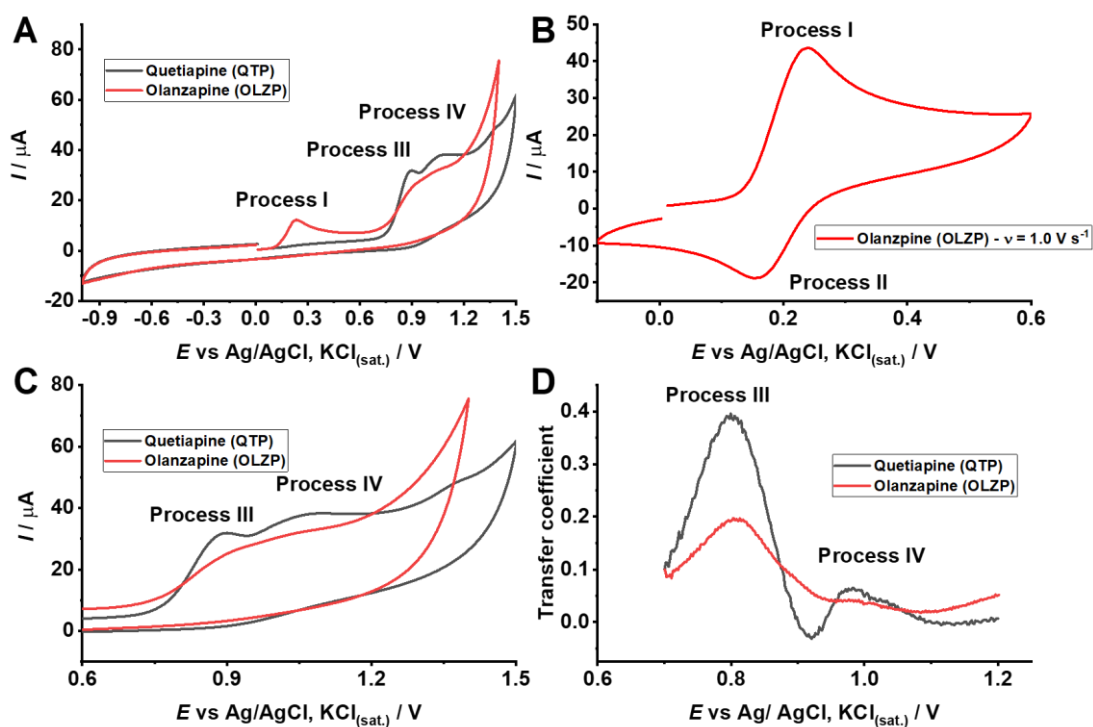


Figure 1: A) CV obtained with GCE in a solution containing 1.0 mM: (red) OLZP, (dark grey) QTP at a wide potential window of -1.0 to 1.4/ 1.5 V in 0.1 M PBS, pH = 7.4.  $v = 0.1 \text{ V s}^{-1}$ ; B) CV obtained with GCE in a solution containing 1.0 mM: (red) OLZP at a restricted potential -0.1 to 0.6 V in 0.1 M PBS, pH = 7.4.  $v = 1.0 \text{ V s}^{-1}$ ; C) CV obtained with GCE in a solution containing 1.0 mM: (red) OLZP at a restricted potential 0.6 V to 1.4/ 1.5 V in 0.1 M PBS, pH = 7.4.  $v = 1.0 \text{ V s}^{-1}$ ; D) Transfer coefficient ( $\beta$ ) as a function of the applied potential obtained from CV presented in figure 1C.

After acknowledging the respective electrochemical processes for each compound, to better study the processes, the scan rate was varied from 0.01 to 1.00  $\text{V s}^{-1}$ . Figure 2A shows that process II only appears at scan rates faster than 0.2  $\text{V s}^{-1}$ , and the peak potential of the process I does not seem to shift as the

scan rate is increased. This result will be further discussed. Simultaneously, the process IV became barely visible. Meanwhile, in figure 2B, processes III and IV are visible and the peak potentials shift to more positive values, as expected to irreversible processes.

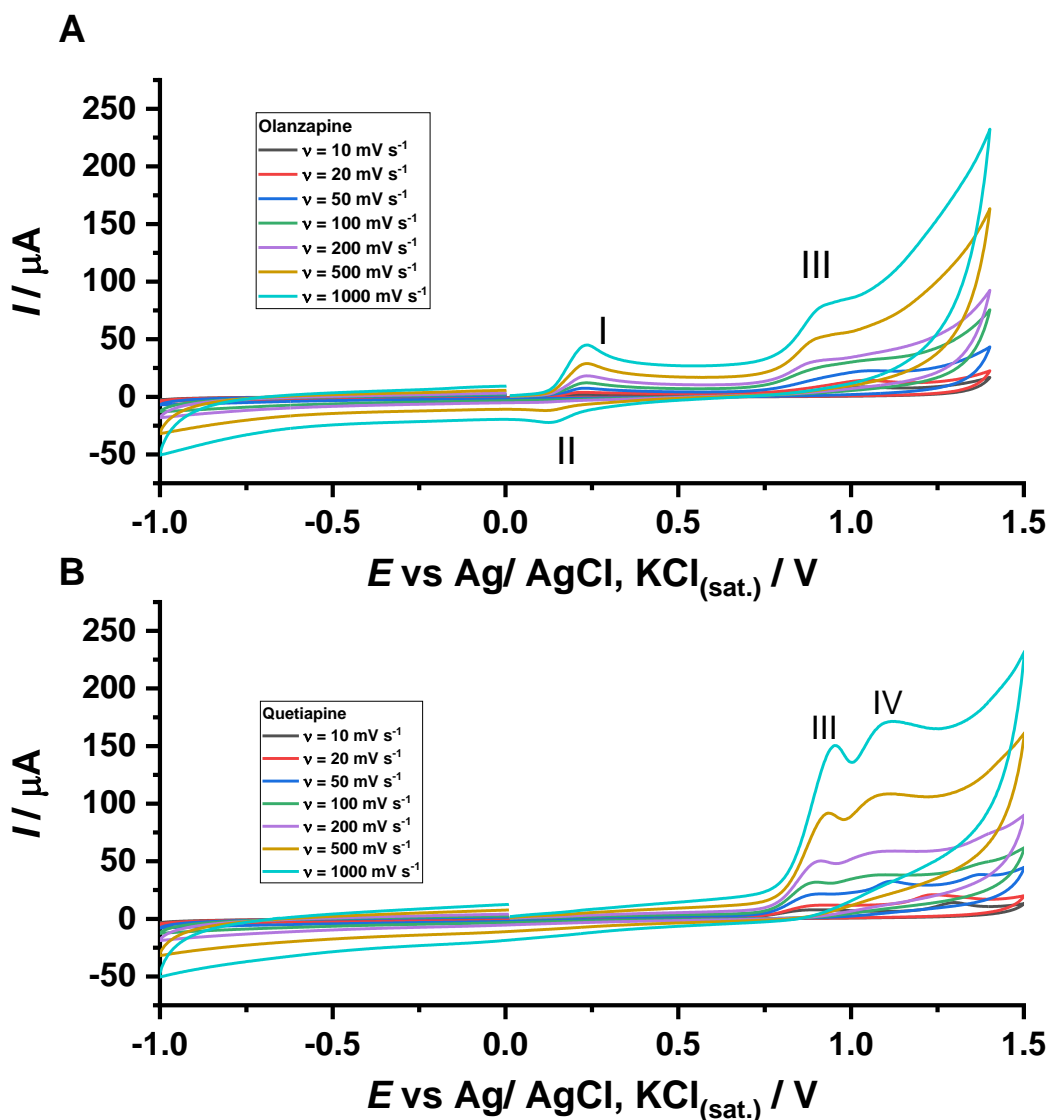


Figure 2: CV obtained with GCE in solutions containing 1.0 mM A) OLZP, B) QTP in 0.1 M PBS, pH = 7.4, the voltage scan rate was varied from 0.01 to 1.00  $\text{V s}^{-1}$ .

### Electrochemical oxidation processes I and II of OLZP

Figure 3A shows CV at a restricted potential window (from -0.1 to 0.6 V) to study the heterogeneous processes I and II of OLZP. At higher scan rates ( $\geq 200 \text{ mV s}^{-1}$ ) the processes I and II of OLZP can be observed as a redox couple. As previously mentioned, the peak potentials of processes I and II barely shifts, as can be observed in figure 3A and table I. Therefore, processes I and II form a reversible process. However, even at very high scan rates, the peak current ratio of the processes I and II tends to 2.5, not the unity, figure 3B. This suggests that process I is followed up by a chemical step that characterizes the process I as an EC mechanism. It is corroborated by the results presented in figure 3C, which shows the Randles-Sevcik theoretical prediction, equations 2, for a reversible process, and 3, for an irreversible process, compared to the experimental peak currents of the oxidation process I of OLZP.

$$I_p = 0.446 nFCA \sqrt{nFvD_0/RT} \quad (2)$$

$$I_p = 0.496 \sqrt{\beta} nFCA \sqrt{nFvD_0/RT} \quad (3)$$

where  $I_p$  is the peak current in A,  $n$  is the overall number of electrons transferred,  $\beta$  is the transfer coefficient,  $F$  is the Faraday Constant in Coulomb  $\text{mol}^{-1}$ ,  $C$  is the concentration in  $\text{mol cm}^{-3}$ ,  $A$  the electrode area in  $\text{cm}^2$ ,  $v$  is the scan rate in  $\text{V s}^{-1}$ ,  $R$  is the Gas Constant in  $\text{J K}^{-1} \text{mol}^{-1}$  and  $T$  is the temperature in K. A diffusion coefficient ( $D_0$ ) of  $4.1 \cdot 10^{-6} \text{ cm}^2 \text{ s}^{-1}$ , was obtained by chronoamperometry, figure S1.

Figure 3C shows that the oxidation mechanism changes with the increase of the scan rate, as the process presents an irreversible behaviour from 0.01 to 188



0.5 V s<sup>-1</sup>, at higher scan rates it changes from irreversible to reversible. This result indicates that the apparent irreversibility of OLZP redox processes occurs due to a follow up chemical step with sufficient fast reaction kinetics, in which even a fast electrons transfer may appear as irreversible.[45,46] Finally, figure 3D shows that the OZLP oxidation process is pH-dependent, as its peak potential shifts as a function of pH with a value of 59 mV per pH unit. Thus, the process I involves the same number of protons as it involves electrons, in this case, one proton and one electron. However, the Pourbaix diagram shows that even in different pH values, the potential peak does not significantly shift as a function of the scan rate.

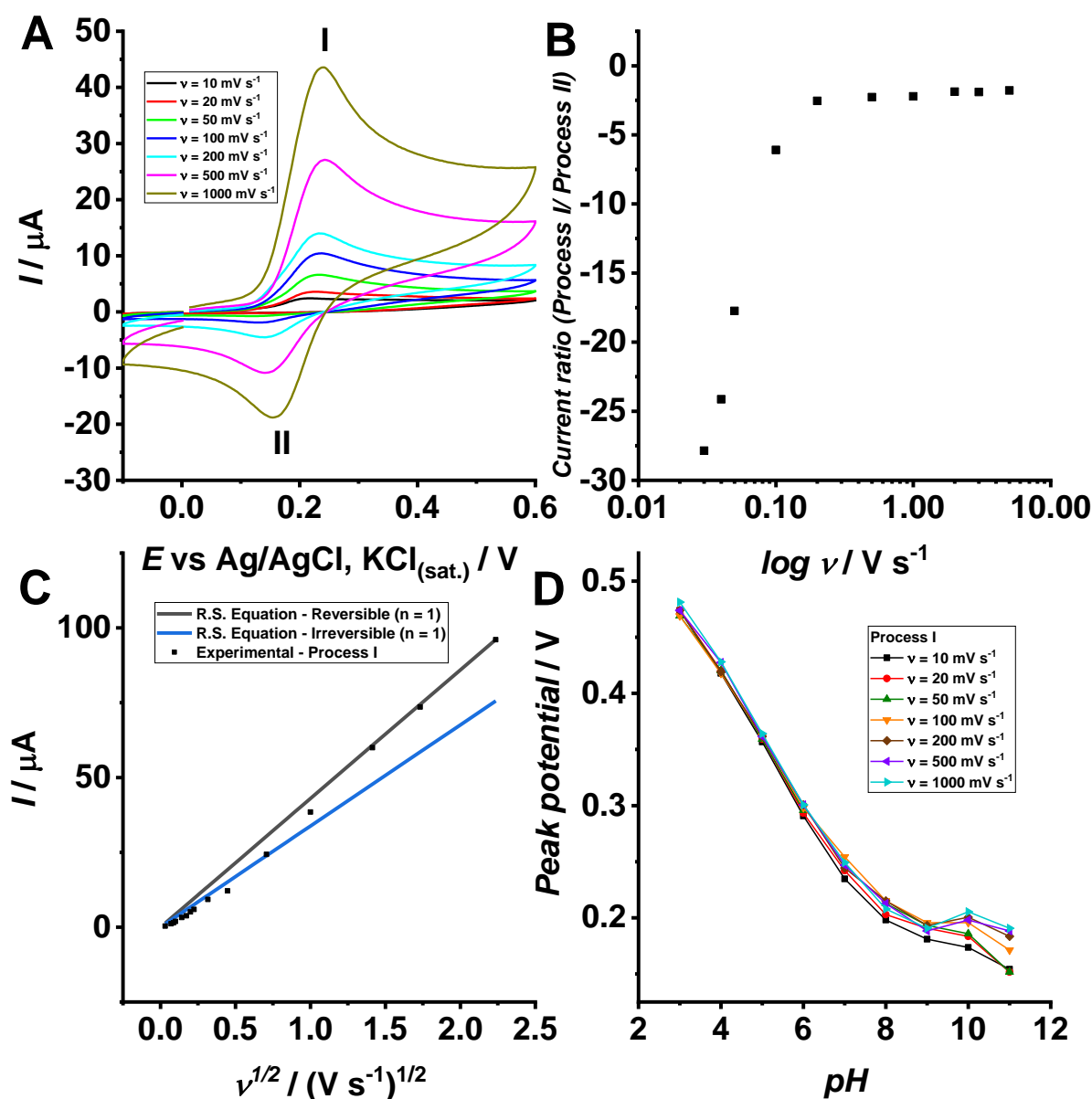


Figure 3: A) CV obtained with GCE in solutions containing 1.0 mM of OLZP in 0.1 M PBS, pH = 7.4, in a restricted window from -0.1 to 0.6 V in various scan rates from 0.01 to 1.00  $\text{V s}^{-1}$ ; B) Peak current ratio (Process I / Process II) as a function of the logarithm of the scan rate; C) Plot of the OLZP oxidation peak current as a function of the square root of the scan rates, compared to the theoretical plots Randles-Sevcik equations (dark grey – reversible, blue – irreversible), Electrode Area = 0.071  $\text{cm}^2$ ; D) OLZP oxidative peak potentials as a function of pH.

Since the transfer coefficient values ( $\beta$ ) are sensitive to the mechanism change in electrochemical processes[47], the Tafel plots were obtained. The values obtained increase as the scan rate is increased from 0.005 to 0.5 V s<sup>-1</sup>, which agrees with the results observed in the comparison between the experimental results and the Randles-Sevcik theoretical prediction. At scan rates higher than 0.5 V s<sup>-1</sup>, the  $\beta$  values decrease from 0.931 to 0.668, suggesting that the electrochemical step kinetics is much faster than the kinetics of the follow-up reaction. Compiling the results obtained to the process I/ II, this process was ascribed to the nitrogen oxidation forming an imine with a radical [48], the radical is then stabilized by the aromatic effect in the benzodiazepine ring, the vicinal already aromatic ring, and the thiophene ring. Therefore, processes I/ II are a proton coupled electron transfer (PCET) which generates a stable radical, that reflects in its fast electrochemical kinetics observed and the electrochemical reversibility even at very high scan rates.

Table 1: Potential peaks of processes I and II from voltammograms presented in figure 3A and  $\beta$  values obtained from the Tafel plots presented in figure 5 at different scan rates.

$v / V s^{-1}$	Ep I / V	Ep II / V	$\beta_1$
0.005	0.206	-	0.649
0.010	0.213	-	0.689

0.030	0.228	-	0.721
0.050	0.231	0.120	0.722
0.100	0.237	0.137	0.726
0.500	0.238	0.143	0.931
1.000	0.241	0.162	0.772
3.000	0.248	0.165	0.739
5.000	0.255	0.166	0.668

---

To better comprehend the follow up chemical step, the peak potentials of the oxidation process I were plotted as a function of the logarithm of the scan rate, figure 4. It shows three different regions, the first one has the follow-up chemical step as the rating determining one, the second region has the heterogeneous process as it rating determining one, and the third region is known as the mixed one due to the ohmic drop and other effects which affect the peak potential. [49,50] At slow scan rates,  $v \leq 0.09 \text{ V s}^{-1}$ , the kinetic region presents a linear fitting that presented a slope of  $24.5 \text{ mV dec}^{-1}$ . This result does not indicate immediately if the follow up chemical step behaves as an EC or EC<sub>2</sub> mechanism since the criteria are of 29.9 and 19.9  $\text{mV dec}^{-1}$  at 25°C [47,51], respectively, as can be observed in equation 4 (EC mechanism) and 5 (EC<sub>2</sub> mechanism).

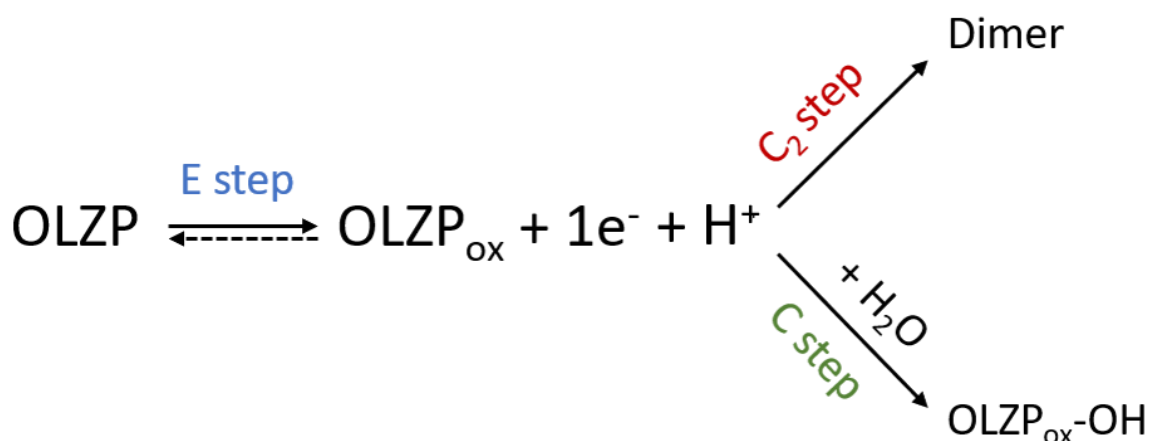
$$\frac{\partial E_p}{\partial \log v} = \frac{2.303RT}{2F} \quad (\text{eq. 4})$$

$$\frac{\partial E_p}{\partial \log v} = \frac{2.303RT}{3F} \quad (\text{eq. 5})$$

where  $E_p$  is the peak potentials in V.

The experimental result is of  $24.5 \text{ mV dec}^{-1}$ , which is the mean value between both criteria, suggesting that both mechanisms could occur in a

competition, as illustrated in scheme 2. This hypothesis is reinforced by Merli et al. in which reports the presence of some products after a exhaustive coulometry that had their products analyzed by HPLC-MS. [2] The first one of a Michael addition of H<sub>2</sub>O after its oxidation (EC mechanism) with a m/z = 329 that corresponds to approximately 60% of the generated product, and an OLZP dimer (EC<sub>2</sub> mechanism) with a m/z = 609. However, Korprasertthaworn et al. reports the products of OLZP after its oxidation with a CYP-450 complex, and the formation of the 7-hydroxyolanzapine (OLZP<sub>ox</sub>-OH) is reported. Therefore, the products of the following chemical steps are the OLZP-OH and a dimer.



Scheme 2: Illustrative competition between chemical steps that follow up OLZP oxidation I process.

From the peak current ratios of the processes I/ II presented in figure 2B, the dimensionless parameter ( $\lambda$ ) was obtained. Through this parameter the chemical rate constant of the following chemical step ( $k_f$ ) was obtained, using the eq. 6. The results are presented in figure 4B.

$$\lambda = \left(\frac{RT}{F}\right)^{k_f/\nu} \quad (\text{eq. 6})$$

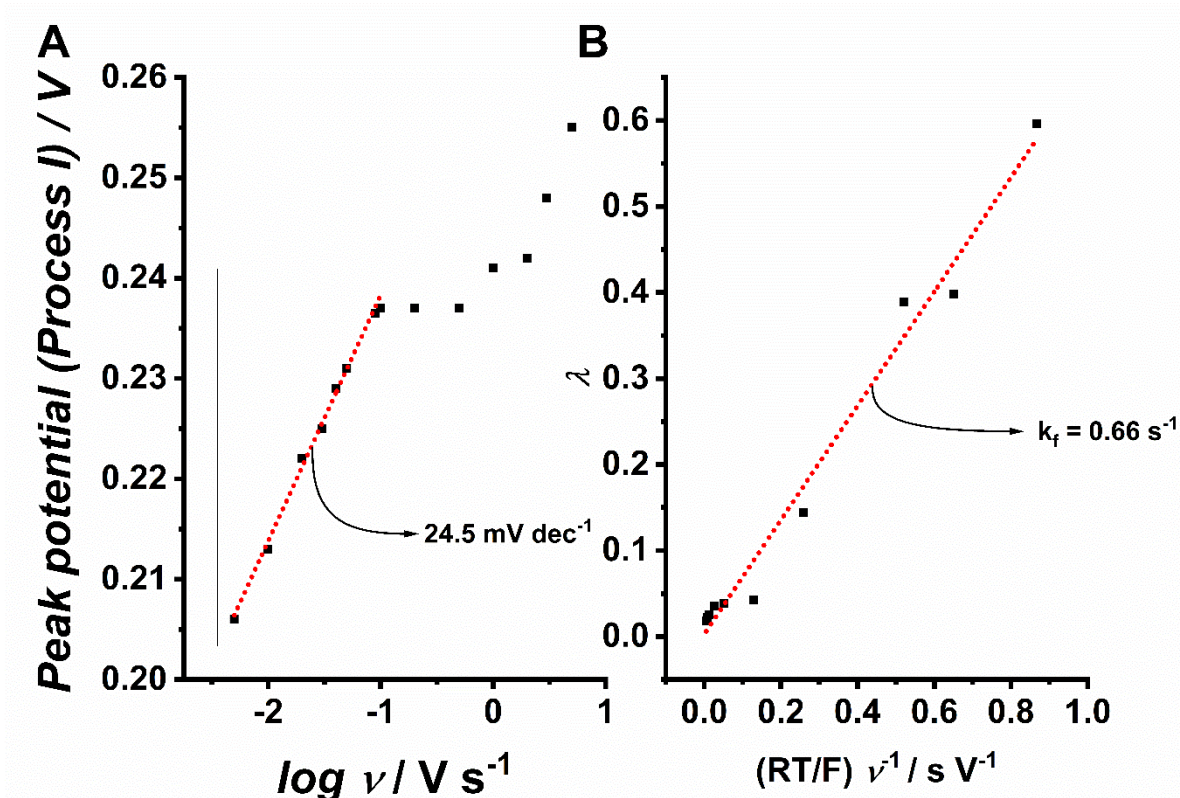


Figure 4: A) Potential peak of OLZP process I as a function of the logarithm of the scan rate.  $E_{p(I)} = 24.5 \cdot 10^{-3} \log v + 0.26$ .  $R^2 = 0.982$  B) Dimensionless parameter ( $\lambda$ ) as a function of the inverse of the scan rate.

### Digital simulations

The EC-Lab software was used to simulate voltammograms at macroelectrodes under linear diffusion conditions with satisfactory precision, using different parameters, such as the heterogeneous rate constant ( $k_0$ ) and the homogeneous rate constants (equilibrium constant, forward reaction rate constant and backward reaction rate constant, represented respectively by  $K$ ,  $k_f$  and  $k_b$ ) which describe the electrochemical and chemical steps, as previously reported by Rudolph et al. [52,53]

As observed in the previous sections, the oxidation process I of OLZP occurs in a competition between an EC and EC<sub>2</sub> mechanism. The simulation

containing the EC<sub>2</sub> mechanism did not present a reasonable fit to the experimental results. Therefore, an electrochemical step with a follow-up chemical reaction (EC mechanism) was simulated, as presented in table 3. The optimization was performed by varying the aforementioned parameters and then comparing the experimental data obtained in a restricted potential window. The optimized parameters used to simulate the system are presented in table 4.

Table 3: Mechanistic steps used to simulate the OLZP system.

Step order	Mechanism simulated	Type of step
1 <sup>st</sup>	$A - e^- \rightarrow B$	Electrochemical
2 <sup>nd</sup>	$B \rightarrow C$	Chemical

Table 4: Optimized parameters for each simulated step, chemical and electrochemical

Step	$E_f^0 / V$	$k^0 / \text{cm s}^{-1}$	$D_0 / \text{cm}^2 \text{s}^{-1}$	$R / \Omega$	$C_{dl} / \mu F$
I/II	0,23	1.0	$4.0 \times 10^{-6}$	125	2.0

Step	K	$K_f / \text{s}^{-1}$	$K_b / \text{s}^{-1}$
Nucleophilic addition	$1 \times 10^5$	0.65	$1.0 \times 10^{-5}$

As previously observed, the processes I/II form a reversible pair. Therefore, a  $k_0$  of  $1.0 \text{ cm s}^{-1}$  was used. The optimized formal potential of the process was 0.23 V. The outline mechanism used to interpret these data can be summarised by the system given in tables 3 and 4. The voltammograms which were simulated with these parameters show a successful fit to the processes I/II with the following chemical step. As previously discussed, at slow scan rates the cathodic peak is not observed, due to the follow up chemical steps, which is reinforced when the scan rate was increased, and the reversibility became visible. Each simulation was evaluated by comparing voltammetric parameters, such as peak currents and peak potentials, the respective peak current ratios and the  $\beta$  values in each scan rate between the simulated voltammograms and the experimental ones. Figures 6A and 6B show the peak current ratios (processes I/II) and the  $\beta$  values obtained from the experimental and simulated voltammograms. Both plots satisfactorily fitted to fast scan rates, above  $0.2 \text{ V s}^{-1}$ . The obtained current ratios were close to the experimental and the  $\beta$  values presented a similar exponential behaviour. However, at slow scan rates, the current ratios presented a similar wavelike shape, although the values were slightly dislocated. In addition, the obtained  $\beta$  values were significantly different, since the  $\beta$  values are sensitive to a mechanism change. This endorses that not only the EC mechanism significantly occurs in both slow and fast scan rates. Although the EC<sub>2</sub> mechanism seems favoured at slow scan rates it probably involves other steps such as adsorption or another complex step, which hindered the simulations involving both mechanisms.



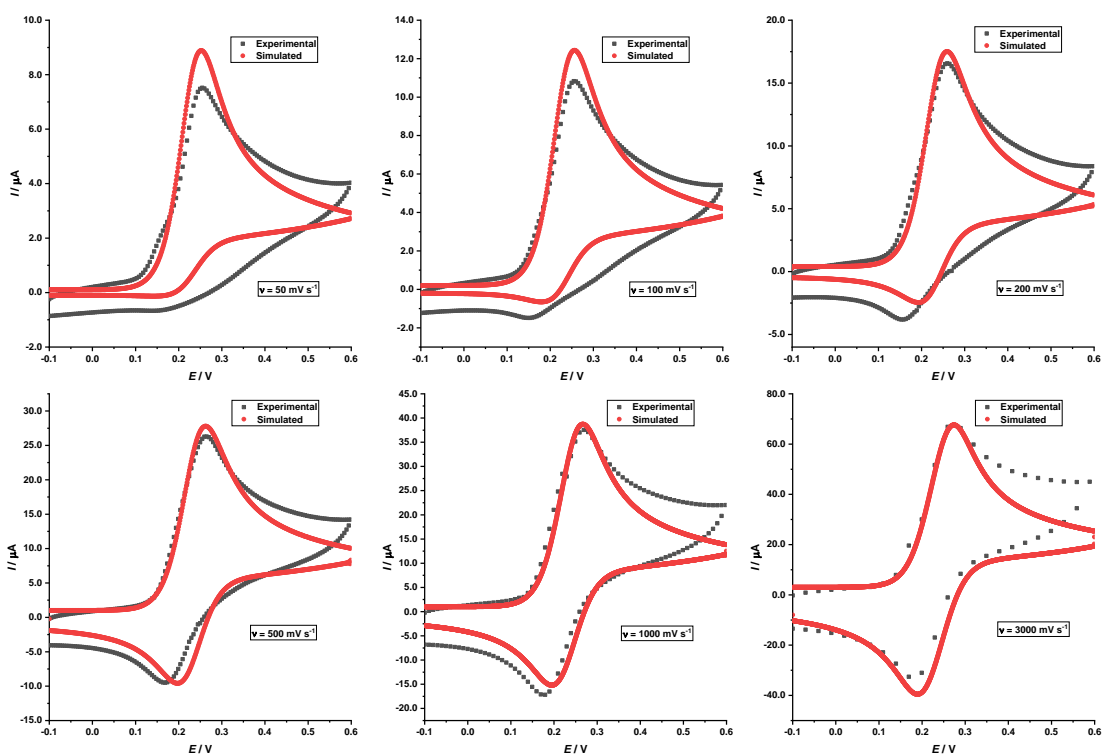


Figure 5: Overlapping between experimental and simulated voltammograms of OLZP process I. The simulations were obtained with the parameters presented in tables 3 and 4.

Table 5: Experimental and simulated  $\beta$  values obtained from the Tafel plots presented in figures S1 and S4 at different scan rates for OLZP oxidation process I.

$v / V s^{-1}$	$\beta$ values - OLZP	
	experimental process	simulated process I
0.05	0.722	0.781
0.10	0.726	0.750
0.20	0.931	0.719
0.50	0.772	0.680

1.00	0.739	0.657
2.00	0.722	0.302
3.00	0.668	0.449

---

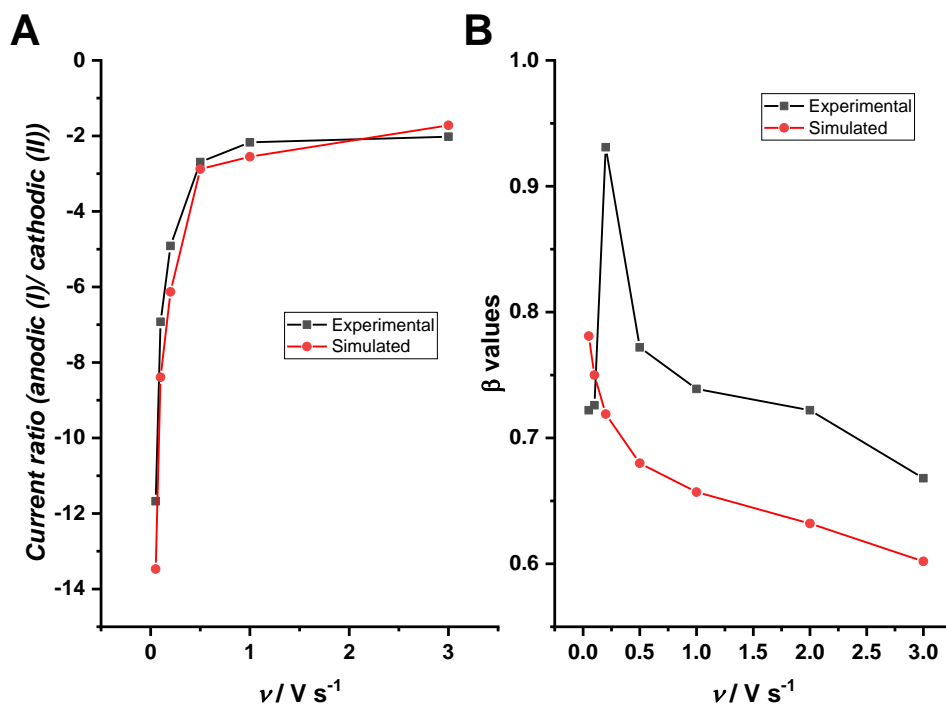


Figure 6: A) Peak current ratios (anodic/cathodic) of the experimental and simulated voltammograms as a function of the scan rates. B) Comparison between the experimental and simulated  $\beta$  values obtained.

### Electrochemical oxidation processes III and IV

This section explores in more detail the processes III and IV of OLZP and QTP using CV at different scan rates and pHs as well as Tafel analysis. It is important to highlight that as previously observed in figure 1, both processes III and IV occur in a similar potential value, and present peaks of transfer coefficients at the same potentials to both molecules.

To discriminate the mechanism of the oxidation processes III and IV of OLZP and QTP the theoretical Randles-Sevcik prediction were used for an irreversible case, equation 3. The figure 7A indicates that process III of OLZP fits the irreversible prediction of the Randles Sevcik equation for a process involving one electron, with a transfer coefficient ( $\beta$ ) of 0.2. This result suggests that the process' kinetics is slow due to the formation of a structurally different intermediary product. A similar result is observed to process IV of QTP, in which the experimental data also fits the irreversible Randles Sevcik equation for a one-electron process with a transfer coefficient of 0.3 (red dots – figure 7B). The experimental results of process III of QTP also fit the theoretical prediction for a one-electron irreversible process, however, presenting a transfer coefficient of 0.9 (black dots – figure 5B), differently than the experimental transfer coefficient of 0.35, obtained in Tafel analysis in figure S6. Figures 7C and 7D show that process III is pH-dependent, shifting approximately 60 mV per pH unit. Therefore, process III is a PCET involving one proton and one electron. The potential peaks shift not only as a function of the pH, but also as a function of the scan rate, as expected to irreversible processes. At last, as observed in figure 1D, processes III and IV are similar to both molecules and its mechanism was attributed based on the the similarities of functional moieties and processes. Since in figures 7C and 7D both presented similar values of pKa around 7.0, and both piperazine moieties present pKas of 7.24 and 7.04, according to software Marvin Sketch predictions, for OLZP and QTP, respectively. The process III in both molecules was ascribed to the formation of an ammonium radical in the piperazine group.

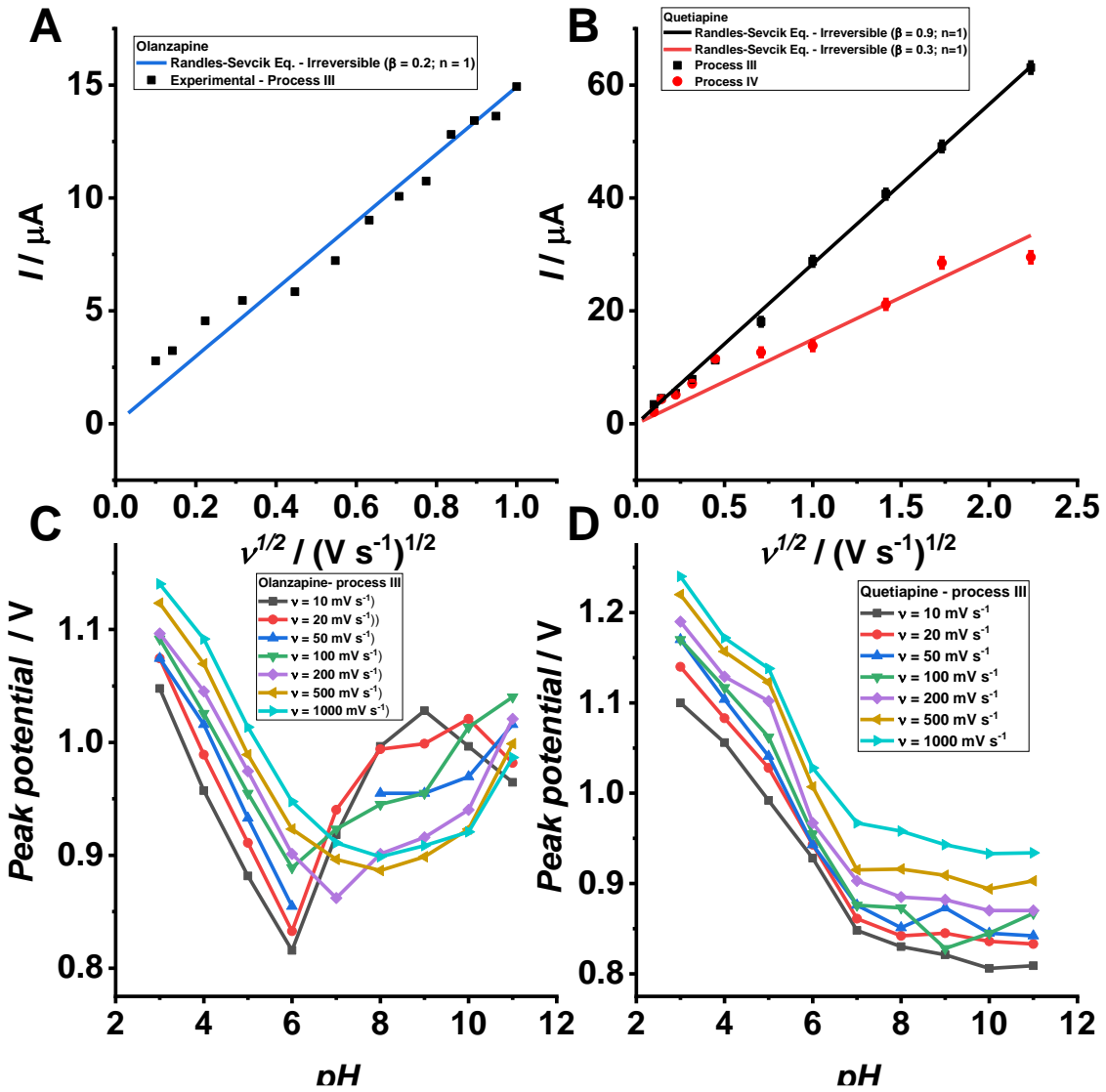


Figure 7: A) Plot of the OLZP oxidation peak current of process III as a function of the square root of the scan rates, compared to the theoretical plots using the Randles-Sevcik equation (blue – irreversible ( $\beta = 0.2; n = 1$ )); B) Plot of the QTP oxidation peak current of process III as a function of the square root of the scan rates, compared to the theoretical plots obtained by Randles-Sevcik equations (black – irreversible ( $\beta = 0.9; n = 1$ ), red – irreversible ( $\beta = 0.3, n=1$ )). Electrode Area =  $0.071 \text{ cm}^2$ ; C) oxidation peak potentials of process III of OLZP as a function of pH; D) oxidation peak potentials of process III of QTP as a function of pH.

As observed in the figures 7A and 7B, the  $\beta$  values of the processes III presented a deviation when compared. Although the Randles-Sevcik theoretical prediction suggests different values, the experimental values obtained from the respective Tafel plots to both compounds presented  $\beta$  values which present a similar exponential behaviour as can be observed in figure 8.

Table 6:  $\beta$  values of oxidative process III of OLZP and QTP, obtained from the Tafel plots at different scan rates presented in figures S5 and S6.

$v / V s^{-1}$	$\beta$ values - OLZP exp process III	$\beta$ values - OLZP exp process IV	$\beta$ values - QTP exp process III	$\beta$ values - QTP exp process IV
0.02	0.136	-	0.316	0.147
0.05	0.158	-	0.344	0.129
0.10	0.174	-	0.348	0.084
0.20	0.180	-	0.351	0.081
0.50	0.185	-	0.354	0.057
1.00	0.192	-	0.356	0.054

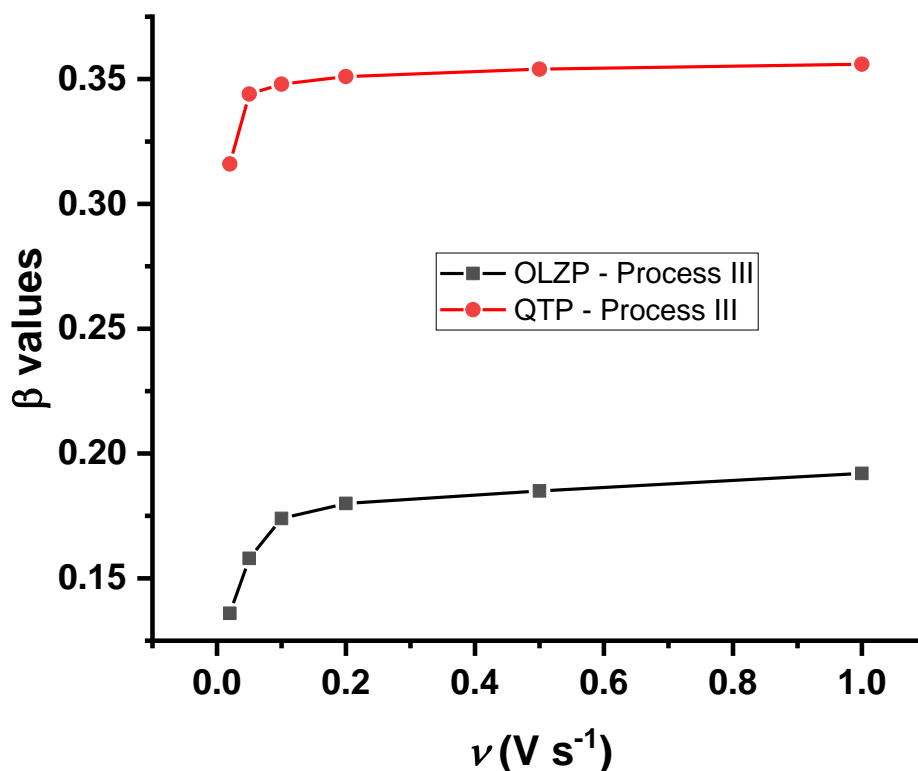


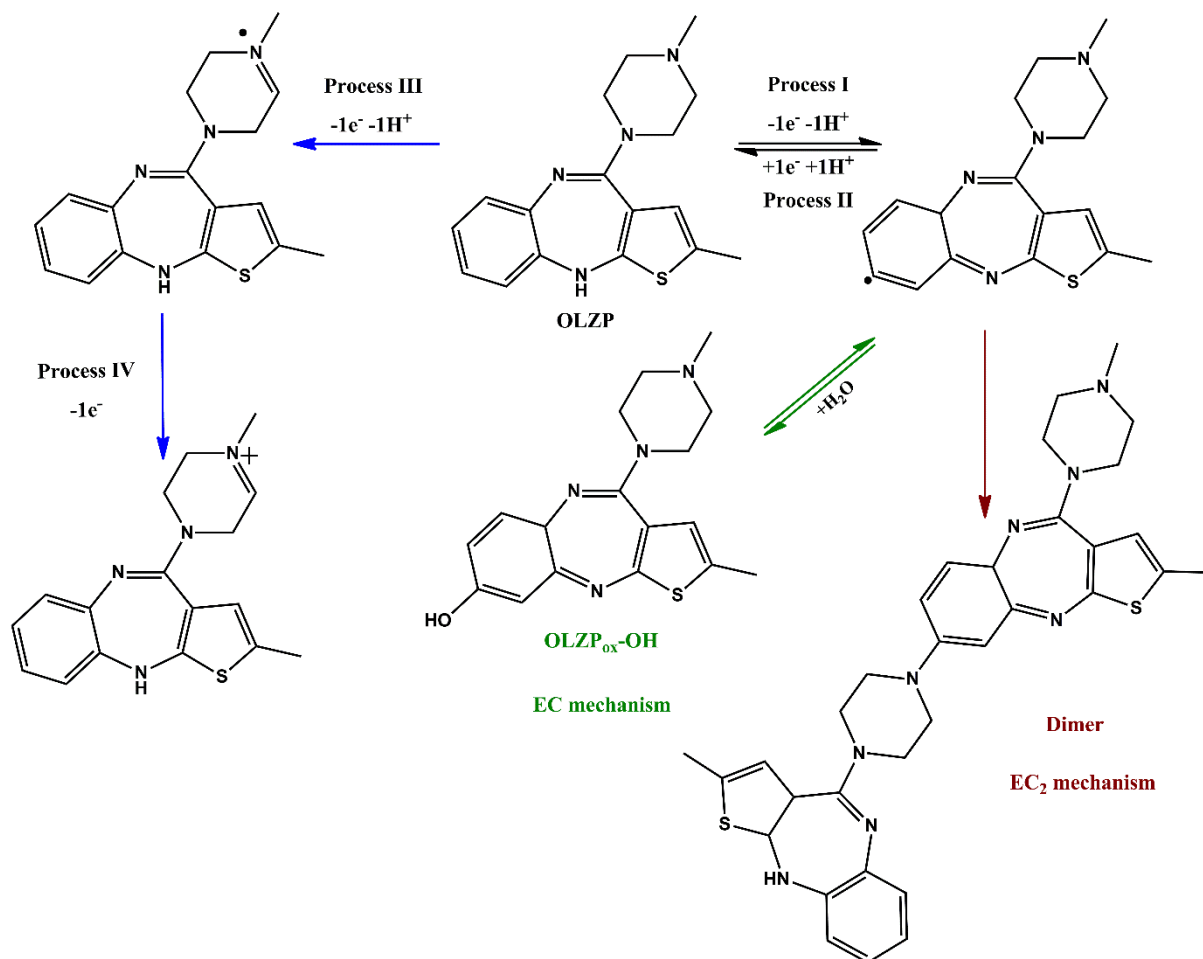
Figure 8: Comparison between the experimental  $\beta$  values of the processes III from OLZP and QTP obtained in the Tafel plots presented in figures S5 and S6.

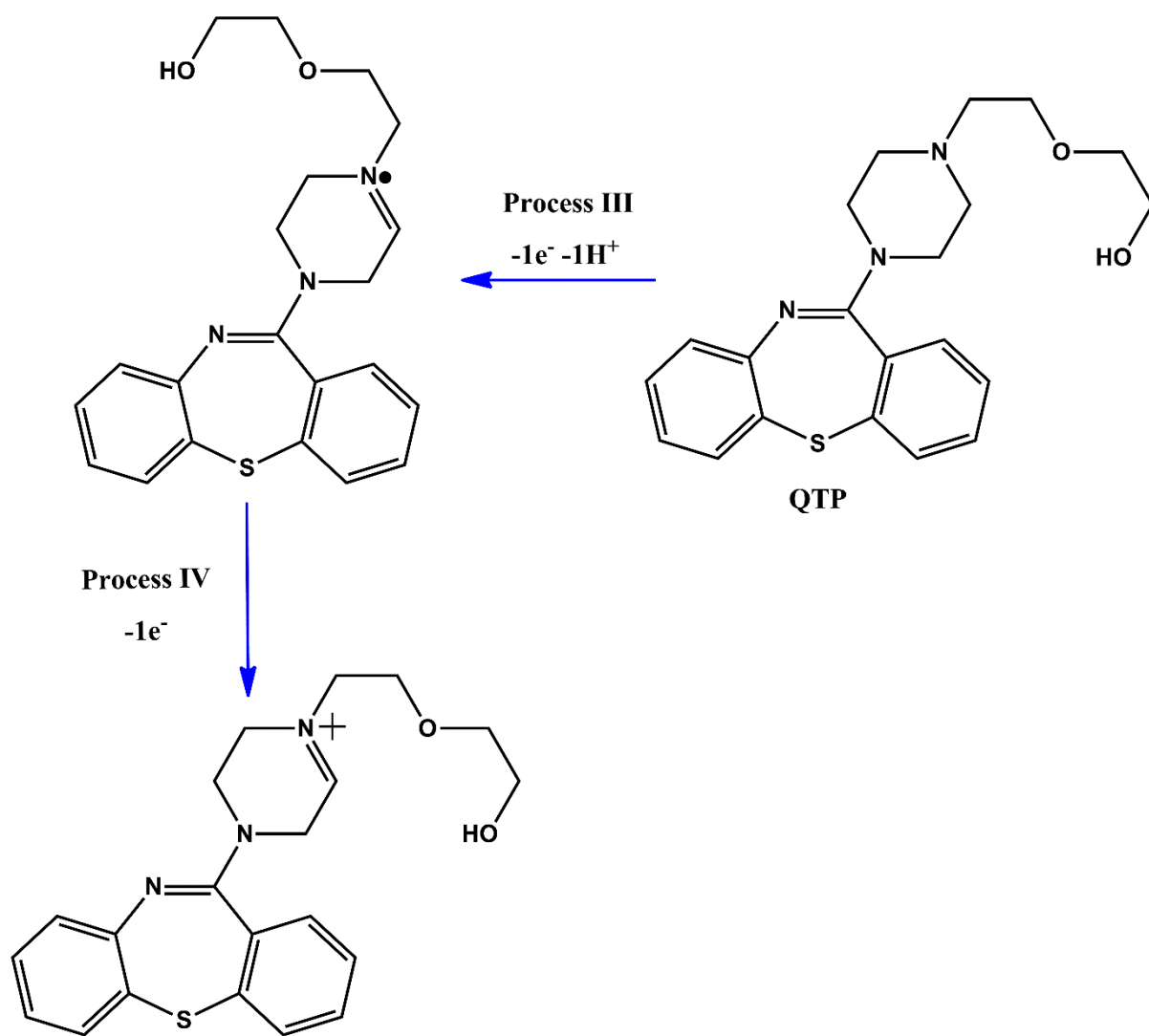
Process IV is only clearly observed in QTP. However, because of the structural similarity, and as both molecules present the same processes at analogous potentials, the QTP results were used to complement the OLZP ones (which are only visible at  $0.1 \text{ V s}^{-1}$ ). The peak potentials of process IV of QTP slightly shift as a function of pH, approximately 150 mV between pHs 3 and 11, which is not significant as observed for process III. Thus, it was concluded that oxidation of process IV only involves one electron and no protons. As a consequence, III and IV, together, are a two-step oxidation process of two electrons and one proton that would occur at the piperazine moiety, forming

initially a tertiary ammonium radical as an intermediary, to in sequence form an imine. It is important to highlight that this process is not reversible because it occurs at an amine and not in an enamine functional group. As observed in previous works from our group, tertiary enamines generate reversible electrochemical processes.[49,54]

### Mechanism proposition

Compiling all the data obtained, the respective electrochemical oxidation mechanism is proposed to both OLZP and QTP at physiological pH.





Scheme 3: Electrochemical oxidation mechanism proposed to OLZP processes I/ II with the follow up chemical processes, III and IV. B) Electrochemical oxidation mechanism proposed to QTP processes III and IV.

### Conclusion

The electrochemical oxidation mechanism of OLZP and QTP was studied using cyclic voltammetry in 0.1 M PBS, at different pH. OLZP presents up to four processes, I/II, which are the reversible redox proton coupled electron transfer involving one proton and one electron that occurs in the outer nitrogen of the benzodiazepine ring and have two follow up chemical steps, a dimerization in an



EC<sub>2</sub> and a nucleophilic addition in an EC mechanism. The EC mechanism was successfully simulated and the kinetic parameters of the chemical step were obtained. The processes III and IV represent sequential oxidation at the outer nitrogen of the piperazine ring, which initially forms an ammonium radical in a proton coupled electron transfer, process III, to later form an imine, process IV. QTP presented only the processes III and IV, and due to the molecular similarity, and analogous results, both were also ascribed to the oxidation of the piperazine ring in the same steps previously described.

### **Acknowledgments**

The authors would like to pay their respects to professor J. M. Savéant (*in memoriam*), who throughout his work inspired and inspires several molecular electrochemists. The authors would like to acknowledge the CNPq projects nº 140833/2016-1 and 310114/2016-0, CAPES project 88881.187396/2018-01 and Fapesp for the grants and funding.

### **References**

- [1] R.P. Bacil, E.A. de O.M. Filho, K. de A. Dias, M.C. Portes, W.R. de Araujo, D. Oliveira-Silva, A.A. dos Santos, L.H. de Andrade, S.H.P. Serrano, The chemical interaction between the neurotransmitter dopamine and the antipsychotic drugs olanzapine and quetiapine., *J. Electroanal. Chem.* (2020).
- [2] D. Merli, D. Dondi, M. Pesavento, A. Profumo, Electrochemistry of olanzapine and risperidone at carbon nanotubes modified gold electrode through classical and DFT approaches, *J. Electroanal. Chem.* 683 (2012) 103–111. doi:10.1016/j.jelechem.2012.08.011.

- [3] S.M. Azab, A.M. Fekry, Role of Green Chemistry in Antipsychotics' Electrochemical Investigations Using a Nontoxic Modified Sensor in McIlvaine Buffer Solution, *ACS Omega*. 4 (2019) 25–30. doi:10.1021/acsomega.8b01972.
- [4] D. Riman, J. Rozsypal, V. Halouzka, J. Hrbac, D. Jirovsky, The use of micro carbon pencil lead electrode for sensitive HPLC-ED analysis of selected antipsychotic drugs, *Microchem. J.* 154 (2020) 104606. doi:10.1016/j.microc.2020.104606.
- [5] J. van Os, S. Kapur, Schizophrenia, *Lancet*. 374 (2009) 635–645. doi:10.1016/S0140-6736(09)60995-8.
- [6] C.-H. Lin, F.-C. Wang, S.-C. Lin, Y.-H. Huang, C.-C. Chen, A randomized, double-blind, comparison of the efficacy and safety of low-dose olanzapine plus low-dose trifluoperazine versus full-dose olanzapine in the acute treatment of schizophrenia, *Schizophr. Res.* 185 (2017) 80–87. doi:10.1016/j.schres.2017.01.004.
- [7] S. Leucht, C. Corves, D. Arbter, R.R. Engel, C. Li, J.M. Davis, Second-generation versus first-generation antipsychotic drugs for schizophrenia: a meta-analysis, *Lancet*. 373 (2009) 31–41. doi:10.1016/S0140-6736(08)61764-X.
- [8] G. K, M. Nagraj, V. R, Olanzapine Induced Fever: A Case Report, *J. Neurobehav. Sci.* 2 (2015) 85. doi:10.5455/JNBS.1443357705.
- [9] L.K. Townsend, W.T. Pepler, N.D. Bush, D.C. Wright, Obesity exacerbates the acute metabolic side effects of olanzapine, *Psychoneuroendocrinology*. 88 (2018) 121–128. doi:10.1016/j.psyneuen.2017.12.004.

- [10] T.N. Peter Bosanac , Graham Burrows, Olanzapine in Anorexia Nervosa, *Aust. New Zeal. J. Psychiatry.* 37 (2003) 494–494. doi:10.1046/j.1440-1614.2003.01221.x.
- [11] A.A. Westin, M. Brekke, E. Molden, E. Skogvoll, I. Castberg, O. Spigset, Treatment With Antipsychotics in Pregnancy: Changes in Drug Disposition, *Clin. Pharmacol. Ther.* 103 (2018) 477–484. doi:10.1002/cpt.770.
- [12] M.-L. Lu, C.-H. Chen, P.-T. Kuo, C.-H. Lin, T.-H. Wu, Application of plasma levels of olanzapine and N -desmethyl-olanzapine to monitor metabolic parameters in patients with schizophrenia, *Schizophr. Res.* 193 (2018) 139–145. doi:10.1016/j.schres.2017.07.022.
- [13] A. Mobed, A. Ahmadalipour, A. Fakhari, S.S. Kazem, G.K. Saadi, Bioassay: A novel approach in antipsychotic pharmacology, *Clin. Chim. Acta.* 509 (2020) 30–35. doi:10.1016/j.cca.2020.05.025.
- [14] L. Patteet, D. Cappelle, K.E. Maudens, C.L. Crunelle, B. Sabbe, H. Neels, Advances in detection of antipsychotics in biological matrices, *Clin. Chim. Acta.* 441 (2015) 11–22. doi:10.1016/j.cca.2014.12.008.
- [15] M. a. Raggi, G. Casamenti, R. Mandrioli, S. Fanali, D. Ronchi, V. Volterra, Determination of the novel antipsychotic drug olanzapine in human plasma using HPLC with amperometric detection, *Chromatographia.* 51 (2000) 562–566. doi:10.1007/BF02490813.
- [16] M.A. Saracino, O. Gandolfi, R. Dall’Olio, L. Albers, E. Kenndler, M.A. Raggi, Determination of Olanzapine in rat brain using liquid chromatography with coulometric detection and a rapid solid-phase extraction procedure, *J. Chromatogr. A.* 1122 (2006) 21–27. doi:10.1016/j.chroma.2006.04.011.

- [17] M. a Raggi, G. Casamenti, R. Mandrioli, V. Volterra, A sensitive high-performance liquid chromatographic method using electrochemical detection for the analysis of olanzapine and desmethylolanzapine in plasma of schizophrenic patients using a new solid-phase extraction procedure., *J. Chromatogr. B. Biomed. Sci. Appl.* 750 (2001) 137–46. <http://www.ncbi.nlm.nih.gov/pubmed/11204214>.
- [18] M.A. Raggi, R. Mandrioli, C. Sabbioni, N. Ghedini, S. Fanali, V. Gobetti, Determination of Olanzapine and Desmethyl-olanzapine in the Plasma of Schizophrenic Patients by Means of an Improved HPLC Method, *Chromatographia*. 54 (2001) 203–207.
- [19] M.A. Raggi, G. Casamenti, R. Mandrioli, G. Izzo, E. Kenndler, Quantitation of olanzapine in tablets by HPLC, CZE, derivative spectrometry and linear voltammetry., *J. Pharm. Biomed. Anal.* 23 (2000) 973–81. <http://www.ncbi.nlm.nih.gov/pubmed/11095298>.
- [20] N. Bergemann, A. Frick, P. Parzer, J. Kopitz, Olanzapine Plasma Concentration, Average Daily Dose, and Interaction with Co-Medication in Schizophrenic Patients, *Pharmacopsychiatry*. 37 (2004) 63–68. doi:10.1055/s-2004-815527.
- [21] P. C. Davis, J. Wong, O. Gefvert, Analysis and pharmacokinetics of quetiapine and two metabolites in human plasma using reversed-phase HPLC with ultraviolet and electrochemical detection, *J. Pharm. Biomed. Anal.* 20 (1999) 271–282. doi:10.1016/S0731-7085(99)00036-9.
- [22] İ. Biryol, N. Erk, Voltammetric, Spectrophotometric, and High Performance Liquid Chromatographic Analysis of Olanzapine, *Anal. Lett.* 36 (2003) 2497–2513. doi:10.1081/AL-120024338.

- [23] G. Zhang, A. V. Terry, M.G. Bartlett, Liquid chromatography/tandem mass spectrometry method for the simultaneous determination of olanzapine, risperidone, 9-hydroxyrisperidone, clozapine, haloperidol and ziprasidone in rat plasma, *Rapid Commun. Mass Spectrom.* 21 (2007) 920–928. doi:10.1002/rcm.2914.
- [24] M. Rouhani, A. Soleymanpour, A new selective carbon paste electrode for potentiometric analysis of olanzapine, *Measurement.* 140 (2019) 472–478. doi:10.1016/j.measurement.2019.04.018.
- [25] H. Arida, A New Coated Wire Selective Electrode for Quetiapine in Biological and Pharmaceutical Analysis, *Int. J. Electrochem. Sci.* 12 (2017) 4120–4133. doi:10.20964/2017.05.76.
- [26] N. El-Enany, A. El-Brashy, F. Belal, N. El-Bahay, Polarographic Analysis of Quetiapine in Pharmaceuticals, *Port. Electrochim. Acta.* 27 (2009) 113–125. doi:10.4152/pea.200902113.
- [27] H.S. El-Desoky, A. Khalifa, M.M. Abdel-Galeil, An advanced and Facile Synthesized Graphene/Magnetic Fe<sub>3</sub>O<sub>4</sub> Nanoparticles Platform for Subnanomolar Voltammetric Determination of Antipsychotic Olanzapine Drug in Human Plasma, *J. Electrochem. Soc.* 167 (2020) 067527. doi:10.1149/1945-7111/ab8366.
- [28] R.P. Shukla, R.H. Belmaker, Y. Bersudsky, H. Ben-Yoav, A platinum black-modified microelectrode for in situ olanzapine detection in microliter volumes of undiluted serum, *J. Neural Transm.* 127 (2020) 291–299. doi:10.1007/s00702-019-02139-0.

- [29] S. a. Ozkan, B. Dogan, B. Uslu, Voltammetric Analysis of the Novel Atypical Antipsychotic Drug Quetiapine in Human Serum and Urine, *Microchim. Acta.* 153 (2006) 27–35. doi:10.1007/s00604-005-0457-x.
- [30] M. Arvand, S. Orangpour, N. Ghodsi, Differential pulse stripping voltammetric determination of the antipsychotic medication olanzapine at a magnetic nano-composite with a core/shell structure, *RSC Adv.* 5 (2015) 46095–46103. doi:10.1039/C5RA00061K.
- [31] M. Arvand, B. Palizkar, Development of a modified electrode with amine-functionalized TiO<sub>2</sub>/multi-walled carbon nanotubes nanocomposite for electrochemical sensing of the atypical neuroleptic drug olanzapine, *Mater. Sci. Eng. C.* 33 (2013) 4876–4883. doi:10.1016/j.msec.2013.08.002.
- [32] L. Mohammadi-Behzad, M.B. Gholivand, M. Shamsipur, K. Gholivand, A. Barati, A. Gholami, Highly sensitive voltammetric sensor based on immobilization of bisphosphoramidate-derivative and quantum dots onto multi-walled carbon nanotubes modified gold electrode for the electrocatalytic determination of olanzapine, *Mater. Sci. Eng. C.* 60 (2016) 67–77. doi:10.1016/j.msec.2015.10.068.
- [33] G. Muthusankar, A. Sangili, S.-M. Chen, R. Karkuzhali, M. Sethupathi, G. Gopu, S. Karthick, R.K. Devi, N. Sengottuvelan, In situ assembly of sulfur-doped carbon quantum dots surrounded iron(III) oxide nanocomposite; a novel electrocatalyst for highly sensitive detection of antipsychotic drug olanzapine, *J. Mol. Liq.* 268 (2018) 471–480. doi:10.1016/j.molliq.2018.07.059.
- [34] M.A. El-Shal, Electrochemical studies for the determination of quetiapine fumarate and olanzapine antipsychotic drugs., *Adv. Pharm. Bull.* 3 (2013) 339–44. doi:10.5681/apb.2013.055.

- [35] M. Ławrywianiec, J. Smajdor, B. Paczosa-Bator, R. Piech, Application of a glassy carbon electrode modified with carbon black nanoparticles for highly sensitive voltammetric determination of quetiapine, *Anal. Methods*. 9 (2017) 6662–6668. doi:10.1039/C7AY02140B.
- [36] B. Nigović, A. Mornar, M. Sertić, Graphene nanocomposite modified glassy carbon electrode for voltammetric determination of the antipsychotic quetiapine, *Microchim. Acta*. 183 (2016) 1459–1467. doi:10.1007/s00604-016-1781-z.
- [37] B. Nigović, J. Spajić, A novel electrochemical sensor for assaying of antipsychotic drug quetiapine., *Talanta*. 86 (2011) 393–9. doi:10.1016/j.talanta.2011.09.033.
- [38] A. Motaharian, K. Naseri, O. Mehrpour, S. Shoeibi, Electrochemical determination of atypical antipsychotic drug quetiapine using nano-molecularly imprinted polymer modified carbon paste electrode, *Anal. Chim. Acta*. 1097 (2020) 214–221. doi:10.1016/j.aca.2019.11.020.
- [39] F.M. Volpe, A.S. Santos, L.S. Rodrigues, R.R. Rocha, P.G. de Magalhães, C.M. Ruas, Current inpatient prescription practices for the treatment of schizophrenia in public hospitals of Minas Gerais, Brazil, *Rev. Bras. Psiquiatr.* 39 (2017) 190–192. doi:10.1590/1516-4446-2016-2047.
- [40] C.J. Carter, Schizophrenia susceptibility genes converge on interlinked pathways related to glutamatergic transmission and long-term potentiation, oxidative stress and oligodendrocyte viability, *Schizophr. Res.* 86 (2006) 1–14. doi:10.1016/j.schres.2006.05.023.

- [41] B.K. Laurence Brunton, Bruce A. Chabner, Goodman and Gilman's The Pharmacological Basis of Therapeutics, Twelfth Ed, 2011. doi:10.1213/00000539-198611000-00041.
- [42] C. Hiemke, P. Baumann, N. Bergemann, A. Conca, O. Dietmaier, K. Egberts, M. Fric, M. Gerlach, C. Greiner, G. Gründer, E. Haen, U. Havemann-Reinecke, E. Jaquenoud Sirot, H. Kirchherr, G. Laux, U. Lutz, T. Messer, M. Müller, B. Pfuhlmann, B. Rambeck, P. Riederer, B. Schoppek, J. Stingl, M. Uhr, S. Ulrich, R. Waschgler, G. Zernig, AGNP Consensus Guidelines for Therapeutic Drug Monitoring in Psychiatry: Update 2011, *Pharmacopsychiatry*. 44 (2011) 195–235. doi:10.1055/s-0031-1286287.
- [43] D. Li, C. Lin, C. Batchelor-McAuley, L. Chen, R.G. Compton, Tafel analysis in practice, *J. Electroanal. Chem.* 826 (2018) 117–124. doi:10.1016/j.jelechem.2018.08.018.
- [44] D. Li, C. Batchelor-McAuley, L. Chen, R.G. Compton, Electrocatalysis via Intrinsic Surface Quinones Mediating Electron Transfer to and from Carbon Electrodes, *J. Phys. Chem. Lett.* 11 (2020) 1497–1501. doi:10.1021/acs.jpcllett.9b03638.
- [45] I. Streeter, S.F. Jenkinson, G.W.J. Fleet, R.G. Compton, Chemical instability promotes apparent electrochemical irreversibility: Studies on the electrode kinetics of the one electron reduction of the 2,6-diphenylpyrylium cation in acetonitrile solution, *J. Electroanal. Chem.* 600 (2007) 285–293. doi:10.1016/j.jelechem.2006.10.006.
- [46] R.P. Bacil, L. Chen, S.H.P. Serrano, R.G. Compton, Dopamine oxidation at gold electrodes: mechanism and kinetics near neutral pH, *Phys. Chem. Chem. Phys.* 22 (2020) 607–614. doi:10.1039/C9CP05527D.



- [47] C.E. Banks, R.G. Compton, *Understanding Voltammetry*, 3rd Ed., World Scientific Press Company, 2018.
- [48] S. Shahrokhian, M. Azimzadeh, P. Hosseini, Modification of a glassy carbon electrode with a bilayer of multiwalled carbon nanotube/benzene disulfonate-doped polypyrrole: application to sensitive voltammetric determination of olanzapine, *RSC Adv.* 4 (2014) 40553–40560. doi:10.1039/C4RA04584J.
- [49] R.P. Bacil, R.M. Buoro, O.S. Campos, M.A. Ramos, C.G. Sanz, S.H.P. Serrano, Electrochemical behaviour of dipyrone (metamizole) and others pyrazolones, *Electrochim. Acta.* 273 (2018) 358–366. doi:10.1016/j.electacta.2018.04.082.
- [50] D. Pletcher, *Instrumental Methods in Electrochemistry*, 1st ed., Woodhead Publishing Limited, Southampton, 2001. <http://books.google.com/books?hl=en&lr=&id=Q6CjAgAAQBAJ&oi=fnd&pg=PP1&dq=Instrumental+Methods+in+Electrochemistry&ots=SjBuoNFS7W&sig=WTGL4H8jY8OCaPLMoulGimWeADY>.
- [51] J.-M. Savéant, *Elements of Molecular and Biomolecular Electrochemistry*, John Wiley & Sons, Inc., Hoboken, NJ, USA, 2006. doi:10.1002/0471758078.
- [52] M. Rudolph, A fast implicit finite difference algorithm for the digital simulation of electrochemical processes, *J. Electroanal. Chem. Interfacial Electrochem.* 314 (1991) 13–22. doi:10.1016/0022-0728(91)85425-O.
- [53] M. Rudolph, Digital simulations with the fast implicit finite difference (FIFD) algorithm, *J. Electroanal. Chem.* 338 (1992) 85–98. doi:10.1016/0022-0728(92)80415-Z.

[54] R.P. Bacil, R.M. Buoro, R.P. Da-Silva, D.B. Medinas, A.W. Lima, S.H. Serrano, Mechanism of Electro-Oxidation of Metamizole Using Cyclic Voltammetry at a Glassy Carbon Electrode, in: ECS Trans., 2012: pp. 251–258. doi:10.1149/1.4704966.

## Appendix 5 - Olanzapine and quetiapine oxidation mechanism in glassy carbon electrode at physiological pH.

### The obtention of the diffusion coefficients of OLZP and QTP

To study the electrochemical mechanisms of OLZP and QTP using the Randles-Sevcik theoretical prediction, the diffusion coefficient ( $D_0$ ) in the experimental conditions must be known. To obtain its value, the chronoamperometry experiment which is described by the Cottrell equation<sup>1</sup>, equation S1, was performed.

$$I = \frac{nFAC\sqrt{D_0}}{\sqrt{\pi t}} \quad (\text{equation S1})$$

$$I = Kt^{-1/2}; K = \frac{nFAC\sqrt{D_0}}{\sqrt{\pi}} \quad (\text{equation S2})$$

where  $I$  is the current in A,  $n$  is the overall number of electrons transferred,  $F$  is the Faraday Constant in Coulomb  $\text{mol}^{-1}$ ,  $C$  is the concentration in  $\text{mol cm}^{-3}$ ,  $A$  the electrode area in  $\text{cm}^2$ ,  $D_0$  is the diffusion coefficient in  $\text{cm s}^{-1}$  and  $t$  is the time in seconds.

Figures S1 and S2 show the typical exponential behaviour of a chronoamperogram, while the inserts show the linear plot of the current as a function of the inverse of the square root of the time. The slopes observed were of  $D_0/n = 4.127 \cdot 10^{-6}$  and  $3.984 \cdot 10^{-6}$ , which in this case is the diffusion coefficient, since the processes involve one electron.

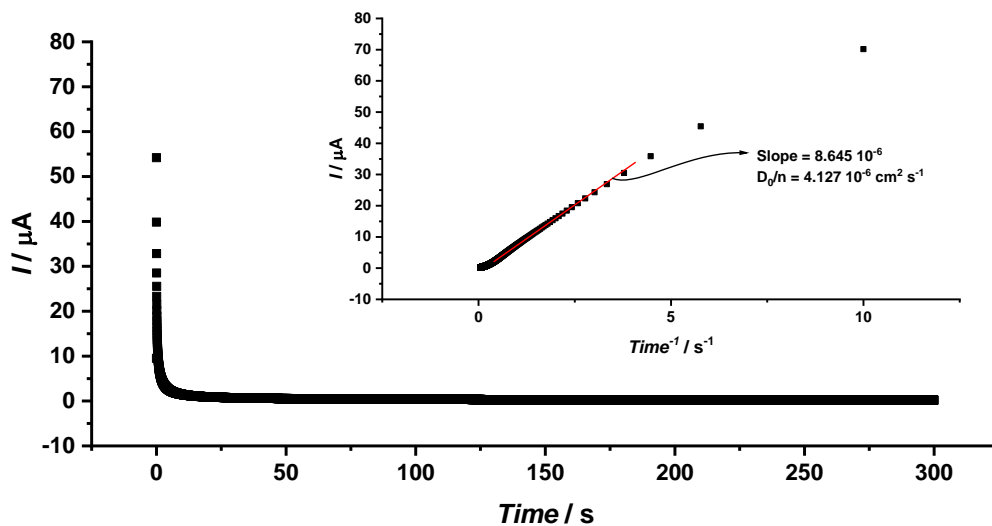


Figure S1: Cronoamperogram at GCE of a solution 1.0mM of OLZP in PBS 0.1M, pH = 7.4,  $E_{\text{app}} = 0.25 \text{ V}$ . Insert: Current as a function of the inverse of the square root of the time, in minutes.

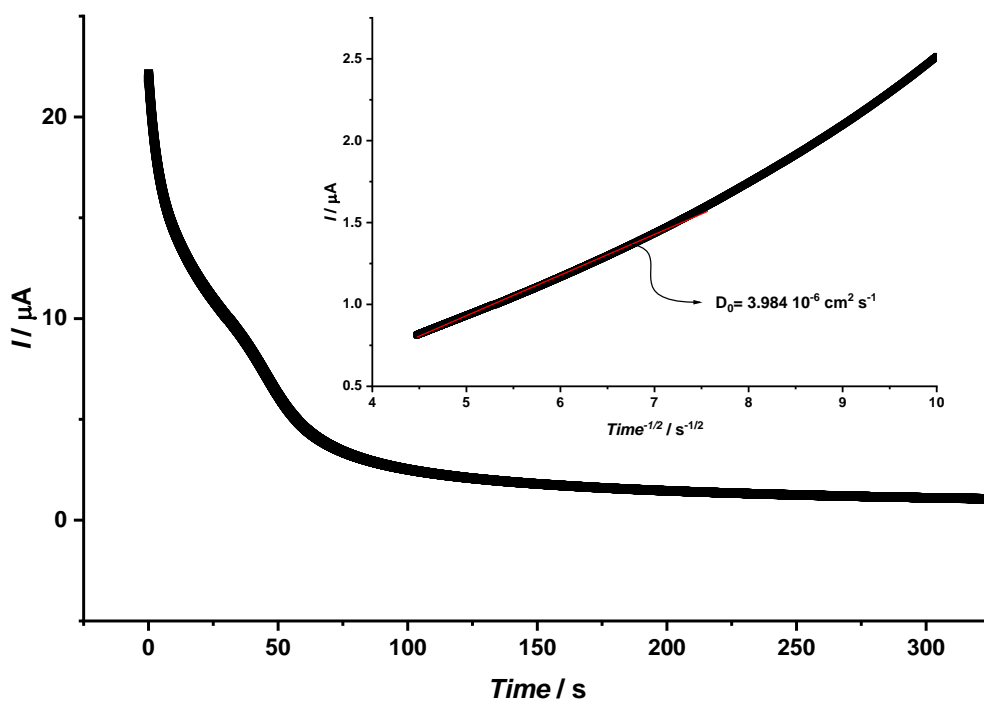


Figure S2: Cronoamperogram at GCE of a solution 1.0mM of QTP in PBS 0.1M, pH = 7.4,  $E_{app} = 1.25$  V. Insert: Current as a function of the inverse of the square root of the time, in seconds.

### **Electrochemical oxidation processes I and II of OLZP**

Since the charge transfer coefficients are related to the electrochemical mechanism, even a subtle mechanism change can be observed. To study the processes I/II of OLZP and processes II and IV in both compounds, the Tafel plots were obtained.

### **Tafel Plots and charge transfer coefficients ( $\beta$ ).**

Figure S3 shows that all obtained  $\beta$  values are between 0 and 1, which is expected considering a process involving one electron. At slow scan rates, from  $0.1 \text{ V s}^{-1}$  and below, a break can be observed in the Tafel analysis, therefore two  $\beta$  values were obtained. This break is a result of the mechanism competition between  $EC_2$  and EC, which as can be observed in figures 5, 6A and 6B. At scan rates above  $0.5 \text{ Vs}^{-1}$ , the  $\beta$  values decrease, indicating that the kinetics of the chemical step in the EC mechanism is being overcome by the heterogeneous kinetics. As a result of the greater electrode kinetics, the cathodic step increases, until it reaches the current ratio of one ( $I_p \text{ I} / I_p \text{ II} = 1$ ).

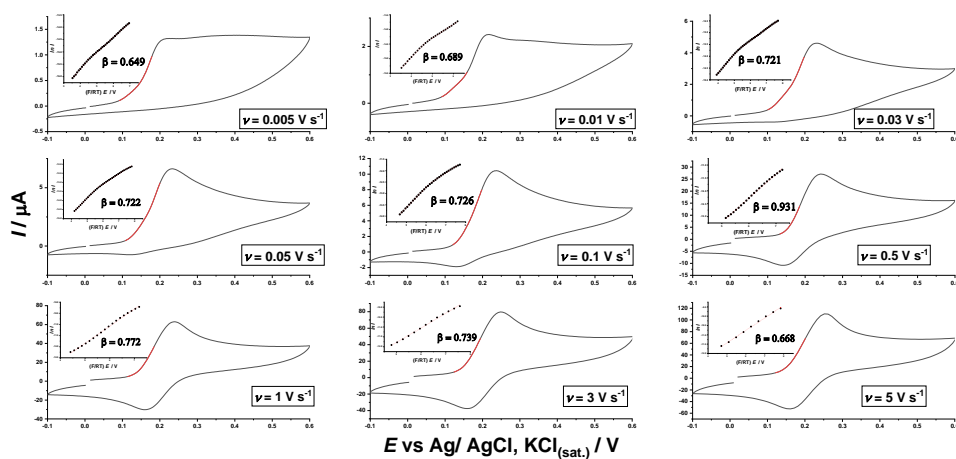


Figure S3: CV presented in figure 3A with the respective Tafel plots as inset. The red parts of the voltammograms show the part of the curve sub-plotted to the Tafel analysis as in the insets. The parameters used in the simulations are presented in table 1.

The digital simulation was performed to a mechanism EC, which occurs more significantly, when compared to the EC<sub>2</sub>. The  $\beta$  values obtained from the simulated voltammograms presented the same exponential profile, observed in the experimental data, at fast scan rates. On the other hand, the EC<sub>2</sub> mechanism heavily impacts the  $\beta$  values at slow scan rates, as shown in figures 6A and 6B.

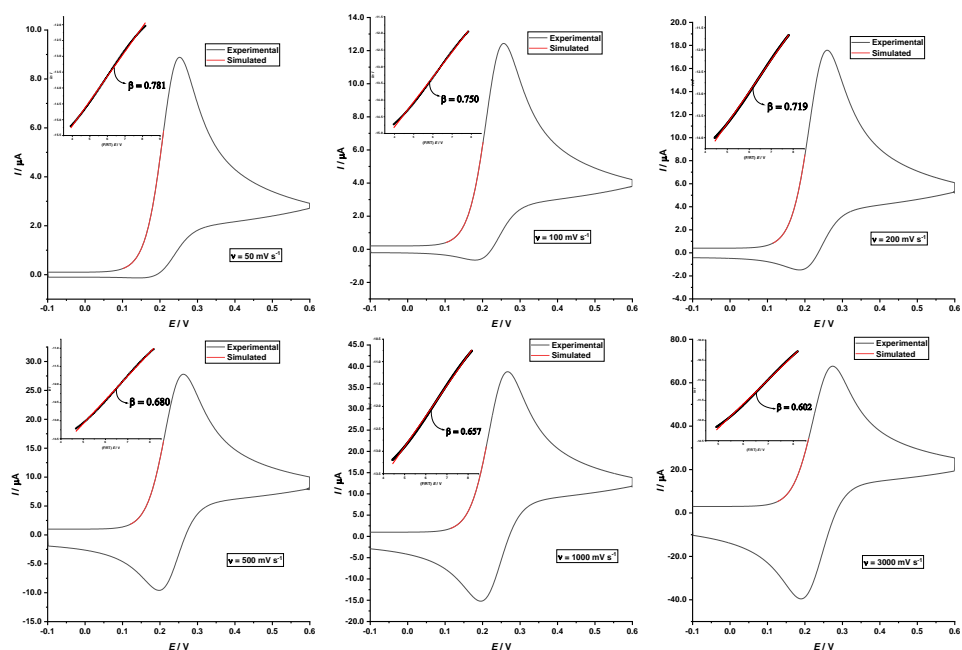


Figure S4: Simulated CVs presented in figure 9 with the respective Tafel plots as inset. The red parts of the voltammograms show the part of the curve sub-plotted to the Tafel analysis as in the insets.

### Electrochemical oxidation processes III and IV

As discussed in the main text, both molecules present the oxidative processes III and IV. To achieve a better understanding of these processes, the scan rate was varied and the Tafel plots of the respective voltammograms were obtained. Figure 5S shows OLZP 1.0 mM CV obtained at different scan rates. Three significant points must be noticed. Firstly, that both processes III and IV merge at slow scan rates ( $< 0.1 \text{ V s}^{-1}$ ), being barely separated at  $0.1 \text{ V s}^{-1}$ . Secondly, both processes are slightly better defined at slow scan rates ( $< 0.1 \text{ V s}^{-1}$ )

1), which suggests that both processes have a slow heterogeneous kinetic. Thirdly, at faster scan rates ( $> 0.1 \text{ V s}^{-1}$ ), OLZP's process IV is barely observed. The latter point suggests that either this process is cloaked by the capacitive current or it is an CE-type mechanism, so that once the scan rate is increased, the prior chemical step does not have time to occur, thus jeopardizing process IV visibility. Figure 6S shows QTP CV at different scan rates and the respective Tafel plots. As observed for the same steps in OLZP, at slow scan rates ( $< 0.1 \text{ V s}^{-1}$ ) the processes are better defined. At faster scan rates ( $> 0.1 \text{ V s}^{-1}$ ), process IV loses its definition, although in QTP it is still visible at higher scan rates. Due to structural similarity, and as both molecules present the same processes at analogous potentials, the QTP's results were complementary to the OLZP's, and that allows us to conclude that oxidative processes III and IV indeed are the same in both molecules. Therefore, occurring at the piperazine moiety in two sequential steps.

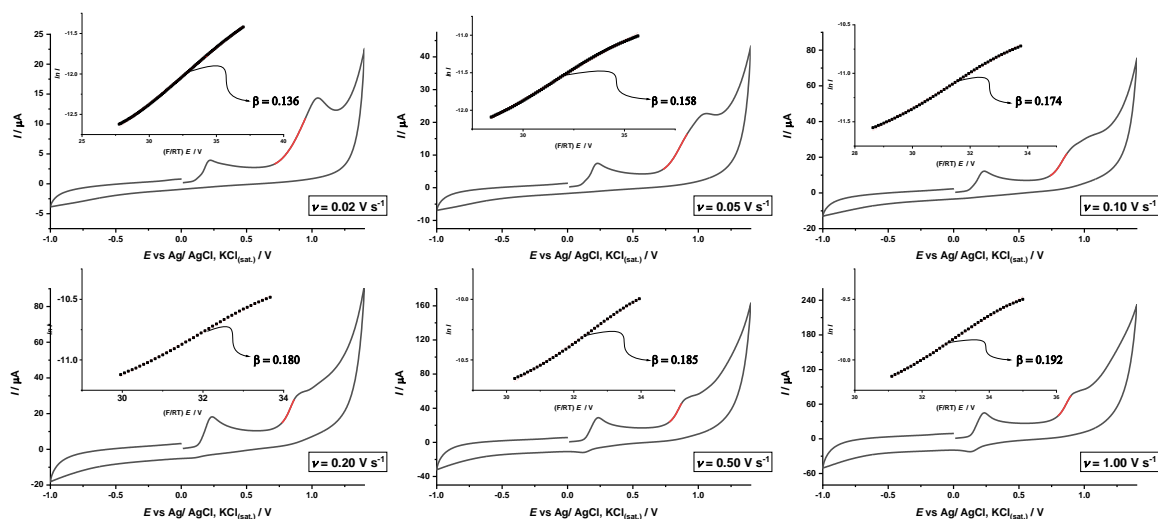


Figure S5: CV presented in figure 2A with the respective Tafel plots as inset. The red parts of the voltammograms show the part of the curve sub-plotted to the Tafel analysis as in the insets.



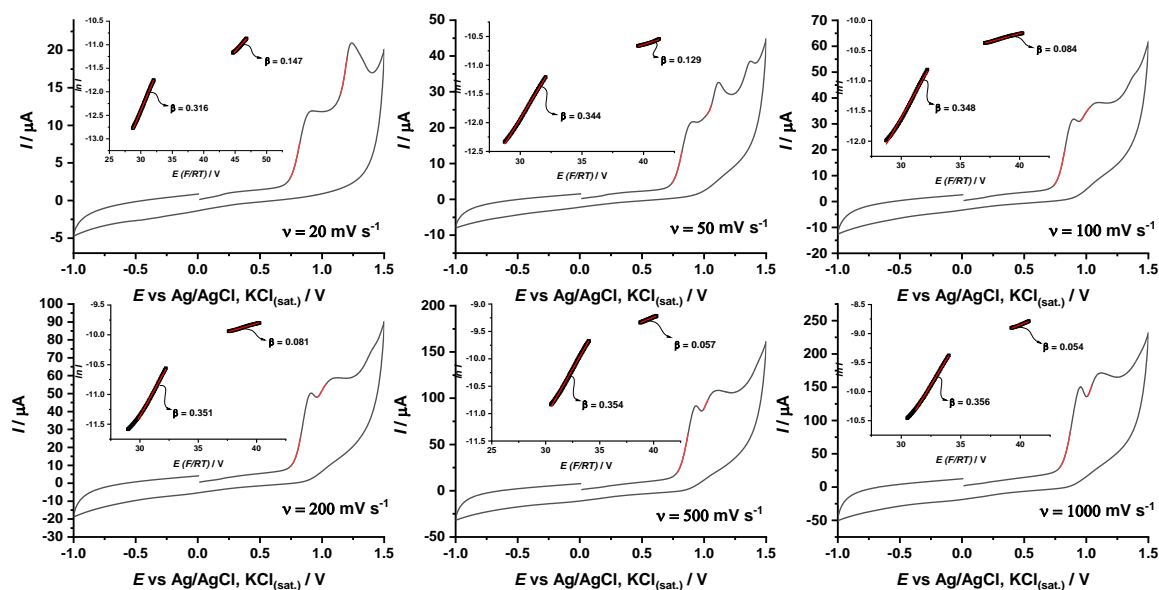


Figure S6: CV presented in figure 2B with the respective Tafel plots as inset. The red parts of the voltammograms show the part of the curve sub-plotted to the Tafel analysis as in the insets.

Table S1: Experimental  $\beta$  values obtained from the Tafel plots presented in figures S5 and S6 at different scan rates for OLZP and QTP oxidative processes III and IV.

$v / \text{V s}^{-1}$	OLZP	OLZP	QTP	QTP
	experimental	experimental	experimental	experimental
	process III	process IV	process III	process IV
0.02	0.136	-	0.316	0.147
0.05	0.158	-	0.344	0.129
0.10	0.174	-	0.348	0.084
0.20	0.180	-	0.351	0.081
0.50	0.185	-	0.354	0.057
1.00	0.192	-	0.356	0.054

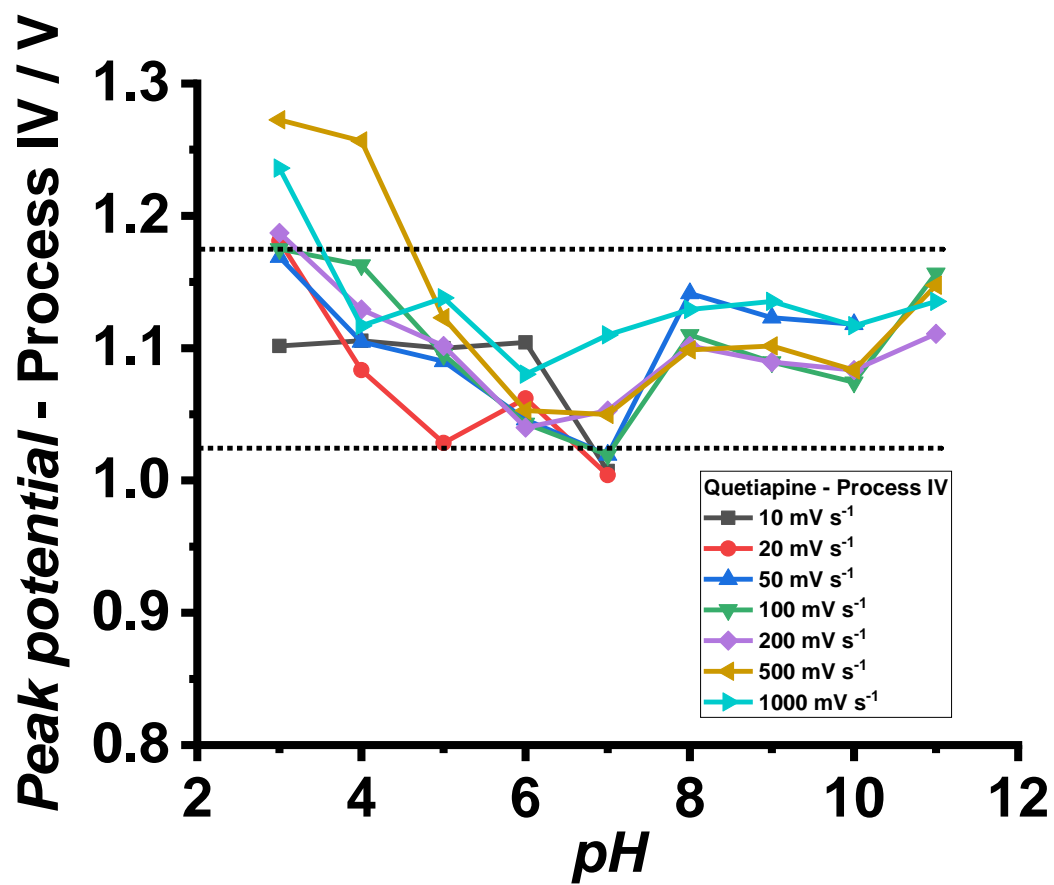


Figure S7: Peak potentials of process IV of QTP as a function of pH.

## Chapter 6

### **Dopamine oxidation at gold electrodes: mechanism and kinetics near neutral pH**

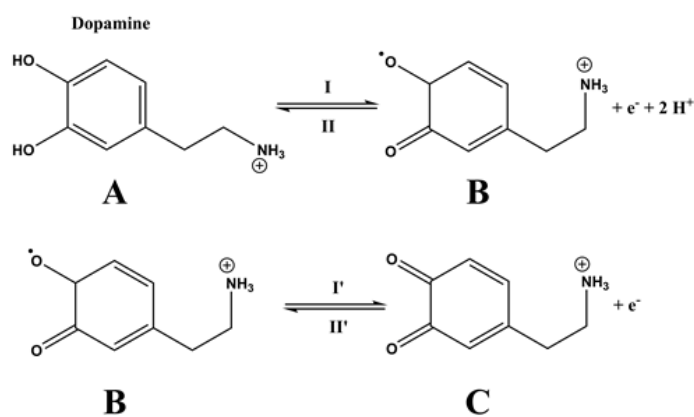
This chapter address to the repagination of the classical dopamine electrochemical mechanism, a work developed during the period abroad. This paper is published at PCCP (Physical Chemistry and Chemical Physics) DOI:10.1039/c9cp05527d and counted with the aid of Dr. Lifu Chen, with the supervision and administration of Professor Silvia Serrano and Professor Richard Compton.

The two-electron electrochemical oxidation of dopamine is studied voltammetrically at gold macro- electrodes around neutral pH with simulations used to give kinetic and mechanistic data. In particular, the system shows “potential inversion” in which the thermodynamic oxidation potential of dopamine to form the corresponding semi-quinone formation occurs at a more positive potential than that of the oxidation of the semi-quinone to the quinone form. The use of Tafel slopes measured from the voltammograms as a function of the voltage scan rate is shown to be a particularly sensitive indicator of mechanism showing the effect of the follow-up chemistry in which the two-electron oxidation product undergoes an irreversible cyclization reaction.

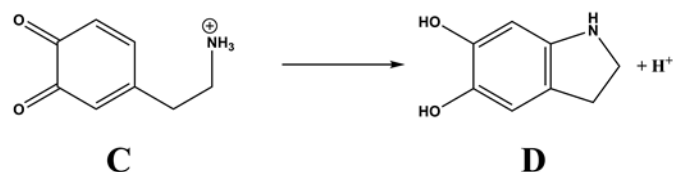
#### **Introduction**

We recently addressed the mechanism of dopamine oxidation under conditions of high acidity (pH = 0), where the overall process is described by Scheme 1 and was studied electrochemically using glassy carbon and carbon

microdisk electrodes.<sup>1</sup> The process was revealed to be multistep with two-electron transfers, the first oxidizing dopamine, A, to the semi-quinone, B, and the second the semi-quinone to the quinone form, C and showing the phenomenon of ‘potential inversion’ in which the formal potential for the A/B oxidation ( $E_{fA/B}^0$ ) was found to have a more positive value than that for the B/C oxidation,  $E_{fB/C}^0$ . Such inversion behaviour has also been observed in the oxidation of catechol<sup>2</sup> and other systems.<sup>3,4</sup> For catechol, a full “scheme of squares” analysis was possible. The potential inversion is attributed to solvation<sup>5</sup> and may be generically typical of hydroquinone/quinone systems in aqueous but not non-aqueous systems.



Scheme 1: Schematic representation of the literature dopamine electrochemical oxidation mechanism. <sup>1</sup>



Scheme 2: Schematic representation of the oxidized dopamine cyclization reaction at pH = 7.4. <sup>6</sup>

Dopamine (DA) has an important physiological role as a neurotransmitter in the central nervous system <sup>7,8</sup> leading to multiple studies which, as summarized in Tables 1 and 2, have revealed that the oxidation leads to ‘follow-up’ chemistry in which the quinone form, C, undergoes a cyclization reaction, Scheme 2, and also polymerization <sup>9–13</sup>. Such chemistry is minimised at low pH values, where the thermodynamics strongly discourages the deprotonation required for a Michael type reaction within or between oxidized dopamine molecules. In terms of understanding and quantifying the kinetics and thermodynamics of the two-electron transfer processes, A/B and B/C, such follow-up chemistry produces an additional complication. On the other hand, it has been shown via computational simulation <sup>14</sup> that, when coupled to follow-up chemical reactions with sufficient fast reaction kinetics, a fast electron transfer process may appear electrochemically irreversible as judged by, in particular, Tafel analysis. Proof of concept was demonstrated experimentally with pyrylium salt reduction and

225

follow-up dimerization.<sup>14</sup> This insight is readily appreciated since in the situation of an electrochemical quasi-reversible oxidation, both the forward (anodic) and backward (cathodic) processes contribute to the net current whilst the latter contribution is lost or diminished if the oxidation product is unstable and the species is lost on a timescale fast compared to electron transfer.

In the present paper, we study the mechanism and kinetics of dopamine oxidation around neutral pH where the follow-up kinetics is voltammetrically visible both in terms of the A/C voltammetric feature and the emergence of a new voltammetric feature attributed to the cyclization product.<sup>15–24</sup> The primary aim is to examine the effect of the follow-up kinetics on the voltammetric wave shape of the A/C process as recorded by Tafel analysis and investigate the dopamine oxidation mechanism at near-neutral pH. In particular it is shown that changing the voltammetric voltage scan rate leads to a marked change in the Tafel slope since at slower scan rates the loss of C in the voltammetric time scale is promoted with a decrease in the apparent reversibility of the A/C reaction. This provides a sensitive measure of the electron transfer kinetics and allows the conclusion to be drawn that the potential inversion mechanism operates at near-neutral pH. Moreover, the difference in the formal potentials,  $\Delta E = E_{f,B/C}^0 - E_{f,A/B}^0$  is shown to be consistent with the value obtained at pH = 0 and also independent of the electrode material so further validating the mechanism suggested.

Table 1. Previous electrochemical studies of dopamine oxidation.

Focus	Electrode material	Reference
Cyclization	Carbon paste	15

Cyclization/ Michael addition	Pyrolitic graphite	16
		17
Cyclization/ Polymerization	Platinum	18
Cyclization	Carbon paste	19
Cyclization/ Michaels addition	Carbon paste	20
Cyclization	Carbon paste	21
Michael Addition/ Cyclization	Carbon paste	22
Cyclization/ Polymerization	Gold	23
Cyclization/ Michael addition	Glassy carbon	24
Scheme of square	Glassy carbon/ carbon microdisk	1
Scheme of square	Glassy carbon/ carbon microdisk	2
Scheme of square	Glassy carbon	25
Scheme of square	Carbon paste	26
Michael addition	Glassy carbon	27
Michael addition	Glassy carbon	28

Michael addition	Glassy carbon	29
Scheme of squares study / pKa values	Gold	6
Disproportionation	Carbon fiber microdisk	30
Polymerization	Gold/ Platinum/ Carbon	31
Polymerization	Pyrolytic graphite	32
Dimerization/ Polymerization	Gold	33
Electrosynthesis	Carbon rod	34
Neurological detection	Carbon fiber microelectrode	7

---

Table 2: Selected non-electrochemical studies of the oxidation of dopamine.

Focus	Methodology	Reference
Cyclization/ Polymerization	UV-Vis	9
Michael addition/ Polymerization	UV-Vis/ XPS	10
Polymerization	NMR/ FT-IR	11



Polymerization	Synthesis and general characterization	12
Cyclization	Theoretical calculations	13

---

## Experimental

### Chemicals and reagents

All reagents used were of analytical grade and acquired from Sigma-Aldrich (Gillingham, UK) and used without any further purification. All solutions were prepared using deionised water from Millipore (Watford, UK) with a measured resistivity of 18.2 M $\Omega$  cm at room temperature (298 K). All the buffers were prepared by dissolving NaHPO<sub>4</sub> and Na<sub>2</sub>HPO<sub>4</sub> in deionised water with a total concentration of 0.1 mol L<sup>-1</sup> and pH = 7.4, resulting in a Phosphate Buffer Solution (PBS). The pH values were measured with a pH meter senseION pH 31 from Hach (Colorado, USA). Adjustments to pH were made by additions of a 3 mol L<sup>-1</sup> NaOH solution. To prevent the dopamine self-oxidation reaction, only fresh solutions were used and were degassed for 20 minutes prior each experiment using pure nitrogen from BOC Gases (Windlesham, UK) to prevent the atmospheric oxygen from oxidizing dopamine.

### Electrochemical procedures

All electrochemical experiments were thermostatted at 25  $\pm$  1  $^{\circ}$ C by a heat-stirrer UC 152 from Stuart (Stone, UK) and performed inside a Faraday cage. A  $\mu$ Autolab type III potentiostat/ galvanostat from Metrohm (Utrecht, Netherlands) for all the electrochemical experiments. A three-electrode system was used with

229

a Gold macroelectrode (GE) from BASi (West Lafayette, Indiana, USA) with an geometrical area of 0.0314 cm<sup>2</sup>, operating as a working electrode, a pyrolytic graphite electrode from IJ Cambridge Scientific (Cambridge, UK) as the counter electrode and a saturated calomel electrode (SCE) (+ 0.244 V vs. SHE) from BASi, Japan) as the reference electrode.

Cyclic voltammograms were performed by sweeping the potential from -0.1 V to +0.5 V, then from +0.5 to -0.5 V, and back to -0.1 V. The scan rates were used between 0.10 and 1.00 V s<sup>-1</sup>. Before every experiment, the GE was polished using diamond spray suspensions with a decreasing particle size of 3.0, 1.0 and 0.1 μm from Kemet (Maidstone, UK) on a polishing pad from Buehler (Lake Bluff, Illinois, USA). All simulations were performed using the Digisim software from BASi (West Lafayette, Indiana, USA) <sup>35,36</sup>.

## **Results and discussion**

This section first presents voltammetric results for dopamine oxidation. These are then compared with the predictions of different Randles-Sevcik equations to give an initial indication of the mechanism of the A/C oxidation. Next, the follow-up reaction of C to D is explored. Full digital simulation is performed to extract kinetic and thermodynamic parameters especially in respect of the potential inversion and the rate of the follow-up cyclization reaction.

### **Cyclic Voltammetry**

Initially, cyclic voltammograms (CV) were recorded over a range of scan rates to overview the DA electrochemical behaviour. CVs were performed on a gold macroelectrode (GE) at near-neutral pH (7.4).

Representative experimental results are shown in figure 1. They show four electrochemical processes, an anodic (I) and a cathodic peak (II), which form a pair around 0.1 V. Another pair, a cathodic (III) and an anodic (IV)) peak, around -0.3 V is also observed. The cathodic peak current of process (II) increased with an increase of the scan rate. The values of peak potentials and peak currents can be seen in Table S1. Moreover, the peak potentials of processes (I) and (II) shifted, to more positive and more negative potentials, respectively. Peaks (I) and (II) are associated with the A/C reaction, scheme 1, whilst peaks III and IV are related to the oxidation of D, scheme 2. The decrease in the size of peaks III and IV with the increase of the scan rate is consistent with the cyclization of D with a chemical reaction with a timescale corresponding to the voltage timescale used.

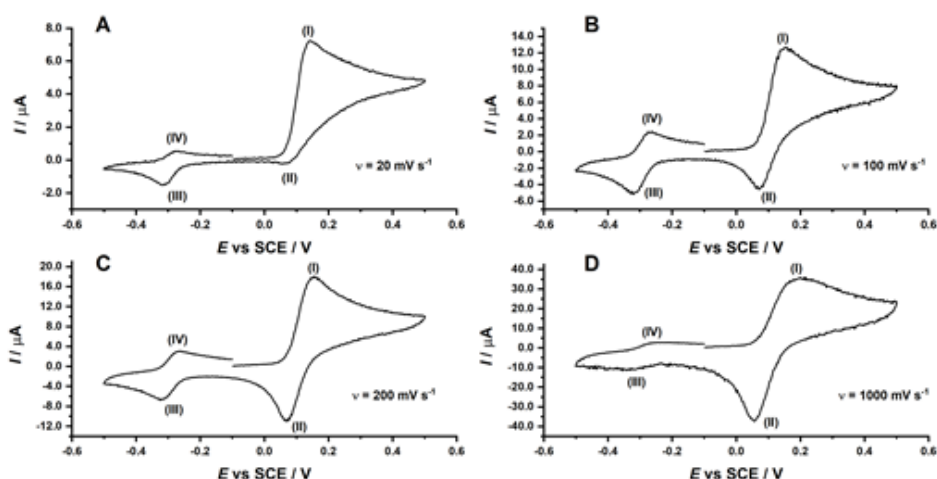


Figure 1. CVs of DA solutions in PBS 0.1 M, pH = 7.4 at different scan rates: A = 0.02 V s<sup>-1</sup>; B = 0.1 V s<sup>-1</sup>; C = 0.20 V s<sup>-1</sup> and D = 1.00 V s<sup>-1</sup>.

### Randles-Sevcik equation and ECE mechanism analysis

The Randles-Sevcik equations are an analytical theoretical prediction of the peak currents of simple electrochemical process, for a reversible case, equation 3, and for an irreversible one, equation 4.

$$I_p = 0.446 n F C A \sqrt{n F v D / R T} \quad (3)$$

$$I_p = 0.446 \sqrt{n' + \beta} F C A \sqrt{n F v D / R T} \quad (4)$$

where  $I_p$  is the peak current in A,  $n$  is the overall number of electrons transferred,  $n'$  is the number of electrons prior to the rate determining step,  $F$  is the Faraday Constant in Coulomb mol<sup>-1</sup>,  $C$  is the concentration in mol cm<sup>-3</sup>,  $A$  the electrode area in cm<sup>2</sup>,  $v$  is the scan rate in V s<sup>-1</sup>,  $R$  is the Gas Constant in J K<sup>-1</sup> mol<sup>-1</sup> and  $T$  is the temperature in K. A diffusion coefficient ( $D$ ) of  $7.7 \cdot 10^{-6}$  cm s<sup>-1</sup>, was obtained by chronoamperometry <sup>37</sup>.

Returning to Figure 1, the A/C process was analysed in terms of a simple EE reaction. Specifically, the experimental results were compared to the theoretical predictions of the Randles-Sevcik Equations. Figure 2 shows the experimental peak currents for the oxidation A to C as a function of the square root of the voltage scan rate. Also shown are the theoretical predictions based in equations (3) and (4) for the following-up cases: a simple reversible two-electron oxidation and an irreversible two-electron processes with either the first or the second step as the rate determining, assuming in each case a charge transfer coefficient of 0.5 in the rate determining step. It is clear that the high scan rate data fits with an overall two-electron process with the initial electron transfer as a rate determining hinting at a potential inversion mechanism but that there is a clear current enhancement over that predicted at lower scan rates.

In order to fully interpret the A/C voltammetry consideration has to be given to the follow-up reaction of C, as discussed in the next section and which explains the current enhancement seen at low scan rates.

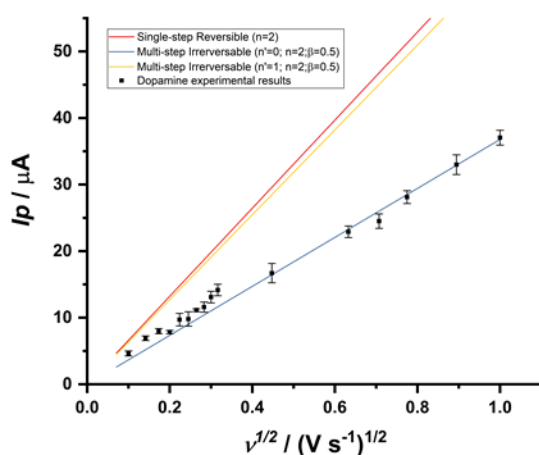


Figure 2. Plot of the dopamine oxidative peak currents as a function of the square root of the scan rates, compared to the theoretical peak currents predicted by the Randles-Sevcik equations for a single step two-electron reversible transfer (-), for a multi-step irreversible ( $n' = 0$ ;  $n = 2$ ;  $\beta = 0.5$ ) process (-), and for a multi-step irreversible ( $n' = 1$ ;  $n = 2$ ;  $\beta = 0.5$ ) (-), together with experimental results (■). Electrode Area =  $0.0314 \text{ cm}^2$ ,  $C = 10^{-3} \text{ mol L}^{-1}$ .

### An analysis of the DA oxidation as an ECCE process

We consider the following mechanism in which the product D can undergo oxidation at the potential of the A/C process:



where  $E_f^0$  is the formal potential,  $k_f$  is the rate constant of formation of D from C.

F is the oxidised cyclization product. The effective number of electrons

transferred ( $n_{\text{eff}}$ ) ( $2 < n_{\text{eff}} < 4$ ), is a function of the dimensionless parameter ( $\lambda$ )

where

$$\lambda = (RT/F) k_f / v \quad (8)$$

and the  $n_{\text{app}}$  values can be obtained by dividing the experimental peak current values by the theoretical prediction for a two-electron process (see above). The low scan rate data such as that shown in figure 2 were analyzed to give  $n_{\text{app}}$  values and then the published<sup>38</sup> working curve used to relate these to  $\lambda$  values.

Then, a plot of  $\lambda$ , as inferred from the working curve against the reciprocal at the scan rate as suggested by equation (9) was made and seen to be linear passing through the origin as shown in Figure 4, which is consistent with the proposed EECEE mechanism. The slope of this plot allowed the interference of a value of  $k_f$  as approximately  $0.2 \text{ s}^{-1}$ , consistent with independent literature values<sup>20,22</sup> At this point the likely basic mechanism summarized in Scheme 1 and 2 has been identified, so attention was next turned to the full modelling of the voltammetry using Digisim as pioneered by Rudolph<sup>35,36</sup>

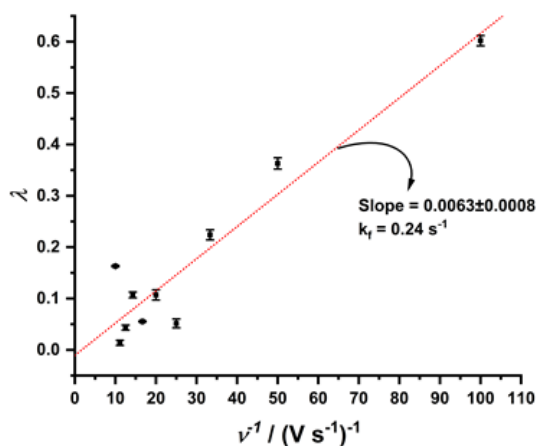


Figure 3: Dimensionless parameter  $\lambda$  parameter versus the inverse of the voltage scan rate. Linear regression:  $\lambda = 0.0063 \pm 0.0008 \text{ v}^{-1} - 0.00873$ .  $R^2 = 0.897$

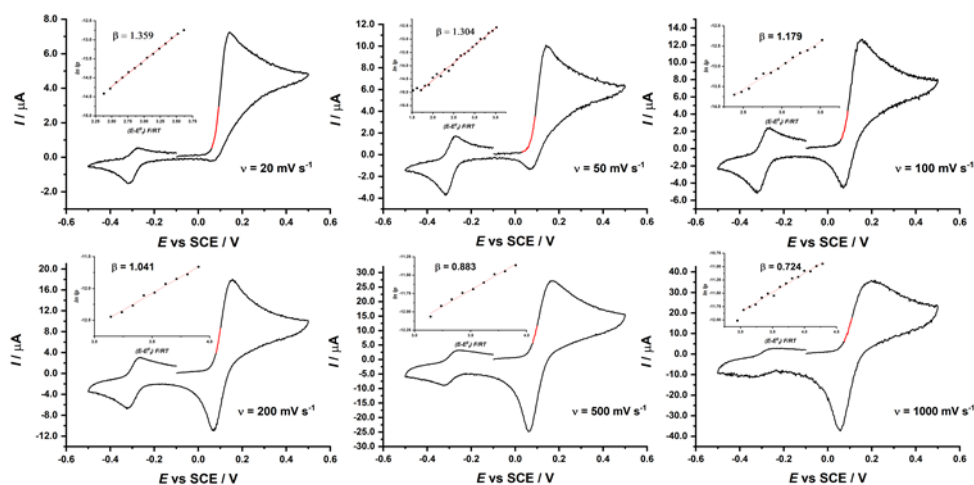


Figure 4: CV presented in figure 1 with the respective Tafel plots as inset. The red parts of the voltammograms show the part of the curve sub-plotted to the Tafel analysis as in the inserts.

### Digisim simulations

Digisim software allows the simulation of voltammograms at macroelectrodes under linear diffusion conditions with various parameters describing the electrochemical and chemical steps. In the following, we use Digisim to fully model the experimental voltammetry of the DA system in the light of the preliminary analysis presented above paying particular attention to the A/C wavelshapes and their associated Tafel slopes. In particular the anodic Tafel slope is given by

$$\beta = \frac{RT}{F} \frac{d \ln I}{dE} \quad (9)$$

provided that relatively little reactant concentration depletion taken place. In experimental practice, this constrains the analysis to the early part of a

voltammetric peak, as shown in red, in Figure 4, following the recommendations of Li et al.<sup>39</sup> Note that as defined by equation (9), the Tafel slope is an experimental quantity independent of the overall number of electrons transferred in the oxidation.<sup>40,41</sup>

In order to probe the voltammetry of the dopamine oxidation system, Tafel plots were obtained from CVs presented in Figure 1, these results are presented in Figure 4.

Table 3:  $\beta$  values obtained from the Tafel plots presented in Figure 4 at different scan rates.

$v / \text{V s}^{-1}$	$\beta$ values (experimental)
0.02	1.36±0.01
0.05	1.30±0.02
0.10	1.18±0.03
0.20	1.04±0.03
0.50	0.83±0.03
1.00	0.72±0.03

The transfer coefficients values ( $\beta$ ) obtained decreased systematically with the increase of the scan rate, Table 3, from 1.36 (20  $\text{mV s}^{-1}$ ) to 0.72 (1000  $\text{mV s}^{-1}$ ). This shift indicates a decrease in the apparent reversibility of the overall two-electron oxidation of A to C combined with the electrochemical of increased loss of C as the voltage timescale increases at slower scan rates. Thus, the decrease in reversibility is associated with the emergence of the D/F voltammetric feature.



The outline mechanism used to interpret these data and informed by the discussion above can be summarised by means of the system given in Table 4. Each simulation was evaluated by comparing the peak currents, peak potentials, peak current ratios and the relation between the  $\beta$  values obtained from the Tafel plots regarding the scan rate between the simulated voltammograms and the experimental ones, to observe which mechanism better represents the latter.

Table 4. Mechanistic steps used to simulate the DA system.

Step order	Mechanism simulated	Correspondence	Type of step
1 <sup>st</sup>	$A - e^- \rightarrow B$	(A/B)	Electrochemical
2 <sup>nd</sup>	$B - e^- \rightarrow C$	(B/C)	Electrochemical
3 <sup>rd</sup>	$C \rightarrow D$	Cyclization (C/D)	Chemical
4 <sup>th</sup>	$D + 2e^- \rightarrow F$	(D/E)	Electrochemical

Table 5: Optimized parameters for each simulated electrochemical and chemical step:

Step	$E_f^0 / V$	$k^0 / \text{cm s}^{-1}$	$D / \text{cm}^2 \text{ s}^{-1}$
A/B	0.2	0.025	$7.7 \cdot 10^{-6}$
B/C	0.0	$10^4$ (Reversible)	$7.7 \cdot 10^{-6}$

D/E	-0.3	$10^4$ (Reversible)	$7.7 \cdot 10^{-6}$
E/F	-0.3	$10^4$ (Reversible)	$7.7 \cdot 10^{-6}$
Step	K	$k_f / \text{s}^{-1}$	$k_b / \text{s}^{-1}$
Cyclization (C/D)	10	0.2	0.02

where K is the chemical step equilibrium constant,  $k_b$  is the homogeneous rate kinetics constant of the inverse reaction,  $k^0$  is the standard electrochemical rate constant of the electron transfer.

To fit the experimental waveshapes with the simulation, the homogeneous rate constant for step 3 and the parameters ( $E^0_f$ ,  $k^0$ , and  $\beta$ ) describing the electrochemical steps were varied and the resulting voltammograms were compared with the experimental ones. The optimized formal potential for A/B process was 0.2 V while the B/C was set at 0.0 V, following the reference presented by Lin et al. <sup>1</sup> which shows the potential inversion occurs before the chemical step. The cyclization (C/D) is a fast and irreversible reaction, as aforementioned. It affects the electrochemical steps at scan rates below 100 mV  $\text{s}^{-1}$ . The peak of the D/F couple was optimized by adding a slow homogeneous first order decomposition of F ( $\sim 1 \text{s}^{-1}$ ).

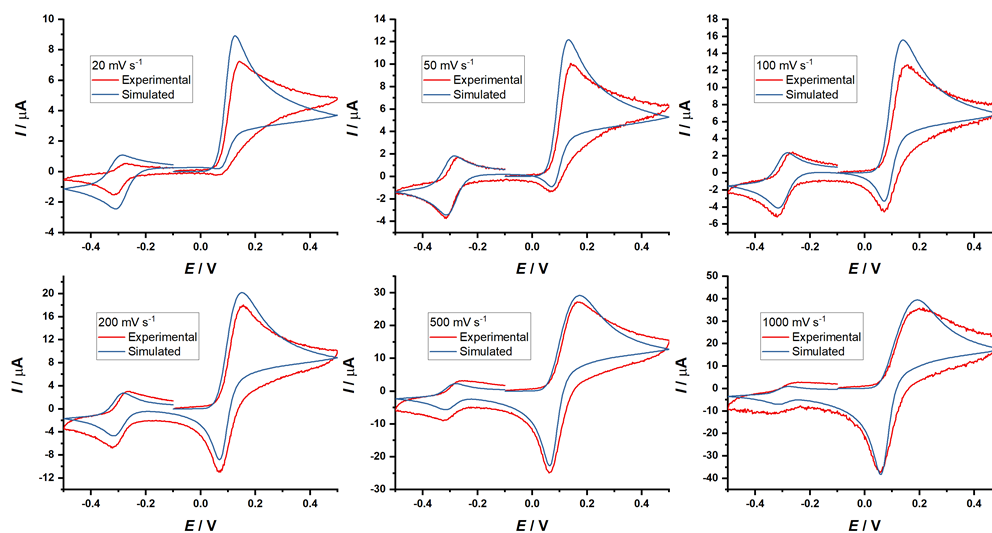


Figure 5: (-) Simulated CV voltammograms; (-) of DA solutions in PBS 0.1 M, pH = 7.4 at different scan rates: A = 0.02 V s<sup>-1</sup>; B = 0.05 V s<sup>-1</sup>; C = 0.10 V s<sup>-1</sup>; D = 0.20 V s<sup>-1</sup>; E = 0.05 V s<sup>-1</sup> and F = 1.00 V s<sup>-1</sup>.

The best fit simulated voltammograms are shown in Figure 5 superimposed on typical experimental data. Figure 6 shows the successful fitting of the A/C voltammograms in terms of the ratio of the forward and reverse peak currents. A reasonable agreement is seen suggesting that several conclusions can be drawn. First and foremost the potential inversion mechanism operates at neutral pH consistent with the conclusion made under strongly acidic conditions.<sup>1</sup> Second, importantly, the simulations successfully reproduce the Tafel slopes and their variation with the voltage scan rate. Figure 7 shows the level of agreement and indicates that concept of chemically induced electrochemical irreversibility in which the cyclization reaction exerts a profound influence on the Tafel slopes. Moreover, if this feature were neglected from the mechanistic analysis quite erroneous inferences the electrochemical kinetics of the A/C system would be drawn. Third, we note the oxidation product F show some slow kinetic lability on the voltammetric timescale.

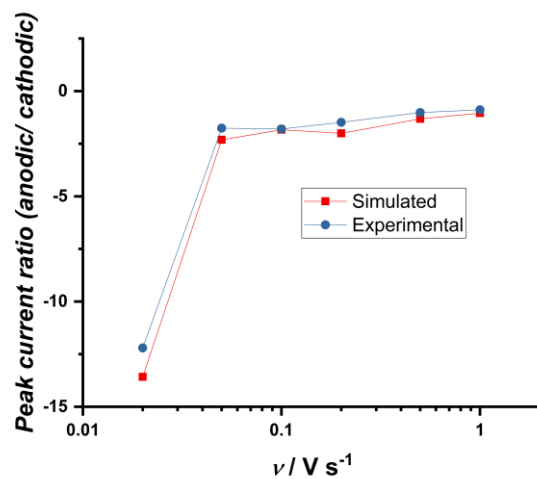


Figure 6: Peak current ratios (anodic/ cathodic) of the experimental and simulated voltammograms as a function of the scan rate, presented in a logarithm scale.

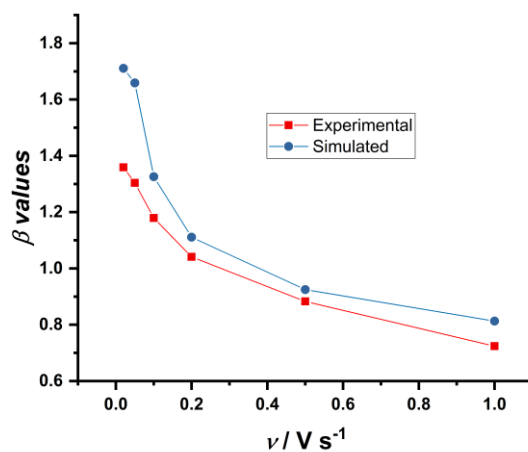
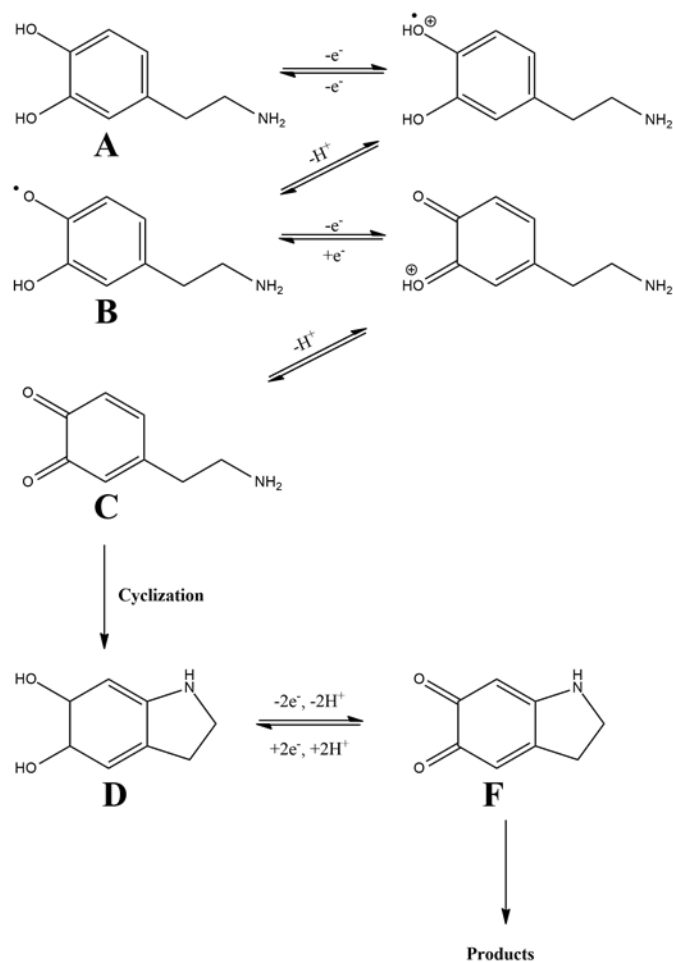


Figure 7.  $\beta$  values for the A/C processes versus the scan rate.

In summary, the DA oxidation mechanism shown in Schemes 1 and 2 has been shown to be consistent with all the voltammetric data.



Scheme 3: Proposed electrochemical oxidation mechanism for dopamine in near-neutral pH.

## Conclusions

Dopamine cyclization was studied at near-neutral pH in aqueous solution using cyclic voltammetry at gold microelectrodes and Digisim software used to digitally simulate the voltammograms. Dopamine oxidizes in a quasi-reversible process, A/C, involving two-electron transfers. The first one is a quasi-reversible transfer, which forms a semi-quinone (A/B) and the second one is a reversible one (B/C), forming a quinone. But, with a potential inversion such that B is more easily oxidized than A. The electrochemical of the follow-up kinetics on the

apparent reversibility of the A/C couple is profound as revealed by the Tafel slopes.

### Acknowledgments

The authors would like to thank the CAPES (Grant number PDSE 88881.187396/2018-01) and CNPq (Grant number 140833/2016-1) for the financial support of this work.

### References

- 1 C. Lin, L. Chen, E. E. L. Tanner and R. G. Compton, Electroanalytical study of dopamine oxidation on carbon electrodes: from the macro- to the micro-scale, *Phys. Chem. Chem. Phys.*, 2018, **20**, 148–157.
- 2 Q. Lin, Q. Li, C. Batchelor-McAuley and R. G. Compton, Two-Electron, Two-Proton Oxidation of Catechol: Kinetics and Apparent Catalysis, *J. Phys. Chem. C*, 2015, **119**, 1489–1495.
- 3 D. H. Evans and K. Hu, Inverted potentials in two-electron processes in organic electrochemistry, *J. Chem. Soc. Faraday Trans.*, 1996, **92**, 3983.
- 4 C. E. Banks and R. G. Compton, *Understanding Voltammetry*, World Scientific Press Company, 3rd Ed., 2018.
- 5 J.-M. Savéant, *Elements of Molecular and Biomolecular Electrochemistry*, John Wiley & Sons, Inc., Hoboken, NJ, USA, 2006.
- 6 M. Salomäki, L. Marttila, H. Kivelä, T. Ouvinen and J. Lukkari, Effects of pH and Oxidants on the First Steps of Polydopamine Formation: A Thermodynamic Approach, *J. Phys. Chem. B*, 2018, **122**, 6314–6327.
- 7 B. J. Venton and R. M. Wightman, Psychoanalytical Electrochemistry: Dopamine and Behavior, *Anal. Chem.*, 2008, **75**, 414 A-421 A.

- 8 M. Shin, Y. Wang, J. R. Borgus and B. J. Venton, Electrochemistry at the Synapse, *Annu. Rev. Anal. Chem.*, 2019, **12**, 297–321.
- 9 E. Herlinger, R. F. Jameson and W. Linert, Spontaneous autoxidation of dopamine, *J. Chem. Soc. Perkin Trans. 2*, 1995, 259.
- 10 Q. Wei, F. Zhang, J. Li, B. Li and C. Zhao, Oxidant-induced dopamine polymerization for multifunctional coatings, *Polym. Chem.*, 2010, **1**, 1430–1433.
- 11 D. R. Dreyer, D. J. Miller, B. D. Freeman, D. R. Paul and C. W. Bielawski, Elucidating the Structure of Poly(dopamine), *Langmuir*, 2012, **28**, 6428–6435.
- 12 J. Liebscher, Chemistry of Polydopamine - Scope, Variation, and Limitation, *European J. Org. Chem.*, 2019, **2019**, 4976–4994.
- 13 N. Umek, B. Geršak, N. Vintar, M. Šoštarič and J. Mavri, Dopamine Autoxidation Is Controlled by Acidic pH, *Front. Mol. Neurosci.*, 2018, **11**, 1–8.
- 14 I. Streeter, S. F. Jenkinson, G. W. J. Fleet and R. G. Compton, Chemical instability promotes apparent electrochemical irreversibility: Studies on the electrode kinetics of the one electron reduction of the 2,6-diphenylpyrylium cation in acetonitrile solution, *J. Electroanal. Chem.*, 2007, **600**, 285–293.
- 15 M. D. Hawley, S. V. Tatawawadi, S. Piekarski and R. N. Adams, Electrochemical studies of the oxidation pathways of catecholamines., *J. Am. Chem. Soc.*, 1967, **89**, 447–50.
- 16 F. Zhang and G. Dryhurst, Oxidation Chemistry of Dopamine: Possible Insights into the Age-Dependent Loss of Dopaminergic Nigrostriatal Neurons, *Bioorg. Chem.*, 1993, **21**, 392–410.
- 17 G. Dryhurst, K. M. Kadish, F. Scheller and R. Renneberg, *Biological Electrochemistry*, Academic Press, London, 1st edn., 1982.

- 18 A. Brun and R. Rosset, Étude électrochimique de l'oxydation de la dihydroxy-3,4 phénylalanine (Dopa), *J. Electroanal. Chem. Interfacial Electrochem.*, 1974, **49**, 287–300.
- 19 S. Corona-Avenidaño, G. Alarcón-Angeles, M. T. Ramírez-Silva, G. Rosquete-Pina, M. Romero-Romo and M. Palomar-Pardavé, On the electrochemistry of dopamine in aqueous solution. Part I: The role of [SDS] on the voltammetric behavior of dopamine on a carbon paste electrode, *J. Electroanal. Chem.*, 2007, **609**, 17–26.
- 20 D. C. S. Tse, R. L. McCreery and R. N. Adams, Potential oxidative pathways of brain catecholamines, *J. Med. Chem.*, 1976, **19**, 37–40.
- 21 T. E. Young and B. W. Babbitt, Electrochemical study of the oxidation of alpha-methyldopamine, alpha-methylnoradrenaline, and dopamine, *J. Org. Chem.*, 1983, **48**, 562–566.
- 22 A. W. Sternson, R. McCreery, B. Feinberg and R. N. Adams, Electrochemical studies of adrenergic neurotransmitters and related compounds, *J. Electroanal. Chem. Interfacial Electrochem.*, 1973, **46**, 313–321.
- 23 Y. Li, M. Liu, C. Xiang, Q. Xie and S. Yao, Electrochemical quartz crystal microbalance study on growth and property of the polymer deposit at gold electrodes during oxidation of dopamine in aqueous solutions, *Thin Solid Films*, 2006, **497**, 270–278.
- 24 X. Wen, Y.-H. Jia and Z.-L. Liu, Micellar effects on the electrochemistry of dopamine and its selective detection in the presence of ascorbic acid, *Talanta*, 1999, **50**, 1027–1033.



- 25 M. R. Deakin, P. M. Kovach, K. J. Stutts and R. M. Wightman, Heterogeneous mechanisms of the oxidation of catechols and ascorbic acid at carbon electrodes, *Anal. Chem.*, 1986, **58**, 1474–1480.
- 26 M. R. Deakin and R. M. Wightman, The kinetics of some substituted catechol/o-quinone couples at a carbon paste electrode, *J. Electroanal. Chem. Interfacial Electrochem.*, 1986, **206**, 167–177.
- 27 H. P. Hendrickson, A. D. Kaufman and C. E. Lunte, Electrochemistry of catechol-containing flavonoids, *J. Pharm. Biomed. Anal.*, 1994, **12**, 325–334.
- 28 L. Khalafi, M. Rafiee, M. Norouznia and Y. A. Asl, Electrochemical oxidation of catecholamines in the presence of aromatic amines: interplay between inter- and intramolecular nucleophilic addition, *Res. Chem. Intermed.*, 2015, **41**, 7151–7162.
- 29 A. Afkhami, D. Nematollahi, L. Khalafi and M. Rafiee, Kinetic study of the oxidation of some catecholamines by digital simulation of cyclic voltammograms, *Int. J. Chem. Kinet.*, 2005, **37**, 17–24.
- 30 E. L. Ciolkowski, K. M. Maness, P. S. Cahill, R. M. Wightman, D. H. Evans, B. Fosset and C. Amatore, Disproportionation During Electrooxidation of Catecholamines at Carbon-Fiber Microelectrodes, *Anal. Chem.*, 1994, **66**, 3611–3617.
- 31 S. Chumillas, T. Palomäki, M. Zhang, T. Laurila, V. Climent and J. M. Feliu, Analysis of catechol, 4-methylcatechol and dopamine electrochemical reactions on different substrate materials and pH conditions, *Electrochim. Acta*, 2018, **292**, 309–321.
- 32 R. P. da Silva, A. W. O. Lima and S. H. P. Serrano, Simultaneous voltammetric detection of ascorbic acid, dopamine and uric acid using a pyrolytic

graphite electrode modified into dopamine solution, *Anal. Chim. Acta*, 2008, **612**, 89–98.

33 S. Schindler and T. Bechtold, Mechanistic insights into the electrochemical oxidation of dopamine by cyclic voltammetry, *J. Electroanal. Chem.*, 2019, **836**, 94–101.

34 D. Nematollahi and M. Rafiee, Electrochemical oxidation of catechols in the presence of acetylacetone, *J. Electroanal. Chem.*, 2004, **566**, 31–37.

35 M. Rudolph, A fast implicit finite difference algorithm for the digital simulation of electrochemical processes, *J. Electroanal. Chem. Interfacial Electrochem.*, 1991, **314**, 13–22.

36 M. Rudolph, Digital simulations with the fast implicit finite difference (FIFD) algorithm, *J. Electroanal. Chem.*, 1992, **338**, 85–98.

37 L. Chen, E. E. L. Tanner, C. Lin and R. G. Compton, Impact electrochemistry reveals that graphene nanoplatelets catalyse the oxidation of dopamine via adsorption, *Chem. Sci.*, 2018, **9**, 152–159.

38 I. Lavagnini, R. Antiochia and F. Magno, An extended method for the practical evaluation of the standard rate constant from cyclic voltammetric data, *Electroanalysis*, 2004, **16**, 505–506.

39 D. Li, C. Lin, C. Batchelor-McAuley, L. Chen and R. G. Compton, Tafel analysis in practice, *J. Electroanal. Chem.*, 2018, **826**, 117–124.

40 R. Guidelli, R. G. Compton, J. M. Feliu, E. Gileadi, J. Lipkowski, W. Schmickler and S. Trasatti, Definition of the transfer coefficient in electrochemistry (IUPAC Recommendations 2014), *Pure Appl. Chem.*, 2014, **86**, 259–262.

41 R. Guidelli, R. G. Compton, J. M. Feliu, E. Gileadi, J. Lipkowski, W. Schmickler and S. Trasatti, Defining the transfer coefficient in electrochemistry: An assessment (IUPAC Technical Report), *Pure Appl. Chem.*, 2014, **86**, 245–258.

**Appendix 6 – Dopamine oxidation at gold electrodes: mechanism and kinetics near neutral pH. - Supplementary Information**

Table S1: Compilation of the values of the potential peak, peak currents per scan rate, from Figure 1.

$v$ (V s <sup>-1</sup> )	Anodic peak potentials (A/C)/ V	Cathodic peak potentials (A/C)/ V	$\Delta E_p$ / V	Anodic peak currents (A/B)/ $\mu$ A	Cathodic peak currents (A/C)/ $\mu$ A
0.01	0.142	0.078	0.064	4.765	-0.118
0.02	0.144	0.077	0.065	6.92	-0.58
0.05	0.149	0.074	0.063	9.71	-5.97
0.10	0.156	0.072	0.084	14.17	-6.65
0.20	0.160	0.069	0.089	16.71	-11.60
0.50	0.164	0.061	0.102	24.51	-25.50
1.00	0.202	0.056	0.156	37.05	-36.85

## Chapter 7

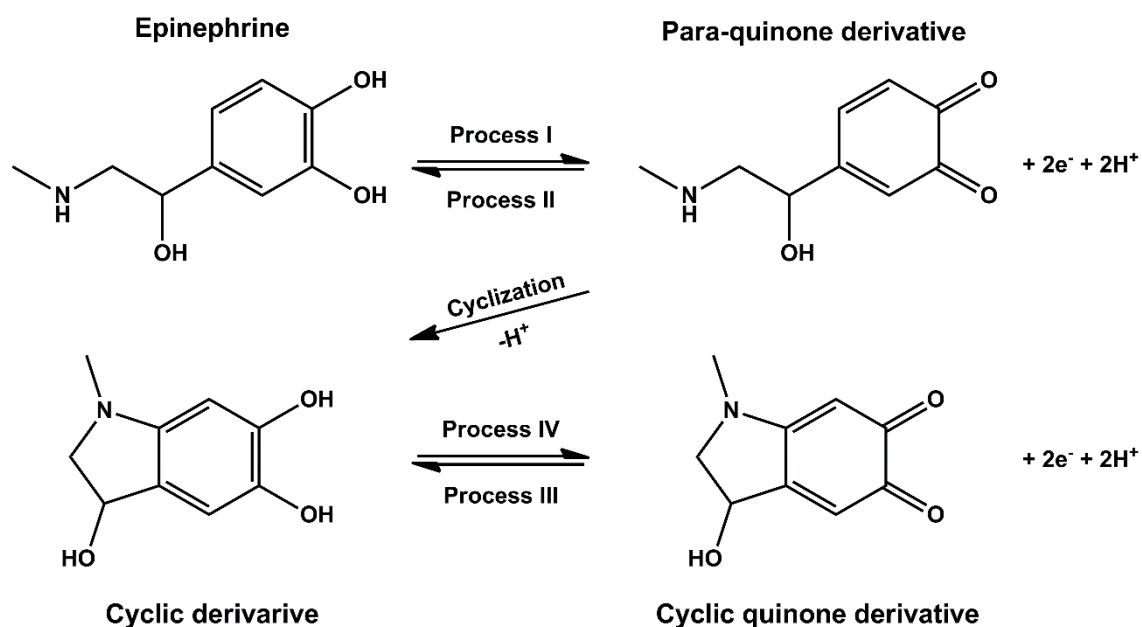
### **New insights on the electrochemical mechanism of epinephrine on glassy carbon electrode.**

In this chapter the epinephrine mechanism was revisited, and its thermodynamical and kinetics parameters were obtained. This work counted with the aid of Pedro Garcia, who helped with data curation and discussions, and Professor Silvia Serrano who administrated the project, and it is published at Journal of Electroanalytical Chemistry, DOI: 10.1016/j.jelechem.2022.116111.

It was observed that it oxidizes in an EECEE mechanism, such as observed for similar molecules such as dopamine. Epinephrine also presents a typical catechol behaviour, a potential inversion was observed in processes I/ II, and III/ IV. The influence of the media on both heterogeneous and homogeneous processes were also studied. It was noticed that epinephrine follow-up chemistry, cyclization, occurs at a much higher rate than other catecholamines and that it is pH-dependent. In acidic media, the reaction is jeopardized due to the protonation of the amine moiety. Hence, a quasi-reversibility was observed to process I/II. In a neutral to basic media, the reaction occurs significantly, as a consequence, it hinders the occurrence of process II. The heterogeneous kinetics was studied and the obtained  $\beta$  values at alkaline media were greater than the ones observed in acidic media due to the occurrence of the cyclization. Finally, the oxidation mechanism to epinephrine was proposed.

## Introduction

Epinephrine (Epi) is a neurotransmitter with a wide biological relevance, not only due to its signalling functions in the central neurosystems but also for its essential cardiac functions. [1] In the 80's, it was also linked with mental disorders, such as anxiety syndrome, [2] panic attacks [3] and post-traumatic stress [4], drawing a lot of attention to Epi as a biomarker to some disorders. Chemically, it is a catecholamine that can be easily oxidized by the atmospheric  $O_2$ , with a subsequent intramolecular Michael addition, which leads to a cyclic compound. [5,6] In aqueous media ( $pH > 3.0$ , using spectroelectrochemistry) [7], its oxidation mechanism is often presented in the literature as an electrochemical-chemical-electrochemical (ECE) mechanism, with each E step being a single-step reversible transfer involving two-protons and two-electrons. The most common representation of Epi oxidation mechanism is illustrated in scheme 1. [6]



Scheme 1: Most accepted oxidation mechanism of Epi in aqueous media ( $pH > 3.0$ ). [6,7]

Recently our group addressed the oxidation mechanism of dopamine at near neutral media. It was observed that dopamine, a molecule which is structurally similar to Epi, oxidizes in an EECEE mechanism with a potential inversion, which is typical of the catechol group. This effect is usually related to a variation on the solvation of reactants and products, hence shifting the formal potential of the following step to a less positive potential than the initial one ( $E_{f1}^0 > E_{f1'}^0$ ). [8,9] Observing the Epi reactivity, it should most likely oxidize as dopamine, in a multi-step oxidation of sequential one-electron processes instead of the traditionally accepted mechanism (Scheme 1). This multi-step process is generally presented as an EECEE, as schematized in equations 1 to 5.



This hypothesis of a multi-step oxidation mechanism is backed up by the literature such as the one by Kalyanaraman et al., who studied the Epi oxidation using electron spin resonance, which shows the formation of the semi-quinone derivative (Epi<sub>Q</sub>). Therefore, presenting a relatively stable intermediary, and strongly suggesting that Epi do not directly oxidize in a single step proton coupled electron transfer involving two electrons and two protons [10]. Similarly, Manini et al., Graham et al., and Garnayak et al., studied the biological oxidation pathways of Epi and also observed the formation of the semi-quinone

intermediary (Epi<sub>o</sub>) and other metabolites [11–13], although Garnayak et al. reported the oxidation with the usual mechanism.

Another typical characteristic of the catecholamines is to undergo an intramolecular Michael addition from the amine moiety in the catechol ring after it oxidizes, forming a quinone derivative. Among the catecholamines, Epi is reported to have the most favoured cyclization rate, followed by norepinephrine and dopamine, with normalized rates of 1, 10 and 1000, respectively. [6,14,15] This chemical step exerts a great influence on the electrochemical processes that both precede and follows it, thus, affecting their respective thermodynamic and kinetic parameters, as observed in dopamine. [8,16].

As aforementioned, Epi is a very relevant biomolecule, which leads several groups to analytically address Epi. Most of them focus on its detection, such as Hernández et al., which uses carbon fiber electrodes to detect Epi using cyclic voltammetry (CV) [17]. Although most of the works use modified electrodes to avoid the fouling effects of Epi oxidation products. Therefore, distinct modification strategies were utilized, such as the use of micellar compounds [18], cobalt (II) hexacyanoferrate films [19], graphene nanoribbons [20], carbon paste modified with extract of yam root (*Dioscorea bulbifera*) [21] and with iron phthalocyanine [22], multi-walled carbon nanotubes (MWCNT) [23], CNT yarn [24], modified with Epi itself [25], graphene oxide nanosheets [26], nano composites (ZnO/ MWCNT) [27], CNT [28], S-functionalized Au nanoparticles [29], flower like zinc oxide nanosheets with in situ growth ferrocene functionalized graphene framework [30].

In addition, to the modified electrodes and functionalized electrodes, biosensors with horseradish enzyme were used [31], Metal-Organic-Frameworks



(MOF) [32], conducting polymers [33], screen-printed graphite polyurethane modified with chitosan and coated with magnetic nanoparticles [34], silica gel film [35], electrochemiluminescence from ZnO nanoparticles modified in pencil graphite electrodes [36]. Most of these works rely on the Epi oxidation as a reversible two-electron single step transfer. A reevaluation of the Epi's oxidation mechanism could not only aid the authors by facilitating their material design to achieve the desired effect, but also help to understand the complex biopathway and signalling effects of the neurotransmitter.

Therefore, this work aims to revisit the most accepted electrochemical mechanism of Epi, which implies an ECE mechanism involving a two-electron single step in each electrochemical process, addressing both thermodynamic and kinetic aspects of the heterogeneous processes as well as the influence that the cyclization reaction exerts on them.

## **Experimental**

### **Chemical and reagents**

All solutions were prepared using deionized water from a reverse osmosis device (Gehara Co., model of ultra-pure OS10LX system, water resistivity 18 M $\Omega$ cm). The 0.1 mol L<sup>-1</sup> phosphate buffer solutions (PBS) were prepared by solubilizing and diluting, respectively, the appropriate amount of NaH<sub>2</sub>PO<sub>4</sub> and H<sub>3</sub>PO<sub>4</sub> (Merck) in deionized water and the pH values were adjusted by the addition of a 4.0 mol L<sup>-1</sup> NaOH (Merck) solution. The 10.0 mmol L<sup>-1</sup> Epi stock solutions were obtained by solubilizing the appropriated amount in 0,1M PBS, pH 7.4. The electrochemical measurements were performed in 1,0 mmol L<sup>-1</sup> solutions. Therefore, 0.5 mL of the stock solution was diluted in 4.5 mL of the appropriated PBS. The Epi stock solutions were freshly prepared before each

experiment, to prevent any previous oxidation of the neurotransmitter. The volumes were measured using EP-10 and EP-100 from Unipette Microliter Pipettes (Uniscience, Brazil). All experiments were performed at room temperature ( $25 \pm 3$  °C).

## **Apparatus**

All pH measurements were performed using a model 654 pHmeter and a combined glass electrode, model 6.0203.100 (OE), both from Metrohm. All electrochemical experiments were performed in a potentiostat/galvanostat PGSTAT 101, Metrohm AUTOLAB, connected to an IME663 interface stirring device. Data processing was done by version 1.11.4 of NOVA software and the software Origin 2019. A Glassy Carbon Electrode (GCE) with a diameter of 3.0 mm was used as a working electrode, a Silver/ Silver Chloride (+ 0.222 V vs. SHE) in a saturated solution of potassium chloride, and a platinum wire were used as a reference and auxiliary electrodes, respectively, in an electrochemical cell of 10 mL. Before each experiment, the electrochemical cell was degassed with industrial N<sub>2</sub>, and the GCE was polished using diamond spray suspensions with a decreasing particle size of 3.0, 1.0 and 0.1 μm from Kemet (Maidstone, UK) on a polishing pad from Buehler (Lake Bluff, Illinois, USA). The solutions were stirred before each electrochemical measurement.

## **Electrochemical procedures**

Cyclic voltammograms (CV) were performed by sweeping the potential from 0.0 V to 1.0 V, then back from 1.0 to -0.6 V, and finally from -0.6 V to 0.0 V. The scan rates were varied between 0.01 and 10.0 V s<sup>-1</sup>. The square wave voltammograms (SWV) were performed by sweeping the potentials from -0.6 V to 1.0 V, and in separate procedures from 1.0 V to -0.6V. The experimental

254

parameters were: step potential of 2.0mV, pulse amplitude of 20.0 mV and a frequency of 50.0 Hz, resulting in a voltage scan rate of 0.1 V s<sup>-1</sup>. All simulations were performed using the DigiElch 8 software from Gamry Instruments (Warminster, PA, USA)

## **Results and Discussion**

For this section, the Epi's oxidation mechanism was constructed using voltammetry. The first part consisted in using CV with varying scan rates to observe the behaviour of epinephrine's processes. In sequence, SVW was used to further elucidate the reversibility of the redox pairs as well as the presence of the chemical reactions. Going further, theoretical predictions allied with experimental data were used to discriminate each Epi's mechanism and identify the number of electrons in each process. Then, by applying the effective number of electrons method, the kinetics involved in each of the electron's transfers was established and the  $k_f$  for the cyclization estimated. Finally, digital simulations were obtained for the voltammograms using the classical and the revised oxidation mechanism and compared with the experimental data to further support the thermodynamic and kinetic parameters obtained experimentally. Finally, Tafel plots and charge transfer coefficient analysis allowed the validation of the simulations and a more detailed oxidation mechanism was proposed.

### **Cyclic and Square Wave Voltammetry – the electrochemical behaviour of epinephrine**

To observe the behaviour of Epi, cyclic voltammograms of 1.0 mM Epi solution in 0.1 M PBS, at pH 7.4 were obtained at different scan rates. Figure 1 shows that Epi presents four processes, two oxidations (process I and IV) and

two reductions (process II and III), in which two redox pairs are formed (steps I/II and III/IV).

It is noteworthy that three of four processes (processes I, III and IV) are present in all scan rates, as process II is only visible at very fast scan rates ( $v \geq 10 \text{ V s}^{-1}$ ). Both I/II and III/IV pairs appear to be irreversible as the peak potentials shift with the increase of the scan rate.

Finally, process II appears to be suppressed by the chemical step which follows process I, resulting in electrochemical irreversibility due to chemical consumption of the product. [37–40] The peak potentials and peak currents of each process at each scan rate are presented in table S1.

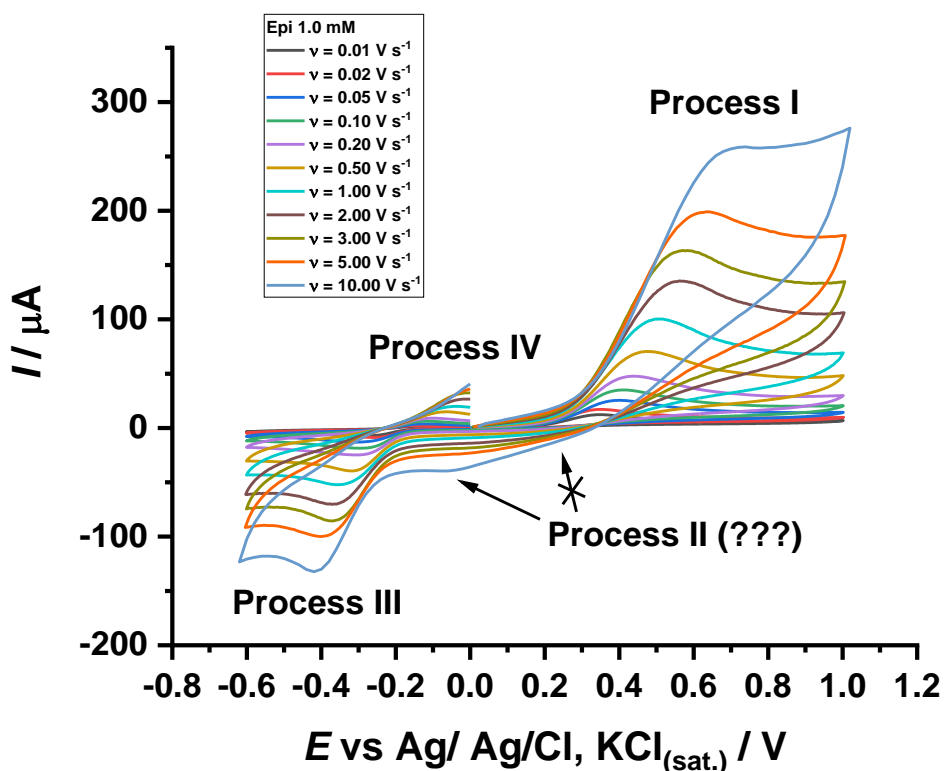


Figure 1: Typical CVs of Epi solutions in 0.1M PBS, pH = 7.4 at different scan rates, from 0.01 to 10.0  $\text{V s}^{-1}$ .

Square wave voltammograms were then performed to better elucidate the electrochemical processes, and observe the chemistry which follows the step I. Figure 2A shows SWV from -0.6 V to 1.0 V. It is possible to observe that both forward and backward current present a similar intensity and the same peak potentials (approximately 0.38 V), confirming that processes I and II form a reversible couple, although the CV suggests an irreversible behaviour. Furthermore, figure 2B shows SWV from 1.0 V to -0.6 V, where, unlike figure 2A, it is possible to see the redox pairs I/ II and III/ IV. The latter processes present a behaviour similar to the former, confirming that III/ IV do form a reversible couple, although the CV results again indicate irreversibility. In addition, the presence of processes III and IV in the SWV recorded with a potential sweep from positive to negative potentials confirm the dependence of processes III/ IV on the processes I/ II and the chemical step that follows.

Therefore, the voltammograms show an ECE mechanism, agreeing with the literature. On the other hand, the literature suggests two reversible processes that will sandwich the chemical step, a result that is in conflict with the ones obtained with the CV. To further explore this divergence, the Randles-Sevcik equations were plotted to provide a theoretical prediction and discrimination of the mechanism.

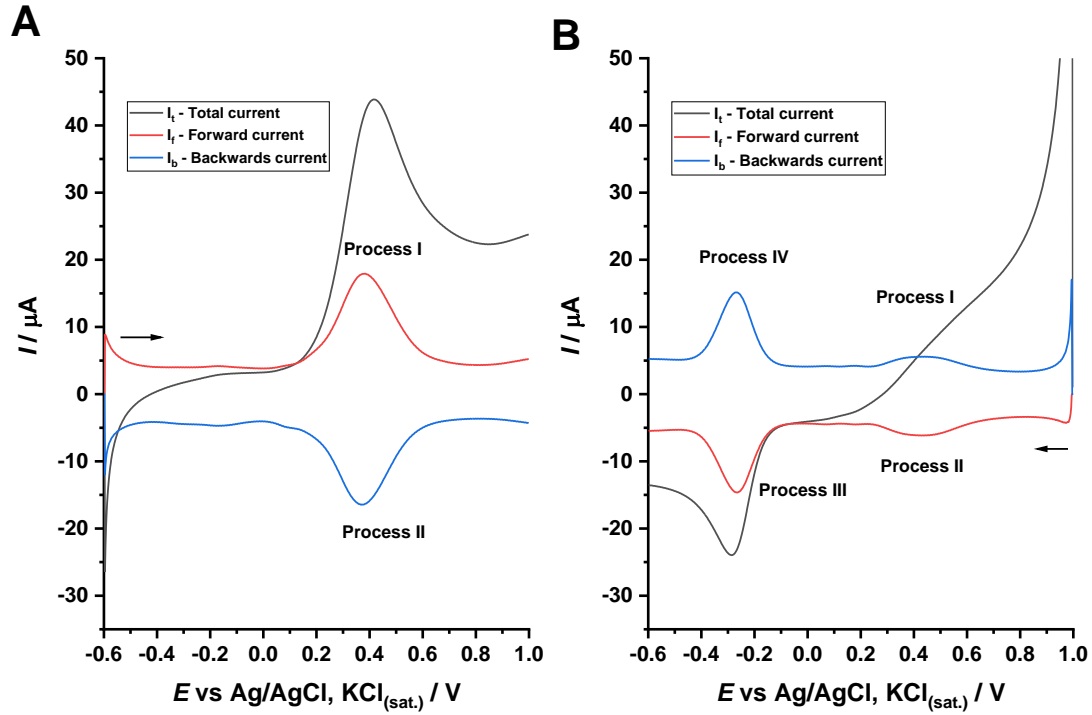


Figure 2: Typical SWV of Epi solutions in 0.1M PBS, pH = 7.4. A) Swept from -0.6 V to 1.0 V. B) Swept from 1.0 V to -0.6 V.

### Randles-Sevcik equation and oxidation mechanism discrimination

To elucidate these results, the Randles-Sevcik theoretical predictions were used. These equations describe the theoretical behaviour of a reversible process, Equation 1, or multi-step irreversible process, Equation 2. [41] Comparing the experimental results with theoretical predictions, not only more information regarding the reversibility of the processes can be acquired, but it also allows us to find the rate-determining step.

$$I_p = 0.446 n F C A \sqrt{n F v D / R T} \quad (6)$$

$$I_p = 0.496 \sqrt{n' + \beta} F C A \sqrt{n F v D / R T} \quad (7)$$

where  $I_p$  is the peak current in A,  $n$  is the overall number of electrons transferred,  $n'$  is the number of electrons prior to the rate-determining step,  $\beta$  is the anodic

charge transfer coefficient,  $F$  is the Faraday Constant in Coulomb mol<sup>-1</sup>,  $C$  is the concentration in mol cm<sup>-3</sup>,  $A$  the electrode area in cm<sup>2</sup>,  $\nu$  is the scan rate in V s<sup>-1</sup>,  $R$  is the Gas Constant in J K<sup>-1</sup> mol<sup>-1</sup> and  $T$  is the temperature in K. A diffusion coefficient ( $D$ ) of  $1.03 \times 10^{-5}$  cm s<sup>-1</sup> was used.

Figure 3 shows the comparison between the Randles-Sevcik theoretical predictions for three distinct mechanisms, a multi-step two-electron oxidation with and without a prior electron being transferred before the rate determining step, and a single step involving two electrons. The experimental results were plotted to show the best fit. Figure 3 also shows the experimental data obtained from the CV.

It can be observed that the experimental values fit the multi-step irreversible case, with the rate-determining first step. Thus, this result strongly suggests that process I occurs in an EE mechanism, two sequential one-electron oxidations, that are then followed by a chemical step, corroborating the data observed in figure 1, rather than supporting the two-electron single step that is commonly proposed in the literature.

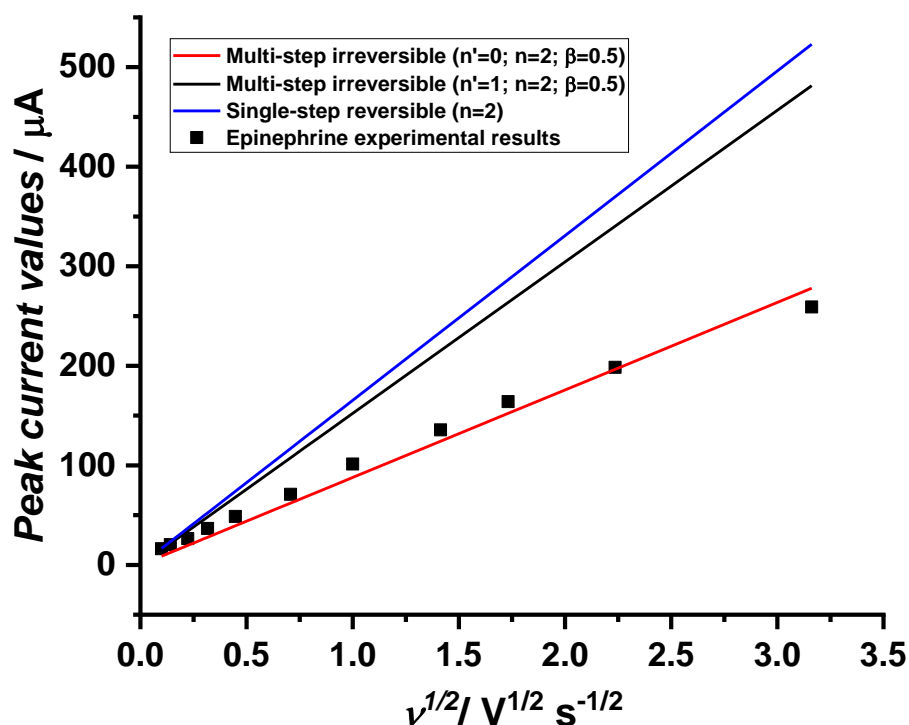


Figure 3: Plot of the Epi oxidation peak current as a function of the square root of the scan rates, compared to the theoretical plots of Randles-Sevcik equations (Black square – Epi experimental peak current values; blue – reversible,  $n=2$ ; dark gray – Multi-step irreversible  $n'=1$ ,  $n=2$ ,  $\beta=0.5$ ; red – Multi-step irreversible  $n'=0$ ,  $n=2$ ,  $\beta=0.5$ ), Electrode Area =  $0.071 \text{ cm}^2$ ,  $D = 1.03 \times 10^{-5} \text{ cm s}^{-1}$ .

### The kinetics of the epinephrine cyclization

The Randles-Sevcik equations show that Epi oxidizes in an EE mechanism. Following the electrochemical steps, an intramolecular Michael addition occurs, as evidenced by the voltammograms. To obtain the kinetics of this chemical step, the method of effective number of electrons transferred was performed. The values of  $n_{app}$  were obtained by the ratio of the experimental peak current values per the theoretical predictions of the multi-step irreversible Randles-Sevcik equation, and the results were then compared with an



experimental working curve in figure S2 ( $n_{app}$  vs  $\log \lambda$ ), where ( $\lambda$ ) is the dimensionless parameter. [42,43] The  $\lambda$  values were then plotted as a function of the inverse of the scan rate to obtain the  $k_f$  of the cyclization reaction, according to equation 8. [8,9,38,41,43]

$$\lambda = (RT/F) k_f / \nu \quad (8)$$

Figure 4 shows an expected linear correlation, with a slope that provides  $k_f = 18.9 \text{ s}^{-1}$ , which is in good agreement with the literature, and a much higher value than the  $0.24 \text{ s}^{-1}$  observed for dopamine. [8,44]

This difference between the rates of the cyclization reactions is due to the methyl-amine moiety of Epi. The donor effect of the methyl group increases the nucleophilic characteristics of the non-ligand electrons of the amine, hence increasing the rate of the chemical step in comparison with dopamine.

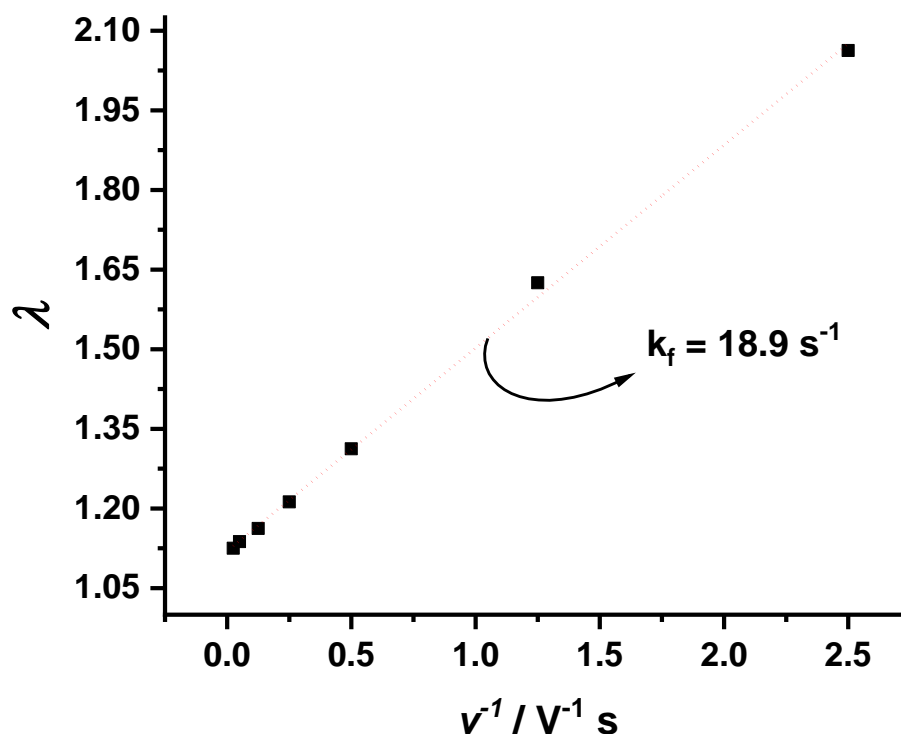


Figure 4: Dimensionless parameter ( $\lambda$ ) as a function of the inverse of the scan rate.

Since the electrochemical steps are proton-coupled electron processes (PCEP) [9], the Pourbaix diagram (Peak process values versus pH) was obtained for each process (I to IV).

### The influence of pH on the cyclization chemical step

To obtain the number of protons and electrons involved in each process, CVs were obtained at different pH values. These results can be seen in figure S3.

In figures 5A, S3, S4 and S5 the peak potential value of process I can be observed as a function of pH. The potential values remain practically constant until approximately pH = 5, after that they decrease about 100 mV per pH unit, indicating that process I involves two protons to each electron transferred. The

pKa of the process can be observed at pH 5.21, which corresponds to the deprotonation of the ammonium moiety that is formed in acidic media ( $HEpi^+ \rightleftharpoons H^+ + Epi$ ), eq. 9, [45] as this step act as a “rate determining step” to the electrochemical mechanism since the non-ligand electrons of the amine moiety are not available to perform the Michael addition, the process II can be observed at pH < 5.21. On the other hand, the deprotonation of HEpi+ acidic media is followed by two sequential proton coupled electron transfers (involving one electron and one proton each) that will convert the Epi into its quinone derivative (Epi<sub>Q</sub>). The latter then undergoes the cyclization process, which also involves a deprotonation, thus supressing the process II. Hence, this ‘C’EEC processes can be summarized by the following equations 9 to 12:



As a consequence of these sequential steps, the peak potentials, as state function, are expressed by the sum of each step, resulting in a complex Nernst equation that involves four protons and two electrons. Hence, two protons for each electron involved, and so differing from the expected 59 mV per dec. [45] These processes are summarized in scheme 2.

In figure 5B the peak potentials of process II can be observed in the same pH window. Process II presents a variation of 52 mV per dec of pH, thus suggesting the transfer of the same number of protons and electrons.

Figure 5C shows the peak potential value of process III as a function of pH. The curve presents a break at pH = 8, which suggests the pKa of the cyclic derivative. It can also be related to a coupled reaction at this value, a polymerization. [46,47]. Besides that, the curve presents a slope of 53 mV per dec of pH. This suggests that process III involves the same number of protons and electrons.

Finally, figure 5D do not present a break, hence no pKa was observed to process IV. In addition, it presents a slope of 52 mV per dec of pH. In conclusion, process IV also involves the same amount of protons and electrons.

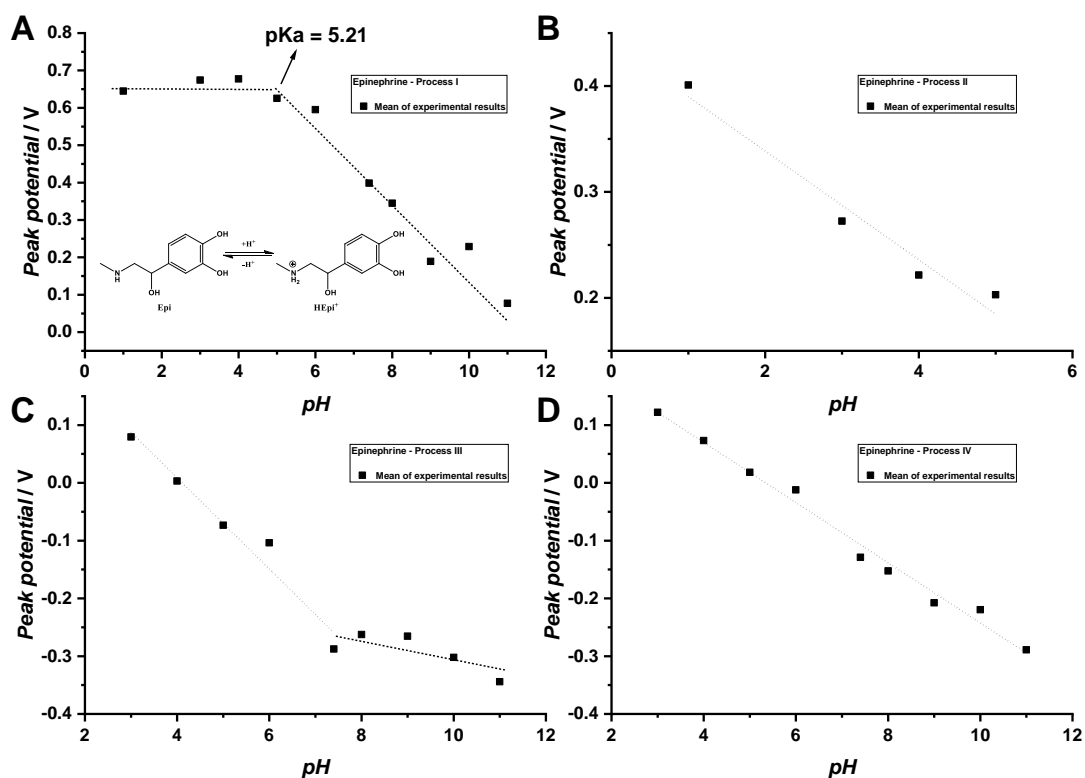
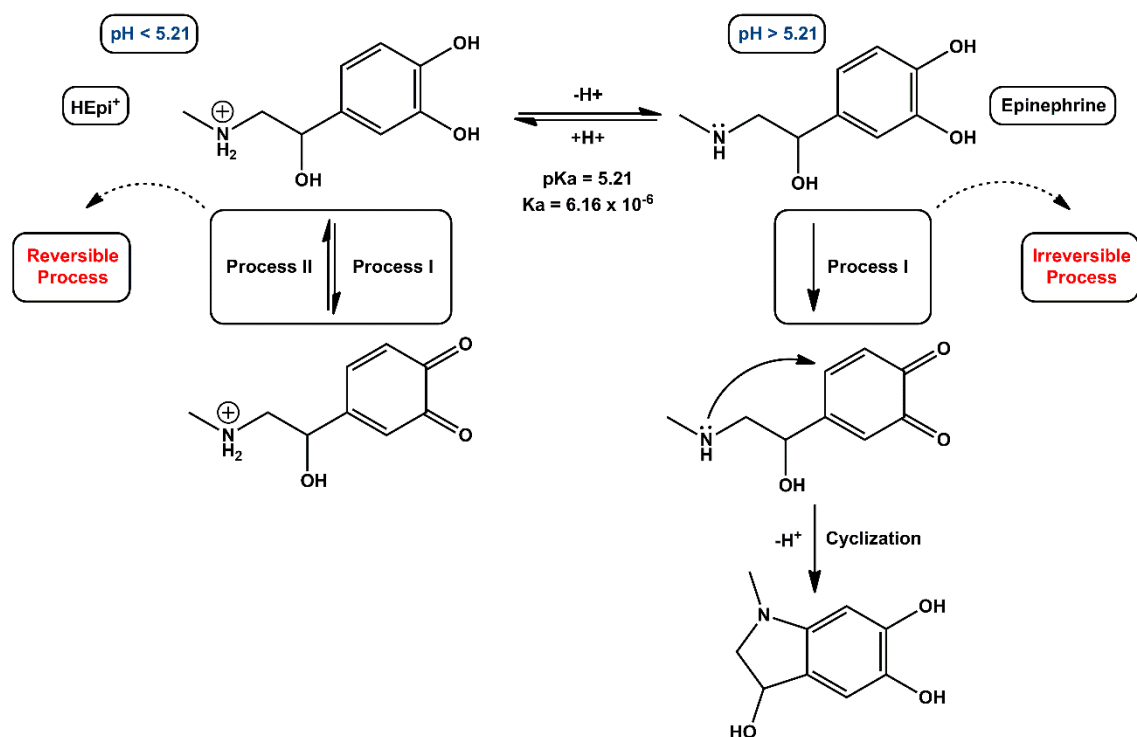


Figure 5: Pourbaix diagram (Peak potential values as a function of pH) of Epi processes. A) Process I, B) Process II, C) Process III, D) Process IV.



Scheme 2: Schematic representation of the Epi oxidation behaviour as a function of pH.

To reinforce the difference between the single-step two-electron reversible transfer and the proposed multi step irreversible process, and to better observe the which mechanism better fits the experimental results, both mechanisms were simulated and compared with the obtained voltammograms.

### Digital simulations

In this section, the experimental data obtained was used to simulate the electrochemical mechanism of Epi and compare with the most accepted one in the literature, a two-electron transfer in a single step. The digital simulations were used due to their capacity to validate the parameters obtained in both thermodynamic and kinetic measurements, even for a complex system such as Epi, as demonstrated by Rudolph. [48,49] As proposed in previous sections, the

oxidation processes of Epi occur in an EECEE mechanism, and so the mechanism imputed in the digital simulations can be observed in Tables 2 and 3.

Table 2: Mechanistic steps used to simulate the Epi multi-step irreversible and single step 2e<sup>-</sup> systems.

Multi-step irreversible mechanism			
Step order	Mechanism simulated	Correspondence	Type of step
1 <sup>st</sup>	$A - e^- \rightarrow B$	A/B	Electrochemical
2 <sup>nd</sup>	$B - e^- \rightarrow C$	B/C	Electrochemical
3 <sup>rd</sup>	$C \rightarrow D$	C/D - Cyclization	Chemical
4 <sup>th</sup>	$D - e^- \rightarrow E$	D/E	Electrochemical
5 <sup>th</sup>	$E - e^- \rightarrow F$	E/F	Electrochemical

Single step 2e <sup>-</sup> reversible			
Step order	Mechanism simulated	Correspondence	Type of step
1 <sup>st</sup>	$A - 2e^- \rightarrow B$	A/B	Electrochemical
2 <sup>nd</sup>	$B \rightarrow C$	B/C - Cyclization	Chemical
3 <sup>rd</sup>	$C - 2e^- \rightarrow D$	C/D	Electrochemical

Table 3: Optimized parameters for each simulated step, chemical and electrochemical.

Multi-step irreversible mechanism				
Step	$E_f^0 / V$	$k^0 / \text{cm} \text{ s}^{-1}$	$\alpha$	$D / \text{cm}^2 \text{ s}^{-1}$

A/B	0.375	0.01	0.5	$1.03 \times 10^{-5}$
B/C	0.175	0.001	0.5	$1.03 \times 10^{-5}$
D/E	-0.175	0.0025	0.5	$1.03 \times 10^{-5}$
E/F	-0.295	0.1	0.5	$1.03 \times 10^{-5}$
Step	K	$k_f / s^{-1}$	$k_b / s^{-1}$	
C/ D -	$1.0 \times 10^5$	18.9	$1.89 \times 10^{-4}$	

Cyclization

Single step 2e- reversible				
Step	$E_f^0 / V$	$k^0 / cm \ s^{-1}$	$\alpha$	$D / cm^2 \ s^{-1}$
A/ B	0.362	$10^3$	0.5	$1.03 \times 10^{-5}$
C/ D	-0.241	$10^3$	0.5	$1.03 \times 10^{-5}$
Step	K	$k_f / s^{-1}$	$k_b / s^{-1}$	
B/ C -	$1.0 \times 10^5$	18.9	$1.89 \times 10^{-4}$	

Cyclization

Figure 6 shows the simulated and experimental CVs at the respective scan rates. When compared with the experimental data, the two-electron transfer in a single reversible step simulation presents higher peak current values and dislocated peak potential values. However, the multi-step irreversible mechanism presents a great fit.

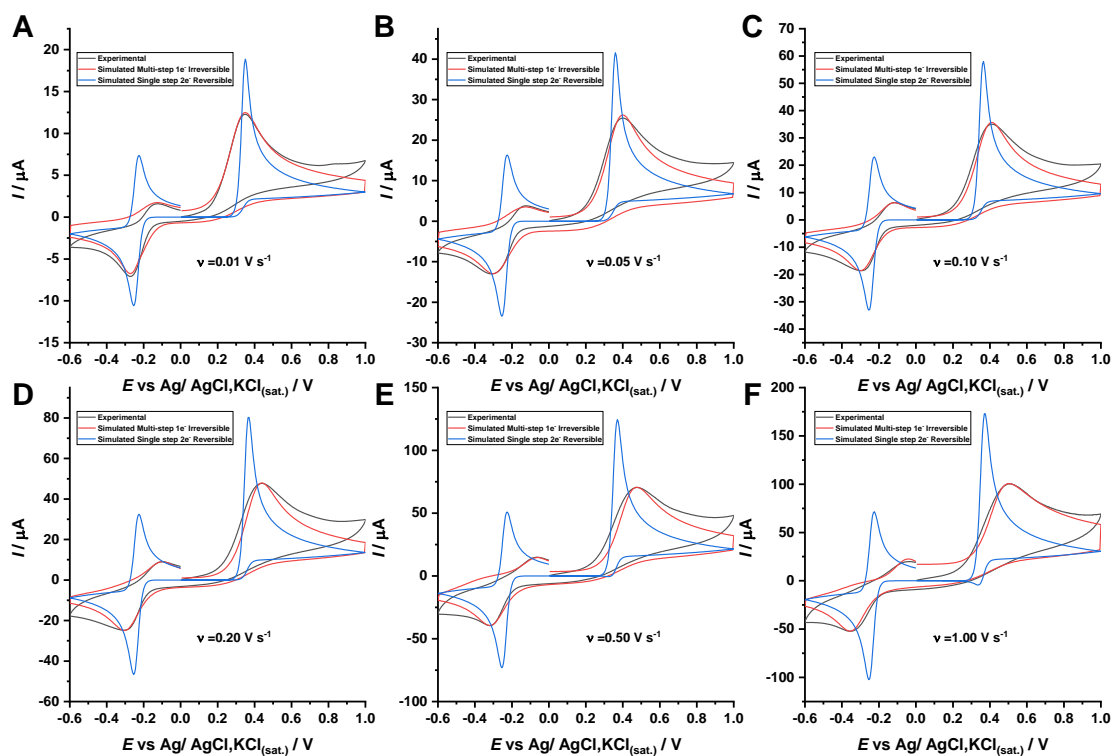


Figure 6: Experimental and simulated CVs of Epi. The simulations were obtained with the parameters presented in Tables 1 and 2.

To further corroborate the multi-step mechanism, the validation of the simulations was performed by Tafel analysis.

### Tafel analysis and validation of the simulations

To better evaluate the heterogeneous kinetics of this process, the Tafel analysis was conducted. It shows a correlation of the wave shapes of the process I with the kinetics of the the respective electrochemical process. In an anodic analysis, the following charge transfer coefficient ( $\beta$ ) can be reckoned according to equation 13. [50,51]

$$\beta(E) = \frac{F}{RT} \frac{d \ln I}{dE} \quad (13)$$

The respective analyses were performed according to Lin et al., [52], and the transfer coefficients of the process I as a function of the scan rate were



compared to both simulated and experimental voltammograms. Since each heterogeneous step was simulated with an  $\alpha$  value of 0.5, any shifts in the  $\beta$  values from the Tafel analyses are a consequence of the mechanism influence on the electrochemical process. These values are presented in Table S1 and Figure 7.

Figure 7 shows  $\beta$  values as a function of the scan rates from the experimental data and both the mechanisms simulated. A significant divergence can be observed between the experimental and single-step two-electron transfer simulated data, but the transfer coefficients of the experimental and multi-step irreversible simulation converge, thus corroborating the multi-step irreversible mechanism prediction, since the  $\beta$  values are directly related to the  $\Delta G^\ddagger$  of the process, as can be observed in equation 14. [53]

$$\beta = \frac{1}{2} \left( 1 + \frac{\Delta G^\ddagger}{\lambda} \right) \quad (14)$$

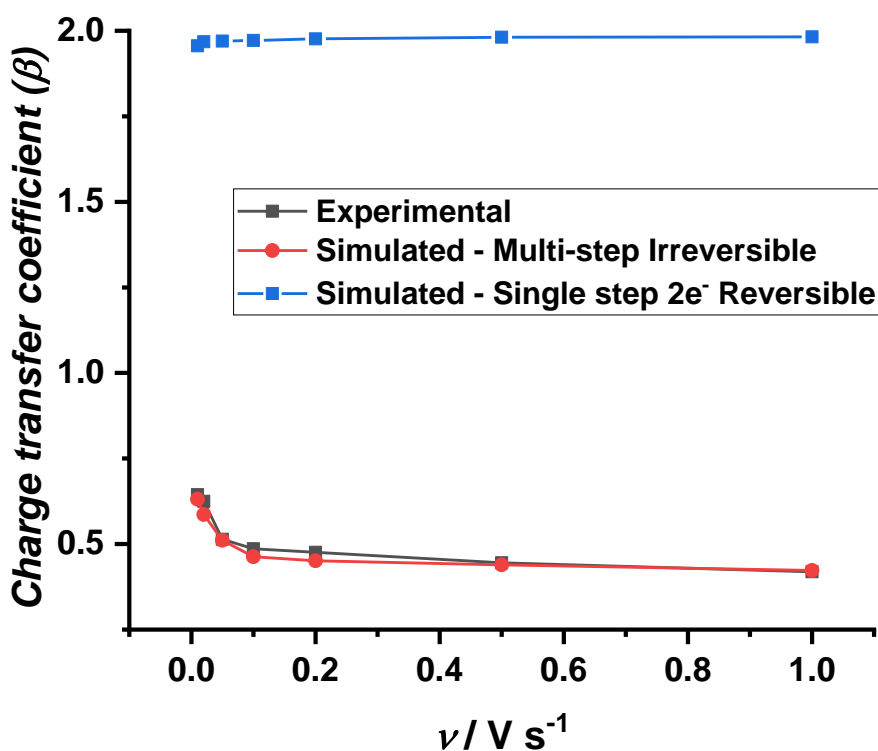


Figure 7: Comparison between the experimental and simulated  $\beta$  values.

In previous sections, the Randles-Sevcik equations predicted a multi-step two-electron process with no prior step to the rating-determining step ( $n'=0$ ) to process I, a result that is in alignment with the obtained Tafel values ( $0 < \beta < 1$ ), indicating the first step as the rating determining one. Using the Gibbs energy prediction provided by the software ChemDraw Ultra version 12.0.2.1076 by Cambridge Soft, the reaction coordinate was obtained, and its results compared with the Randles-Sevcik and charge-transfer coefficient predictions.

Figure 8 shows the Gibbs energy obtained for each of Epi's intermediate derivatives. The results suggest that the first step presents a higher energy, thus being the rating determining step, which matches the previous predictions.

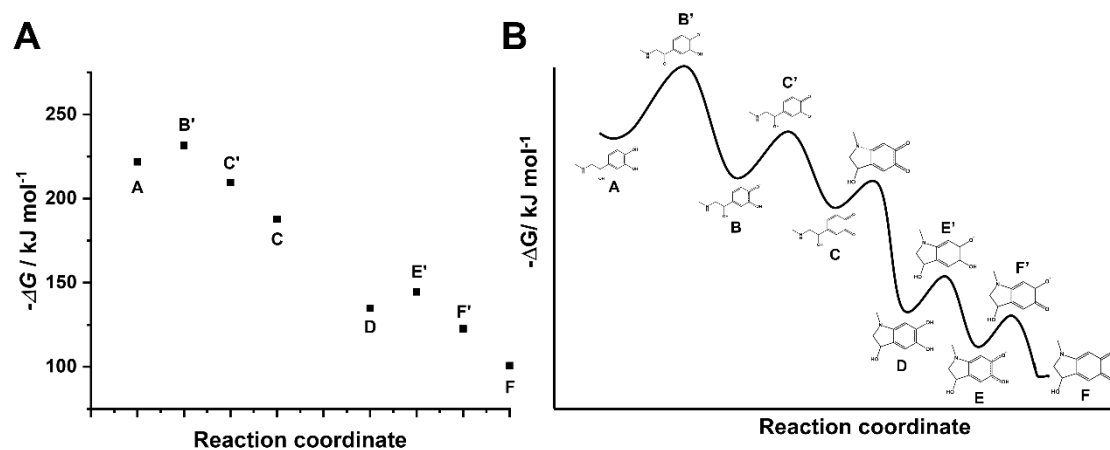
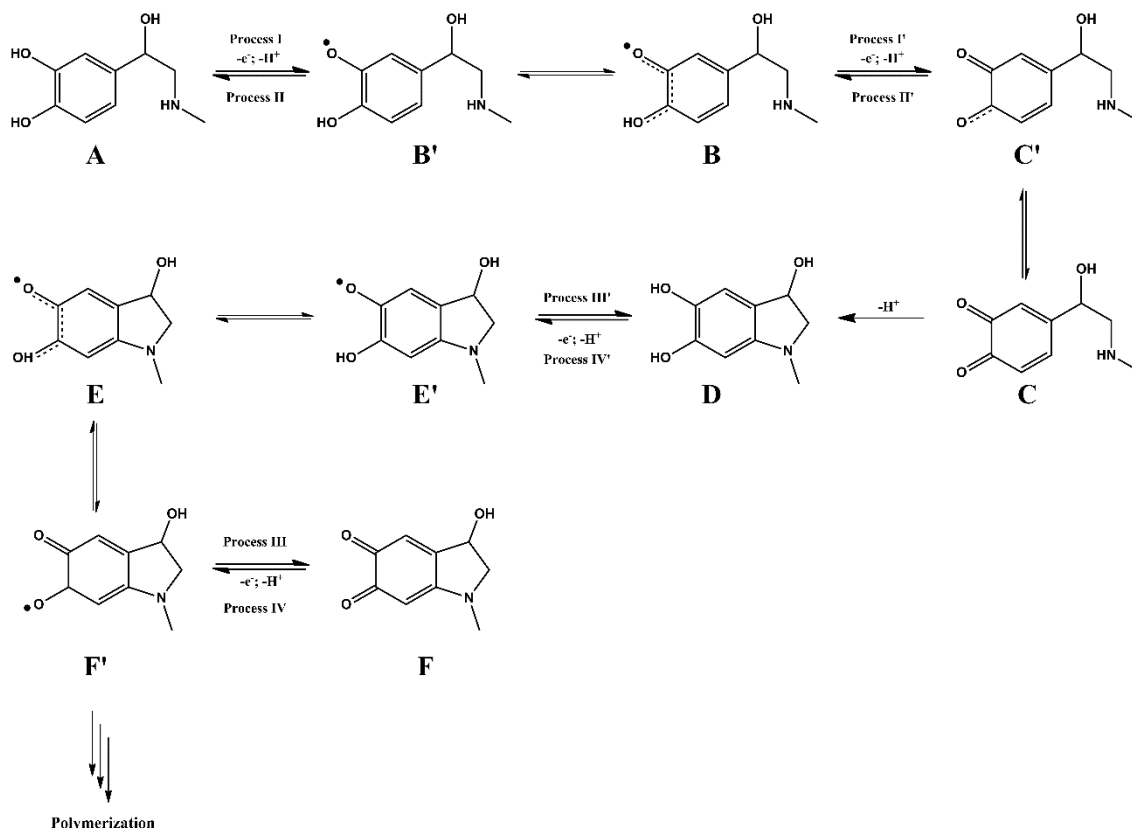


Figure 8: A) Diagram of Gibbs energy as a function of the reaction coordinate of the oxidation of Epi. B) Schematic representation of the Gibbs energy as a function of the reaction coordinate, illustrating each product and intermediate formed.

Based on the obtained data, the digital simulations, Gibbs energy and Tafel analysis, the following mechanism is proposed.



Scheme 3: Proposed electrochemical mechanism to Epi's processes I, II, III and IV with the follow-up cyclization.

## Conclusions

In summary, the classic epinephrine's ECE mechanism was revisited. The data obtained suggests that its mechanism is in fact a multi-step irreversible mechanism with a very fast intramolecular cyclization, an EECEE with a potential inversion, instead of a couple of two-electron processes in a single-step transfer. Moreover, the electrochemical and chemical steps are pH dependent. Based on Tafel analysis, digital simulations, and Gibbs energy and Randles-Sevcik predictions, a more detailed electrochemical mechanism was proposed to epinephrine.

## Acknowledgements

The main author would like to thank Roberto Bacil (*in memoriam*) for all the perspectives he taught. The authors would like to acknowledge the CNPq projects n° 140833/2016-1 and 150250/2021-5, CAPES project 88881.187396/2018-01 and Fapesp for the grants and funding to this project, and also thanks to Professor Mauro Bertotti who kindly allowed us to use the DigiElch 8 software for the digital simulations and Professor Richard G. Compton for the contributions in this work. Finally, the authors would like to thank Estênio Augusto de Oliveira Marcondes Filho for the proofreading this work.

## References

- [1] M. Esler, D. Kaye, J. Thompson, G. Jennings, H. Cox, A. Turner, G. Lambert, D. Seals, Effects of aging on epinephrine secretion and regional release of epinephrine from the human heart., *J. Clin. Endocrinol. Metab.* 80 (1995) 435–442. <https://doi.org/10.1210/jcem.80.2.7852502>.
- [2] R.J. Mathew, B.T. Ho, D.J. Francis, D.L. Taylor, M.L. Weinman, Catecholamines and anxiety, *Acta Psychiatr. Scand.* 65 (1982) 142–147. <https://doi.org/10.1111/j.1600-0447.1982.tb00833.x>.
- [3] G.A. Van Zijderveld, D.J. Veltman, R. Van Dyck, L.J.P. Van Doornen, Epinephrine-induced panic attacks and hyperventilation, *J. Psychiatr. Res.* 33 (1999) 73–78. [https://doi.org/10.1016/S0022-3956\(98\)00051-X](https://doi.org/10.1016/S0022-3956(98)00051-X).
- [4] R. Martinho, A. Oliveira, G. Correia, M. Marques, R. Seixas, P. Serrão, M. Moreira-Rodrigues, Epinephrine May Contribute to the Persistence of Traumatic Memories in a Post-traumatic Stress Disorder Animal Model, *Front. Mol. Neurosci.* 13 (2020) 1–16. <https://doi.org/10.3389/fnmol.2020.588802>.

- [5] T.D. Sokoloski, T. Higuchi, Kinetics of Degradation in Solution of Epinephrine by Molecular Oxygen, *J. Pharm. Sci.* 51 (1962) 172–177. <https://doi.org/10.1002/jps.2600510220>.
- [6] D.C.S. Tse, R.L. McCreery, R.N. Adams, Potential oxidative pathways of brain catecholamines, *J. Med. Chem.* 19 (1976) 37–40. <https://doi.org/10.1021/jm00223a008>.
- [7] H. Cui, L. Wu, J. Chen, X. Lin, Multi-mode in situ spectroelectrochemical studies of redox pathways of adrenaline, *J. Electroanal. Chem.* 504 (2001) 195–200. [https://doi.org/10.1016/S0022-0728\(01\)00444-2](https://doi.org/10.1016/S0022-0728(01)00444-2).
- [8] R.P. Bacil, L. Chen, S.H.P. Serrano, R.G. Compton, Dopamine oxidation at gold electrodes: Mechanism and kinetics near neutral pH, *Phys. Chem. Chem. Phys.* 22 (2020) 607–614. <https://doi.org/10.1039/c9cp05527d>.
- [9] J.-M. Savéant, C. Costentin, *Elements of Molecular and Biomolecular Electrochemistry: An Electrochemical Approach to Electron Transfer Chemistry*, 2nd editio, Wiley, 2019. <https://www.wiley.com/en-br/Elements+of+Molecular+and+Biomolecular+Electrochemistry%3A+An+Electrochemical+Approach+to+Electron+Transfer+Chemistry%2C+2nd+Edition-p-9781119292333>.
- [10] B. Kalyanaraman, C.C. Felix, R.C. Sealy, Electron spin resonance-spin stabilization of semiquinones produced during oxidation of epinephrine and its analogues., *J. Biol. Chem.* 259 (1984) 354–358. [https://doi.org/10.1016/S0021-9258\(17\)43666-0](https://doi.org/10.1016/S0021-9258(17)43666-0).
- [11] P. Manini, L. Panzella, A. Napolitano, M. D'Ischia, Oxidation Chemistry of Norepinephrine: Partitioning of the O -Quinone between Competing Cyclization and Chain Breakdown Pathways and Their Roles in Melanin

- Formation, *Chem. Res. Toxicol.* 20 (2007) 1549–1555.  
<https://doi.org/10.1021/tx700254q>.
- [12] D.G. Graham, Oxidative pathways for catecholamines in the genesis of neuromelanin and cytotoxic quinones., *Mol. Pharmacol.* 14 (1978) 633–43.  
<http://www.ncbi.nlm.nih.gov/pubmed/98706>.
- [13] S. Garnayak, S. Patel, Oxidation of Epinephrine to Adrenochrome by Cetyltrimethylammonium Dichromate: A Mechanistic Study, *Ind. Eng. Chem. Res.* 53 (2014) 12249–12256. <https://doi.org/10.1021/ie500037x>.
- [14] S. Ito, A Chemist's View of Melanogenesis, *Pigment Cell Res.* 16 (2003) 230–236. <https://doi.org/10.1034/j.1600-0749.2003.00037.x>.
- [15] M.D. Hawley, S. V Tatawawadi, S. Piekarski, R.N. Adams, Electrochemical Studies of the Oxidation Pathways of Catecholamines, *J. Am. Chem. Soc.* 89 (1967) 447–450. <https://doi.org/10.1021/ja00978a051>.
- [16] C. Lin, L. Chen, E.E.L. Tanner, R.G. Compton, Electroanalytical study of dopamine oxidation on carbon electrodes: from the macro- to the micro-scale, *Phys. Chem. Chem. Phys.* 20 (2018) 148–157.  
<https://doi.org/10.1039/C7CP07450F>.
- [17] P. Hernández, I. Sánchez, F. Patón, L. Hernández, Cyclic voltammetry determination of epinephrine with a carbon fiber ultramicroelectrode, *Talanta.* 46 (1998) 985–991. [https://doi.org/10.1016/S0039-9140\(97\)00353-6](https://doi.org/10.1016/S0039-9140(97)00353-6).
- [18] X. Wen, Y.-H. Jia, Z.-L. Liu, Micellar effects on the electrochemistry of dopamine and its selective detection in the presence of ascorbic acid, *Talanta.* 50 (1999) 1027–1033. [https://doi.org/10.1016/S0039-9140\(99\)00207-6](https://doi.org/10.1016/S0039-9140(99)00207-6).

- [19] S.-M. Chen, K.-T. Peng, The electrochemical properties of dopamine, epinephrine, norepinephrine, and their electrocatalytic reactions on cobalt(II) hexacyanoferrate films, *J. Electroanal. Chem.* 547 (2003) 179–189. [https://doi.org/10.1016/S0022-0728\(03\)00220-1](https://doi.org/10.1016/S0022-0728(03)00220-1).
- [20] R. Sainz, M. del Pozo, M. Vilas-Varela, J. Castro-Esteban, M. Pérez Corral, L. Vázquez, E. Blanco, D. Peña, J.A. Martín-Gago, G.J. Ellis, M.D. Petit-Domínguez, C. Quintana, E. Casero, Chemically synthesized chevron-like graphene nanoribbons for electrochemical sensors development: determination of epinephrine, *Sci. Rep.* 10 (2020) 14614. <https://doi.org/10.1038/s41598-020-71554-1>.
- [21] C.S. Caruso, I. da Cruz Vieira, O. Fatibello-Filho, Determination of Epinephrine and Dopamine in Pharmaceutical Formulations Using a Biosensor Based on Carbon Paste Modified with Crude Extract of Cara Root ( *Dioscorea bulbifera* ), *Anal. Lett.* 32 (1999) 39–50. <https://doi.org/10.1080/00032719908542597>.
- [22] S. Shahrokhian, M. Ghalkhani, M.K. Amini, Application of carbon-paste electrode modified with iron phthalocyanine for voltammetric determination of epinephrine in the presence of ascorbic acid and uric acid, *Sensors Actuators B Chem.* 137 (2009) 669–675. <https://doi.org/10.1016/j.snb.2009.01.022>.
- [23] R.N. Goyal, S. Bishnoi, A novel multi-walled carbon nanotube modified sensor for the selective determination of epinephrine in smokers, *Electrochim. Acta.* 56 (2011) 2717–2724. <https://doi.org/10.1016/j.electacta.2010.12.047>.
- [24] Z. Shao, P. Puthongkham, K.K. Hu, R. Jia, M. V. Mirkin, B.J. Venton, *Thin* 276



- layer cell behavior of CNT yarn and cavity carbon nanopipette electrodes: Effect on catecholamine detection, *Electrochim. Acta.* 361 (2020) 137032. <https://doi.org/10.1016/j.electacta.2020.137032>.
- [25] S.-M. Chen, J.-Y. Chen, V.S. Vasantha, Electrochemical preparation of epinephrine/Nafion chemically modified electrodes and their electrocatalytic oxidation of ascorbic acid and dopamine, *Electrochim. Acta.* 52 (2006) 455–465. <https://doi.org/10.1016/j.electacta.2006.05.027>.
- [26] S. Immanuel, R. Sivasubramanian, Fabrication of two-dimensional chemically reduced graphene oxide nanosheets for the electrochemical determination of epinephrine, *Bull. Mater. Sci.* 43 (2020) 79. <https://doi.org/10.1007/s12034-019-2034-7>.
- [27] P. Shaikshavali, T. Madhusudana Reddy, T. Venu Gopal, G. Venkataprasad, V.S. Kotakadi, V.N. Palakollu, R. Karpoornath, A simple sonochemical assisted synthesis of nanocomposite (ZnO/MWCNTs) for electrochemical sensing of Epinephrine in human serum and pharmaceutical formulation, *Colloids Surfaces A Physicochem. Eng. Asp.* 584 (2020) 124038. <https://doi.org/10.1016/j.colsurfa.2019.124038>.
- [28] M.E. Ghica, C.M.A. Brett, Simple and Efficient Epinephrine Sensor Based on Carbon Nanotube Modified Carbon Film Electrodes, *Anal. Lett.* 46 (2013) 1379–1393. <https://doi.org/10.1080/00032719.2012.762584>.
- [29] T. Łuczak, Comparison of electrochemical oxidation of epinephrine in the presence of interfering ascorbic and uric acids on gold electrodes modified with S-functionalized compounds and gold nanoparticles, *Electrochim. Acta.* 54 (2009) 5863–5870. <https://doi.org/10.1016/j.electacta.2009.05.047>.

- [30] D. Zhu, H. Ma, Q. Zhen, J. Xin, L. Tan, C. Zhang, X. Wang, B. Xiao, Hierarchical flower-like zinc oxide nanosheets in-situ growth on three-dimensional ferrocene-functionalized graphene framework for sensitive determination of epinephrine and its oxidation derivative, *Appl. Surf. Sci.* 526 (2020) 146721. <https://doi.org/10.1016/j.apsusc.2020.146721>.
- [31] S. Adak, U. Bandyopadhyay, D. Bandyopadhyay, R.K. Banerjee, Mechanism of Horseradish Peroxidase Catalyzed Epinephrine Oxidation: Obligatory Role of Endogenous O<sub>2</sub> - and H<sub>2</sub>O<sub>2</sub> †, *Biochemistry.* 37 (1998) 16922–16933. <https://doi.org/10.1021/bi980899l>.
- [32] S.A. Hira, S. Nagappan, D. Annas, Y.A. Kumar, K.H. Park, NO<sub>2</sub>-functionalized metal–organic framework incorporating bimetallic alloy nanoparticles as a sensor for efficient electrochemical detection of dopamine, *Electrochem. Commun.* 125 (2021) 107012. <https://doi.org/10.1016/j.elecom.2021.107012>.
- [33] F. Meloni, M.I. Pilo, G. Sanna, N. Spano, A. Zucca, Ru(terpy)-Based Conducting Polymer in Electrochemical Biosensing of Epinephrine, *Appl. Sci.* 11 (2021) 2065. <https://doi.org/10.3390/app11052065>.
- [34] I.A. Mattioli, P. Cervini, É.T.G. Cavaleiro, Screen-printed disposable electrodes using graphite-polyurethane composites modified with magnetite and chitosan-coated magnetite nanoparticles for voltammetric epinephrine sensing: a comparative study, *Microchim. Acta.* 187 (2020) 318. <https://doi.org/10.1007/s00604-020-04259-x>.
- [35] M. Porcel-Valenzuela, F. Huerta, E. Morallón, F. Montilla, Affinity of Electrochemically Deposited Sol–Gel Silica Films towards Catecholamine Neurotransmitters, *Sensors.* 19 (2019) 868.

<https://doi.org/10.3390/s19040868>.

- [36] R. Zheng, C. Zhao, J. Zhong, Z. Qiu, Z. Hu, Determination of Epinephrine using a Novel Sensitive Electrochemiluminescence Sensor based on ZnO Nanoparticles Modified Pencil Graphite Electrode, *Int. J. Electrochem. Sci.* 14 (2019) 9380–9390. <https://doi.org/10.20964/2019.09.51>.
- [37] I. Streeter, S.F. Jenkinson, G.W.J. Fleet, R.G. Compton, Chemical instability promotes apparent electrochemical irreversibility: Studies on the electrode kinetics of the one electron reduction of the 2,6-diphenylpyrylium cation in acetonitrile solution, *J. Electroanal. Chem.* 600 (2007) 285–293. <https://doi.org/10.1016/j.jelechem.2006.10.006>.
- [38] R.P. Bacil, P.H.M. Garcia, W.R. de Araujo, S.H.P. Serrano, Mechanism and kinetics of olanzapine and quetiapine oxidations at glassy carbon electrode, *Electrochim. Acta.* 368 (2021) 137683. <https://doi.org/10.1016/j.electacta.2020.137683>.
- [39] R.P. Bacil, R.M. Buoro, O.S. Campos, M.A. Ramos, C.G. Sanz, S.H.P. Serrano, Electrochemical behaviour of dipyrone (metamizole) and others pyrazolones, *Electrochim. Acta.* 273 (2018) 358–366. <https://doi.org/10.1016/j.electacta.2018.04.082>.
- [40] R.P. Bacil, R.M. Buoro, R.P. Da-Silva, D.B. Medinas, A.W. Lima, S.H. Serrano, Mechanism of Electro-Oxidation of Metamizole Using Cyclic Voltammetry at a Glassy Carbon Electrode, *ECS Trans.* 43 (2012) 251–258. <https://doi.org/10.1149/1.4704966>.
- [41] C.E. Banks, R.G. Compton, *Understanding Voltammetry*, 3rd Ed., World Scientific Press Company, 2018.
- [42] R.S. Nicholson, I. Shain, *Theory of Stationary Electrode Polarography*: 279

- Single Scan and Cyclic Methods Applied to Reversible, Irreversible, and Kinetic Systems, *Anal. Chem.* 36 (1964) 706–723. <https://doi.org/10.1021/ac60210a007>.
- [43] A.J. Bard, L.R. Faulkner, N. York, C. @bullet, W. Brisbane, S.E. Toronto, *ELECTROCHEMICAL METHODS Fundamentals and Applications*, Electrochem. I. Faulkner, Larry R. (1944) 3–7. <https://doi.org/10.1016/B978-0-12-381373-2.00056-9>.
- [44] N. Umek, Cyclization step of noradrenaline and adrenaline autoxidation: a quantum chemical study, *RSC Adv.* 10 (2020) 16650–16658. <https://doi.org/10.1039/D0RA02713H>.
- [45] ChemAxon, Marvin Sketch 19.18, (2019). [www.chemaxon.com](http://www.chemaxon.com).
- [46] R. Abdel-Hamid, E.F. Newair, Adsorptive stripping voltammetric determination of gallic acid using an electrochemical sensor based on polyepinephrine/glassy carbon electrode and its determination in black tea sample, *J. Electroanal. Chem.* 704 (2013) 32–37. <https://doi.org/10.1016/j.jelechem.2013.06.006>.
- [47] T.K. Das, S. Remanan, S. Ghosh, S.K. Ghosh, N.C. Das, Efficient synthesis of catalytic active silver nanoparticles illuminated cerium oxide nanotube: A mussel inspired approach, *Environ. Nanotechnology, Monit. Manag.* 15 (2021) 100411. <https://doi.org/10.1016/j.enmm.2020.100411>.
- [48] M. Rudolph, A fast implicit finite difference algorithm for the digital simulation of electrochemical processes, *J. Electroanal. Chem. Interfacial Electrochem.* 314 (1991) 13–22. [https://doi.org/10.1016/0022-0728\(91\)85425-O](https://doi.org/10.1016/0022-0728(91)85425-O).
- [49] M. Rudolph, Digital simulations with the fast implicit finite difference (FIFD)

- algorithm, *J. Electroanal. Chem.* 338 (1992) 85–98.  
[https://doi.org/10.1016/0022-0728\(92\)80415-Z](https://doi.org/10.1016/0022-0728(92)80415-Z).
- [50] P. Delahay, *Double layer and electrode kinetics*, Interscience Publishers, 1965.
- [51] R. Guidelli, R.G. Compton, J.M. Feliu, E. Gileadi, J. Lipkowski, W. Schmickler, S. Trasatti, Defining the transfer coefficient in electrochemistry: An assessment (IUPAC Technical Report), *Pure Appl. Chem.* 86 (2014) 245–258. <https://doi.org/10.1515/pac-2014-5026>.
- [52] D. Li, C. Lin, C. Batchelor-McAuley, L. Chen, R.G. Compton, Tafel analysis in practice, *J. Electroanal. Chem.* 826 (2018) 117–124.  
<https://doi.org/10.1016/j.jelechem.2018.08.018>.
- [53] R.P. Bacil, E.A. de O. Marcondes Filho, K. de A. Dias, M.C. Portes, W.R. de Araujo, D. Oliveira-Silva, A.A. dos Santos, S.H.P. Serrano, The chemical interaction between the neurotransmitter dopamine and the antipsychotic drugs olanzapine and quetiapine, *J. Electroanal. Chem.* 881 (2021) 114946. <https://doi.org/10.1016/j.jelechem.2020.114946>.

## Appendix 7 - New insights on the electrochemical mechanism of epinephrine on glassy carbon electrode – Supplementary material

Table S1: Peak potentials and peak currents of the processes I, II, III and IV in each scan rate from figure 1.

v/ V	Peak potential process I/ V	Peak potential process II/ V	Peak potential process III/ V	Peak potential process IV/ V	Peak current process I/ $\mu\text{A}$	Peak current process II/ $\mu\text{A}$	Peak current process III/ $\mu\text{A}$	Peak current process IV/ $\mu\text{A}$
0.01	0.343	--	-0.266	-0.141	16.28	--	-5.52	1.65
0.02	0.343	--	-0.252	-0.159	20.04	--	-7.07	2.89
0.05	0.391	--	-0.295	-0.139	26.44	--	-8.78	3.30
0.10	0.3991	--	-0.286	-0.129	36.56	--	-9.98	5.09
0.20	0.426	--	-0.288	-0.117	48.70	--	-15.25	5.72
0.50	0.462	--	-0.309	-0.091	70.95	--	-22.99	6.75
1.00	0.490	--	-0.337	-0.079	101.3	--	-26.13	5.76
2.00	0.539	--	-0.357	-0.059	135.7	--	-32.53	4.74
3.00	0.541	--	-0.351	-0.042	164.0	--	-39.55	4.29
5.00	0.594	--	-0.373	-0.040	198.4	--	-39.31	4.06
10.0	0.639	-0.020	-0.399	-0.040	259.1	-7.35	-50.69	3.15
0								

## Randles-Sevcik equation and oxidation mechanism discrimination

The chronoamperogram was obtained by applying a potential of 0.7 V vs Ag/AgCl, KCl<sub>(sat.)</sub> for 200 s, and the diffusion coefficient was obtained by the linearization of the Cottrell equation ( $I$  vs  $t^{1/2}$ ).

To obtain the Randles-Sevcik theoretical predictions, a chronoamperometry of the system was obtained. The linearization of the chronoamperogram indicates a diffusion coefficient of  $1.03 \cdot 10^{-5} \text{ cm s}^{-1}$ .

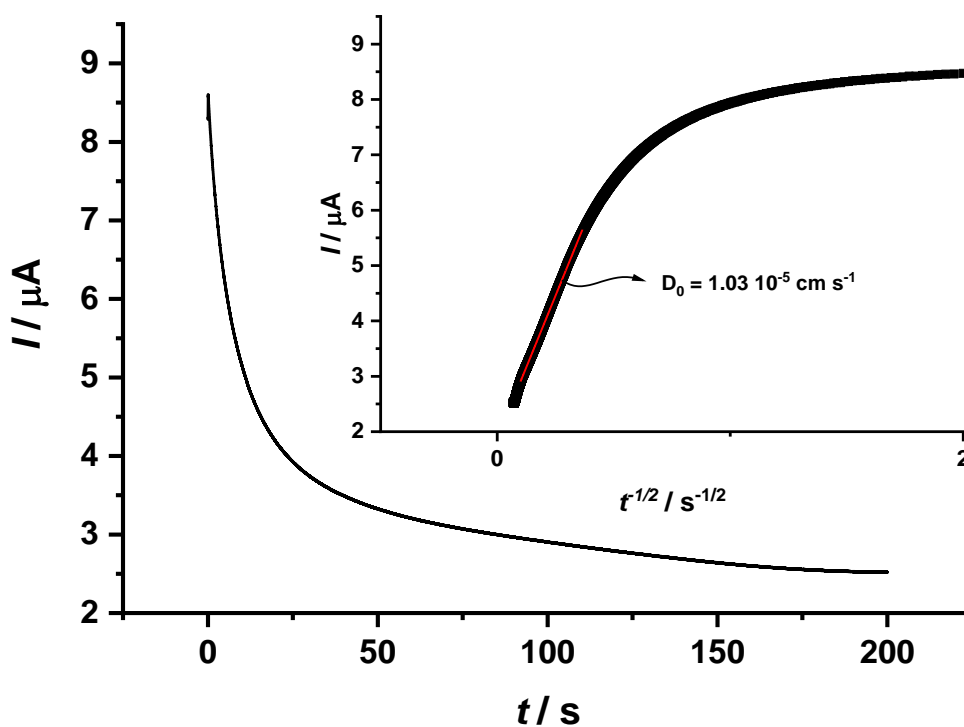


Figure S1: Chronoamperogram of 1.0 mM of Epi in 0.1 PBS, pH=7.4 and its respective linearization (insert)

## Kinetic analysis of the Epinephrine cyclization chemical step

### The number of effective electrons method

This method consists of the correlation between the number of electrons ( $n_{app}$ ) and the peak current observed in a system in which a chemical step is coupled to the electrochemical one. This correlation was obtained throughout an experimental working curve of the dimensionless parameter  $\lambda$  and the number of electrons observed ( $n_{app}$ )

$$n_{app} = n_1 + n_2 (1 - e^{-\lambda}) \quad (S1)$$

where  $n_1$  is the number of electrons involved in the heterogeneous steps prior to a chemical reaction and  $n_2$  is the number of electrons involved in electrochemical steps following the chemical step [41]

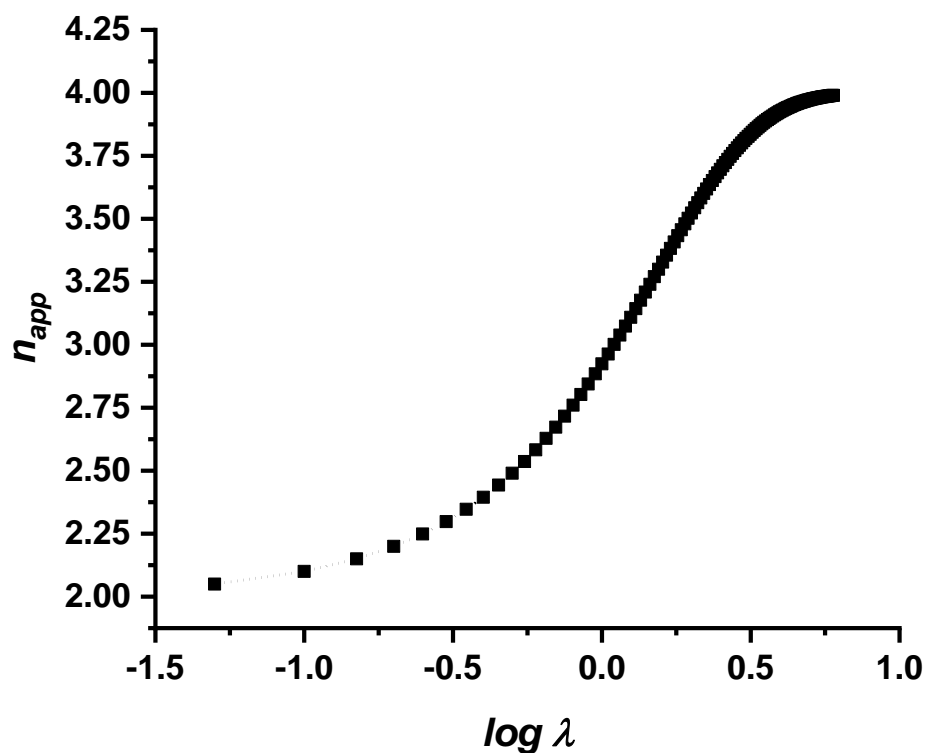




Figure S2: Experimental working curve that correlates the apparent number of electrons and the dimensionless parameter  $\lambda$ .

### The influence of pH at the cyclization chemical step

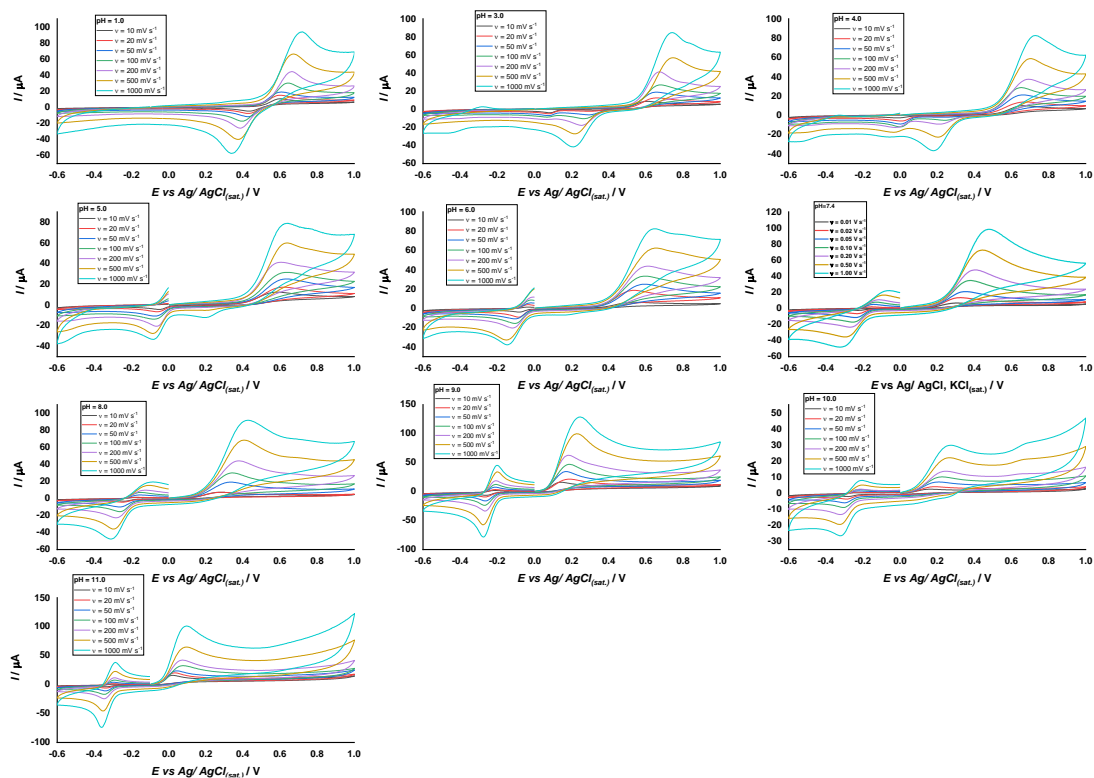


Figure S3: CVs of Epi solutions in 0.1M PBS, pHs = 1.0, 3.0, 4.0, 5.0, 6.0, 7,4 at different scan rates, from 0.01 to 10.0 V s<sup>-1</sup>.

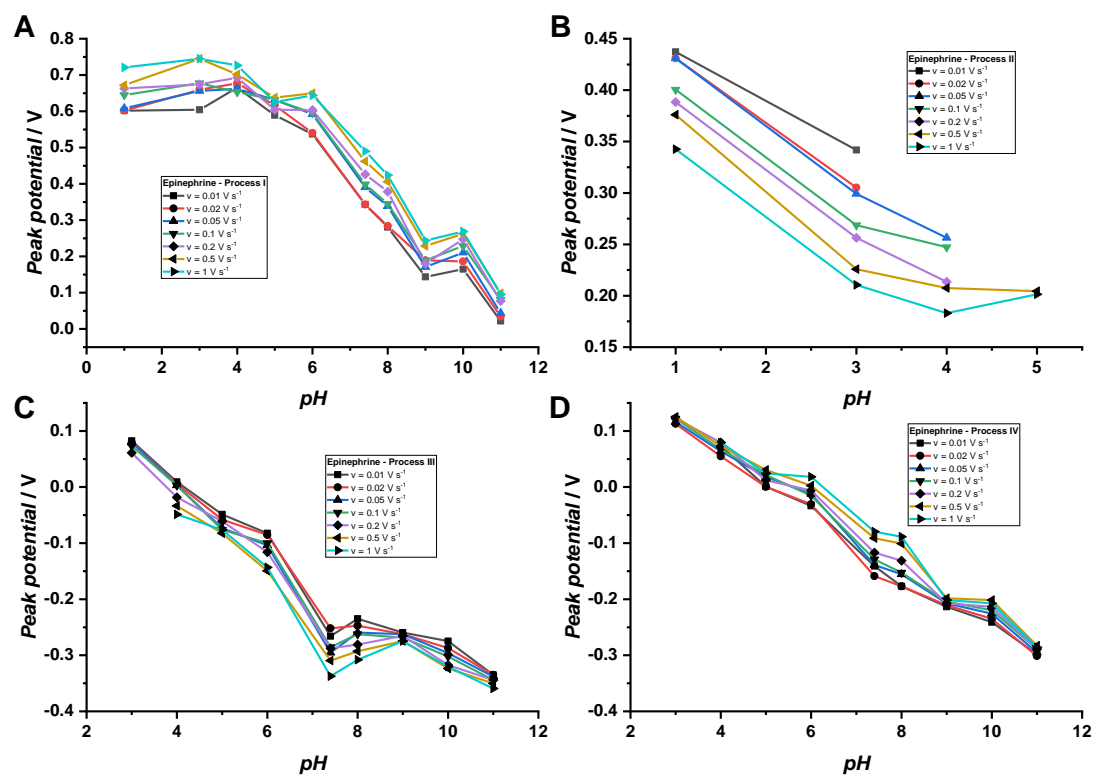


Figure S4: Pourbaix diagrams (Peak potential x pH) of processes A) I; B) II, C) III and D) IV.

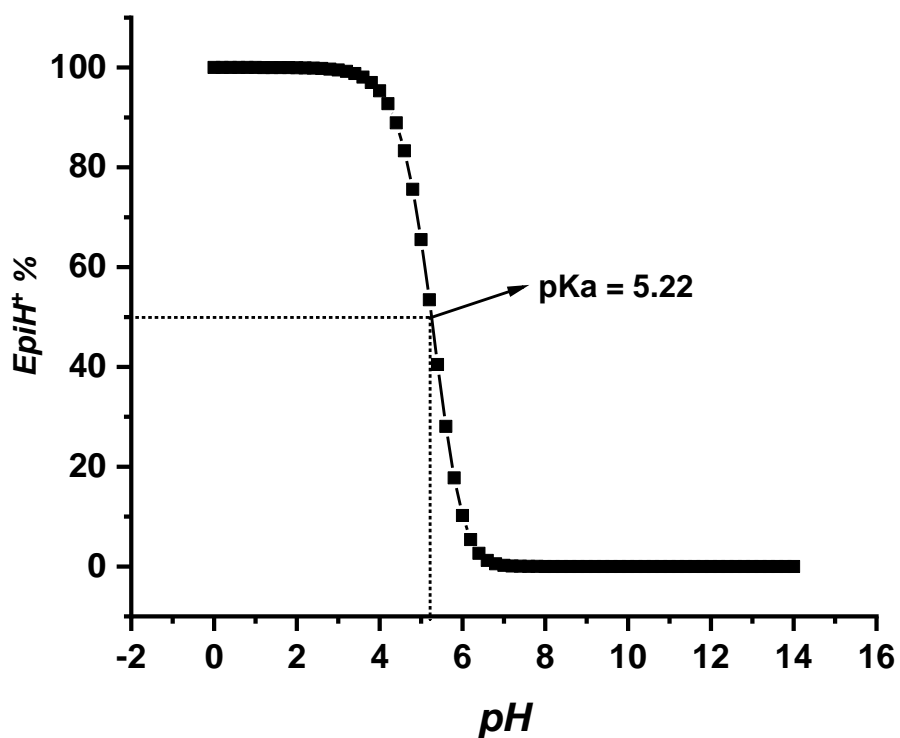


Figure S5: Plot of HEpi<sup>+</sup> % of species as a function of pH obtained with the software Marvin Sketch v21.20.0 from ChemAxon Ltd.

### Digital simulations

Table S2: Peak potentials and peak currents of cyclic voltammograms 1.0 mM

Epi solutions at 0.1M PBS, pH = 7.4

Experimental Data						
v/ V s-	EapI/	EapIII/	EapIV/	IapI/	IapIII/	IapIV/
1	V	V	V	μA	μA	μA
0.01	0.351	-0.272	-0.165	12.36	-7.12	1.61
0.05	0.400	-0.292	-0.126	25.42	-13.12	3.83
0.10	0.414	-0.301	-0.117	35.12	-18.60	6.43

0.20	0.439	-0.302	-0.103	47.87	-24.86	9.24
0.50	0.479	-0.317	-0.060	70.65	-39.29	14.82
1.00	0.509	-0.352	-0.039	100.10	-52.36	20.0

Table S3: Peak potentials and peak currents of Simulated Multi-step Irreversible simulated cyclic voltammograms, conditions presented at Table 2.

Simulated Multi-step Irreversible						
v/ V s <sup>-1</sup>	E <sub>apI</sub> /	E <sub>apIII</sub> /	E <sub>apIV</sub> /	I <sub>apI</sub> /	I <sub>apIII</sub> /	I <sub>apIV</sub> /
1	V	V	V	μA	μA	μA
0.01	0.351	-0.272	-0.164	12.47	-6.83	1.88
0.05	0.401	-0.292	-0.127	26.35	-13.13	3.40
0.10	0.413	-0.299	-0.116	35.19	-18.39	6.39
0.20	0.439	-0.301	-0.103	48.09	-24.53	9.34
0.50	0.478	-0.315	-0.060	69.89	-39.00	15.18
1.00	0.510	-0.353	-0.038	101.09	-52.02	22.51

Table S4: Peak potentials and peak currents of Simulated Simulated Single-step 2e<sup>-</sup> Reversible simulated cyclic voltammograms, conditions presented at Table 2.

Simulated Single-step 2e- Reversible						
v/ V s <sup>-1</sup>	E <sub>apI</sub> /	E <sub>apIII</sub> /	E <sub>apIV</sub> /	i <sub>apI</sub> /	i <sub>apIII</sub> /	i <sub>apIV</sub> /
1	V	V	V	μA	μA	μA
0.01	0.348	-0.250	-0.229	18.79	-10.44	7.36
0.05	0.354	-0.259	-0.226	41.82	-23.18	16.01
0.10	0.359	-0.261	-0.226	57.84	-32.84	23.58
0.20	0.364	-0.261	-0.226	80.88	-46.12	31.94
0.50	0.366	-0.262	-0.225	125.13	-72.90	51.83
1.00	0.371	-0.263	-0.244	173.45	-102.53	70.51

### Tafel analysis and validation of the simulations

Table S5: Charge transfer coefficients ( $\beta$ ) of the process I to the experimental data, multi-step irreversible and single step simulation as a function of the voltage scan rate.

v / (V s <sup>-1</sup> ) <sup>1)</sup>	Experimental	Simulated Multi-step irreversible	Simulated 2e- Single-step reversible
0.01	0.644	0.631	1.956
0.02	0.625	0.586	1.968
0.05	0.514	0.511	1.970
0.10	0.486	0.463	1.972
0.20	0.476	0.451	1.976
0.50	0.445	0.439	1.981
1.00	0.419	0.423	1.982

Table S6: Gibbs energy obtained from ChemDraw for each molecule presented in figure 8

Molecule	$\Delta G/ \text{kJ mol}^{-1}$
A	221.8
B'	231.58
C'	209.64
C	187.7
D	134.75
E'	144.53
F'	122.59
F	100.65

## References

[41] A.J. Bard, L.R. Faulkner, N. York, C. @bullet, W. Brisbane, S.E. Toronto, ELECTROCHEMICAL METHODS Fundamentals and Applications,

Electrochem. I. Faulkner, Larry R. (1944) 3–7. <https://doi.org/10.1016/B978-0-12-381373-2.00056-9>.

## Chapter 8

### **The chemical interaction between the neurotransmitter dopamine and the antipsychotic drugs olanzapine and quetiapine.**

This chapter addresses the chemical reaction between the neurotransmitter dopamine and the antipsychotics olanzapine and quetiapine. The development of this work count with the aid of Estenio Marcondes, who participated in the data curation, writing and revising the original draft, Dr. Kevin Dias and Professor Leandro Helgueira whom extracted and purified the drugs, Marcelo Portes, who acquired the EPR data, Professor William Reis who aided in the discussions, data curation and revising the original manuscript, Professor Diogo Silva and Professor Alcindo dos Santos, whom aided with HPLC-MS to comprove the adduct formation, and Professor Silvia Serrano who administrated the project. This manuscript is published at Journal of Electroanalytical Chemistry (DOI: 10.1016/j.jelechem.2020.114946)

Mental disorders like schizophrenia affect about 0.7% of the world population. Nowadays, the treatment consists of atypical antipsychotic drugs, mainly olanzapine and quetiapine. In this paper, we observed the chemical interaction between both olanzapine and quetiapine, antipsychotic drugs, with dopamine in phosphate buffer solutions at physiological pH using cyclic and differential voltammetry techniques, UV-Vis and EPR spectra. A solution containing both antipsychotic drugs and dopamine resulted in a shift of dopamine's redox processes, hindering its electrochemical oxidation. The chemical interaction was voltametrically investigated and a mechanism is



proposed. In addition, it was observed that the reactions of both drugs with DA are first-order, presenting kinetic rate constants of  $1.5 \cdot 10^{-2} \text{ s}^{-1}$  and  $9.0 \cdot 10^{-3} \text{ s}^{-1}$  for olanzapine and quetiapine, respectively, at  $\text{pH} = 7.4$ . To further evaluate the chemical reaction, a minimalist model between PIPES molecule and catechol was proposed and tested. The model presented a similar signal decrease and kinetic rate constant to those observed for both olanzapine and quetiapine reaction with dopamine, reinforcing the data obtained which strongly suggests that the chemical reaction occurs between piperazine and catechol moieties.

## **Introduction**

Neurotransmitters are biomolecules which perform critical signalling functions, being responsible for the "communication" between cells and organs in animals and humans. [1] They are classified as catecholamines, indoleamines, amino acids, neuropeptides, cholinergic and free radicals. [1] The malfunctions of these neural signalling pathways have been associated with some mental disorders, like schizophrenia. [2] This disease affects about 0.7% of the world population. [3] Nowadays, the treatment consists mainly of the use of atypical antipsychotic drugs, among the highly used ones are Olanzapine (OLZP) and Quetiapine (QTP). [4] Although this new generation of drugs presents fewer side effects than the typical ones [4], it could still affect patient health. The precise causes of the side effects remain to be explored, as there are no conclusive reports in the literature. According to the biochemical hypothesis of schizophrenia, the excess of neurotransmitters interacting with the dopaminergic receptors would lead to hypersignallism, triggering the effects of the disease. [2,5]

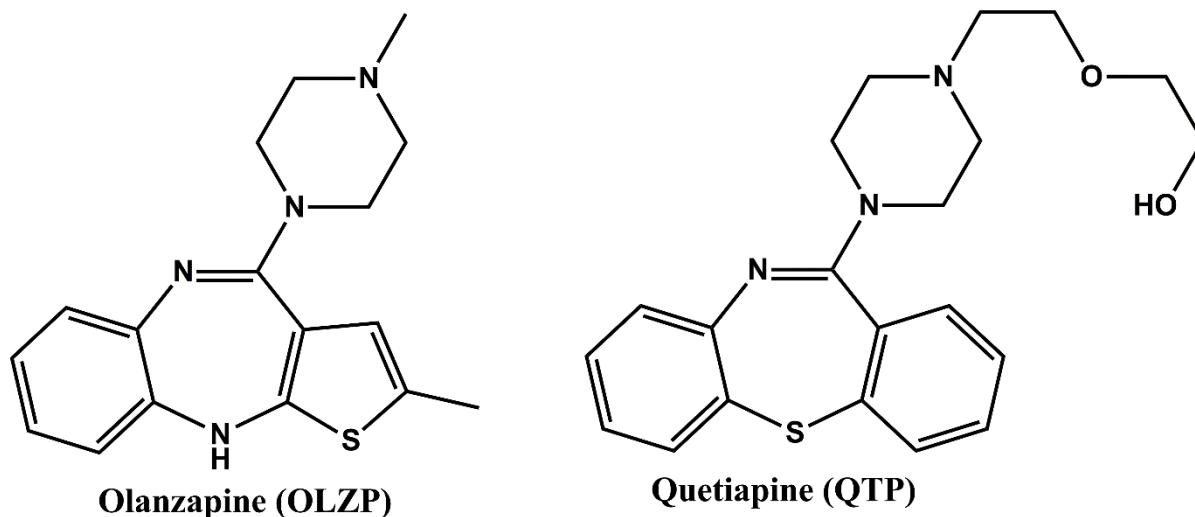
To counter the disease, an antipsychotic drug should be able to interact with the receptors preventing this effect. [6,7]

Before the 20<sup>th</sup> century, mental illnesses were treated with horrifying inhumane procedures such as electroshock therapy and lobotomy. [8,9] These “treatments” resulted in the intense stigmatization of patients in society, which persists until nowadays, regardless of the disease’s severity. Therefore, psychiatric patients are a frequent target of discrimination, which aggravates their psychological and psychiatric situation and hinders the lives of their families. [10–14]

As a response, mental illnesses such as schizophrenia, mood disorders, and depression have been the focus of much attention by the medical and psychological fields, as well as by related ones. [9,10] Throughout the years, care provided to the patients has been changing significantly and periodical drug dosage revisions as well as psychological therapy are now usual procedures. [15–17]

Recently, therefore, psychiatric diseases have been recognized and treated as such, even though the treatments, antipsychotic drugs, still presents extrapyramidal side effects. [3] To counter that, a new class, known as atypical antipsychotic drugs was created. [18–21] However minor the atypical antipsychotic-related extrapyramidal side effects may be. [4,22–24] they are significant and the literature still lacks studies regarding the chemical interactions between the drugs and neurotransmitters, which may be the cause of the side effects. [6,25]

Among the atypical medicines, two of the most used are olanzapine (OLZP) and quetiapine (QTP). [26] The chemical structures of both drugs are presented in Scheme 1.

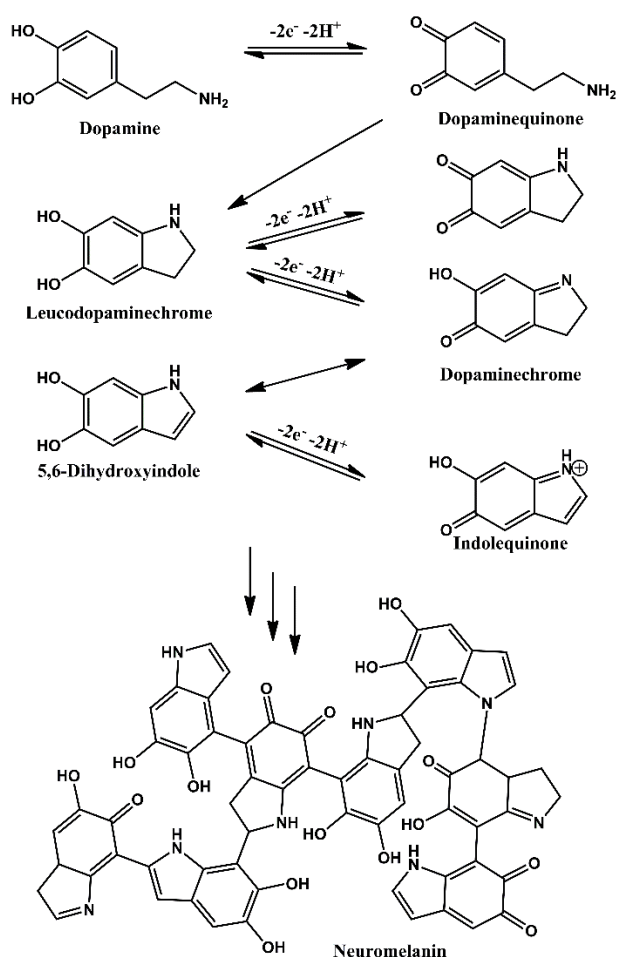


Scheme 1: Chemical structures of Olanzapine (OLZP) and Quetiapine (QTP).

Chemically, OLZP is a diazepine derivative, which has attached to it a piperazine ring by an amidine group. QTP is a tiodiazepine derivative that also presents an amidine group followed by a piperazine group, as can be observed in scheme 1. The electrochemical oxidation mechanism of OLZP is partially described by Shahrokhian et al. [27] However, up to the moment, the literature still lacks information regarding the electrochemical mechanism of QTP. Due to their widespread utilization, analytical methods were developed to detect and quantify OLZP and QTP using several different techniques such as spectrophotometric techniques [28,29], chromatographic [30–32], and electrochemical methods. [27,33–35]

Since the '60s, neurotransmitters have been widely studied with electrochemical techniques and as a result, their electron transfer mechanisms

are well described in the literature. [36–38] Among neurotransmitters, Dopamine (DA) stands out due to its signalling functions not only in the brain but also in the peripheral organs. [1] Its oxidation occurs in the catechol moiety [38–42], in a process involving two electrons and two protons. [42,43] In sequence, the oxidation product of DA undergoes a follow-up chemical step, consisting of a Michael addition reaction performed by the amine moiety forming an indole ring [38], which can also be oxidized, in a redox process that also involves two electrons and two protons. Ultimately, dopaminechrome converts into indolequinone, which then polymerizes forming neuromelanin. This oxidation mechanism is illustrated in scheme 2. [38,42]



Scheme 2: Schematic representation of the electrochemical redox mechanism of dopamine (DA), leading to neuromelanin. [38,42]

Due to its utmost biological relevance, several studies utilize electrochemical methods to detect this vital metabolite, which may adsorb on glassy carbon surfaces, and so demands the use of modified electrodes to be accurately quantified. Different types of electrode modification were used, like melanin films on pyrolytic graphite [42], molecularly imprinted polymers (MIPs) [44], graphene sheets [45], and others using ionic liquid electrodes [46], carbon nanorods [47], etc.

As mentioned above, the literature lacks a description of this chemical interaction between antipsychotic drugs and neurotransmitters, such as DA. Based on this, this paper aims to evaluate the occurrences of direct chemical interaction between the drugs OLZP and QTP and the neurotransmitter DA, as well as to obtain kinetic information of the related interaction reactions.

## **Materials and methods**

### **Apparatus**

All pH measurements were performed using a model 654 pH meter and a combined glass electrode, model 6.0203.100 (OE), both from Metrohm. NMR spectra were obtained from the IQ-USP Analytical Centre using a 300 MHz Bruker equipment with ACS laboratory software. All the NMR data were obtained at an ambient temperature of  $25 \pm 3$  °C.

### **Chemicals and reagents**

All used reagents, except QTP and OLZP, were of analytical grade and used without prior purification. The solutions were prepared using deionized water from

a reverse osmosis device (Gehara Co., model of ultra-pure OS10LX system, water resistivity 18MΩcm). 0.1 mol L<sup>-1</sup> phosphate buffer solutions (PBS) were prepared by solubilizing and diluting, respectively, the appropriate amount of NaH<sub>2</sub>PO<sub>4</sub> and H<sub>3</sub>PO<sub>4</sub> (Merck) in deionized water, and the pH values were adjusted by the addition of a 4.0 mol L<sup>-1</sup> NaOH (Merck) solution. The volumes were measured using EP-10 and EP-100 from Unipettemicroliter Pipettes (Uniscience, Brazil). All experiments were performed at room temperature (25 ± 3 °C)

### **Olanzapine (OLZP) Extraction, Purification and <sup>1</sup>H-NMR Analysis**

Ten tablets of Olanzapine (30 mg each) (Crisália Produtos Químicos Farmaceuticos Ltda, Production number: 17040039L) were pulverized in a ball mill until a fine powder (300-400 mesh) was obtained. Silica gel for flash chromatography (100 g) was added and the resulting solid mixture was transferred to a sintered glass Büchner funnel. Under vacuum, the solid mixture was washed with CHCl<sub>3</sub>:AcOEt (9:1) (250 mL x 2). The filtrate was concentrated under reduced pressure and a pale yellow powder was obtained. The residue was analysed by <sup>1</sup>H-NMR (DMSO-D<sub>6</sub>, 300 MHz), where the presence of the excipient monocrySTALLINE cellulose was verified along with OLZP. The residue was resolubilized in CHCl<sub>3</sub> (300 mL) and subjected to successive liquid-liquid extractions. The first one was achieved by the formation of a biphasic system with an aqueous saturated solution of NH<sub>4</sub>Cl<sub>(aq)</sub> (150 mL x 2). After phase separation, NaHCO<sub>3</sub>(aq) saturated solution (150 mL x 2) was added to the organic phase. The remaining organic phase was washed with pH = 7.4 PBS (300 mL). The organic phase was dried over anhydrous MgSO<sub>4</sub>(s), filtered and concentrated

under reduced pressure. OLZP was obtained as yellow crystals (246 mg, extraction efficiency = 82%).

OLZP CAS Number: #CAS: 132539-06-1;  $^1\text{H}$  NMR (DMSO- $d_6$ , 300 MHz):  $\delta$  (ppm) = 7.12 (dt, 1H,  $J = 1.5$  Hz,  $J = 5.7$  Hz), 6.87–6.77 (m, 2H), 6.68 (dd, 1H,  $J = 2.0$  Hz,  $J = 5.7$  Hz), 6.34 (d, 1H,  $J = 1.2$  Hz), 2.41 (t, 4H,  $J = 5.1$  Hz), 2.26 (d, 3H,  $J = 1.2$  Hz), 2.24 (s, 3H), 2.18 (t t, 4H,  $J = 5.1$  Hz); m.p. ( $^{\circ}\text{C}$ ): 193-196 (lit. 195). [48] The  $^1\text{H}$  NMR spectra obtained from OLZP extraction product is presented in figure S1.

### **Quetiapine (QTP) Extraction, Purification and $^1\text{H}$ -NMR Analysis**

Twenty tables of Quetiapine hemifumarate (2 mg each) (Crisália Produtos Químicos Farmaceuticos Ltda, Production number: 17070009L) were pulverized in a ball mill until a fine powder (300-400 mesh) was obtained. Silica gel for flash chromatography (70 g) was added and the resulting solid mixture was transferred to a sintered glass Büchner funnel. Under vacuum, the solid mixture was washed with MeOH:CH<sub>2</sub>Cl<sub>2</sub> mixture (7:3 v/v) (100 mL x 5), followed by MeCN (100 ml x 5). The filtrate was concentrated under reduced pressure and resolubilized in MeOH:MeCN (5:5 v/v) (50 mL). To the solution, NaOH (0.5 mmol, 20 mg) was added. The reaction mixture was kept under magnetic stirring for 4h at 50  $^{\circ}\text{C}$ . After this period, the reaction mixture was concentrated under reduced pressure and the residue was resolubilized in CH<sub>2</sub>Cl<sub>2</sub> (100 mL) and subjected to successive liquid-liquid extractions. The first was achieved by the formation of a biphasic system with ultrapure water (50 mL x 2). After phase separation, NaHCO<sub>3(aq)</sub> saturated solution (50 mL x 2) washing was performed and after phase separation, the resulting organic phase was sequentially washed with 0.5

molL<sup>-1</sup> HCl<sub>(aq)</sub> solution (50 mL x 2). The last extraction took place by washing the organic phase with a saturated solution of NaCl<sub>(aq)</sub> (100 mL). The organic phase was dried over anhydrous MgSO<sub>4(s)</sub> and, after filtration, the solution was concentrated under reduced pressure. QTP was obtained in the form of beige oil (29 mg, extraction efficiency = 73%). The <sup>1</sup>H NMR of the product obtained after the extraction procedure is present in figure S2.

QTP CAS Number: #CAS: 111974-69-7; <sup>1</sup>H NMR (CDCl<sub>3</sub>, 300 MHz): δ (ppm) = 7.51 (d, 1H, J = 7.2 Hz), 7.41–7.29 (m, 4H), 7.18 (dt, 1H, J = 1.5 Hz, J = 7.8 Hz), 7.07 (dd, 1H, J = 1.5 Hz, J = 7.2 Hz), 6.89 (dt, 1H, J = 1.5 Hz, J = 7.8 Hz), 3.72–3.53 (m, 11H), 2.75–2.63 (m, 6H).[49]

### **Electrochemical procedures**

All electrochemical experiments were performed in a potentiostat/galvanostat PGSTAT 101, Metrohm AUTOLAB, connected to an IME663 interface stirring device. Data processing was done by version 1.11.4 of NOVA software and the software Origin 2019. A Glassy Carbon Electrode (GCE) with a diameter of 3.0 mm was used as a working electrode, a Silver/ Silver Chloride in a saturated solution of potassium chloride, (+0.222 V vs. SHE) and a platinum wire were used as a reference and auxiliary electrodes, respectively, in an electrochemical cell of 20 mL. Before each experiment, the GCE was polished using diamond spray suspensions with a decreasing particle size of 3.0, 1.0, and 0.1 μm from Kemet (Maidstone, UK) on a polishing pad from Buehler (Lake Bluff, Illinois, USA). The solutions were stirred before each electrochemical measurement.

Cyclic voltammetry (CV) was performed by sweeping the potential ranging from -1.0 V to 1.5 V, then from 1.5 back to -1.0 V, and in a restricted potential



window from -0.3 V to 0.6 V. The scan rates were varied between 0.10 and 10.0 V s<sup>-1</sup>. Differential pulse voltammograms (DPV) were performed by sweeping the potential from 0.0 V to 1.6 V. The parameters used were 25.0 mV of modulation amplitude, a modulation time of 50 ms, a potential step of 2.5 mV, and time interval between the pulses of 0.5 s resulting in a scan rate of  $v = 5.0 \text{ mV s}^{-1}$ . The system was degassed with nitrogen gas for 15 minutes prior to the experiment when the potential window used was below -0.3 V to prevent any oxygen interference.

### **EPR characterization**

EPR measurements were carried out utilizing continuous wave Bruker EMX equipment at X-Band (9,5Ghz), 20mW power and 3G of modulation amplitude with a high sensitivity cavity. The samples were analysed a quartz flat cell at room temperature (RT).

### **Results and discussion**

This section initially describes the voltammetric behaviour of OLZP, QTP, DA, and of the solutions containing each drug and the neurotransmitter using cyclic voltammetries. The following section presents the differential pulse voltammograms and the kinetics studies of the chemical interaction between DA, OLZP, and QTP. The last section presents a minimalist model between PIPES and catechol to reinforce the role of the moieties responsible for the chemical interaction between the antipsychotic drugs with the neurotransmitter.

## **Cyclic voltammetry and the electrochemical behaviour of the molecules involved.**

The cyclic voltammograms were obtained in a wide potential window -1.0 V to 1.4/ 1.5 V vs Ag/AgCl, KCl<sub>(sat.)</sub> to observe any voltammetric profile changes in solutions containing both the drugs (separately) and DA.

Figure 1A shows the voltammetric profile of DA (grey line), OLZP (blue line), and the mixture of DA with OLZP (red line). DA presented the typical profile, two redox couples in an EEC<sub>EE</sub> mechanism [38] around 0.2 V and -0.3 V and an irreversible oxidation process around 0.85 V. OLZP presents two oxidation processes, the first one in about 0.2 V, like DA. The second one occurs around 0.9 V.

In the solutions containing both compounds, DA's first reduction peak (II) disappeared while the second reduction peak shifted to a more negative potential region around -0.5 V, while the DA and OLZP oxidation peaks turn into a barely defined voltammetric peak, which extends from 0.2 to 0.4 V, and from 0.8 to 1.0 V, respectively. In both cases, the sum of their current levels is less than those observed in a solution containing only DA (Figure 1A, black line) or OLZP (Figure 1A, blue line). The potential shifts observed in DA's electrochemical processes suggests that OLZP interacts with the electroactive groups, the catechol moiety, of DA.

In figure 1B, the QTP voltammogram (blue line) presents three irreversible oxidation processes at 0.8, 1.1, and 1.4 V. The solution containing both QTP and DA presented the first and last processes at the same potentials. However, the second process shifted from 1.1 V to 1.2 V. It is also noticed that a peak around

0.4 V appears, suggesting that it is DA's 0.2 V oxidation peak that shifted when in the presence of QTP or OLZP. To better comprehend these processes around 0.2 V in both interactions, the potential windows were restricted to the range of -0.1/ -0.3 V to 0.6 V, and the scan rates were varied.

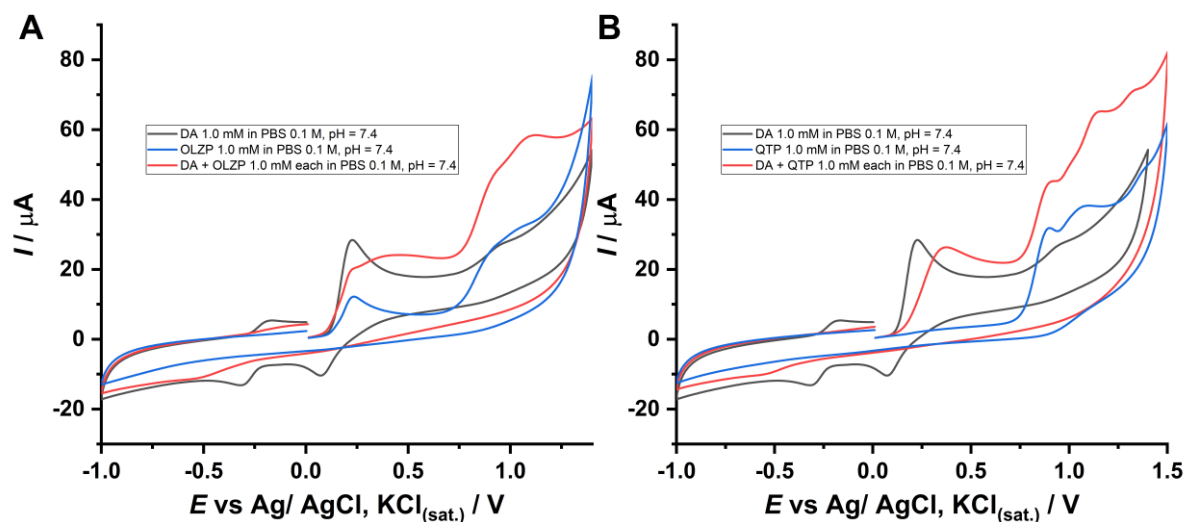


Figure 1: CV obtained using GCE in a solution containing: A) 1.0 mM DA solution (grey); 1.0 mM OLZP solution (blue); 1.0 mM DA and OLZP (red), in 0.1 M PBS, pH = 7.4, at the scan rate of  $100 \text{ mV s}^{-1}$ . B) 1.0 mM DA solution (grey); 1.0 mM QTP solution (blue); and 1.0 mM DA and QTP (red), in 0.1 M PBS, pH = 7.4, at the scan rate of  $100 \text{ mV s}^{-1}$ .

The potential window was then restricted to the first electrochemical steps of both OLZP and DA, to observe the potential chemical interaction between them. As previously reported [38], DA oxidizes in a quasi-reversible process involving a two-step one electron transfer mechanism, which is followed by a chemical step in gold electrodes; a similar oxidation was observed at GCE. As presented in figure 2A, at slow scan rates ( $20 \text{ mV s}^{-1}$ ), DA's oxidation process does not present a cathodic component, due to the chemical step. As the scan

rate increases, the heterogeneous rate constant becomes more significant than the homogeneous one, and as a result the cathodic process can be observed. As expected to a quasi-reversible process, the peak potentials shift with the increase of the scan rate.

OLZP presents a reversible process with a formal potential ( $E^0_f$ ) of 0.197 V vs Ag/AgCl, KCl<sub>(sat.)</sub>. As can be observed by the oxidation peak potential, it barely shifts with the increase of scan rate. On the other hand, unlike DA, it does not present the reversible component at slow scan rates, figure 2B. Therefore, OLZP's oxidation process is also followed by a chemical step, resulting in an electrochemical irreversibility caused by a chemical follow up step.[50]

As previously observed in figure 1A, the OLZP and DA interaction results in a shift of the DA's oxidation process to more positive potentials, figures 2C and D.

It was attributed to DA's oxidation process because it is quasi-reversible, and the first oxidation process presents a peak potential that barely shifts, as OLZP's process. Moreover, the OLZP's cathodic process only becomes visible in the mixture at higher scan rates ( $>1,000 \text{ mV s}^{-1}$ ) when compared to the voltammetric profile of OLZP alone, that appears at  $v=50 \text{ mV s}^{-1}$ . This result suggests that the oxidation product of OLZP interacts with DA in a chemical step, which consumes this product, and therefore OLZP's cathodic process is not visible until very higher scan rates. It also shifts the DA's oxidation process, which is no longer observed in about 0.2 V vs Ag/AgCl, KCl<sub>(sat.)</sub>.

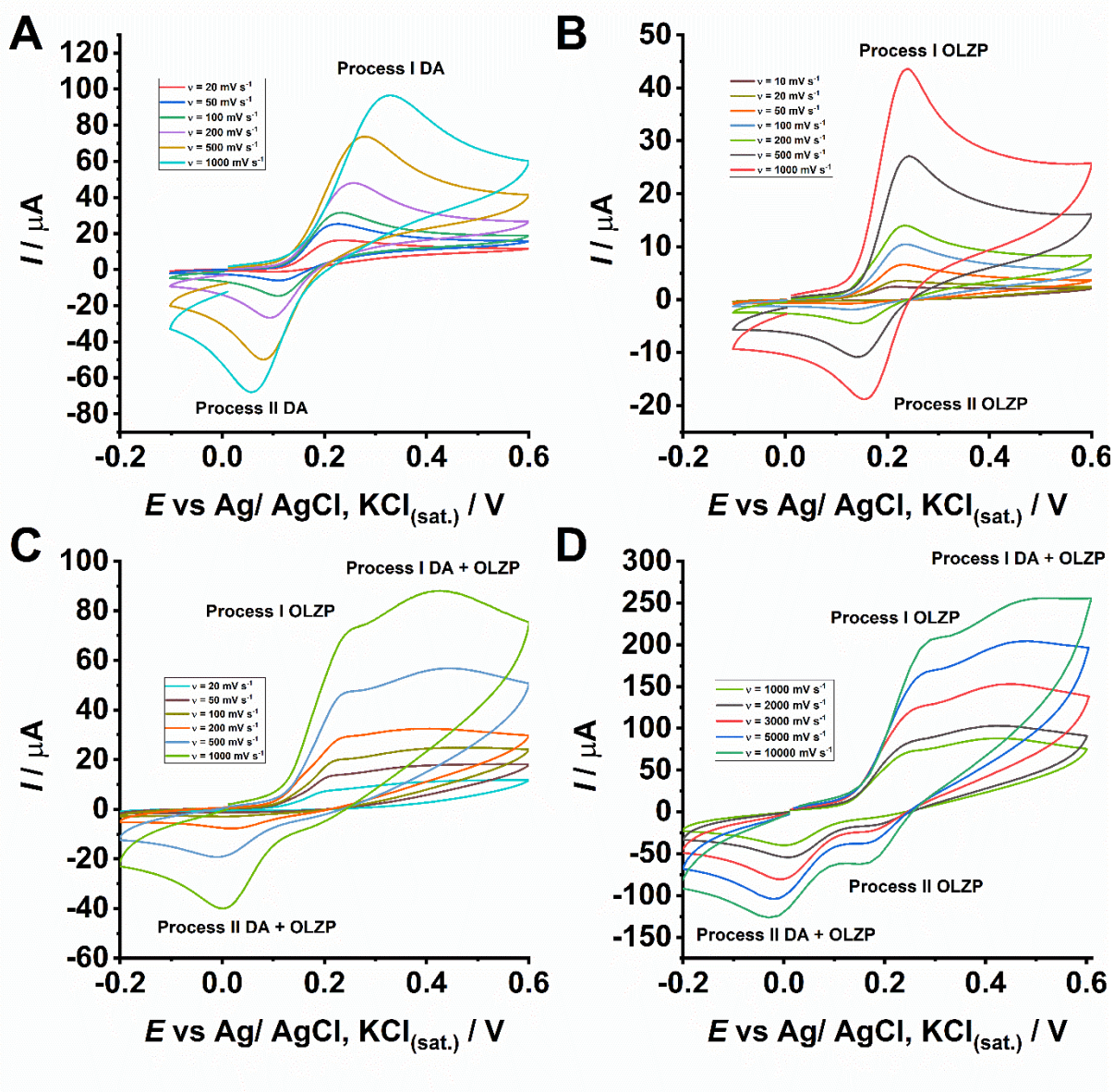


Figure 2: CV obtained using GCE in a solution containing: A) 1.0 mM DA solution; B) 1.0 mM OLZP solution; C) and D) 1.0 mM DA and OLZP, in 0.1 M PBS, pH = 7.4, at different scan rates.

Figure 3B shows that QTP only presents three oxidation processes at scan rates below  $200 \text{ mV s}^{-1}$ , and does not present any oxidation process in the potential windows between -0.1 and 0.6 V. However, in a solution containing both DA and QTP, DA's oxidation processes shifted in a similar way to that which was previously observed to OLZP, figures 3C and 3D. This result corroborates the

305

previous conclusion (figures 2C and 2D) that DA's peaks shifted and OLZP's one remained at the same potential.

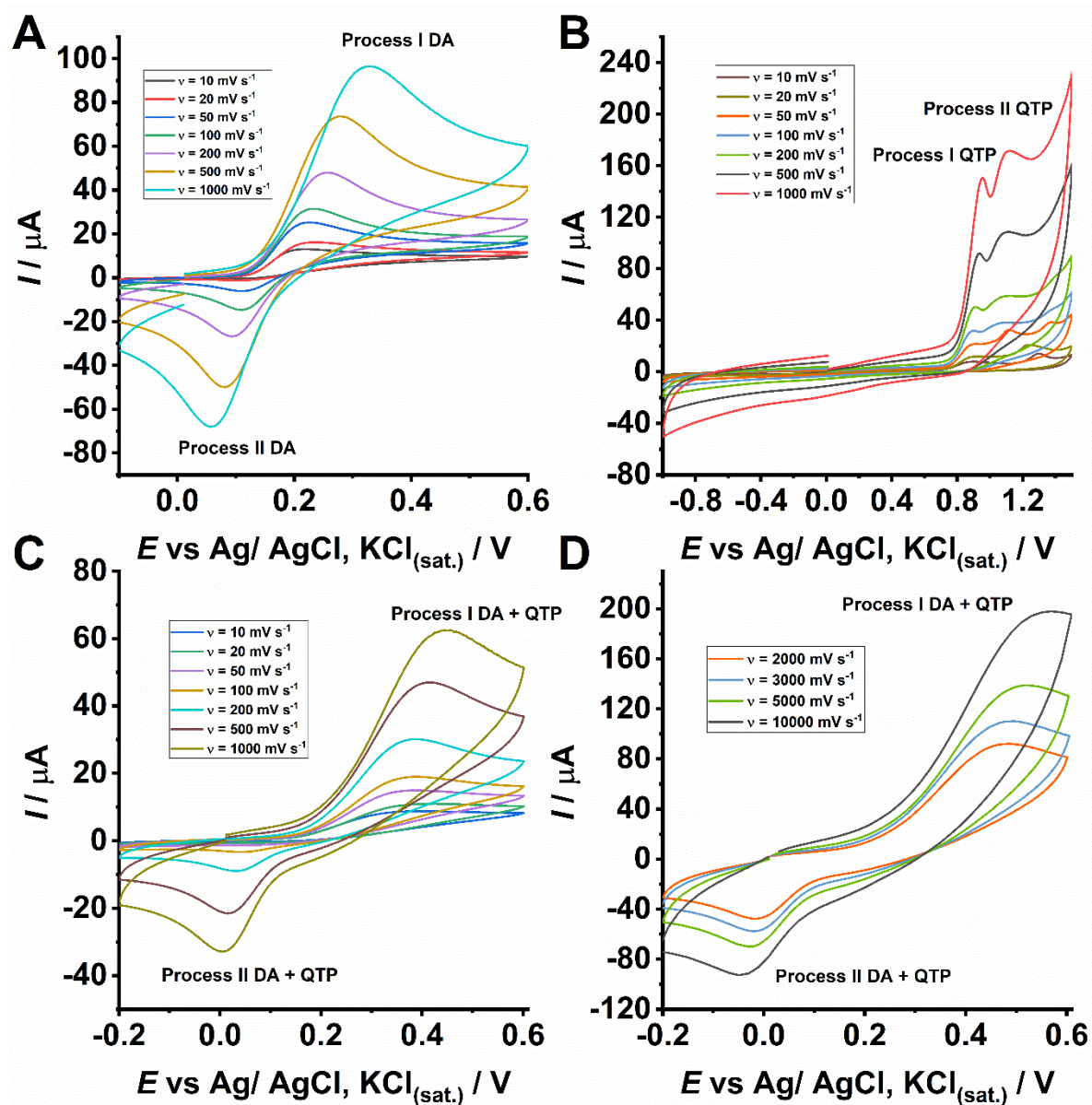


Figure 3: CV obtained using GCE in a solution containing: A) 1.0 mM DA; B) 1.0 mM QTP; C) and D) 1.0 mM DA and QTP, in 0.1 M PBS, pH = 7.4, at different scan rates.

Comparing the results presented in figures 2C and 2D with figures 3C and 3D, it was noticed that the peak potentials from DA's first oxidation process shift

306

similarly when in the presence of the drugs, as can be observed in figure 4A, which strongly suggests that a reaction occurs involving the moiety which is common to both molecules, the piperazine ring. This group tends to undergo oxidation around 1.0 V vs Ag/AgCl. [51,52]

To endorse that the reaction occurs via a similar mechanism to both OLZP's and QTP's reactions, and therefore in the analogous moieties of the drugs, the charge transfer coefficients were obtained since the  $\beta$  values can be described as:

$$\beta = \frac{1}{2} \left( 1 + \frac{\Delta G^\ddagger}{\lambda} \right) \quad (1)$$

where  $\beta$  is the charge transfer coefficient,  $\Delta G^\ddagger$  is the standard Gibbs energy of activation in  $\text{kJ mol}^{-1}$  and  $\lambda$  is the reorganization energy in  $\text{mol kJ}^{-1}$ . [53] Figure 4B shows the  $\beta$  values ( $d \ln // d E$ ) as a function of the potential applied, to obtain the charge transfer coefficients of the process I of DA, and of DA in the presence of OLZP and QTP. [54] Both processes I of DA when in presence of the antipsychotics presented a  $\beta$  value around 0.5 at 0,34 V. In conclusion, differently from the DA's oxidation at slow scan rates ( $v = 20 \text{ mV s}^{-1}$ ) which presents a  $\beta$  value around 1.2, the oxidation step has the first electron transfer as the rate determining step, suggesting that the transition state of the oxidation is a radical. In addition, the reaction with each drug presents a similar factor  $\frac{\Delta G^\ddagger}{\lambda}$ , that implies a similar mechanism and therefore reaction.

Subsequently, to endorse that a radical is generated in this process, the electron paramagnetic resonance analysis (EPR) was performed. Figure S3A shows a series of 'silent' EPR spectra from DA, piperazine (PPZ), PIPES, OLZP, and QTP, leading to the conclusion that none of the molecules presents an

unpaired electron. Thus, no signal is observed in the spectra. On the other hand, when DA is in the presence of the PPZ, OLZP or QTP, a signal is observed around 3481 Gauss, indicating that an unpaired electron with a radical characteristic is being generated, corroborating the result observed in the Tafel analysis. Another signal is observed in around 3484 Gauss, which is from a polydopamine (PDA) sample. Therefore, the presence of a piperazine group in a DA solution seems to catalyse the oxidation of DA, which results in the formation of PDA. Based on this premise, reports describing a reaction between DA and PPZ were found in the literature. Moreover, according to Ang et al. and van der Leeden [55,56], PPZ reacts with DA via a Michael addition generating a peak at 288 nm in UV-Vis spectra. Torriero et al. also describe a similar reaction, but between catechol (CAT) and PPZ. [57] This peak at 288 nm can be observed in both spectra of DA in the presence of the drugs (figures 4C and 4D). Finally, You et al. describe and propose a Michael addition between piperidine and dopamine in which the piperidine may attack not only at position 4, but also at position 2 of the catechol moiety of DA, resulting in an alternative cyclization of DA. [58] These results are corroborated by figure 1. Furthermore, where in the presence of the drugs, DA's process II is not observed, indicating that the oxidation product formed in the oxidative process I is being consumed. Moreover, the DA's redox processes around -0,5 V, which are related to its cyclization product [38], present a shift in their peak potential. This result suggests that after oxidation DA undergoes a Michael addition in position 4, which is less sterically hindered, being attacked by the non-ligand electron pair of electrons from the piperazine moiety of the drugs, thereby forcing the cyclization to occur in the position 2, as analogously proposed by You et al. for DA and piperidine. [58]



At last, figures 4E, 4F, 4G and 4H show photos of the solutions of DA in the presence of PPZ, DA solution, DA in the presence of OLZP and DA in the presence of QTP, after 6 hours of their preparation. As can be observed, the solution becomes dark brown colour, indicating that an oxidation product is being formed, with a distinct kinetics of the DA oxidation.

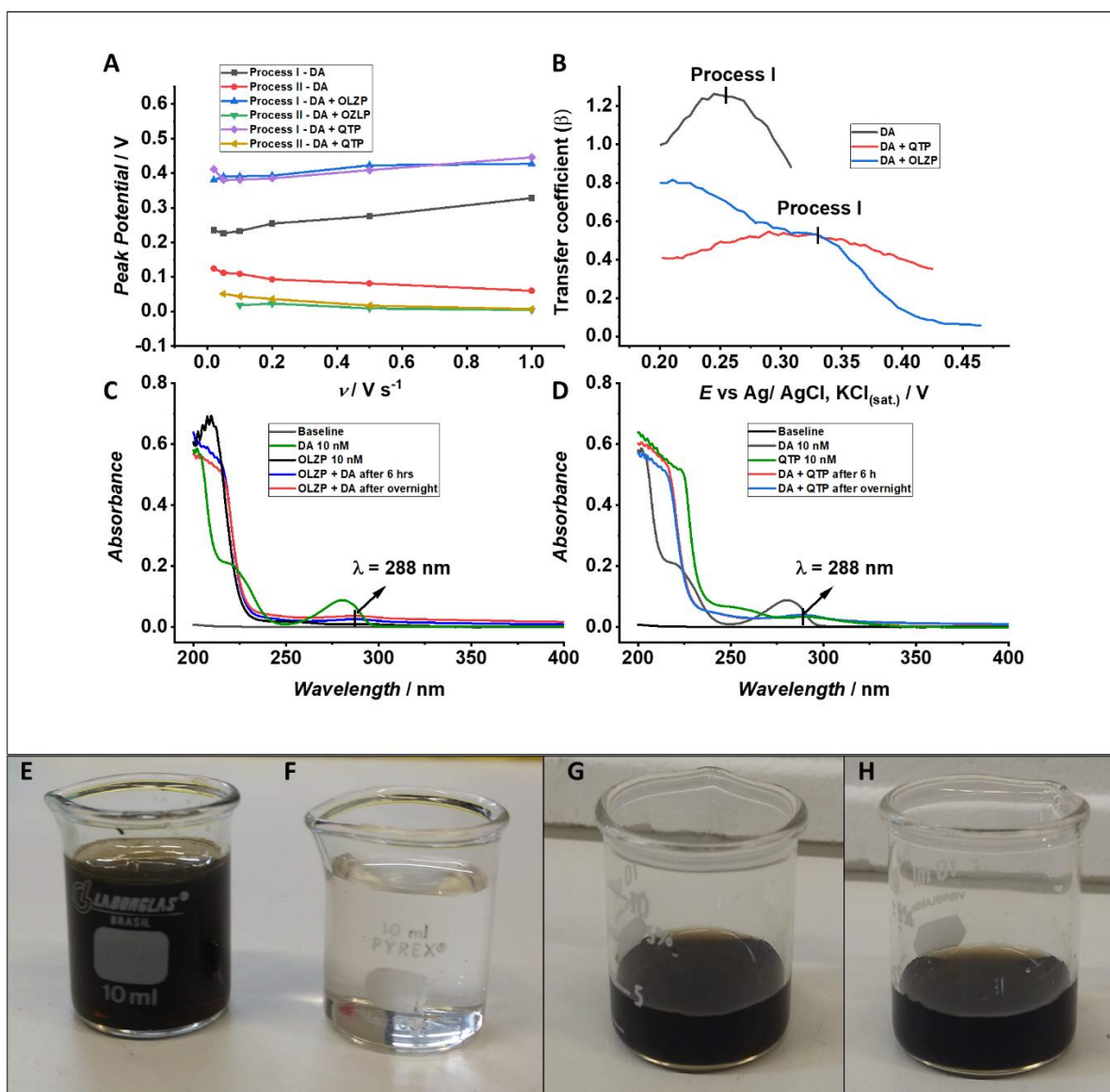
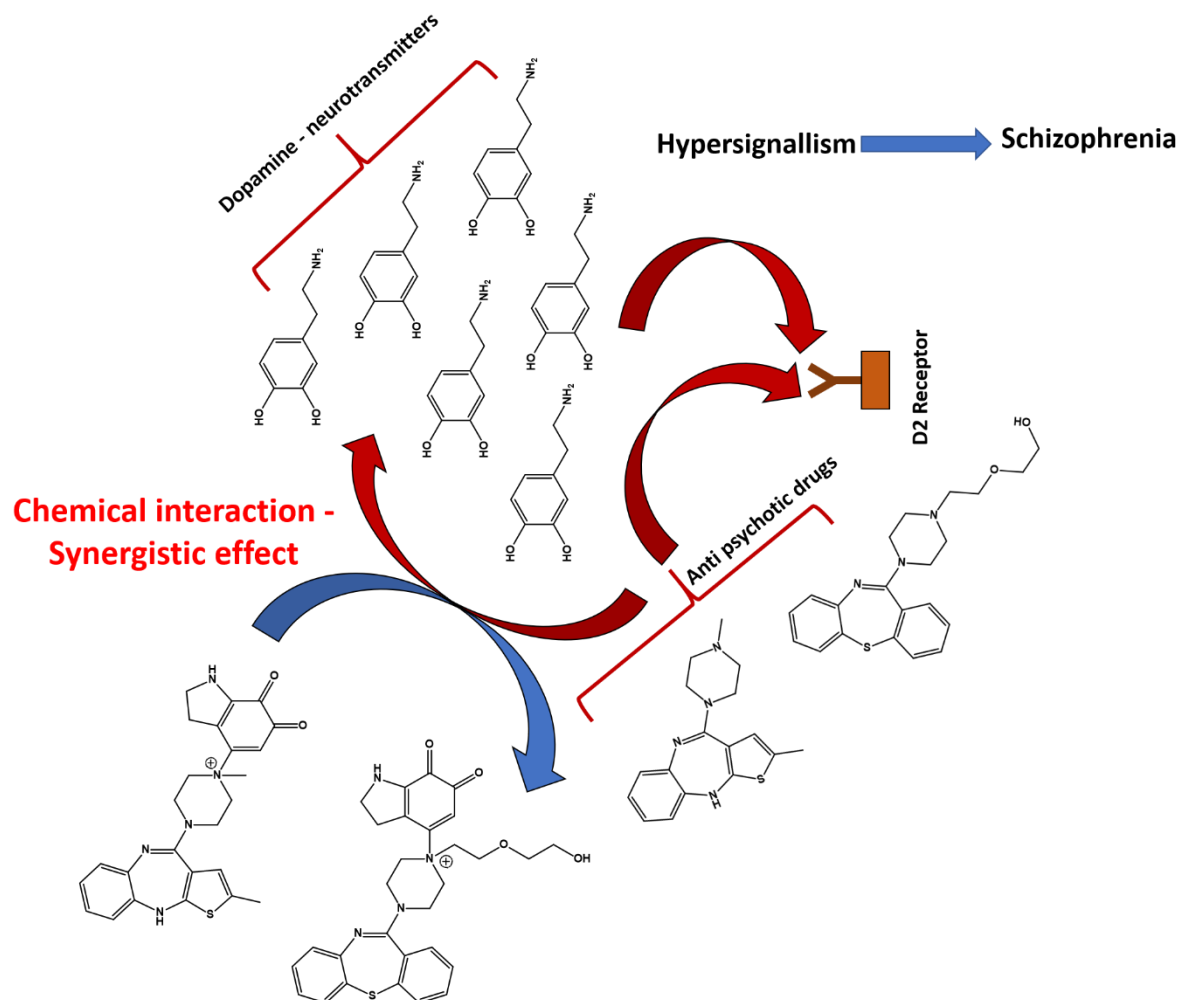


Figure 4: A) Peak potential of processes I and II of DA (dark grey and red, respectively), DA in the presence of OLZP (blue and green, respectively), and DA

in the presence of QTP (purple and dark yellow, respectively) as a function of the scan rate. B) Charge transfer coefficient ( $\ln // dE$ ) as a function of the potential obtained from respective CVs at  $20 \text{ mV s}^{-1}$ ; C) UV-Vis spectra of a  $90 \text{ nM}$  of DA,  $90 \text{ nM}$  of OLZP, OLZP in the presence of DA,  $90 \text{ nM}$  (1:1) after 6 hours and overnight; D)  $90 \text{ nM}$  of DA,  $90 \text{ nM}$  of QTP, QTP in the presence of DA,  $90 \text{ nM}$  (1:1) after 6 hours and overnight; Photo of E) a  $10 \text{ mM}$  (1:1) DA + PIPES solution after 6 hrs, F)  $10 \text{ mM}$  solution of DA used as control, G) a  $10 \text{ mM}$  (1:1) DA + OLZP solution after 6 hours, H) a  $10 \text{ mM}$  (1:1) DA + QTP solution after 6 hours.

Hence, as the antipsychotic drugs act by hindering the contact between the D2 receptors and DA [5,59–61], it can be concluded that the drugs which present a piperazine moiety will not only diminish this interaction between the neurotransmitter and its receptor but will also react with DA, decreasing its effective concentration nearby the receptors. Therefore, the antipsychotics present a synergistic effect in decreasing the natural interaction that DA will perform with this receptor, most likely amplifying the effect of the drug.

Based on the results obtained and in the already described reaction between these moieties, the following mechanism is proposed, Scheme 3.



Scheme 3: Mechanism proposition of the chemical reaction between dopamine and the antipsychotic drugs.

Since DA oxidation process I shifted in the presence of both drugs, a DPV protocol using this process was performed to evaluate the kinetics of the chemical interaction between DA and both OLZP and QTP.

### Differential pulse voltammetry and the chemical rate constants

#### Interaction between olanzapine and dopamine

Initially, DPVs were obtained in 1.0 mM DA solution in 0.1 M PBS, pH 7.4, for one hour to evaluate the stability of signal and to guarantee that the current decrease is only attributed to the DA-antipsychotic interaction. The current values

obtained in a solution containing only DA presented a stable signal during the full experiment. These results can be observed in figures S3A and S3B. The current stability observed throughout DA's oxidation process guarantees that any variation occurs due to the chemical interaction between DA and the drugs.

The same protocol was performed in solutions containing DA and OLZP, 1.0 mM each. Figure 5A shows DPV in which both DA and OLZP oxidation signals overlap around 0.2 V vs Ag/AgCl, KCl<sub>(sat.)</sub>, resulting in a current signal, which is the sum of both currents. After 15 minutes, a decrease of approximately 25% in the signal was observed, and it progressively decreases until approximately 35% of the original signal remains after at 60 minutes, as can be seen in figure 5B, indicating that a chemical reaction between DA and OLZP occurs. The current values versus time present an exponential decreasing behaviour, representing the reaction kinetics. Moreover, it was noticed that the prediction of the fitted curve ends approximately at the current value observed for the first oxidation process of the OLZP. This result corroborates with those previously shown in Figure 2, and suggests that DA's catechol moiety is being oxidized. On the other hand, the OLZP process is practically unaffected, suggesting as did figure 3, that the reaction does not involve the OLZP diazepine ring. It was also noticed a slight decrease in the current of OLZP's second oxidation process, strongly suggesting an interaction between the catechol and the piperazine moieties. Finally, figure 5C shows a first-order kinetics for DA in the reaction, with a kinetic rate constant (k) of  $1.5 \cdot 10^{-2} \text{ s}^{-1}$ .

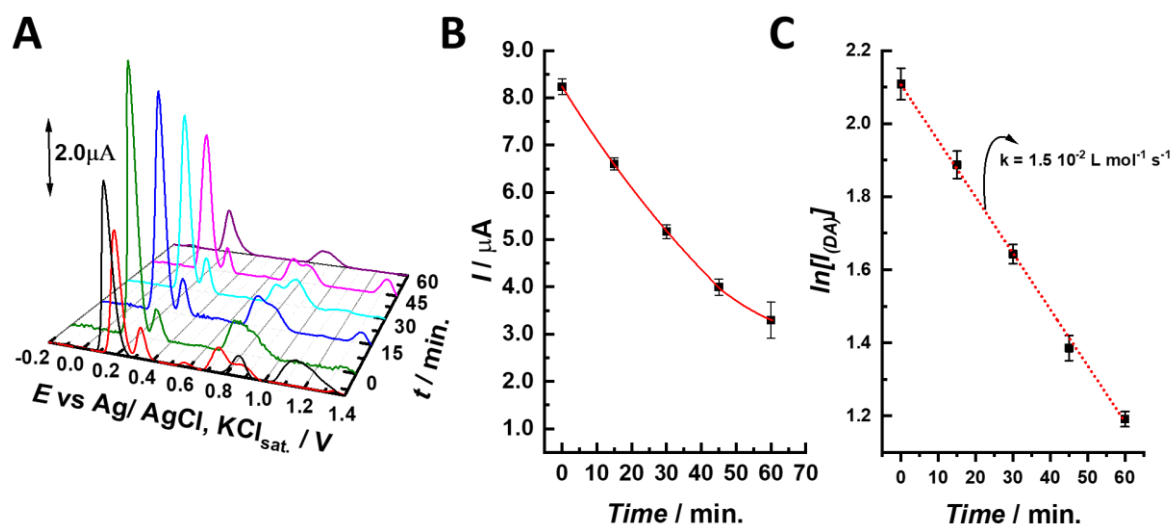


Figure 5: A) DPV obtained for the individual solutions of 1.0 mM DA (black line) and 1.0 mM of OLZP (red line) in 0.1 M PBS, pH = 7.4, and for the mixture of 1.0 mM of OLZP and DA solutions, along the time of reaction, with DPV data obtained every 15 min; B) Peak current extracted from DPV data for different time of reaction; C) Logarithm of the DA oxidation peak current versus time in minutes ( $\ln I_{DA} = -1.5 \cdot 10^{-2}t + 2.2$ ,  $R^2 = 0.99$ )

### Interaction between quetiapine and dopamine

As observed in figures 1 and 3, QTP interacts with DA. Therefore, we conducted the same DPV approach to evaluate the chemical kinetics of this reaction.

Figure 6A shows the DA (black line), as well as the QTP (red line) signal at a “negative time”. At time equals 0 minutes, the voltammetric response of each QTP and DA solutions can be observed. As it follows, after 15 minutes the voltammogram shows a significant decrease in DA’s oxidation peak current. The decrease in current was then monitored every 15 minutes and an exponential decrease was observed in a similar result as previously observed for OLZP in figure 5.

These results strongly suggest that the piperazine moiety in QTP reacts with the catechol portion in DA, therefore, being responsible for the interaction between the drug and the neurotransmitter, such as observed for OLZP. Once again, an exponential decrease was observed, which presented a linear curve when plotted as a logarithm function versus time, showing that DA presents a first-order kinetics in the reaction with QTP. In addition, a kinetic constant of  $9.0 \cdot 10^{-3} \text{ s}^{-1}$  was obtained.

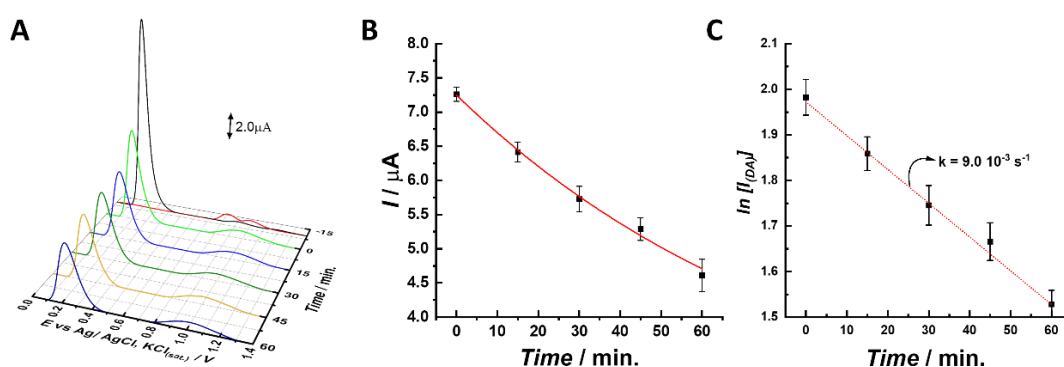


Figure 6: A) DPVs obtained for individual solutions of 1.0 mM QTP (red line) and 1.0 mM DA (black line) and for the mixture of 1.0 mM QTP+DA along the time of reaction, recording the DPV data every 15 min. B); Peak current extracted from DPV data presented in A along the time of reaction. C) logarithm of DA's oxidation peak current versus time in minutes ( $\ln I_{\text{DA}} = -9.0 \cdot 10^{-3} t + 2.07$ ,  $R^2 = 0.99$ )

To confirm the chemical interaction between the piperazine and catechol moieties, in the antipsychotics and DA, respectively, a minimalist model, using only PIPES and CAT as a molecular model was proposed. The model works as a proof of concept. If the same reaction is observed between the model molecules, it allows us to conclude that these particular moieties are responsible for the chemical interaction.

## The catechol-piperazine minimalist model

To endorse PIPES as a model molecule, its interaction with DA was observed with the same experiment previously performed to observe the interaction between the drugs and DA. These results are presented in figure S4, and the obtained rate constant to the reaction between DA and PIPES was  $2.1 \cdot 10^{-2} \text{ s}^{-1}$ , certifying PIPES as a model to the antipsychotic drugs. In sequence to validate the model hypothesis that an interaction occurs between the piperazine and catechol moieties, the same DPV protocol was used to CAT and PIPES. As expected, a similar chemical interaction effect was observed.

An exponential decrease was observed in the CAT's oxidation current signal when the PIPES was added to the electrochemical cell. The decay was analogous to the already observed results of both OLZP and QTP reactions with DA; therefore, validating the model. A kinetic constant of  $1.7 \cdot 10^{-2} \text{ s}^{-1}$  was obtained, which agrees with the previously obtained constants, especially the one related to OLZP interaction.

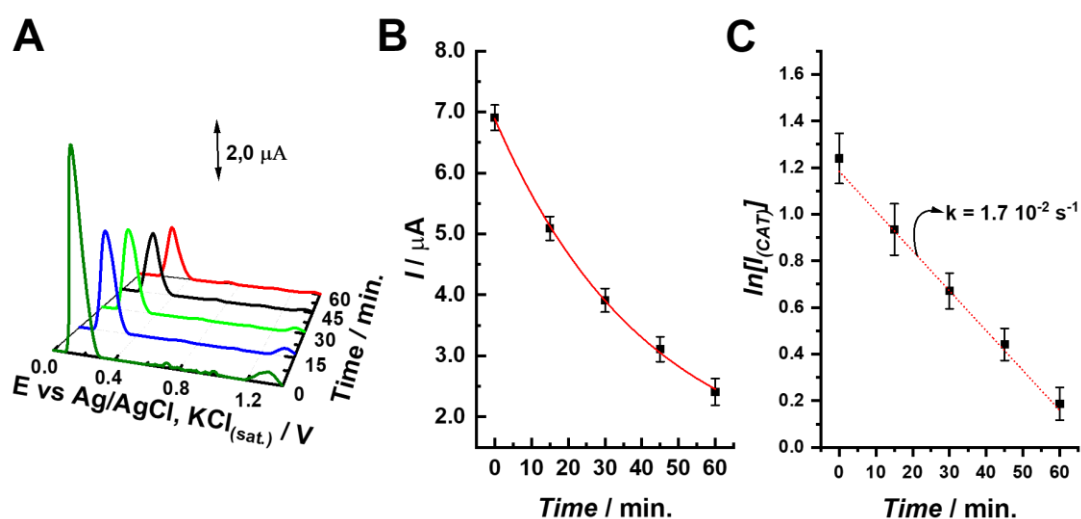


Figure 7: A) DPVs obtained for the mixture of CAT and PIPES solutions, 1.0 mM, each along the time of reaction, recording the DPV data every 15 min. B); Peak

current extracted from DPV data presented in A along the time of reaction. C) logarithm of the DA oxidation peak current versus time in minutes ( $\ln I_{\text{CAT}} = -1.7 \cdot 10^{-2} t + 1.3$ ,  $R^2 = 0.87$ )

Compiling the presented electrochemical data, it is possible to conclude that DA reacts with both OLZP and QTP. This reaction most likely occurs between the catechol moiety of DA and the piperazine moiety of OLZP or QTP. The reactions presented rate constants of  $1.5 \cdot 10^{-2} \text{ s}^{-1}$  and  $9.0 \cdot 10^{-3} \text{ s}^{-1}$  for OLZP and QTP interaction with DA, respectively. These values are considered moderated since a fast kinetic such as dopamine cyclization presents a rate constant of  $0.24 \text{ s}^{-1}$ . [38] That conclusion was also supported by the reaction observed in the molecular model, between CAT and PIPES, including a kinetic rate constant similar to the ones observed between the antipsychotic drugs and dopamine.

## Conclusions

In summary, the chemical interaction between both antipsychotic drugs, olanzapine, and quetiapine, with dopamine were electrochemically studied, using a glassy carbon electrode in 0.1 M PBS solutions at pH = 7.4. The voltammograms, UV-Vis, EPR spectra, and photos showed that both olanzapine and quetiapine interact chemically with dopamine. Based on the data, a mechanism for this reaction is proposed. Using a differential pulse voltammetry protocol, PIPES and catechol were used as molecular models, to mimic the drugs and the neurotransmitter. confirming not only that this reaction develops involving the catechol moiety of dopamine and the piperazine moiety of the drugs, but also that this reaction is first-order with a moderate chemical rate.



## Acknowledgments

The main author would like to thank Spinell Bacil (*in memoriam*) for all the support and friendship throughout the years. The authors would like to thank the CNPq projects nº 140833/2016-1 and 310114/2016-0, CAPES project 88881.187396/2018-01 and Fapesp for the grants and funding. Finally, the authors would like thank Professor Ana Maria da Costa Ferreira for the access to EPR instrument, supported by the CEPID-Redoxoma Network (FAPESP grant 2013/07937-8).

## References

- [1] J.D. Harvey Lodish, Arnold Berk, Paul Matsudaira, Chris A. Kaiser, Monty Krieger, Matthew P. Scott, Lawrence Zipursky, Molecular cell biology, 4th ed., W. H. Freeman, New York, 2000. <https://www.ncbi.nlm.nih.gov/books/NBK21521/>.
- [2] H.Y. Meltzer, S.M. Stahl, The Dopamine Hypothesis of Schizophrenia: A Review\*, *Schizophr. Bull.* 2 (1976) 19–76. doi:10.1093/schbul/2.1.19.
- [3] J. van Os, S. Kapur, Schizophrenia, *Lancet.* 374 (2009) 635–645. doi:10.1016/S0140-6736(09)60995-8.
- [4] S. Leucht, C. Corves, D. Arbter, R.R. Engel, C. Li, J.M. Davis, Second-generation versus first-generation antipsychotic drugs for schizophrenia: a meta-analysis, *Lancet.* 373 (2009) 31–41. doi:10.1016/S0140-6736(08)61764-X.
- [5] P. Seeman, Dopamine receptors and the dopamine hypothesis of schizophrenia, *Synapse.* 1 (1987) 133–152. doi:10.1002/syn.890010203.
- [6] B.K. Madras, History of the Discovery of the Antipsychotic Dopamine D2 Receptor: A Basis for the Dopamine Hypothesis of Schizophrenia, *J. Hist. Neurosci.* 22 (2013) 62–78. doi:10.1080/0964704X.2012.678199.

- [7] O.D. Howes, S. Kapur, The Dopamine Hypothesis of Schizophrenia: Version III--The Final Common Pathway, *Schizophr. Bull.* 35 (2009) 549–562. doi:10.1093/schbul/sbp006.
- [8] A. Kucharski, History of Frontal Lobotomy in the United States, 1935-1955, *Neurosurgery.* 14 (1984) 765–772. doi:10.1227/00006123-198406000-00022.
- [9] J. Johnson, A Dark History: Memories of Lobotomy in the New Era of Psychosurgery, *Med. Stud.* 1 (2009) 367–378. doi:10.1007/s12376-009-0031-7.
- [10] R. Warner, D. Taylor, M. Powers, J. Hyman, Acceptance of the mental illness label by psychotic patients: Effects on functioning., *Am. J. Orthopsychiatry.* 59 (1989) 398–409. doi:10.1111/j.1939-0025.1989.tb01675.x.
- [11] C. Heimberg, R.E. Gur, R.J. Erwin, D.L. Shtasel, R.C. Gur, Facial emotion discrimination: III. Behavioral findings in schizophrenia, *Psychiatry Res.* 42 (1992) 253–265. doi:10.1016/0165-1781(92)90117-L.
- [12] G. Thornicroft, E. Brohan, D. Rose, N. Sartorius, M. Leese, Global pattern of experienced and anticipated discrimination against people with schizophrenia: a cross-sectional survey, *Lancet.* 373 (2009) 408–415. doi:10.1016/S0140-6736(08)61817-6.
- [13] S. Lee, M.Y.L. Chiu, A. Tsang, H. Chui, A. Kleinman, Stigmatizing experience and structural discrimination associated with the treatment of schizophrenia in Hong Kong, *Soc. Sci. Med.* 62 (2006) 1685–1696. doi:10.1016/j.socscimed.2005.08.016.
- [14] B. Schulze, M.C. Angermeyer, Subjective experiences of stigma. A focus group study of schizophrenic patients, their relatives and mental health professionals, *Soc. Sci. Med.* 56 (2003) 299–312. doi:10.1016/S0277-9536(02)00028-X.

- [15] G.E. Hogarty, C.M. Anderson, D.J. Reiss, S.J. Kornblith, D.P. Greenwald, C.D. Javna, M.J. Madonia, Family Psychoeducation, Social Skills Training, and Maintenance Chemotherapy in the Aftercare Treatment of Schizophrenia, *Arch. Gen. Psychiatry*. 43 (1986) 633. doi:10.1001/archpsyc.1986.01800070019003.
- [16] G.E. Hogarty, C.M. Anderson, D.J. Reiss, S.J. Kornblith, D.P. Greenwald, R.F. Ulrich, M. Carter, Family Psychoeducation, Social Skills Training, and Maintenance Chemotherapy in the Aftercare Treatment of Schizophrenia, *Arch. Gen. Psychiatry*. 43 (1986) 633. doi:10.1001/archpsyc.1986.01800070019003.
- [17] K.G. TERKELSEN, Schizophrenia and the Family: II. Adverse Effects of Family Therapy, *Fam. Process*. 22 (1983) 191–200. doi:10.1111/j.1545-5300.1983.00191.x.
- [18] J.W. Newcomer, Second-Generation (Atypical) Antipsychotics and Metabolic Effects, *CNS Drugs*. 19 (2005) 1–93. doi:10.2165/00023210-200519001-00001.
- [19] J. Geddes, N. Freemantle, P. Harrison, P. Bebbington, Atypical antipsychotics in the treatment of schizophrenia: systematic overview and meta-regression analysis, *BMJ*. 321 (2000) 1371–1376. doi:10.1136/bmj.321.7273.1371.
- [20] D.M. Taylor, R. McAskill, Atypical antipsychotics and weightgain - a systematic review, *Acta Psychiatr. Scand*. 101 (2000) 416–432. doi:10.1034/j.1600-0447.2000.101006416.x.
- [21] P.M. Haddad, S.G. Sharma, Adverse Effects of Atypical Antipsychotics, *CNS Drugs*. 21 (2007) 911–936. doi:10.2165/00023210-200721110-00004.

- [22] S.W. Woods, Chlorpromazine Equivalent Doses for the Newer Atypical Antipsychotics, *J. Clin. Psychiatry.* 64 (2003) 663–667. doi:10.4088/JCP.v64n0607.
- [23] C.W. Ritchie, E. Chiu, S. Harrigan, K. Hall, A. Hassett, S. Macfarlane, M. Mastwyk, D.W. O'Connor, J. Opie, D. Ames, The impact upon extra-pyramidal side effects, clinical symptoms and quality of life of a switch from conventional to atypical antipsychotics (risperidone or olanzapine) in elderly patients with schizophrenia, *Int. J. Geriatr. Psychiatry.* 18 (2003) 432–440. doi:10.1002/gps.862.
- [24] A. Ceci, A. Brambilla, P. Duranti, M. Grauert, N. Grippa, F. Borsini, Effect of antipsychotic drugs and selective dopaminergic antagonists on dopamine-induced facilitatory activity in prelimbic cortical pyramidal neurons. An in vitro study, *Neuroscience.* 93 (1999) 107–115. doi:10.1016/S0306-4522(99)00123-2.
- [25] R.L. Jakab, P.S. Goldman-Rakic, 5-Hydroxytryptamine<sub>2A</sub> serotonin receptors in the primate cerebral cortex: Possible site of action of hallucinogenic and antipsychotic drugs in pyramidal cell apical dendrites, *Proc. Natl. Acad. Sci.* 95 (1998) 735–740. doi:10.1073/pnas.95.2.735.
- [26] S. Inc., Top antipsychotic drugs in the US based in revenue in 2011 - 2012, (n.d.). [www.statista.com](http://www.statista.com).
- [27] S. Shahrokhian, M. Azimzadeh, P. Hosseini, Modification of a glassy carbon electrode with a bilayer of multiwalled carbon nanotube/benzene disulfonate-doped polypyrrole: application to sensitive voltammetric determination of olanzapine, *RSC Adv.* 4 (2014) 40553–40560. doi:10.1039/C4RA04584J.

- [28] A. Jasińska, E. Nalewajko, Batch and flow-injection methods for the spectrophotometric determination of olanzapine, *Anal. Chim. Acta.* 508 (2004) 165–170. doi:10.1016/j.aca.2003.11.069.
- [29] M.A. Saracino, O. Gandolfi, R. Dall'Olio, L. Albers, E. Kenndler, M.A. Raggi, Determination of Olanzapine in rat brain using liquid chromatography with coulometric detection and a rapid solid-phase extraction procedure, *J. Chromatogr. A.* 1122 (2006) 21–27. doi:10.1016/j.chroma.2006.04.011.
- [30] Q. Zheng, F. Wang, H. Li, P. Xu, H. Tang, L. Li, R. Cheng, Quantitative analysis of olanzapine in rat brain microdialysates by HPLC-MS/MS coupled with column-switching technique, *J. Chromatogr. B Anal. Technol. Biomed. Life Sci.* 905 (2012) 127–132. doi:10.1016/j.jchromb.2012.07.024.
- [31] C. Krishnaiah, M. Vishnu Murthy, R. Kumar, K. Mukkanti, Development of a stability-indicating UPLC method for determining olanzapine and its associated degradation products present in active pharmaceutical ingredients and pharmaceutical dosage forms, *J. Pharm. Biomed. Anal.* 54 (2011) 667–673. doi:10.1016/j.jpba.2010.10.013.
- [32] M.A. Raggi, G. Casamenti, R. Mandrioli, G. Izzo, E. Kenndler, Quantitation of olanzapine in tablets by HPLC, CZE, derivative spectrometry and linear voltammetry., *J. Pharm. Biomed. Anal.* 23 (2000) 973–81. <http://www.ncbi.nlm.nih.gov/pubmed/11095298>.
- [33] M.A. El-Shal, Electrochemical studies for the determination of quetiapine fumarate and olanzapine antipsychotic drugs., *Adv. Pharm. Bull.* 3 (2013) 339–44. doi:10.5681/apb.2013.055.
- [34] D. Merli, D. Dondi, M. Pesavento, A. Profumo, Electrochemistry of olanzapine and risperidone at carbon nanotubes modified gold electrode through
- 321

classical and DFT approaches, *J. Electroanal. Chem.* 683 (2012) 103–111. doi:10.1016/j.jelechem.2012.08.011.

[35] M.H. Mashhadizadeh, E. Afshar, Electrochemical investigation of clozapine at TiO<sub>2</sub> nanoparticles modified carbon paste electrode and simultaneous adsorptive voltammetric determination of two antipsychotic drugs, *Electrochim. Acta.* 87 (2013) 816–823. doi:10.1016/j.electacta.2012.09.004.

[36] D.C.S. Tse, R.L. McCreery, R.N. Adams, Potential oxidative pathways of brain catecholamines, *J. Med. Chem.* 19 (1976) 37–40. doi:10.1021/jm00223a008.

[37] B.J. Venton, R.M. Wightman, Psychoanalytical Electrochemistry: Dopamine and Behavior, *Anal. Chem.* 75 (2008) 414 A-421 A. doi:10.1021/ac031421c.

[38] R.P. Bacil, L. Chen, S.H.P. Serrano, R.G. Compton, Dopamine oxidation at gold electrodes: mechanism and kinetics near neutral pH, *Phys. Chem. Chem. Phys.* 22 (2020) 607–614. doi:10.1039/C9CP05527D.

[39] L. Chen, E.E.L. Tanner, C. Lin, R.G. Compton, Impact electrochemistry reveals that graphene nanoplatelets catalyse the oxidation of dopamine via adsorption, *Chem. Sci.* 9 (2018) 152–159. doi:10.1039/C7SC03672H.

[40] Y. Li, M. Liu, C. Xiang, Q. Xie, S. Yao, Electrochemical quartz crystal microbalance study on growth and property of the polymer deposit at gold electrodes during oxidation of dopamine in aqueous solutions, *Thin Solid Films.* 497 (2006) 270–278. doi:10.1016/j.tsf.2005.10.048.

[41] T.A. Enache, A.M. Oliveira-Brett, Phenol and para-substituted phenols electrochemical oxidation pathways, *J. Electroanal. Chem.* 655 (2011) 9–16. doi:10.1016/j.jelechem.2011.02.022.

- [42] R.P. da Silva, A.W.O. Lima, S.H.P. Serrano, Simultaneous voltammetric detection of ascorbic acid, dopamine and uric acid using a pyrolytic graphite electrode modified into dopamine solution, *Anal. Chim. Acta.* 612 (2008) 89–98. doi:10.1016/j.aca.2008.02.017.
- [43] Q. Lin, Q. Li, C. Batchelor-McAuley, R.G. Compton, Two-Electron, Two-Proton Oxidation of Catechol: Kinetics and Apparent Catalysis, *J. Phys. Chem. C.* 119 (2015) 1489–1495. doi:10.1021/jp511414b.
- [44] D. Lakshmi, A. Bossi, M.J. Whitcombe, I. Chianella, S.A. Fowler, S. Subrahmanyam, E. V Piletska, S.A. Piletsky, Electrochemical Sensor for Catechol and Dopamine Based on a Catalytic Molecularly Imprinted Polymer-Conducting Polymer Hybrid Recognition Element, *Anal. Chem.* 81 (2009) 3576–3584. doi:10.1021/ac802536p.
- [45] F. Gao, X. Cai, X. Wang, C. Gao, S. Liu, F. Gao, Q. Wang, Highly sensitive and selective detection of dopamine in the presence of ascorbic acid at graphene oxide modified electrode, *Sensors Actuators B Chem.* 186 (2013) 380–387. doi:10.1016/j.snb.2013.06.020.
- [46] A. Safavi, N. Maleki, O. Moradlou, F. Tajabadi, Simultaneous determination of dopamine, ascorbic acid, and uric acid using carbon ionic liquid electrode, *Anal. Biochem.* 359 (2006) 224–229. doi:10.1016/j.ab.2006.09.008.
- [47] D. Yuan, X. Yuan, S. Zhou, W. Zou, T. Zhou, N-Doped carbon nanorods as ultrasensitive electrochemical sensors for the determination of dopamine, *RSC Adv.* 2 (2012) 8157. doi:10.1039/c2ra21041j.
- [48] K.A. Chu, S.H. Yalkowsky, An interesting relationship between drug absorption and melting point, *Int. J. Pharm.* 373 (2009) 24–40. doi:10.1016/j.ijpharm.2009.01.026.

- [49] E.J. Warawa, B.M. Migler, C.J. Ohnmacht, A.L. Needles, G.C. Gatos, F.M. McLaren, C.L. Nelson, K.M. Kirkland, Behavioral approach to nondyskinetic dopamine antagonists: identification of seroquel., *J. Med. Chem.* 44 (2001) 372–89. doi:10.1021/jm000242+.
- [50] I. Streeter, S.F. Jenkinson, G.W.J. Fleet, R.G. Compton, Chemical instability promotes apparent electrochemical irreversibility: Studies on the electrode kinetics of the one electron reduction of the 2,6-diphenylpyrylium cation in acetonitrile solution, *J. Electroanal. Chem.* 600 (2007) 285–293. doi:10.1016/j.jelechem.2006.10.006.
- [51] O.M. Popa, V.C. Diculescu, Electrochemical and spectrophotometric characterisation of protein kinase inhibitor and anticancer drug danusertib, *Electrochim. Acta.* 112 (2013) 486–492. doi:10.1016/j.electacta.2013.09.017.
- [52] C.S.H. Jesus, V.C. Diculescu, Redox mechanism, spectrophotometrical characterisation and voltammetric determination in serum samples of kinases inhibitor and anticancer drug dasatinib, *J. Electroanal. Chem.* 752 (2015) 47–53. doi:10.1016/j.jelechem.2015.06.006.
- [53] C.E. Banks, R.G. Compton, *Understanding Voltammetry*, 3rd Ed., World Scientific Press Company, 2018.
- [54] D. Li, C. Batchelor-McAuley, L. Chen, R.G. Compton, Electrocatalysis via Intrinsic Surface Quinones Mediating Electron Transfer to and from Carbon Electrodes, *J. Phys. Chem. Lett.* 11 (2020) 1497–1501. doi:10.1021/acs.jpcllett.9b03638.
- [55] M.B.M.Y. Ang, Y.-L. Ji, S.-H. Huang, K.-R. Lee, J.-Y. Lai, A facile and versatile strategy for fabricating thin-film nanocomposite membranes with



polydopamine-piperazine nanoparticles generated in situ, *J. Memb. Sci.* 579 (2019) 79–89. doi:10.1016/j.memsci.2019.02.064.

[56] M.C. van der Leeden, Are Conformational Changes, Induced by Osmotic Pressure Variations, the Underlying Mechanism of Controlling the Adhesive Activity of Mussel Adhesive Proteins?, *Langmuir*. 21 (2005) 11373–11379. doi:10.1021/la0515468.

[57] A.A.J. Torriero, E. Salinas, J. Raba, J.J. Silber, Sensitive determination of ciprofloxacin and norfloxacin in biological fluids using an enzymatic rotating biosensor, *Biosens. Bioelectron.* 22 (2006) 109–115. doi:10.1016/j.bios.2005.12.004.

[58] I. You, H. Jeon, K. Lee, M. Do, Y.C. Seo, H.A. Lee, H. Lee, Polydopamine coating in organic solvent for material-independent immobilization of water-insoluble molecules and avoidance of substrate hydrolysis, *J. Ind. Eng. Chem.* 46 (2017) 379–385. doi:10.1016/j.jiec.2016.11.007.

[59] P. Seeman, T. Tallerico, Antipsychotic drugs which elicit little or no Parkinsonism bind more loosely than dopamine to brain D2 receptors, yet occupy high levels of these receptors, *Mol. Psychiatry*. 3 (1998) 123–134. doi:10.1038/sj.mp.4000336.

[60] K.J. Broadley, The vascular effects of trace amines and amphetamines, *Pharmacol. Ther.* 125 (2010) 363–375. doi:10.1016/j.pharmthera.2009.11.005.

[61] N.H. Jensen, R.M. Rodriguiz, M.G. Caron, W.C. Wetsel, R.B. Rothman, B.L. Roth, N-Desalkylquetiapine, a Potent Norepinephrine Reuptake Inhibitor and Partial 5-HT<sub>1A</sub> Agonist, as a Putative Mediator of Quetiapine's Antidepressant Activity, *Neuropsychopharmacology*. 33 (2008) 2303–2312. doi:10.1038/sj.npp.1301646.

## Appendix 8 - The chemical interaction between the neurotransmitter dopamine and the anti-psychotic drugs olanzapine and quetiapine.

### Olanzapine (OLZP) Extraction, Purification and <sup>1</sup>H-NMR Analysis

The NMR spectra obtained from the extracted samples of OLZP and QTP are presented in figures S1 and S2.

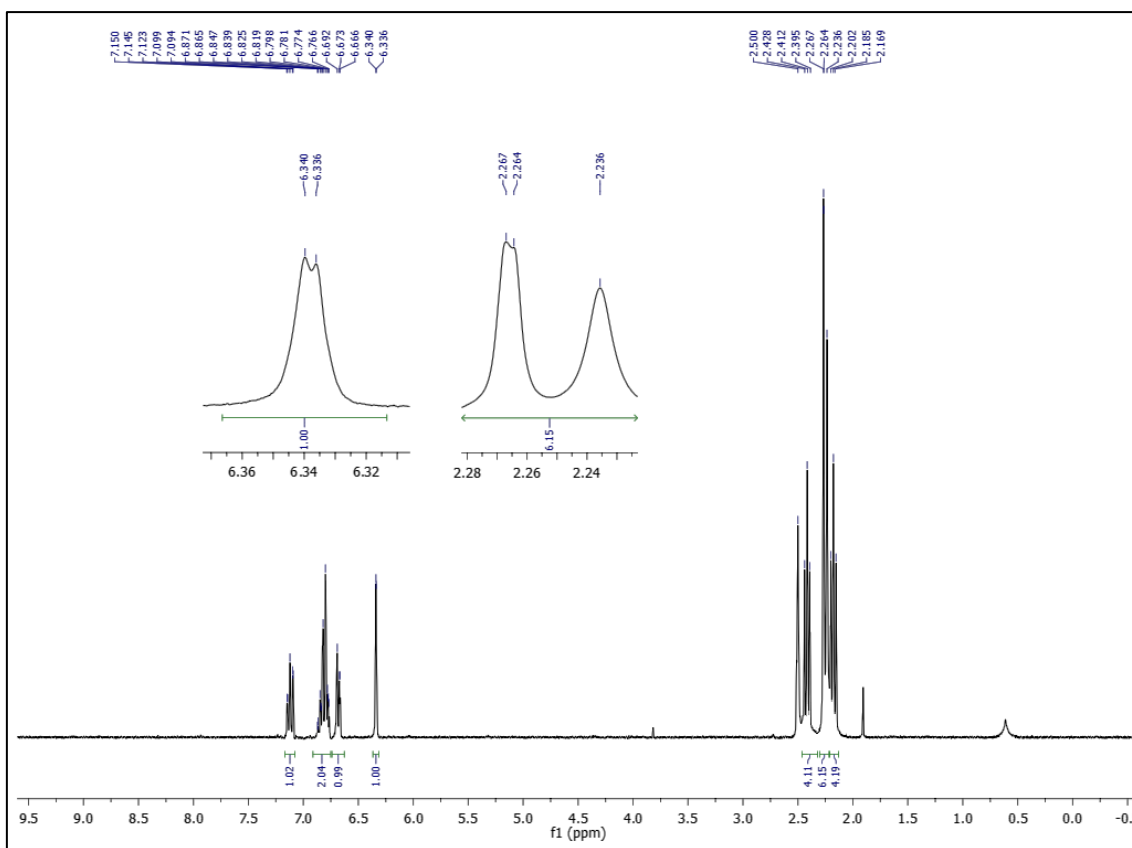
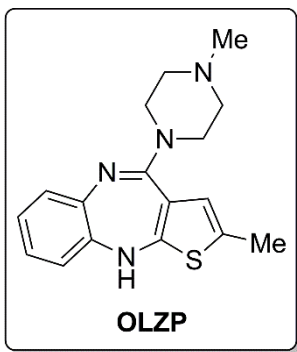


Figure S1: <sup>1</sup>H NMR (DMSO-d<sub>6</sub>, 300 MHz) of OLZP samples obtained after the extraction procedure.



**#CAS:** 132539-06-1; **<sup>1</sup>H NMR (DMSO-D<sub>6</sub>, 300 MHz):** δ (ppm) = 7.12 (dt, 1H, *J* = 1.5 Hz, *J* = 5.7 Hz), 6.87–6.77 (m, 2H), 6.68 (dd, 1H, *J* = 2.0 Hz, *J* = 5.7 Hz), 6.34 (d, 1H, *J* = 1.2 Hz), 2.41 (t, 4H, *J* = 5.1 Hz), 2.26 (d, 3H, *J* = 1.2 Hz), 2.24 (s, 3H), 2.18 (t t, 4H, *J* = 5.1 Hz); **m.p.** (°C): 193-196 (lit. 195).<sup>48</sup>

### Quetiapine (QTP) Extraction, Purification and <sup>1</sup>H-NMR Analysis

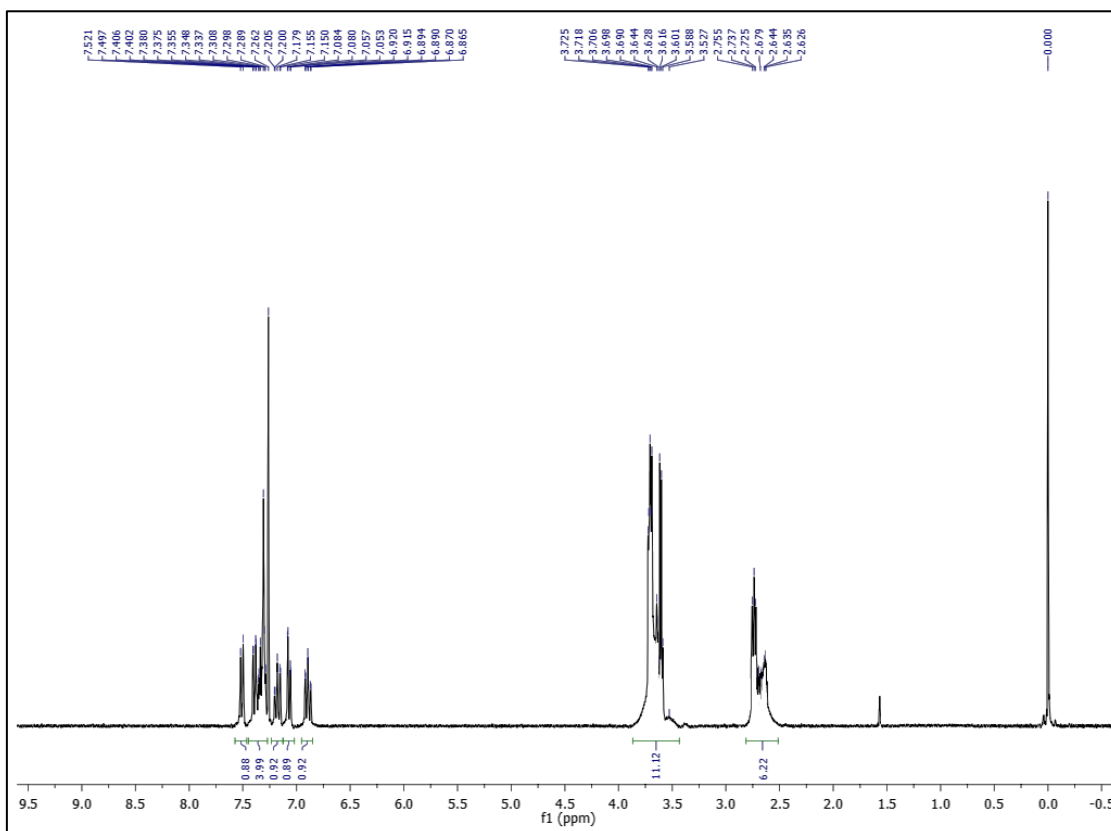
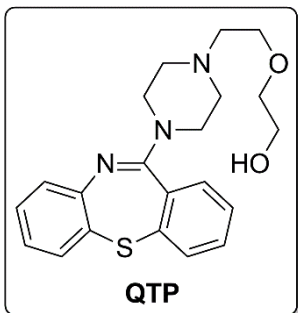


Figure S2: <sup>1</sup>H NMR (CDCl<sub>3</sub>, 300 MHz) of QTP samples obtained after the extraction procedure.



**#CAS:** 111974-69-7;  **$^1\text{H NMR}$  ( $\text{CDCl}_3$ , 300 MHz):**  $\delta$  (ppm) = 7.51 (d, 1H,  $J = 7.2$  Hz), 7.41–7.29 (m, 4H), 7.18 (dt, 1H,  $J = 1.5$  Hz,  $J = 7.8$  Hz), 7.07 (dd, 1H,  $J = 1.5$  Hz,  $J = 7.2$  Hz), 6.89 (dt, 1H,  $J = 1.5$  Hz,  $J = 7.8$  Hz),

3.72–3.53 (m, 11H), 2.75–2.63 (m, 6H). <sup>49</sup>

### Cyclic voltammetry and the electrochemical behaviour of the molecules involved.

The potential peaks and the peak currents obtained in the voltammograms from figures 2 and 3 are presented in the tables bellow.

Table S1: Compilation of the potential peak and peak currents values of DA per scan rate, from figure 2A.

$v$ ( $\text{V s}^{-1}$ )	Ep I (V)	Ep II (V)	$I_{pI}$ ( $\mu\text{A}$ )	$I_{pII}$ ( $\mu\text{A}$ )
0.02	0.235	0.124	16.94	-1.24
0.05	0.226	0.112	25.85	-6.519
0.10	0.233	0.109	31.51	-14.61
0.20	0.254	0.093	41.7	-26.75
0.50	0.276	0.081	73.59	-50.22
1.00	0.328	0.060	96.26	-68.02

Table S2: Compilation of the potential peak and peak currents values of OLZP

per scan rate, from figure 2B.

$v$ ( $V s^{-1}$ )	Ep I (V)	Ep II (V)	IpI ( $\mu A$ )	IpII ( $\mu A$ )
0.02	0.218	-	3.63	-
0.05	0.227	-	6.66	-
0.10	0.232	0.146	10.53	-0.74
0.20	0.235	0.148	14.15	-1.85
0.50	0.240	0.150	27.12	-4.60
1.00	0.240	0.157	43.67	-10.95

Table S3: Compilation of the peak potential values of solutions containing DA and OLZP, DA and QTP per scan rate, from figures 2C and 2D, and 3C and 3D.

$v$	EpI DA + OLZP (V)	EpII DA + OLZP (V)	EpI DA + QTP (V)	EpII DA + QTP (V)
0.02	0.340	-	0.412	-
0.05	0.390	-	0.380	0.051
0.10	0.391	0.018	0.381	0.044
0.20	0.393	0.023	0.385	0.036
0.50	0.423	0.009	0.409	0.017
1.00	0.427	0.004	0.446	0.007
2.00	0.443	0.001	0.471	-0.009
3.00	0.447	-0.005	0.489	-0.018
5.00	0.482	-0.016	0.520	-0.024
10.00	0.522	-0.029	0.565	-0.049

Table S4: Compilation of the peak current values of solutions containing DA and OLZP, DA and QTP per scan rate, from figures 2C and 2D, and 3C and 3D.

	IpI DA + OLZP	IpII DA + OLZP	Ip I DA + QTP	IpII DA + QTP
v	( $\mu$ A)	( $\mu$ A)	( $\mu$ A)	( $\mu$ A)
0.02	11.40	-	11.01	-
0.05	18.07	-	15.11	-1.39
0.10	24.89	-2.88	19.41	-3.38
0.20	32.51	-7.82	30.41	-9.17
0.50	57.15	-20.56	47.63	-21.6
1.00	88.32	-41.26	62.93	-33.08
2.00	103.39	-55.24	92.83	-47.99
3.00	152.84	-81.45	109.96	-58.00
5.00	205.78	-104.70	139.58	-70.88
10.00	256.45	-126.21	198.80	-94.05

### Electron Paramagnetic Resonance (EPR) analysis

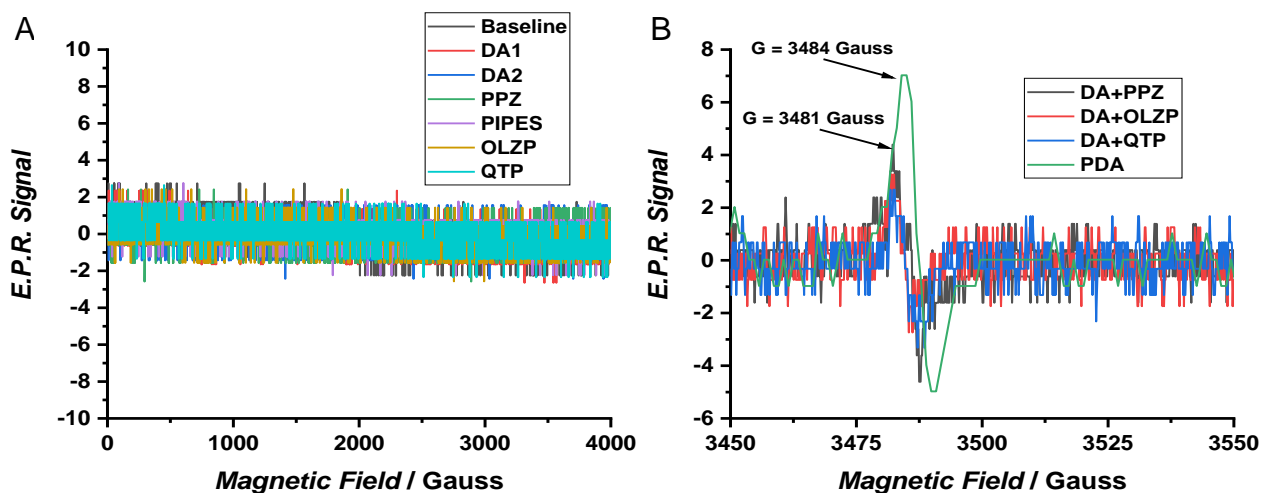


Figure S3: EPR spectra of A) DA, PPZ, OLZP and QTP samples; B) DA+ PPZ, DA+OLZP, DA+QTP and PDA samples.

## Differential pulse voltammetry and the chemical rate constants

### Dopamine stability

The DA stability along the experiment was observed using the same protocol used to study the chemical interactions to guarantee that DA oxidation during the experiment would not be significant and therefore, generate false-positive results. DA presents a stable signal after 15 minutes of experiment. The initial signal decreased approximately 10% of the initial current obtained, even with the electrochemical cell hidden from light and the DA solution degassed. Thus, the obtained results were only considered significant when the DA oxidation signal decreased more than 10%, which occurred for each studied solution.

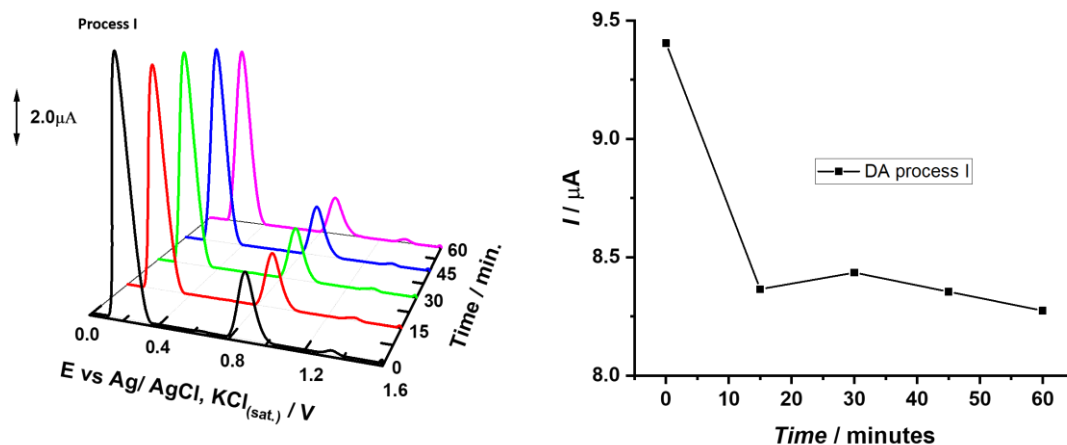


Figure S4: A) DPVs obtained using GCE in a solution containing a mixture of DA solutions, 1.0 mM along the time of reaction, recording the DPV data every 15 min. B); Peak current extracted from DPV data presented in A along the time of reaction. CV

### The catechol-piperazine minimalist model

Before the essay with CAT, it was observed if PIPES could be used as a model. Therefore, being able to react with DA, in a comparable interaction that was observed within the anti psychotic drugs. The same experiment used to observe the interaction between the neurotransmitter DA and OLZP and QTP was performed.

As the DA was introduced in a cell it was observed a sharp decrease of the DA oxidation signal that was succeeded by slight decreases every 15 minutes, until one hour. It generates an analogous result as observed to the interaction between the drugs and DA, which in conclusion validates the PIPES to be used as a model. The kinetic curve obtained also presented a similar rate constant to the one observed for the studied reactions.

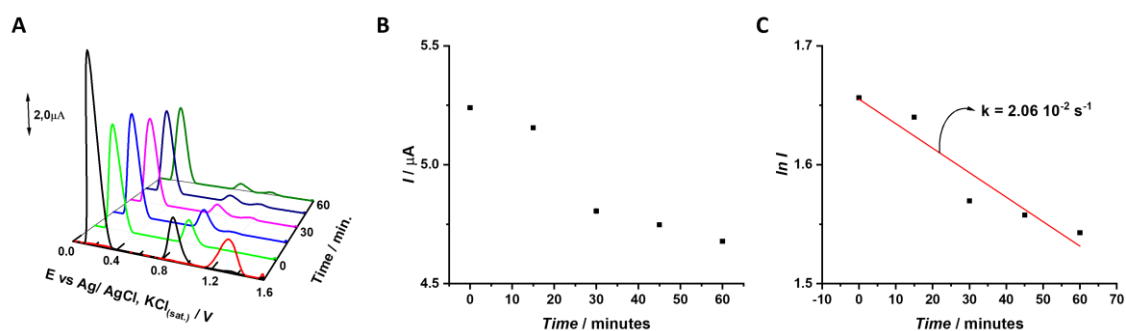




Figure S5: A) DPVs obtained using GCE in a solution containing a mixture of DA and PIPES solutions, 1.0 mM, each along the time of reaction, recording the DPV data every 15 min. B); Peak current extracted from DPV data presented in A along the time of reaction. C) logarithm of the DA oxidation peak current versus time in minutes ( $\ln I_{CAT} = -2.06 \cdot 10^{-2} t + 1.65$ ,  $R^2 = 0.92$ )

## References

- [48] K. A. Chu and S. H. Yalkowsky, An interesting relationship between drug absorption and melting point, *Int. J. Pharm.*, 2009, **373**, 24–40.
- [49] E. J. Warawa, B. M. Migler, C. J. Ohnmacht, A. L. Needles, G. C. Gatos, F. M. McLaren, C. L. Nelson and K. M. Kirkland, Behavioral approach to nondyskinetic dopamine antagonists: identification of seroquel., *J. Med. Chem.*, 2001, **44**, 372–89.

## Chapter 9

### **A reaction between neurotransmitter epinephrine and antipsychotics drugs olanzapine and quetiapine at physiological pH.**

#### **Abstract**

This chapter shows the complementary study of the chemical interaction between the catecholamine neurotransmitter epinephrine and the atypical antipsychotics olanzapine and quetiapine. This work counted with the aid of Pedro Garcia and Elaine Mattos in data acquirement data curation, discussions and writing the original draft and revision, Professor Silvia Serrano administrated the project.

This study shows that epinephrine quinone derivative reacts with the atypical antipsychotic olanzapine and quetiapine in a Michael addition which involves the piperazine moiety from the drugs and the o-quinone moiety from oxidized epinephrine, changing the cyclization reaction of epinephrine to a different position. These formed adducts oxidizes in a two-electrons and two protons multi-step irreversible processes that present the first step as the rate determining one, in a thermodynamically favourable exergonic process. Both reaction and following oxidation were proposed.

## Introduction

The epinephrine (Epi) is a hormone which performs a signalling function. [1] Its major influence resents in the cardiac system as well as some neural functions [2], therefore been responsible for the increase of the vascularization and the heart rate. [3,4] Elevated levels of Epi result of stress are linked with hypertension. [3] On the other hand, Epi is used as a cardiac stimulator in cardiac arrests and severely low blood pressure, or low oxygenation [5], as well as been used in treatments of acute asthma. [6]

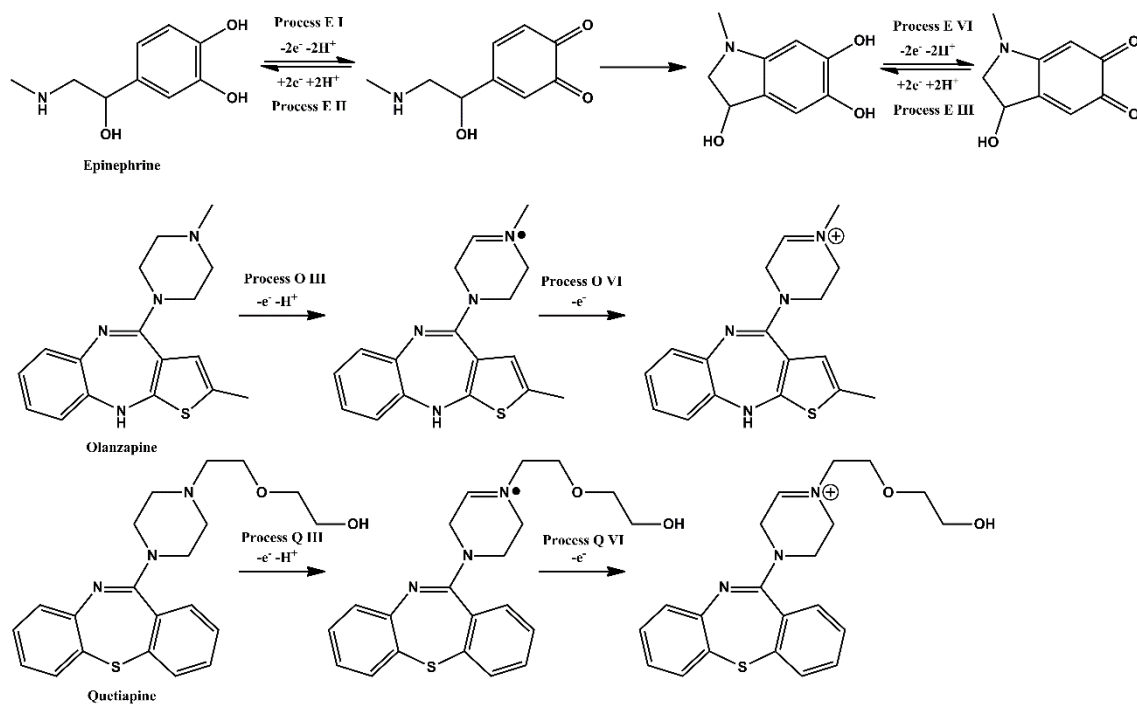
This catecholamine is mainly generated in the suprarenal glands, and it interacts with the adrenergic receptors that have different subtypes, divided in  $\alpha$  and  $\beta$  subtypes. Epi interacts with both subtypes of adrenoreceptors, as the  $\alpha$  units are responsible for a vasoconstriction response, as the  $\beta$  vasodilation. [7] In general, the  $\alpha$ -adrenoreceptors are less sensible to the Epi interaction when compared to the  $\beta$  one. Thus, low levels of Epi are enough to result in a vasodilation effect. On the other hand, when elevated levels of Epi are in the system, the result in an enhanced activity of the  $\alpha$  subtypes that overrides the vasodilation effects, therefore resulting in a vasoconstriction. [8] The adrenal system is most known to act in extreme situations in which one is exposed to dangerous situations or elevated surprise. In these cases, the Epi level released by the glands sharply increase resulting in flight or fight reaction, that develops in a temporary supersaturation of the receptors, and per consequence a vasoconstriction effect and enhanced physical abilities. [4,9]

Since the levels of Epi can change the effects of the adrenergic receptors, affecting the cardiac functions, the quantification and determination of Epi is of

335

the utmost importance. Therefore, several works study different methods to analyse Epi. Most studies use electroanalytical methods such as cyclic voltammetry and/ or amperometry [10–19]-[20,21] Square Wave Voltammetry (SWV), [22–24] FIA with UV-Vis [25] and amperometric detection [26], differential pulse voltammetry, [27–36]-[37–40] Stripping Voltammetry, [41,42] HPLC, [43] capillary electrophoresis, [44] and fluorimetry. [45]

The adrenergic receptors can be antagonized by several different types of molecules, known as  $\alpha$  or  $\beta$  blockers. Among these molecules, one of the major antagonists for the  $\alpha$ -adrenoreceptors are the antipsychotic drugs, since the suppression of this receptors can act positively in the reduction of the symptoms of schizophrenia by inhibiting the presynaptic levels and striatal hyperdopaminergia. [46,47] It is known that Epi presents an oxidation which is similar to dopamine, in a proton coupled electron transfer (PCET) process that involves two electrons and two protons, as presented in scheme 1. The atypical antipsychotics olanzapine (OLZP) and quetiapine (QTP) oxidation mechanism is also described [48]. OLZP presents two oxidation processes, both are PCET, the first one involves one electron and one proton, that occurs in the benzodiazepine moiety, in approximately 0.2 V vs Ag/ AgCl, KCl<sub>(sat.)</sub> (+0.222V vs SHE) as the second one is sequential process involving two-electrons and one proton in the piperazine moiety of the drug. [49] QTP only presents the process of the piperazine moiety, which is similar to the one observed in OLZP. [49] The oxidation processes of the drugs are presented in the scheme 1.



Scheme 1: Schematic representation of the oxidation mechanisms of epinephrine, olanzapine and quetiapine.

As previously observed, the antipsychotics not only interact with the dopaminergic receptor D2, it also interacts with dopamine. [50] Thus, the aim of this work is to evaluate if Epi reacts with the atypical antipsychotics, as dopamine.

## Materials and methods

### Apparatus

All pH measurements were performed using a model 654 pH meter and a combined glass electrode, model 6.0203.100 (OE), both from Metrohm. NMR spectra were obtained from the IQ-USP Analytical Centre using a 300 MHz Bruker equipment with ACS laboratory software. All the NMR data were obtained at an ambient temperature of  $25 \pm 3$  °C.

### Chemicals and reagents

All used reagents, except QTP and OLZP, were of analytical grade and used without prior purification. The solutions were prepared using deionized

water from a reverse osmosis device (Gehara Co., model of ultra-pure OS10LX system, water resistivity 18MΩcm). The 0.1 mol L<sup>-1</sup> phosphate buffer solutions (PBS) were prepared by solubilizing and diluting, respectively, the appropriate amount of NaH<sub>2</sub>PO<sub>4</sub> and H<sub>3</sub>PO<sub>4</sub> (Merck) in deionized water, and the pH values were adjusted by the addition of a 4.0 mol L<sup>-1</sup> NaOH (Merck) solution. The volumes were measured using EP-10 and EP-100 from Unipettemicroliter Pipettes (Uniscience, Brazil). All experiments were performed at room temperature (25 ± 3 °C)

### **Olanzapine (OLZP) Extraction, Purification and <sup>1</sup>H-NMR Analysis**

Olanzapine was obtained by extraction from commercial tablets as presented in previous study [51,52]

### **Quetiapine (QTP) Extraction, Purification and <sup>1</sup>H-NMR Analysis**

Quetiapine was also obtained by extraction from commercial tablets as presented in previous study [51,52]

### **Electrochemical procedures**

All electrochemical experiments were performed using a potentiostat/galvanostat PGSTAT 101, Metrohm AUTOLAB, connected to an IME663 interface stirring device. Data was obtained and treated with software NOVA version 1.11.4 and the software Origin 2019. The electrochemical procedures were performed using a Glassy Carbon Electrode (GCE) with a diameter of 3.0 mm as working electrode, a Silver/ Silver Chloride electrode in a saturated solution of potassium chloride, (+0.222 V vs. SHE) [52] as reference electrode, and a platinum wire as an auxiliary electrode, in an electrochemical cell of 10 mL. Before each electrochemical procedure, the GCE was polished using diamond spray suspensions with decreasing particle sizes of 3.0, 1.0, and 338

0.1  $\mu\text{m}$  from Buehler (Lake Buff, IL, USA) on a polishing pad also from Buehler, and the solutions were stirred before each electrochemical measurement.

Cyclic voltammetry (CV) was performed by sweeping the potential from 0.0 V to 1.5 V, then from 1.5 V to -1.0 V and from -1.0 V back to 0.0 V, and in a restricted potential window from 0.0 V to 1.0 V, then from 1.0 V to -0.6 V and finally, from -0.6 V to 0.0 V. The scan rates changed from 0.10 to 10.0  $\text{V s}^{-1}$ . Square Wave Voltammetry (SWV) was performed by sweeping the potential from -0.6 V to 1.2 V and from 1.2 V to -0.6 V. The parameters used were: potential step of 2.0 mV, pulse amplitude of 20.0 mV and frequency of 50 Hz, resulting in a scan rate of  $\nu = 100 \text{ mV s}^{-1}$ . The system was degassed with nitrogen gas for 15 minutes prior to the experiment when the potential window used was below -0.3 V, to prevent any oxygen interference.

### **UV-Vis procedures**

UV-vis spectra were performed using a Shimadzu UV-1601PC with both deuterium and tungsten lamps, and a quartz cuvette with a 1.0 cm optical path. Blank spectra were performed in deionized water.

### **Results and discussions**

This study initially presents an electrochemical analysis of the processes of the neurotransmitter epinephrine, and the antipsychotics olanzapine and quetiapine. The cyclic voltammograms were obtained to both characterize the processes as a function of the scan rates and as a function of the time. Following, the square wave voltammograms were obtained to observe the influence of the reaction in each of the electrochemical processes. Then, the UV-Vis spectra were

obtained to observe the formation or shifts of the bands. Finally, the mechanism of the chemical reaction was proposed.

### **Cyclic voltammetry, and the general behaviour of the system**

The CV were obtained to observe the processes of each molecule individually, and then the neurotransmitter together with each of the drugs. The voltammograms were initially obtained in different scan rates to observe the heterogeneous kinetics related each process in all the molecules.

Figure 1A shows the voltammograms of Epi in solutions 0.1 M PBS at scan rates from 0.01 to 1.00 V s<sup>-1</sup>. It shows that Epi present four processes, (E I, E II, E III, and E IV) three well defined and one barely visible (E II). The process E I, E III, and E IV presented a quasi-reversible behaviour as their peak potential values shift with the increase of the scan rate. Process E I is the oxidation of Epi at the catechol moiety, which involves two-electrons and two protons. As previously stated, the reduction pair of this process, E II, is barely visible. This is most likely due to the following chemical step, a cyclization, that generates an electrochemical irreversibility as a consequence of a fast chemical reaction that follows the heterogeneous process, as previously discussed in scheme 1. [51] The peak potential values for Epi processes are presented in table 1. The processes E III and E IV are both quasi-reversible, as similarly to E I, their peak potential values shift as the scan rate is increased. These processes E III and E IV can be ascribed to the oxidation and reduction of the catechol moiety after the cyclization occurs, scheme 1.

Figure 1B shows the voltammograms for solutions 1.0 mM of OLZP 0.1 M PBS at scan rates from 0.01 to 1.00 V s<sup>-1</sup>. As Epi, OLZP also presents four processes. The processes O I and O II form a redox pair, in a proton coupled



electron transfer, which involves one electron and one proton. [48] The other two processes, E III and E IV, are schematized in scheme 1, they are a sequential process, involving one electron and one proton, and only one electron, occurring at the piperazine moiety of OLZP. Figure 1C shows voltammograms of 1.0 mM of OLZP 0.1 M PBS QTP. It presents two processes, Q III and Q IV, which correspond to the oxidation in the piperazine moiety, similarly as observed to OLZP, scheme 1.

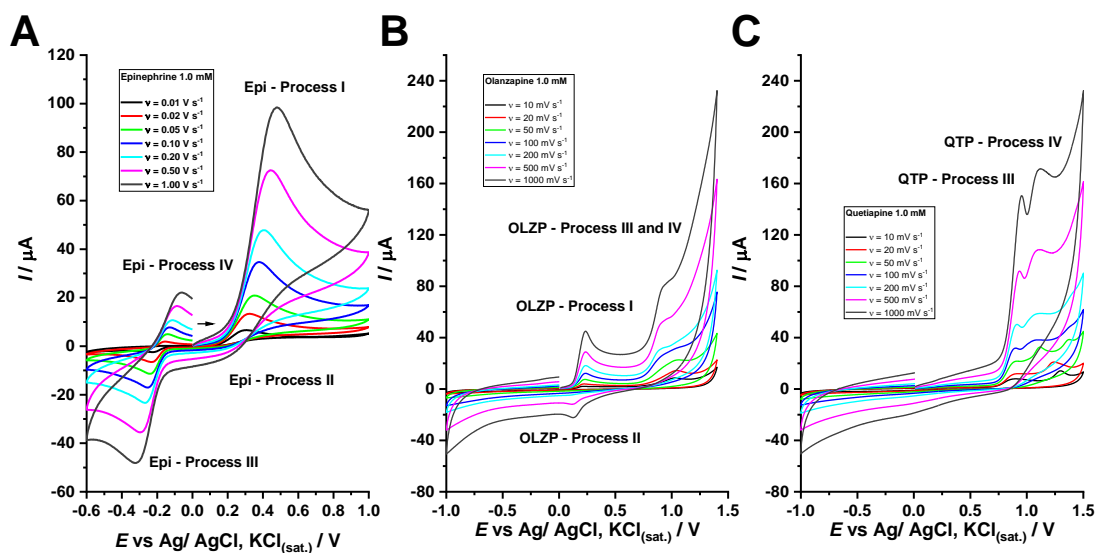


Figure 1: CV of 1.0 mM solutions in PBS of A) Epi, B) OLZP, and C) QTP at different scan rates.

To observe the chemical reaction between the Epi and the drugs, the CV of solutions containing the neurotransmitter and one of the antipsychotics were obtained. The results of a solution containing Epi in the presence of OLZP can be seen in figure 2A, as the results to the solutions containing Epi with QTP are

presented in figure 2B. Moreover, the CV were obtained in different scan rates to observe the heterogeneous kinetics of the processes of the molecules together.

Figure 2A shows that in the presence of OLZP the Epi processes shift to different peak potentials, strongly suggesting that a chemical interaction occurs, as previously reported. [50] The process E I and E IV shift to more positive potentials as the process E III peak potentials slightly shift to more negative values. On the other hand, the oxidation process of OLZP O I remains in the same peak potential and with similar peak current values. A result that indicates that the chemical reaction does not occur involving the nitrogen of the benzodiazepine ring of OLZP. Therefore, as observed to dopamine, the interaction most likely proceeds involving the piperazine moiety.

Figure 2B shows that when in the presence of QTP, the processes of Epi also shift their peak potential values, analogously to the observed in figure 2A. However, the values observed for process E I are slightly more positive than the ones observed for OLZP. Despite that, the values observed for the process E III are similar to both drugs. The peak potential values are presented in table 1.

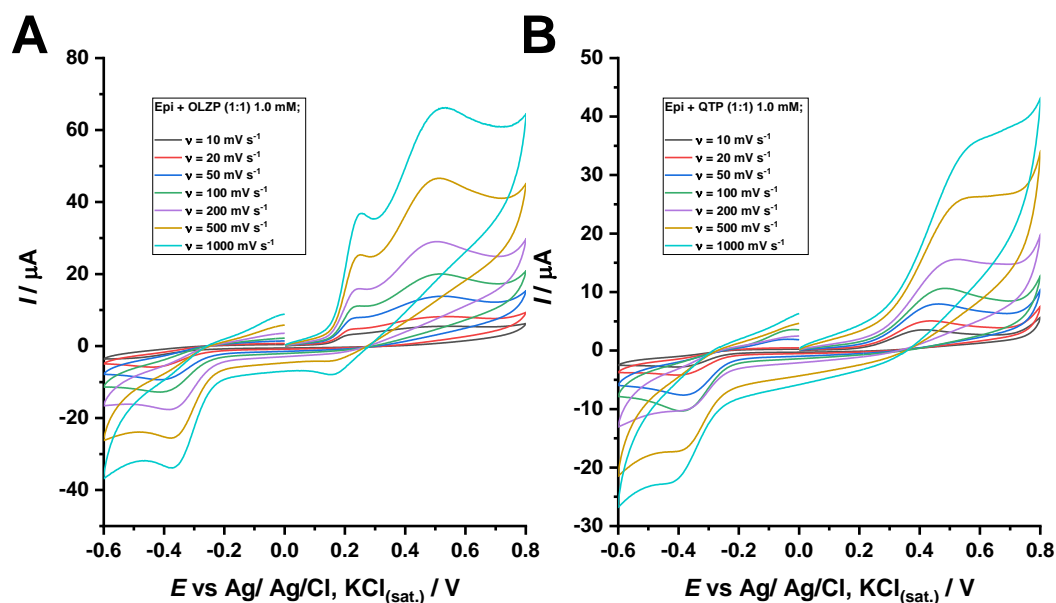


Figure 2: CV of 1.0 mM solutions of A) Epi with OLZP, B) Epi with QTP at different scan rates.

Table 1: Peak potential values of Epi, and Epi in the presence of OLZP and QTP as a function of the scan rate.

$v / V s^{-1}$	E I (in the presence of OLZP) / V	E I (in the presence of QTP) / V
0.01	0.490	0.435
0.02	0.510	0.451
0.05	0.517	0.482
0.10	0.527	0.496
0.20	0.529	0.522
0.50	0.537	0.527
1.00	0.538	0.530

To observe the correlation between the processes EI of Epi in the presence of both drugs OLZP and QTP the plots of the peak potentials of EI, and the peak current values were plotted as a function of the scan rate.

Figure 3A shows that the peak potential values as a function of the scan rate present an exponential behaviour, evidencing the quasi-reversible behaviour of the oxidation process of the adduct formed between the neurotransmitter and OLZP. Moreover, despite the divergence of the peak potential values observed for the interaction product at slow scan rates ( $< 0.2 \text{ V s}^{-1}$ ), the peak potentials tend to converge to scan rates above  $0.2 \text{ V s}^{-1}$ . A result that can be explained by presence of oxidation process O I of OLZP in the potential window studied. After the oxidation, two following chemical steps occur, leading to two distinct products. The first one is an EC, which has a Michael addition generating a hydroxylated derivative of OLZP, the OLZP-OH, and a the second one is an EC<sub>2</sub> mechanism which forms a dimer of OLZP. The dimerization only occurs at slow scan rates as the Michael addition is a fast chemical step that occurs even at high scan rates. [48] Therefore, the major divergence is caused by these side chemical steps, although neither of them affects the chemical reaction observed between the Epi and OLZP because the interaction occurs in a different moiety of the drugs, the piperazine, as can be evidenced in figure 3B.

Figure 3B shows the peak current values as a function of the square root of the scan rate, a comparison between the experimental values obtained of an Epi mixture each of the drugs and the multi-step irreversible Randles Sevcik theoretical prediction described by the equation 1, this comparison allows not only to discriminate the mechanism of the process E I in the presence of the

antipsychotics, but also to show that both drugs interact with the neurotransmitter, generating a similar process.

$$I_p = 0.496 \sqrt{n' + \beta_{rds}} nFAC \sqrt{FvD_0/RT} \quad (1)$$

where  $I_p$  is the peak current in A,  $n'$  the number of electrons transferred in the steps prior to the rating determining step,  $\beta_{rds}$  is the charge transfer coefficient of the rating determining step,  $n$  is the total number of electrons transferred,  $F$  is the Faraday constant in  $A \text{ mol}^{-1}$ ,  $C$  is the concentration in  $\text{mol cm}^{-3}$ ,  $v$  is the scan rate in  $V \text{ s}^{-1}$ ,  $D_0$  is the diffusion coefficient in  $\text{cm}^2 \text{ s}^{-1}$ ,  $R$  is the gas constant in  $J \text{ K}^{-1} \text{ mol}^{-1}$  and  $T$  is the temperature in K.

Figure 3B shows that both process E I with the drugs present similar currents values, which best corresponds to the multi-step irreversible Randles Sevcik prediction with no prior step to the rating determining one. Is it noteworthy that the peak currents of the E I process in the presence of OLZP were obtained by subtracting the total current of E I of the process O I, to prevent the change of the baseline. Therefore, the results show that to both drugs the adduct oxidation process is the same two-electrons process with the first step as the rating determining one, which is in agreement with the results observed to dopamine.

[50]

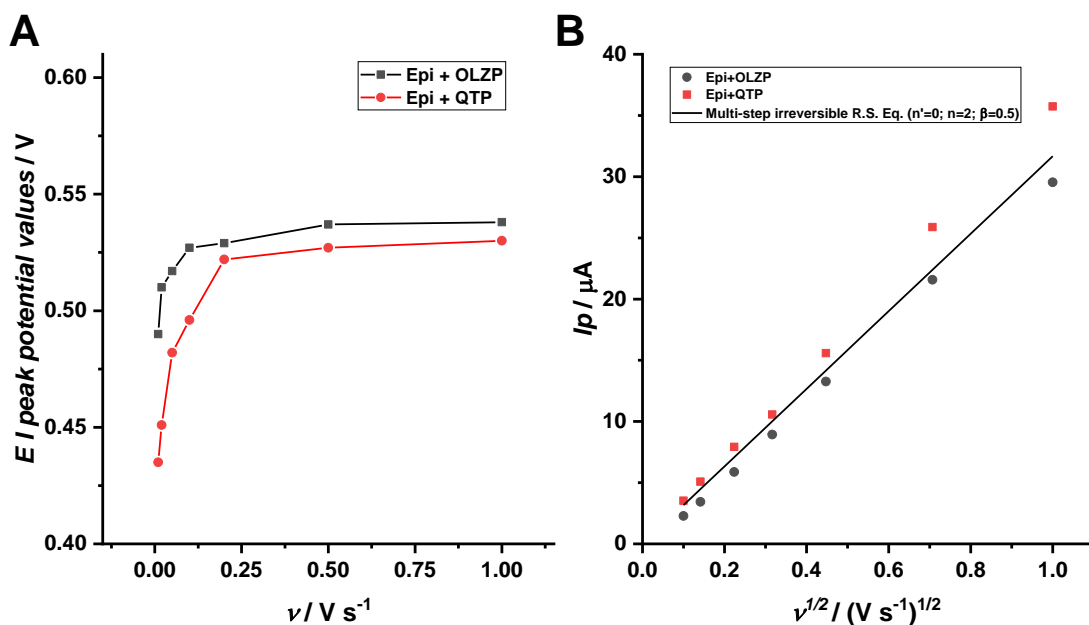


Figure 3: A) Peak potential values of process E I in the presence of the drugs as a function of the scan rate. B) Plot of the experimental peak current values of process E I in the presence of the drugs as a function of the square root of the scan rate, compared with the theoretical predictions of the multi-step irreversible Randles-Sevcik equation ( $n'=0$ ;  $n=2$ ,  $\beta=0.5$ ), electrode area =  $0.071 \text{ cm}^2$ ,  $C = 1.0 \cdot 10^{-6} \text{ mol cm}^{-3}$ ,  $D_0=2.5 \cdot 10^{-6} \text{ cm}^2 \text{ s}^{-1}$ .

In sequence, the kinetics of the reaction between the drugs and the Epi were studied, as the Epi undergoes a much faster cyclization than dopamine.

Figure 4A and 4B show CVs shifts in the voltammetric wavelshape that occur after the addition of the drugs in the solution A) addition of OLZP and B) addition of QTP. It was noticed that to both drugs the voltammetric wave shape obtained in  $t = 0$ , was observed for half an hour, showing that, as expected, the

reaction is fast reaching its equilibrium hastily, thus, presenting a waveshape that endures.

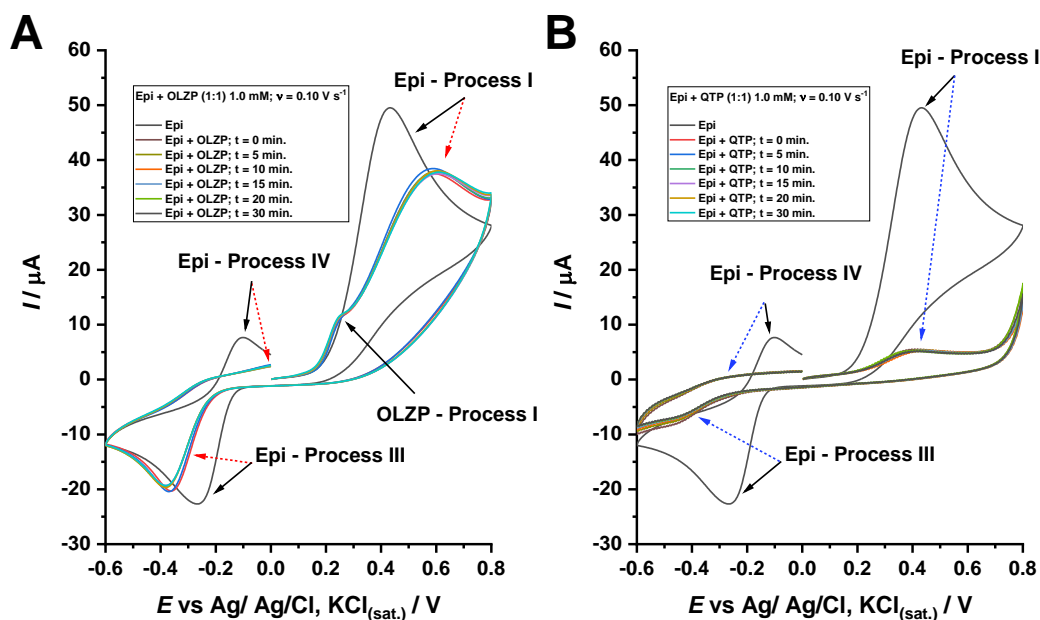


Figure 4: CV of 1.0 mM solutions of A) Epi with OLZP, B) Epi with QTP at  $0.1 \text{ V s}^{-1}$  and different times.

### Square wave voltammetry and the influence of the chemical reaction between the neurotransmitter and the drugs

Since the processes are the same to both molecules, SWV were performed to observe how the reaction between the neurotransmitter and the antipsychotics affect the reversibility of the processes.

Initially, SWV of Epi without the drugs was performed in both sweeping directions. Following, the same procedure was performed to each mixture containing the catecholamine and one of the remedies.

Figure 5A and 5B shows the total, forward and backwards currents of voltammograms that were swept from negative to positive potentials, and from more positive to negative potentials, respectively. In figure 5A, a reversible couple can be seen in processes E I and EII. It is important to observe that in the SWV the process E II can be seen, differently than previously observed to the CVs, even at high scan rates. Figure 5B shows the reversible couple in approximately -0.25 V, processes E III and E IV. These results confirm the ECE mechanism which is well known for Epi, as the processes E III and E IV only appears the negative sweeping voltammogram, after the processes E I and E II already occur, been followed by the cyclization reaction, as presented in scheme 1.

Figures 5C and 5D present the total forward and backwards currents of voltammograms that were swept from negative to positive, and from positive to negative potential directions, respectively. In figure 5C shows that process E II is not visible, which agrees to results priorly obtained. Indicating that Epi undergoes a different reaction than the cyclization, and therefore, the reduction process E II is hindered by the reaction with OLZP, and the process becomes irreversible. [51,52] Figure 5D shows that when in the presence of OLZP, the voltammogram swept form positive to negative the processes E I is not visible. A result that indicates that the chemical reaction with OLZP induces the oxidation of Epi by dislocating the equilibrium to the formation of the product, as predict by the Le Chatelier principle. [53] This result is corroborated by the shift of process E I towards less positive potentials and a decrease in the current values in figure 5C, and also by differences in the processes E III and E IV not only presented a shift in the peak potentials, but also shows a decrease in the peak current values.



Figure 5D and 5E displays SWV of solutions of Epi and QTP that were swept from negative to positive, and from positive to negative potentials, respectively. Figure 5E, similarly to the priorly observed in figure 5C, the oxidation process E I shifts to less positive potentials whilst the peak current values decreased. Figure 5F shows that processes E III and E IV presented both the shift in the peak potentials and the decrease in the current values. In summary, the results voltammetric results suggest that both drugs react with the oxidized Epi, and this chemical step induce the oxidation of Epi according to the Le Chatelier principle. Moreover, it can be also concluded that the cyclization still occurs, but forming a different product, as evidenced by the shift in the potential values of E III and E IV when in the presence of both OLZP and QTP.

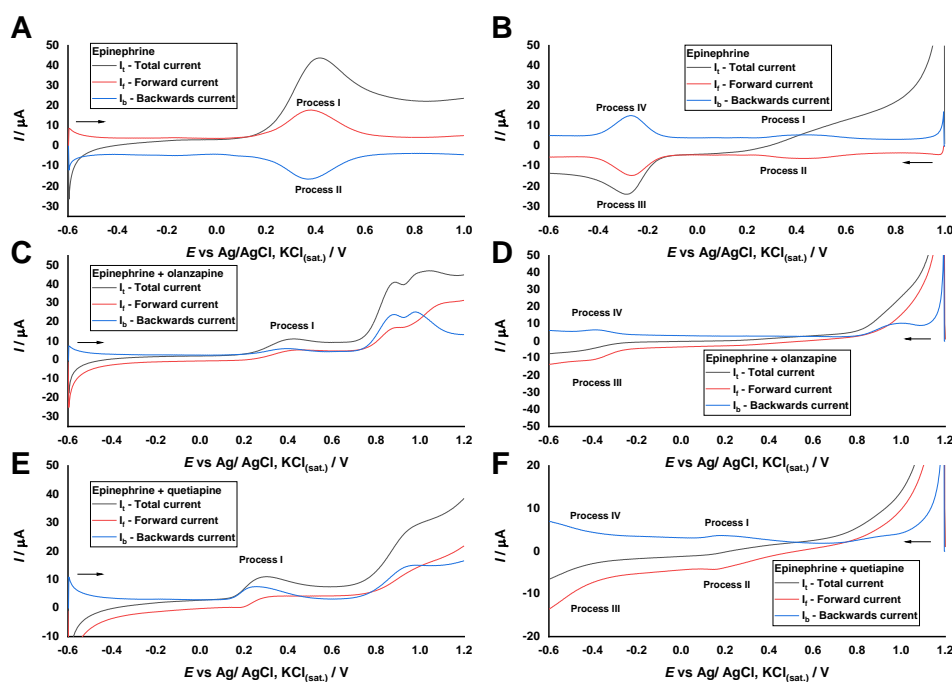


Figure 5: SWV of 1.0 mM solutions of A and B Epi, C and D Epi with OLZP, and E and F Epi with QTP. A, C and E were obtained by sweeping the potential from

negative to positive potentials. B, D and F were obtained by sweeping the potential from positive to negative potentials.

To corroborate that both drugs react in the same moiety with Epi, in a similar way, the Tafel analysis were performed to obtain and compare the values of the charge transfer coefficients ( $\beta$ ) of the adducts oxidation.

### **Tafel analysis and electrode kinetics**

The Tafel analysis allows to better comprehend the kinetics of the heterogeneous processes, indicating if a process is endergonic ( $\beta > 0.5$ ), isogonic ( $\beta = 0.5$ ) or exergonic ( $\beta < 0.5$ ) by the obtention of the charge transfer coefficient ( $\beta$ ). [54] The  $\beta$  values can be obtained from the Tafel plot, with the equation 2.

$$\beta(E) = (F/RT) (d \ln I / d E) \quad (2)$$

This correlation with the transition state is due to an intimal correlation between the Tafel analysis, the Butler Volmer theory, and the Arrhenius Law of kinetics [55] This association allows to compare the activation energy with the charge transfer coefficient, as presented by the Marcus theory, equation 3. [56–58]

$$\beta = 1/2 (1 + \Delta G/\lambda) \quad (3)$$

where  $\lambda$  is the reorganization energy, and  $\Delta G$  is the variation of the activation Gibbs energy in  $\text{kJ mol}^{-1}$ . Therefore, the Tafel analysis was performed to compare the  $\beta$  values of the adduct oxidation process E I and observe if chemical reaction between the Epi and the antipsychotics presents similar values, which would indicate a similar transition energy, and consequently a similar reaction pathway and mechanism.

Figure 6 shows the charge transfer coefficients obtained from the derivation of the natural logarithm of the peak currents as a function of the applied potential from CV of A) Epi in the presence of OLZP, B) Epi in the presence of QTP, at  $0.1 \text{ V s}^{-1}$ . Both figures show that Epi's process E I when in the solution with the drugs present  $\beta$  values of 0.244 and 0.224 to interactions with OLZP and QTP, respectively. Allowing not only to conclude that both drugs react similarly with the neurotransmitter, but also that both reactions are exergonic. Thus, been heavily favoured energetically.

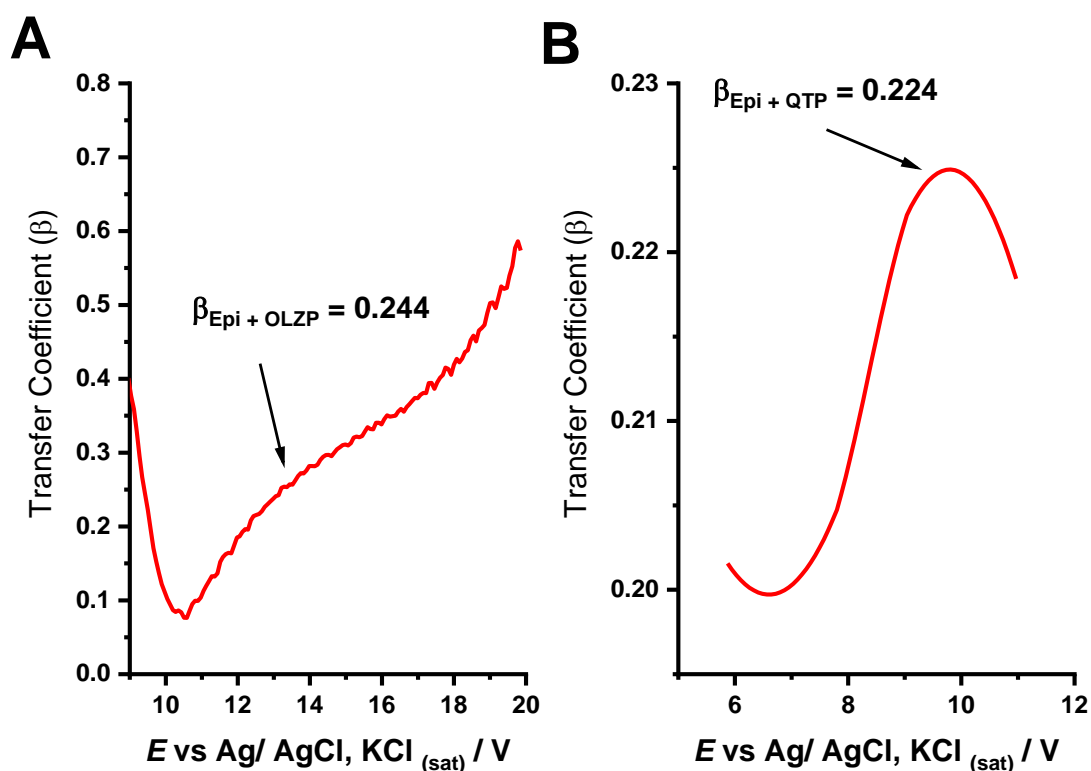


Figure 6: Charge transfer coefficient as a function of potential from CV of A) Epi with OLZP, B) Epi with QTP at a scan rate of  $0.1 \text{ V s}^{-1}$ .

### UV-Vis analysis of the adducts

To corroborate the conclusion of a similar reaction which involves the same moieties of the antipsychotics performing a Michael addition that changes

the cyclization of Epi, the UV-Vis spectra of Epi solutions were obtained. Following, each of the drugs were added to the neurotransmitter solution to observe the formation of distinct bands. Since the previous data support that both OLZP and QTP react with Epi in a similar mechanism, it is expected that a common transition should be observed to both reactions.

Figure 7 shows that Epi presents four transitions, the first one ( $\lambda_1$ ) of around 200 nm, that corresponds to the  $\pi$  to  $\pi^*$  aromatic transitions, the second ( $\lambda_2$ ) in approximately 225 nm, which is also a  $\pi$  to  $\pi^*$  transition, but ascribed to the carbonyl moiety, a third transition ( $\lambda_3$ ) in 280 nm also related to the carbonyl, but being a non-ligand to  $\pi^*$  transition, and at last a barely defined transition ( $\lambda_4$ ) between 335 and 350 nm, that corresponds to the non-ligand to  $\pi^*$  transition of the amine moiety. [59]

Figure 7A shows the addition of OLZP in an Epi solution results not only in the shift of transitions  $\lambda_1$ , from ~200 nm to 210 nm, but also in the appearance of a new transition ( $\lambda_{\text{adduct}}$ ) in 254 nm. Similarly, figure 7B shows the addition of QTP in an Epi solution. As prior observed, the transition  $\lambda_1$  shift from approximately 200 nm to 210 nm and a shift of  $\lambda_3$  from 280 nm to 290 nm. Distinctively from the interaction with OLZP, the addition of QTP results in the shift of  $\lambda_4$  from 335 nm to 325 nm. Finally, the transition  $\lambda_{\text{adduct}}$  appears in 254 nm, this transition was ascribed to the electrons of the bond between the piperazine moiety of the drugs and the aromatic moiety of the neurotransmitter, in agreement with the priorly reaction of dopamine with the same drugs and references which report the reaction between the catechol and piperazine. [50,60,61] Thus, not only indicating that dopamine and Epi reacts with these drugs, but any catecholamine or derivatives.

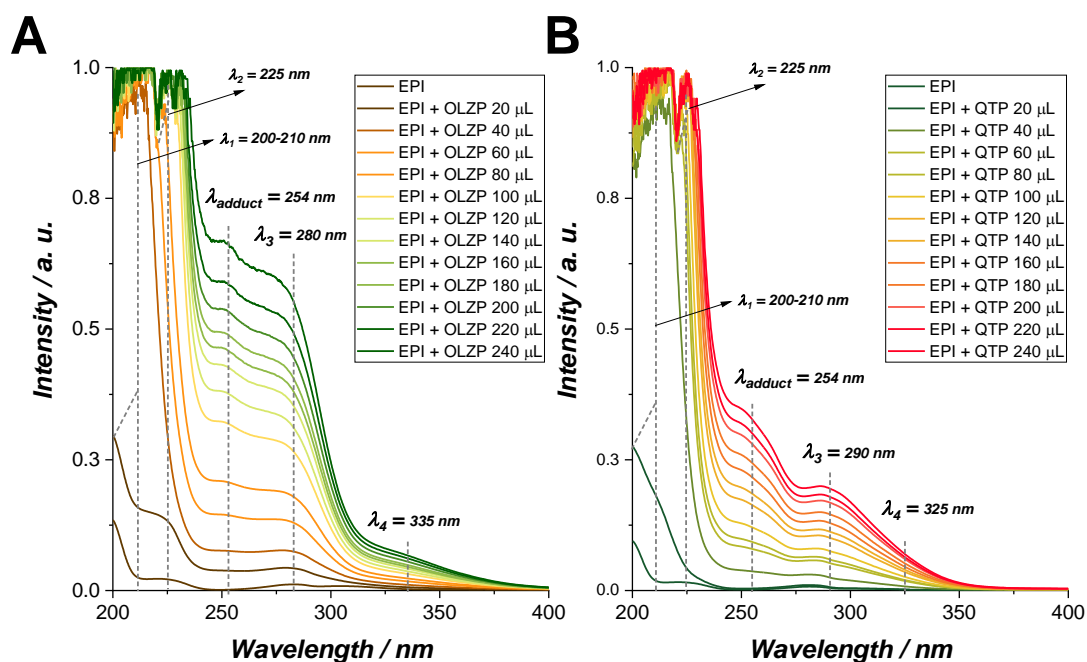
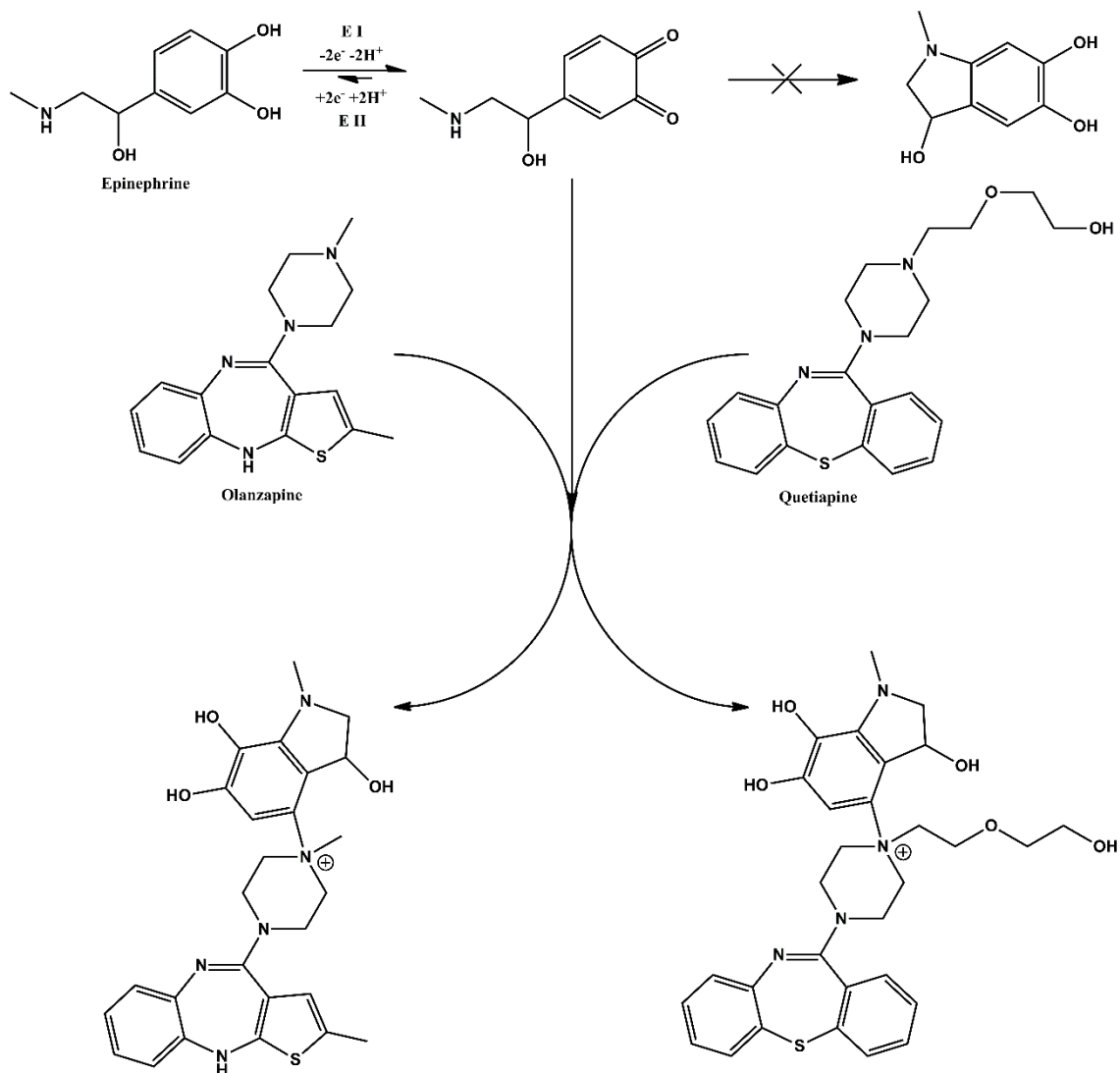


Figure 7: UV-Vis spectra of solutions 1.0 mM of A) Epi, OLZP and QTP, separately. B) Epi with OLZP, C) Epi with QTP.

### Mechanism proposition

Based on the voltammetric, the Tafel analysis and UV-Vis data it can be concluded that Epi reacts with both OLZP and QTP in a hastily reaction which is energetically favoured. Both formed adducts present similar oxidation processes, a two electrons process with the first one being the rating determining step. Moreover, in the UV-Vis spectra it was observed similar bands in 254 nm. Therefore, the results strongly indicate that both adducts are formed by a Michael addition between an oxidized derivative of Epi and the antipsychotics, changing the cyclization reaction of Epi in the process, as can be observed in scheme 2.



Scheme 2: Mechanism proposition of the chemical reaction between epinephrine and the antipsychotic drugs olanzapine and quetiapine.

## Conclusions

In summary this study shows that epinephrine quinone derivative reacts with both olanzapine and quetiapine in a Michael addition which involves the piperazine moiety from the drugs and the o-quinone moiety from oxidized epinephrine, changing the cyclization reaction of epinephrine to a different position. These formed adducts oxidize in a two-electrons and two protons multi-

step irreversible processes that present the first step as the rating determining one, in a thermodynamically favourable exergonic process. Both reaction and following oxidation were proposed.

## References

[1] M. Lieberman, A.D. Marks, A. Peet, Marks' basic medical biochemistry, a clinical approach, Fourth Edi, Lippincott Williams & Wilkinsa Wolters Kluwer Publishers, Baltimore, MD, US, 2013.  
<http://dx.doi.org/10.1016/j.encep.2012.03.001>.

[2] M. Longmore, I. Wilkinson, T. Turmezei, C.K. Cheung, Oxford Handbook of Clinical Medicine, 9th Editio, Oxford University Press, Oxford, UK, 2014.

[3] Y. Azuma, K. Ohura, Immunological Modulation by Lidocaine-Epinephrine and Prilocaine- Felypressin on the Functions Related to Natural Immunity in Neutrophils and Macrophages, *Curr. Drug Targets - Immune, Endocr. Metab. Disord.* 4 (2004) 29–36. <https://doi.org/10.2174/1568008043339974>.

[4] H.F. BROWN, D. DIFRANCESCO, S.J. NOBLE, How does adrenaline accelerate the heart?, *Nature.* 280 (1979) 235–236.  
<https://doi.org/10.1038/280235a0>.

[5] J.M. Field, M. Bressler, R. O'Connor, J. Tobas, T. VandenHoek, M.J. Bresler, P.J. Kudenchuk, A. Mattu, S.M. Silvers, *The Textbook of Emergency Cardiovascular Care and CPR*, Lippincott Williams and Wilkins / Wolters Kluwer Health, 2008.

[6] D.L. Uden, D.R. Goetz, D.P. Kohen, G.C. Fifield, Comparison of nebulized terbutaline and subcutaneous epinephrine in the treatment of acute asthma, *Ann. Emerg. Med.* 14 (1985) 229–232. [https://doi.org/10.1016/S0196-0644\(85\)80445-](https://doi.org/10.1016/S0196-0644(85)80445-5)

- [7] J.O. Ruuskanen, H. Xhaard, A. Marjamäki, E. Salaneck, T. Salminen, Y.-L. Yan, J.H. Postlethwait, M.S. Johnson, D. Larhammar, M. Scheinin, Identification of Duplicated Fourth  $\alpha$ 2-Adrenergic Receptor Subtype by Cloning and Mapping of Five Receptor Genes in Zebrafish, *Mol. Biol. Evol.* 21 (2004) 14–28. <https://doi.org/10.1093/molbev/msg224>.
- [8] P.A. van Zwieten, Interaction Between  $\alpha$  and  $\beta$ -Adrenoceptor-Mediated Cardiovascular Effects, *J. Cardiovasc. Pharmacol.* 8 (1986). [https://journals.lww.com/cardiovascularpharm/Fulltext/1986/08004/Interaction\\_Between\\_\\_\\_and\\_\\_\\_Adrenoceptor\\_Mediated.4.aspx](https://journals.lww.com/cardiovascularpharm/Fulltext/1986/08004/Interaction_Between___and___Adrenoceptor_Mediated.4.aspx).
- [9] D.M. Perez, *The Adrenergic Receptors In the 21st Century*, 1st ed., Springer INC, Totowa, NJ, 2006.
- [10] L.V. da Silva, N.D. dos Santos, A.K.A. de Almeida, D.D.E.R. dos Santos, A.C.F. Santos, M.C. França, D.J.P. Lima, P.R. Lima, M.O.F. Goulart, A new electrochemical sensor based on oxidized capsaicin/multi-walled carbon nanotubes/glassy carbon electrode for the quantification of dopamine, epinephrine, and xanthurenic, ascorbic and uric acids, *J. Electroanal. Chem.* 881 (2021) 114919. <https://doi.org/10.1016/j.jelechem.2020.114919>.
- [11] F. Meloni, K. Spsychalska, D. Zając, M.I. Pilo, A. Zucca, J. Cabaj, Application of a Thiadiazole-derivative in a Tyrosinase-based Amperometric Biosensor for Epinephrine Detection, *Electroanalysis.* 33 (2021) 1639–1645. <https://doi.org/10.1002/elan.202060610>.
- [12] H. Kang, Y. Jin, Q. Han, Electrochemical Detection of Epinephrine Using an L-Glutamic Acid Functionalized Graphene Modified Electrode, *Anal. Lett.* 47 (2014) 1552–1563. <https://doi.org/10.1080/00032719.2013.876541>.



- [13] H. Zhang, Studies of the electrochemical behavior of epinephrine at a homocysteine self-assembled electrode, *Talanta*. 56 (2002) 1081–1088. [https://doi.org/10.1016/S0039-9140\(01\)00642-7](https://doi.org/10.1016/S0039-9140(01)00642-7).
- [14] H. Beitollahi, M.M. Ardakani, B. Ganjipour, H. Naeimi, Novel 2,2'-[1,2-ethanediylbis(nitriloethylidyne)]-bis-hydroquinone double-wall carbon nanotube paste electrode for simultaneous determination of epinephrine, uric acid and folic acid, *Biosens. Bioelectron.* 24 (2008) 362–368. <https://doi.org/10.1016/j.bios.2008.04.009>.
- [15] M.D. Hawley, S. V Tatawawadi, S. Piekarski, R.N. Adams, Electrochemical studies of the oxidation pathways of catecholamines., *J. Am. Chem. Soc.* 89 (1967) 447–450. <http://www.ncbi.nlm.nih.gov/pubmed/6031636>.
- [16] A.G. Ramu, A. Umar, A.A. Ibrahim, H. Algadi, Y.S.A. Ibrahim, Y. Wang, M.M. Hanafiah, P. Shanmugam, D. Choi, Synthesis of porous 2D layered nickel oxide-reduced graphene oxide (NiO-rGO) hybrid composite for the efficient electrochemical detection of epinephrine in biological fluid, *Environ. Res.* 200 (2021) 111366. <https://doi.org/10.1016/j.envres.2021.111366>.
- [17] K. Chetankumar, B.E. Kumara Swamy, S.C. Sharma, Safranin amplified carbon paste electrode sensor for analysis of paracetamol and epinephrine in presence of folic acid and ascorbic acid, *Microchem. J.* 160 (2021) 105729. <https://doi.org/10.1016/j.microc.2020.105729>.
- [18] K. Chetankumar, B.E.K. Swamy, H.S.B. Naik, MgO and MWCNTs amplified electrochemical sensor for guanine, adenine and epinephrine, *Mater. Chem. Phys.* 267 (2021) 124610. <https://doi.org/10.1016/j.matchemphys.2021.124610>.

- [19] C. Wu, J. Li, X. Liu, H. Zhang, R. Li, G. Wang, Z. Wang, Q. Li, E. Shangguan, Simultaneous voltammetric determination of epinephrine and acetaminophen using a highly sensitive CoAl-OOH/reduced graphene oxide sensor in pharmaceutical samples and biological fluids, *Mater. Sci. Eng. C.* 119 (2021) 111557. <https://doi.org/10.1016/j.msec.2020.111557>.
- [20] P. Thondaiman, R. Manikandan, C.J. Raj, A.D. Savariraj, S.E. Moulton, B.C. Kim, Boron and nitrogen doped graphene quantum dots on a surface modified Cu mesh for the determination of dopamine and epinephrine, *Synth. Met.* 278 (2021) 116831. <https://doi.org/10.1016/j.synthmet.2021.116831>.
- [21] C. Erkmen, Y. Demir, S. Kurbanoglu, B. Uslu, Multi-Purpose electrochemical tyrosinase nanobiosensor based on poly (3,4 ethylenedioxythiophene) nanoparticles decorated graphene quantum dots: Applications to hormone drugs analyses and inhibition studies, *Sensors Actuators B Chem.* 343 (2021) 130164. <https://doi.org/10.1016/j.snb.2021.130164>.
- [22] D. Brondani, C.W. Scheeren, J. Dupont, I.C. Vieira, Biosensor based on platinum nanoparticles dispersed in ionic liquid and laccase for determination of adrenaline, *Sensors Actuators, B Chem.* 140 (2009) 252–259. <https://doi.org/10.1016/j.snb.2009.04.037>.
- [23] R.N. Goyal, S. Bishnoi, Simultaneous determination of epinephrine and norepinephrine in human blood plasma and urine samples using nanotubes modified edge plane pyrolytic graphite electrode, *Talanta.* 84 (2011) 78–83. <https://doi.org/10.1016/j.talanta.2010.12.034>.
- [24] S. Saghiri, M. Ebrahimi, M.R. Bozorgmehr, NiO nanoparticle / 1-hexyl-3-methylimidazolium hexafluorophosphate composite for amplification of
- 358

epinephrine electrochemical sensor, *Asian J. Nanosci.* 4 (2021) 46–52.  
<https://doi.org/10.26655/AJNANOMAT.2021.1.4>.

[25] P. Solich, C.K. Polydorou, M.A. Koupparis, C.E. Efstathiou, Automated flow-injection spectrophotometric determination of catecholamines (epinephrine and isoproterenol) in pharmaceutical formulations based on ferrous complex formation, *J. Pharm. Biomed. Anal.* 22 (2000) 781–789.  
[https://doi.org/10.1016/S0731-7085\(00\)00291-0](https://doi.org/10.1016/S0731-7085(00)00291-0).

[26] C. Wang, Q. Han, P. Liu, G. Zhang, L. Song, X. Zou, Y. Fu, A Superstable Luminescent Lanthanide Metal Organic Gel Utilized in an Electrochemiluminescence Sensor for Epinephrine Detection with a Narrow Potential Sweep Range, *ACS Sensors.* 6 (2021) 252–258.  
<https://doi.org/10.1021/acssensors.0c02272>.

[27] M. Hischke, G. Arroyo, R.F. Reiser, J. Rosecrance, A Comparison of Sensor Placement for Estimating Trunk Postures in Manual Material Handling, in: *Adv. Intell. Syst. Comput.*, 2019: pp. 85–99. [https://doi.org/10.1007/978-3-319-96089-0\\_9](https://doi.org/10.1007/978-3-319-96089-0_9).

[28] X. Liu, D. Ye, L. Luo, Y. Ding, Y. Wang, Y. Chu, Highly sensitive determination of epinephrine by a MnO<sub>2</sub>/Nafion modified glassy carbon electrode, *J. Electroanal. Chem.* 665 (2012) 1–5.  
<https://doi.org/10.1016/j.jelechem.2011.06.030>.

[29] P.S. Dorraji, F. Jalali, Novel sensitive electrochemical sensor for simultaneous determination of epinephrine and uric acid by using a nanocomposite of MWCNTs-chitosan and gold nanoparticles attached to thioglycolic acid, *Sensors Actuators, B Chem.* 200 (2014) 251–258.  
<https://doi.org/10.1016/j.snb.2014.04.036>.

- [30] E. Wierzbicka, M. Szultka-Młyńska, B. Buszewski, G.D. Sulka, Epinephrine sensing at nanostructured Au electrode and determination its oxidative metabolism, *Sensors Actuators B Chem.* 237 (2016) 206–215. <https://doi.org/10.1016/j.snb.2016.06.073>.
- [31] S. Chen, M. Shi, Q. Xu, J. Xu, X. Duan, Y. Gao, L. Lu, F. Gao, X. Wang, Y. Yu, Ti<sub>3</sub>C<sub>2</sub>T<sub>x</sub> MXene/nitrogen-doped reduced graphene oxide composite: a high-performance electrochemical sensing platform for adrenaline detection, *Nanotechnology.* 32 (2021) 265501. <https://doi.org/10.1088/1361-6528/abef94>.
- [32] S. Pradhan, M. Bhattacharyya Banerjee, S. Biswas, N. Aliya Hamizi, D.K. Das, R. Bhar, R. Bandyopadhyay, P. Pramanik, An Efficient Simultaneous Electrochemical Detection of Nanomolar Epinephrine and Uric Acid using Low Temperature Synthesized Nano-sized Copper Telluride, *Electroanalysis.* 33 (2021) 383–392. <https://doi.org/10.1002/elan.202060283>.
- [33] M.M. Charithra, J.G. Manjunatha, Electrochemical sensing of adrenaline using surface modified carbon nanotube paste electrode, *Mater. Chem. Phys.* 262 (2021) 124293. <https://doi.org/10.1016/j.matchemphys.2021.124293>.
- [34] R. Sadhana, P. Abraham, A. Vidyadharan, Solar Exfoliated Graphene Oxide: A Platform for Electrochemical Sensing of Epinephrine, *Curr. Anal. Chem.* 16 (2020) 393–403. <https://doi.org/10.2174/1573411015666190104110928>.
- [35] S. Zheng, Preparation of Eosin Y/Graphene Oxide Modified Glassy Carbon Electrode as a Sensing Platform for Dopamine and Epinephrine Detection, *Int. J. Electrochem. Sci.* 15 (2020) 3681–3693. <https://doi.org/10.20964/2020.05.27>.
- [36] R. Sainz, M. del Pozo, M. Vilas-Varela, J. Castro-Esteban, M. Pérez Corral, L. Vázquez, E. Blanco, D. Peña, J.A. Martín-Gago, G.J. Ellis, M.D. Petit-360

Domínguez, C. Quintana, E. Casero, Chemically synthesized chevron-like graphene nanoribbons for electrochemical sensors development: determination of epinephrine, *Sci. Rep.* 10 (2020) 14614. <https://doi.org/10.1038/s41598-020-71554-1>.

[37] Q. Wang, H. Si, L. Zhang, L. Li, X. Wang, S. Wang, A fast and facile electrochemical method for the simultaneous detection of epinephrine, uric acid and folic acid based on ZrO<sub>2</sub>/ZnO nanocomposites as sensing material, *Anal. Chim. Acta.* 1104 (2020) 69–77. <https://doi.org/10.1016/j.aca.2020.01.012>.

[38] C. Li, Y. Zhang, C. Li, Q. Wan, Q. Ke, N. Yang, Tailoring the CeO<sub>2</sub> morphology and its electrochemical reactivity for highly sensitive and selective determination of dopamine and epinephrine, *Microchim. Acta.* 187 (2020) 143. <https://doi.org/10.1007/s00604-019-4100-7>.

[39] A. Dehdashti, A. Babaei, Designing and characterization of a novel sensing platform based on Pt doped NiO/MWCNTs nanocomposite for enhanced electrochemical determination of epinephrine and tramadol simultaneously, *J. Electroanal. Chem.* 862 (2020) 113949. <https://doi.org/10.1016/j.jelechem.2020.113949>.

[40] Y. Luo, Y. Zhang, L. Lu, H. Luo, A flexible CVD graphene platform electrode modified with L-aspartic acid for the simultaneous determination of acetaminophen, epinephrine and tyrosine, *J. Electroanal. Chem.* 856 (2020) 113737. <https://doi.org/10.1016/j.jelechem.2019.113737>.

[41] T. A. Ahmed, Stripping voltammetric determination of Epinephrine applying sulfacetamide modified glassy carbon electrode, *Int. J. Electrochem. Sci.* 15 (2020) 3143–3156. <https://doi.org/10.20964/2020.04.38>.

- [42] X.-H. Zhang, S.-F. Wang, DIFFERENTIAL PULSE ADSORPTIVE STRIPPING VOLTAMMETRY DETERMINATION OF EPINEPHRINE WITH  $\beta$ -MERCAPTOETHANOL SELF-ASSEMBLED MONOLAYERS MODIFIED ELECTRODE, *Anal. Lett.* 35 (2002) 995–1006. <https://doi.org/10.1081/AL-120004551>.
- [43] V. Carrera, E. Sabater, E. Vilanova, M.A. Sogorb, A simple and rapid HPLC–MS method for the simultaneous determination of epinephrine, norepinephrine, dopamine and 5-hydroxytryptamine: Application to the secretion of bovine chromaffin cell cultures, *J. Chromatogr. B.* 847 (2007) 88–94. <https://doi.org/10.1016/j.jchromb.2006.09.032>.
- [44] Y. Zhao, S. Zhao, J. Huang, F. Ye, Quantum dot-enhanced chemiluminescence detection for simultaneous determination of dopamine and epinephrine by capillary electrophoresis, *Talanta.* 85 (2011) 2650–2654. <https://doi.org/10.1016/j.talanta.2011.08.032>.
- [45] W.K. Adeniyi, A.R. Wright, Novel fluorimetric assay of trace analysis of epinephrine in human serum, *Spectrochim. Acta Part A Mol. Biomol. Spectrosc.* 74 (2009) 1001–1004. <https://doi.org/10.1016/j.saa.2009.09.028>.
- [46] H.P. Rang, M.M. Dale, J.M. Ritter, R.J. Flower, G. Henderson, Rang and Dale's Pharmacology, 9th Editio, Elsevier, New York, NY, US, 2020.
- [47] T.H. Svensson,  $\alpha$ -Adrenoceptor modulation hypothesis of antipsychotic atypicality, *Prog. Neuro-Psychopharmacology Biol. Psychiatry.* 27 (2003) 1145–1158. <https://doi.org/10.1016/j.pnpbp.2003.09.009>.
- [48] R.P. Bacil, P.H.M. Garcia, W.R. de Araujo, S.H.P. Serrano, Mechanism and kinetics of olanzapine and quetiapine oxidations at glassy carbon electrode,

Electrochim. Acta. 368 (2020) 137683.

<https://doi.org/10.1016/j.electacta.2020.137683>.

[49] R.G. Bates, J.B. Macaskill, Standard Potential of the Silver-Silver Chloride Electrode, *Pure Appl. Chem.* 50 (1978) 1701–1706.

<https://doi.org/10.1351/pac197850111701>.

[50] R.P. Bacil, E.A. de O. Marcondes Filho, K. de A. Dias, M.C. Portes, W.R. de Araujo, D. Oliveira-Silva, A.A. dos Santos, S.H.P. Serrano, The chemical interaction between the neurotransmitter dopamine and the antipsychotic drugs olanzapine and quetiapine, *J. Electroanal. Chem.* 881 (2021) 114946.

<https://doi.org/10.1016/j.jelechem.2020.114946>.

[51] I. Streeter, S.F. Jenkinson, G.W.J. Fleet, R.G. Compton, Chemical instability promotes apparent electrochemical irreversibility: Studies on the electrode kinetics of the one electron reduction of the 2,6-diphenylpyrylium cation in acetonitrile solution, *J. Electroanal. Chem.* 600 (2007) 285–293.

<https://doi.org/10.1016/j.jelechem.2006.10.006>.

[52] R.P. Bacil, L. Chen, S.H.P. Serrano, R.G. Compton, Dopamine oxidation at gold electrodes: Mechanism and kinetics near neutral pH, *Phys. Chem. Chem. Phys.* 22 (2020) 607–614. <https://doi.org/10.1039/c9cp05527d>.

[53] H.L. Le Chatelier, A General Statement of the Law of Chemical Equilibrium, *Comptes Rendus.* 99 (1884) 786–789.

[54] J.-M. Savéant, C. Costentin, *Elements of Molecular and Biomolecular Electrochemistry: An Electrochemical Approach to Electron Transfer Chemistry*, 2nd editio, Wiley, 2019. <https://www.wiley.com/en-br/Elements+of+Molecular+and+Biomolecular+Electrochemistry%3A+An+Electr>

ochemical+Approach+to+Electron+Transfer+Chemistry%2C+2nd+Edition-p-9781119292333.

[55] S. Arrhenius, Über die Dissociationswärme und den Einfluss der Temperatur auf den Dissociationsgrad der Elektrolyte, Zeitschrift Für Phys. Chemie. 4U (1889). <https://doi.org/10.1515/zpch-1889-0408>.

[56] R. Guidelli, R.G. Compton, J.M. Feliu, E. Gileadi, J. Lipkowski, W. Schmickler, S. Trasatti, Defining the transfer coefficient in electrochemistry: An assessment (IUPAC Technical Report), Pure Appl. Chem. 86 (2014) 245–258. <https://doi.org/10.1515/pac-2014-5026>.

[57] R.A. Marcus, On the Theory of Electron-Transfer Reactions. VI. Unified Treatment for Homogeneous and Electrode Reactions, J. Chem. Phys. 43 (1965) 679–701. <https://doi.org/10.1063/1.1696792>.

[58] C.E. Banks, R.G. Compton, Understanding Voltammetry, 3rd Ed., World Scientific Press Company, 2018.

[59] D. Pavia, G. Lampman, G. Kriz, J. Vyvyan, Introduction to spectroscopy, 4th editio, BOOKS/ COLE CENGAGE Learning, Washington D.C., 2008. <http://books.google.com/books?hl=en&lr=&id=uX0GAAAAQBAJ&oi=fnd&pg=PR5&dq=Introduction+to+Spectroscopy&ots=loT7cSdq1R&sig=vF04fja6tJBBTB MGNnNI66jwiRM>.

[60] M.B.M.Y. Ang, Y.L. Ji, S.H. Huang, K.R. Lee, J.Y. Lai, A facile and versatile strategy for fabricating thin-film nanocomposite membranes with polydopamine-piperazine nanoparticles generated in situ, J. Memb. Sci. 579 (2019) 79–89. <https://doi.org/10.1016/j.memsci.2019.02.064>.

[61] I. You, H. Jeon, K. Lee, M. Do, Y.C. Seo, H.A. Lee, H. Lee, Polydopamine coating in organic solvent for material-independent immobilization of water-364



insoluble molecules and avoidance of substrate hydrolysis, *J. Ind. Eng. Chem.*  
46 (2017) 379–385. <https://doi.org/10.1016/j.jiec.2016.11.007>.

## General conclusions

In this work electrochemical techniques were used to show that non-steroidal anti-inflammatory drugs (NSAIDs) such as dipyrrone, are capable to interact with their target, the *cyclooxygenase* enzyme via redox reactions, thus deactivating the Fe (IV) in the enzyme's active site. In addition, some NSAIDs deactivate the enzyme by interacting and changing its structure, resulting in an allosteric regulation. This work also shows that electrochemical techniques can be used to elucidate the occurrence of complex reactions, such as chemical interactions between antipsychotics and neurotransmitters. The results show the occurrence of a chemical interaction between the orto-quinine derivative of dopamine and epinephrine. Additional and more specific biomedical studies are required, as these reactions could better explain the effectiveness variation of antipsychotics, such as quetiapine and olanzapine in distinct patients.

## Perspectives

The present interaction results should be further explored not only into *in vivo* experiments, but also extended to antipsychotic drugs, for instance, to clozapine. The interaction of other catecholamines, such as norepinephrine should also be evaluated with drugs containing a piperazine moiety to further evaluate this chemical interaction. Finally, interactions with different neurotransmitters, like nitrous oxide, should also be evaluated, as it could be a significant breakthrough in psychiatric conditions, as post-traumatic stress disorder and panic syndrome.

## **Abbreviations used by chapter**

### **Chapter 1 - Mechanism of Electro-Oxidation of Metamizole using Cyclic Voltammetry at a Glassy Carbon Electrode**

Non Steroidal Anti-Inflammatory Drug – NSAIDs

Metamizole/ dipyrone - (MTM)

4-methyl-aminoantipyrine - (MAA)

Britton Robinson Buffer - (BRB)

Dimethylformamide (DMF)

Cyclooxygenase-2 enzyme (COX)

4-formyl-amino-antipyrine (FAA)

4-amino-antipyrine (4AA)

4-acetyl-amino-antipyrine (AAA)

High pressure liquid chromatography (HPLC)

Flow injection analysis (FIA)

Cyclic voltammetry (CV)

Glassy carbon electrode (GCE)

Electrochemical anodic process (Eap)

Electrochemical cathodic process (Ecp)

Differential Pulse voltammetry (DPV)

Electrochemical process from hydrolysis product (Ehp)

## **Chapter 2 - Electrochemical behaviour of dipyrone (metamizole) and others pyrazolones**

dipyrone (MTM)

antipyrine (AA)

4-aminoantipyrine (4AA)

4-methyl-aminoantipyrine (MAA)

4-dimethyl-aminoantipyrine (DMAA)

Electrochemical anodic process (Eap)

Electrochemical cathodic process (Ecp)

4-amino-2,3-dimethyl-1-phenyl-3-pyrazol-5-one (FAA)

4-dimethylamino-1,5-dimethyl-2-phenylpyrazol-3-one (AAA)

High performance liquid chromatography (HPLC)

Flow injection analysis (FIA)

Nuclear magnetic resonance – (NMR)

Gas chromatography - (GC)

Cyclic voltammetry (CV)

Phosphate buffer solution – (PBS)

Dimethylformamide (DMF)

Tetrabutylammonium tetrafluoroborate – (TFBTBA)

Peak width at half height - ( $w_{1/2}$ )

Differential Pulse voltammetry (DPV)

Square wave voltammetry (SWV)

electrochemical-chemical (EC) mechanism

electrochemical-chemical dimerization (EC<sub>2</sub>) mechanism

**Chapter 3 - Electrochemical oxidation of dipyrone and pyrazolone derivatives complexes with Fe (III), and its EC' mechanism.**

Electrochemical-chemical catalytic (EC') mechanism

Dipyrone (MTM)

Antipyrine (AA)

4-aminoantipyrine (4AA)

4-methyl-aminoantipyrine (MAA)

4-dimethyl-aminoantipyrine (DMAA)

Electrochemical anodic process (Eap)

Electrochemical cathodic process (Ecp)

High performance liquid chromatography (HPLC)

Flow injection analysis (FIA)

Cyclic voltammetry (CV)

**Chapter 4 - Electrochemical Cyclooxygenase biosensor to evaluate target  
– drug viability and interactions.**

Non-steroidal-anti-inflammatory drugs (NSAIDs)

Cyclooxygenase-2 enzyme (COX)

Electron paramagnetic resonance (EPR)

Deoxyribonucleic acid (DNA)

arachidonic acid (AA)

prostaglandins (PG)

Tyrosine (Tyr)

Hematin (Htin)

Prostaglandin G2 (PGG2)

Phosphate buffer solution – (PBS)

Salicylic Acid (AS)

Acetylsalicylic Acid (ASA)

Acetaminophen (APAP)

Ibuprofen (IBU)

Naproxen (NPX)

4-methyl-aminoantipyrine (MAA)

Cyclic voltammetry (CV)

Differential Pulse voltammetry (DPV)

Square wave voltammetry (SWV)

Tyrosine (Tyr)

**Chapter 5 - Mechanism and kinetics of olanzapine and quetiapine oxidations at glassy carbon electrode.**

Dopamine (DA)

electrochemical-chemical (EC) mechanism

electrochemical-chemical catalytical (EC') mechanism

Olanzapine (OLZP)

Quetiapine (QTP)

World Health Organization (WHO)

High performance liquid chromatography HPLC

Hepatic cytochrome enzymes (CYP 450)

Phosphate buffer solution – (PBS)

Cyclic voltammetry (CV)

Glassy carbon electrode GCE

Charge transfer coefficient ( $\beta$ )

Diffusion coefficient ( $D_0$ )

Proton coupled electron transfer (PCET)

High performance liquid chromatography hyphenated with a mass spectrometry

HPLC-MS

dimensionless parameter ( $\lambda$ )

chemical rate ( $k_f$ )

heterogeneous standard rate constant ( $k_0$ )

## Chapter 6 - Dopamine oxidation at gold electrodes: mechanism and kinetics near neutral pH

Dopamine (DA)

electrochemical-chemical-electrochemical (ECE) mechanism

cyclic voltammograms (CV)

gold macroelectrode (GE)

Phosphate buffer solution – (PBS)

$E_f^0$  is the formal potential

apparent number of electrons – ( $n_{app}$ )

dimensionless parameter ( $\lambda$ )

equilibrium constant (K)

homogeneous rate kinetics constant of the forward reaction  $k_f$

homogeneous rate kinetics constant of the inverse reaction  $k_b$

heterogeneous standard rate constant ( $k_0$ )

Charge transfer coefficient ( $\beta$ )



## **Chapter 7 - New insights on the electrochemical mechanism of epinephrine on glassy carbon electrode.**

Epinephrine (Epi)

Electrochemical-chemical-electrochemical (ECE) mechanism

Cyclic voltammetry (CV)

Multi-walled carbon nanotubes (MWCNT)

Zinc oxide/ multi-walled carbon nanotubes nano composites (ZnO/ MWCNT)

Metal-Organic-Frameworks (MOF)

Square wave voltammograms (SWV)

Homogeneous rate kinetics constant of the forward reaction  $k_f$

Phosphate buffer solution – (PBS)

Charge transfer coefficient ( $\beta$ )

proton-coupled electron processes (PCEP)

**Chapter 8 - The chemical interaction between the neurotransmitter dopamine and the antipsychotic drugs olanzapine and quetiapine.**

Electron paramagnetic resonance (EPR)

Dopamine DA

piperazine-N,N'-bis(2-ethanesulfonic acid) PIPES

Olanzapine (OLZP)

Quetiapine (QTP)

Molecularly imprinted polymers (MIPs)

Nuclear paramagnetic resonance (NMR)

Glassy carbon electrode (GCE)

Formal potential ( $E^0_f$ )

Reorganization energy ( $\lambda$ )

Piperazine (PPZ)

Polydopamine (PDA)

Catechol (CAT)

Differential pulse voltammetry (DPV)

Kinetic rate constant (k)

## **Chapter 9 - A reaction between neurotransmitter epinephrine and antipsychotics drugs olanzapine and quetiapine at physiological pH.**

Epinephrine (Epi)

Square wave voltammetry (SWV)

High performance liquid chromatography (HPLC)

Flow injection analysis (FIA)

Proton coupled electron transfer (PCET)

Olanzapine (OLZP)

Quetiapine (QTP)

Cyclic voltammetry (CV)

Phosphate buffer solution (PBS)

Epinephrine's electrochemical process I (E I)

Epinephrine's electrochemical process II (E II)

Epinephrine's electrochemical process III (E III)

Epinephrine's electrochemical process IV (E IV)

Olanzapine's electrochemical process I (O I)

Olanzapine's electrochemical process II (O II)

Olanzapine's electrochemical process III (O III)

Olanzapine's electrochemical process IV (O IV)

Quetiapine's electrochemical process III (Q III)

Quetiapine's electrochemical process IV (Q IV)

Electrochemical-Chemical-Electrochemical mechanism (ECE mechanism)

Charge transfer coefficient ( $\beta$ )

Reorganization energy ( $\lambda$ )

Variation of the activation Gibbs energy ( $\Delta G$ )

## List of figures and schemes captions by chapter

### Chapter 1 - Mechanism of Electro-Oxidation of Metamizole using Cyclic Voltammetry at a Glassy Carbon Electrode

Figure 1. Cyclic Voltammograms obtained at GCE in solution  $1.0 \text{ mmol L}^{-1}$  of MTM in DMF with  $0.1 \text{ mol L}^{-1}$  of TT and  $100 \text{ mVs}^{-1}$ . Experimental Conditions: **1A**.  $E_i = 0.1 \text{ V}$ ;  $E_\lambda = 1.4 \text{ V}$ ;  $E_f = 0.1 \text{ V}$  and **1B**.  $E_i = 0.1 \text{ V}$ ;  $E_\lambda = 0.8 \text{ V}$ ;  $E_f = 0.1 \text{ V}$ .

Figure 2. Current Function ( $I_p / C \times v^{1/2}$ ) versus. Plots obtained from cyclic voltammograms performed with a GCE in a DMF containing  $1.0 \text{ mmol L}^{-1}$  of MTM and  $0.10 \text{ mol L}^{-1}$  of TT. Curve Equations:  $I_{pa1} / C \times v^{1/2} = 413.5 - 4.79 v$ ;  $I_{pa2} / C \times v^{1/2} = 282.5 - 3.98 v$ ;  $I_{pa3} / C \times v^{1/2} = -11.7 \times 521.9 e^{(-x/0.184)} v$ .

Figure 3. Cyclic voltammograms obtained in a solution of  $1.0 \text{ mmol L}^{-1}$  of MTM in BR solution using GCE. Experimental conditions:  $v = 100 \text{ mV s}^{-1}$ . **3A**.  $E_i = 0.0 \text{ V}$ ;  $E_\lambda = 1.0 \text{ V}$ ;  $E_f = 0.0 \text{ V}$ , pH 4.0. **3B**.  $E_i = 0.1 \text{ V}$ ;  $E_\lambda = 0.8 \text{ V}$ ;  $E_f = 0.1 \text{ V}$ , pH 4.0; **3C**.  $E_i = 0.1 \text{ V}$ ;  $E_\lambda = 0.8 \text{ V}$ ;  $E_f = 0.1 \text{ V}$ , pH 8.0; **3D**. Ehp vs pH curve, constructed using the results obtained from cyclic voltammograms performed with a GCE in a solution containing  $1.0 \text{ mmol L}^{-1}$  of MTM in BR solutions; Ehp vs pH plot (Ehp =  $584 - 38\text{pH}$ ).

Figure 4. (a) Cyclic Voltammograms obtained in a solution  $1.0 \text{ mmol L}^{-1}$  of MTM in BR solution, pH 8.0 using GCE. (MTM solution aged for two weeks); Experimental Conditions:  $v = 100 \text{ mV s}^{-1}$ .  $E_i = 0.1 \text{ V}$ ;  $E_\lambda = 1.3 \text{ V}$ ;  $E_f = 0.1 \text{ V}$  and (b) Differential pulse voltammograms obtained in  $1.0 \text{ mmol L}^{-1}$  MAA (MTM solution aged for one month) at BR buffer pH 2.1 ( $-\square-$ ); 4.0 ( $--$ ); 8.0 ( $-\Delta-$ ); and

10 (-\*-). Experimental Conditions: potential range of 0.0 V to + 0.7 V;  $\nu = 5.0 \text{ mV s}^{-1}$ , pulse amplitude = 25 mV and pulse width = 50 ms. Taking in account the presented results, an electro-oxidation mechanism, in which both products have the same electroactive groups, was proposed, Schemes 1a and 1b.

Scheme 1a. Proposition for MTM electro-oxidation mechanism in DMF.<sup>26,27</sup>

Scheme 1b. Proposition for MTM hydrolysis step to produce MAA and MAA electro-oxidation mechanism in BR buffer media.<sup>26,27</sup>

## Chapter 2 - Electrochemical behaviour of dipyrone (metamizole) and others pyrazolones

Scheme 1. The MTM hydrolysis and its generated products.

Scheme 2. Structure of the pyrazolones studied in this work.

Figure 1. Cyclic voltammograms obtained with GCE in 0.1M PBS, pH = 7.4, containing 1mM of each of the compounds: AA (A); 4AA (B); MAA (C); DMAA (D); MTM (E).

Figure 2. Pourbaix diagrams:  $E_{ap0}$  from MAA (red line) and 4AA (black line).

Figure 3. Differential pulse voltammograms obtained with GCE in 0.1 mol L<sup>-1</sup> PBS, pH 7.4, containing 1.0 mmol L<sup>-1</sup> of AA (**A**); 4AA (**B**); MAA (**C**); DMAA (**D**) and MTM (**E**). The peak width at half height values ( $w_{1/2}$ ) were obtained after the voltammogram deconvolution processes (colored lines).

Figure 4. Differential pulse voltammograms obtained with GCE in DMF containing 0.1 M of TFBTBA and 1.0 mmol L<sup>-1</sup> of A) AA; B) 4AA; C) MAA; D) DMAA; E) MTM. Deconvolution processes were performed, when necessary, to obtain the values of  $w_{1/2}$ . Experimental data are shown as black lines while deconvolutions are displayed as colored lines.

Figure 5: Square wave voltammograms (SWV) obtained with GCE in 0.1 M PBS, pH = 7.4, containing 1.0 mM of each of the compounds: (A) AA; (B) 4AA; (C) MAA; (D) DMAA; (E) MTM. (1) Total current; (2) forward current; (3) backward current.

Figure 6: Cyclic voltammograms obtained with GCE in DMF containing 0.1 mol L<sup>-1</sup> of TFBTBA and 1.0 mmol L<sup>-1</sup> of MTM: (A) 10 mV s<sup>-1</sup> (1); 50 mV s<sup>-1</sup> (2); 100 mV s<sup>-1</sup> (3); 500 mV s<sup>-1</sup> (4) and 1000 mV s<sup>-1</sup> (5); (B)  $E_0 = 0.0$  V;  $E_\lambda = 1.4$  V;  $E_f = 0.0$  V and 10 mV s<sup>-1</sup> (1); 50 mV s<sup>-1</sup> (2); 100 mV s<sup>-1</sup> (3); 500 mV s<sup>-1</sup> (4) and 1000 mV s<sup>-1</sup> (5);  $E_0 = 0.0$  V;  $E_\lambda = 0.7$  V;  $E_f = 0.0$  V .

Figure 7:  $i_{ap1} / i_{cp}$  ratio as a function of scan rate ( $\nu$ ). Applied potential window restricted to the interval in which only the first electrochemical process occurs.

Figure 8:  $E_{ap1}$  vs  $\log \nu$  plot obtained in DMF containing 0.1 mol L<sup>-1</sup> TFBTBA and 1.0 mmol L<sup>-1</sup> MTM. ( $E_{p1} = 0.030 \log \nu + 0.495$ ,  $R^2 = 0.975$ ).

Scheme 3. Schematic representation of the possible reaction pathways after the  $E_{ap1}$  process.

Scheme 4. Electrochemical oxidation mechanism proposed for dipyrone and antipyrine molecules.

Figure 9: DMAA and MTM analytical curves obtained in PBS pH 7.4 (black line) and DMF containing 0.1 mol L<sup>-1</sup> of TFBTBA (red line), respectively. DMAA solutions in PB, pH = 7.4. Data obtained from square wave voltammograms in 10–100  $\mu\text{mol L}^{-1}$  range (average of five measurements).

$i_{p(\text{DMAA})}/\mu\text{A} = 0.96[\text{DMAA}]\mu\text{M} - 0.45$  ( $R^2 = 0.998$ ) and  $i_{p(\text{MTM})}/\mu\text{A} = 0.92[\text{MTM}]\mu\text{M} - 0.59$  ( $R^2 = 0.998$ ).

## **Appendix 2 - Electrochemical behaviour of dipyrone (metamizole) and others pyrazolones – Supplementary material**

Figure S1. Chromatograms obtained in MeOH 55/ PB 45 (V/V),  $\text{pH}_{\text{apparent}} = 2.5$ , containing  $1.0 \text{ m molL}^{-1}$  of (-) MTM, (-) 4AA and (-) AA individual solutions (A) and

(-) MTM, (-) MAA and (-) MTM, after 10 minutes (B).

Figure S2A. H1 NMR Spectrum vs  $\text{CDCl}_3$  at 500 MHz, obtained in MAA, extracted with  $\text{CHCl}_3$ , from 1.0 mM of MTM aging solutions.

Figure S2B. C13 NMR Spectrum vs  $\text{CDCl}_3$  at 500 MHz, obtained in MAA, extracted with  $\text{CHCl}_3$ , from 1.0 mM of MTM aging solutions.

Figure S3: UV-VIS Spectra obtained from solutions containing  $50.0 \text{ } \mu\text{mol L}^{-1}$  of MTM (Inset), MAA ( -.-.), 4AA, ( - - -) and AA (...) in PBS  $\text{pH} = 7.4$ .



### **Chapter 3 - Electrochemical oxidation of dipyrone and pyrazolone derivatives complexes with Fe (III), and its EC' mechanism.**

Scheme 1: Electrochemical oxidation mechanism of the antipyrines and MTM's hydrolysis reaction. [6]

Figure 1: UV-Vis spectra as a function of the iron (III) addition for: A) AA, B) 4AA, C) DMAA and D) MTM

Figure 2: Raman spectra from crystal and solutions of A) AA and AA + Fe (III), B) 4AA and 4AA + Fe (III), C) DMAA and DMAA + Fe (III) and D) MTM and MTM + Fe (III).

Scheme 2: Proposition of the structures of the complexes formed between the phenazones and iron III.

Figure 3: CV of A) 1.0 mM AA B) 1.0 mM AA + Fe (III) C) 1.0 mM 4AA D) 1.0 mM AA + Fe (III) E) 1.0 mM DMAA F) 1.0 mM AA + Fe (III) G) 1.0 mM MTM H) 1.0 mM AA + Fe (III) in solutions of 0.1 M HCl.

Figure 4: Randles Sevcik theoretical predictions compared to the experimental peak current values obtained to the processes A)  $E_{ap3}$  of AA, B)  $E_{ap0}$  of 4AA, C)  $E_{ap1}$  of DMAA, D) combined values of  $E_{ap0}$  and  $E_{ap1}$  of MTM.

Figure 5: Plots of the charge transfer coefficient ( $\beta$ ) as a function of the applied potential.

Figure 6: A) CV obtained in (1:1) 1.0 mM 4AA with DMAA solutions in 0.1 KCl, pH = 2.0 at different scan rates, B) CV obtained in (1:1:1) 1.0 mM 4AA, DMAA, and Fe (III) solutions in 0.1 KCl, pH = 2.0 at different scan rates C) CV obtained in (1:1) 1.0 mM 4AA with DMAA solutions in 0.1 KCl, pH = 2.0 at different times D) Charge transfer coefficients of the CVs presented in C, E) Turnover frequency as a function of the driving force for the systems presented in A and in B, F) Catalytic Tafel plots of the systems presented in A and B G) CV obtained in (1:1) 1.0 mM MTM with Fe (III) solutions in 0.1 KCl, pH = 2.0 at different times H) Tafel Plots from the voltammograms presented in F I) Catalytic Tafel plots of the system presented in G.

**Appendix 3 - Electrochemical oxidation of dipyrone and pyrazolone derivatives complexes with Fe (III), and its EC' catalytic mechanism – Supplementary material**

Figure S1: Complexation of MTM with Iron (III) 1.0 mM (1:1) at different pH values.

Figure S2: Complexation of A) AA; B) 4AA; C) DMAA; D) MTM with Iron (III) 1.0 mM (1:1) at acidic media (pH 2,0).

Figure S3: UV-Vis spectra of  $1.0 \mu\text{ mol L}^{-1}$  of AA in  $0.1 \text{ mol L}^{-1}$  KCl solutions, pH = 2.0 and the subsequent additions of  $\text{Fe (III)}_{(\text{aq.})}$

Figure S4: UV-Vis spectra of  $1.0 \mu\text{ mol L}^{-1}$  of  $\text{Fe (III)}_{(\text{aq.})}$  in  $0.1 \text{ mol L}^{-1}$  KCl solutions, pH = 2.0 and the subsequent additions of AA

Figure S5: UV-Vis spectra of  $0.5 \cdot 10^{-9} \text{ mol L}^{-1}$  of AA in  $0.1 \text{ mol L}^{-1}$  KCl solutions, pH = 2.0 at different times, and the subsequent additions of  $\text{Fe (III)}_{(\text{aq.})}$

Figure S6: UV-Vis spectra of  $1.0 \mu\text{ mol L}^{-1}$  of 4AA in  $0.1 \text{ mol L}^{-1}$  KCl solutions, pH = 2.0 and the subsequent additions of  $\text{Fe (III)}_{(\text{aq.})}$

Figure S7: UV-Vis spectra of  $1.0 \mu\text{ mol L}^{-1}$  of AA in  $0.1 \text{ mol L}^{-1}$  KCl solutions, pH = 2.0 and the subsequent additions of  $\text{Fe (III)}_{(\text{aq.})}$

Figure S8: UV-Vis spectra of  $1.0 \mu\text{ mol L}^{-1}$  of 4AA in  $0.1 \text{ mol L}^{-1}$  KCl solutions, pH = 2.0 and the subsequent additions of  $\text{Fe (III)}_{(\text{aq.})}$

Figure S9: Cronoamperogram of a 1,0 mM AA solution in PBS, pH = 7,4.

Figure S10: Cronoamperogram of a 1,0 mM 4AA solution in PBS, pH = 7,4.

Figure S11: Cronoamperogram of a 1,0 mM DMAA solution in PBS, pH = 7,4.

Figure S12: UV-Vis spectra as a function of the iron (III) addition for a 4AA and DMAA solution.

## **Chapter 4 - Electrochemical Cyclooxygenase biosensor to evaluate target – drug viability and interactions.**

Scheme 1: Schematic representation of the COX enzyme; 1A) the active site of the enzyme and its chemical steps. 1B) the cyclooxygenase and peroxidase reactions of the enzyme to convert the AA into PGH<sub>2</sub>. (Tsai et al., 1995; Tsai and Kulmacz, 2010)

Figure 1: A) CV obtained in GCE-COX at PB 0.1 M, pH 7.4 (1<sup>st</sup> scan GCE-COX – Black, Blank scan – Red); B) DPV obtained in GCE-COX at PB 0.1 M, pH 7.4 (Scan GCE-COX – Black, Blank scan – Red); C) SWV obtained in GCE-COX at PB 0.1 M, pH 7.4 ((1) Backward Current, (2) Forward Current, (3) Total Current), the experimental conditions were presented in the previous section.

Figure 2: DPV obtained in GCE-COX 50 μM Tyr solutions in PB 0.1 M, pH 7.4 A) Without the presence of 5mM H<sub>2</sub>O<sub>2</sub>; B) Within the presence of 5mM H<sub>2</sub>O<sub>2</sub>.

Figure 3: DPV obtained in GCE-COX at several different H<sub>2</sub>O<sub>2</sub> concentrations in PB 0.1 M, pH 7.4 solutions; Figure 4 Inset: *i* versus concentration curve obtained from 4 voltammograms.

Scheme 2: Proposed catalytic electrochemical mechanism of COX.

Figure 4: DPV in GCE-COX at 5.0 mM H<sub>2</sub>O<sub>2</sub> and 50 μmol L<sup>-1</sup> of A) SA, B) ASA, C) APAP, D) MAA, E) IBU, F) NPX, in PB 0.1 M solutions, pH 7.4;. Inset) DPV

was obtained in GCE-COX after a gentle wash in a new 5.0 mM H<sub>2</sub>O<sub>2</sub> solution PB 0.1 M solution, pH 7.4 without the presence of the NSAID.

Figure 5: Plots of the inhibition percentage versus time for some NSAIDs; A) Salicylic Acid (SA); B) Acetyl Salicylic Acid (ASA); C) Acetaminophen (APAP); D) 4-Methyl-Aminoantipyrine (MAA); E) Ibuprofen (IBU); F) Naproxen (NPX)

Figure 6: X-band EPR plots of hematin-induced tyrosyl radicals and their spectra in the presence of NSAIDs.

Figure 7: A) Bar graph of COX inhibitions in % observed for each NSAIDs at DPV, obtained at GCE-COX in 5mM H<sub>2</sub>O<sub>2</sub> at PBS, pH 7.4; B) Bar graph of Htin inhibitions in % observed for each NSAIDs at EPR, obtained at Htin 100 μM and Tyr 100 μM at H<sub>2</sub>O. 50μM and 5μM of drugs were used, respectively.

#### **Appendix 4 – Electrochemical Cyclooxygenase biosensor to evaluate target – drug viability and interactions – Supplementary material**

Figure S1. Detection of COX-2 protein expression by western blotting assay. The protein samples were obtained from C3H/HeJ mice's liver from a control group, whose animals were submitted to a fibrosis-associated hepatocarcinogenesis model.

Figure S2: A) CV obtained in GCE-COX at PB 0.1 M, pH 7.4 (1st scan GCE-COX – Black, Blank scan – Red); B) DPV obtained in GCE-COX at PB 0.1 M, pH 7.4;

C) SWV obtained in GCE-COX at PB 0.1 M, pH 7.4 ((1) Backward Current, (2) Forward Current, (3) Total Current), the experimental conditions were presented in the previous section.

Figure S3: DPV obtained in GCE-COX 50 $\mu$ M Tyr solutions in PB 0.1 M, pH 7.4  
A) Without the presence 5mM H<sub>2</sub>O<sub>2</sub>; B) Within the presence of 5mM H<sub>2</sub>O<sub>2</sub>.

Figure 3: Linear Sweep Voltammetry and the Tafel plots of processes Ecp2 and Ecp3.

Figure 4: DPV obtained in GCE-COX at several different H<sub>2</sub>O<sub>2</sub> concentration in PB 0.1 M, pH 7.4 solutions; Figure 4 Inset:  $-i$  versus concentration curve obtained from 4 voltammograms.

Scheme 2: Proposed catalytic electrochemical mechanism of COX.

## Chapter 5 - Mechanism and kinetics of olanzapine and quetiapine oxidations at glassy carbon electrode.

Scheme 1: Molecular structure of the anti-psychotic drugs olanzapine (OLZP) and quetiapine (QTP).

Figure 1: A) CV obtained with GCE in a solution containing 1.0 mM: (red) OLZP, (dark grey) QTP at a wide potential window of -1.0 to 1.4/ 1.5 V in 0.1 M PBS, pH = 7.4.  $v = 0.1 \text{ V s}^{-1}$ ; B) CV obtained with GCE in a solution containing 1.0 mM: (red) OLZP at a restricted potential -0.1 to 0.6 V in 0.1 M PBS, pH = 7.4.  $v = 1.0 \text{ V s}^{-1}$ ; C) CV obtained with GCE in a solution containing 1.0 mM: (red) OLZP at a restricted potential 0.6 V to 1.4/ 1.5 V in 0.1 M PBS, pH = 7.4.  $v = 1.0 \text{ V s}^{-1}$ ; D) Transfer coefficient ( $\beta$ ) as a function of the applied potential obtained from CV presented in figure 1C.

Figure 2: CV obtained with GCE in solutions containing 1.0 mM A) OLZP, B) QTP in 0.1 M PBS, pH = 7.4, the voltage scan rate was varied from 0.01 to 1.00  $\text{V s}^{-1}$ .

Figure 3: A) CV obtained with GCE in solutions containing 1.0 mM of OLZP in 0.1 M PBS, pH = 7.4, in a restricted window from -0.1 to 0.6 V in various scan rates from 0.01 to 1.00  $\text{V s}^{-1}$ ; B) Peak current ratio (Process I/ Process II) as a function of the logarithm of the scan rate; C) Plot of the OLZP oxidation peak current as a function of the square root of the scan rates, compared to the theoretical plots Randles-Sevcik equations (dark grey – reversible, blue – irreversible), Electrode Area = 0.071  $\text{cm}^2$ ; D) OLZP oxidative peak potentials as a function of pH.

Scheme 2: Illustrative competition between chemical steps that follow up OLZP oxidation I process.



Figure 4: A) Potential peak of OLZP process I as a function of the logarithm of the scan rate.  $E_{p(I)} = 24.5 \cdot 10^{-3} \log v + 0.26$ .  $R^2 = 0.982$  B) Dimensionless parameter ( $\lambda$ ) as a function of the inverse of the scan rate.

Figure 5: Overlapping between experimental and simulated voltammograms of OLZP process I. The simulations were obtained with the parameters presented in tables 3 and 4.

Figure 6: A) Peak current ratios (anodic/cathodic) of the experimental and simulated voltammograms as a function of the scan rates. B) Comparison between the experimental and simulated  $\beta$  values obtained.

Figure 7: A) Plot of the OLZP oxidation peak current of process III as a function of the square root of the scan rates, compared to the theoretical plots using the Randles-Sevcik equation (blue – irreversible ( $\beta = 0.2$ ;  $n = 1$ )); B) Plot of the QTP oxidation peak current of process III as a function of the square root of the scan rates, compared to the theoretical plots obtained by Randles-Sevcik equations (black – irreversible ( $\beta = 0.9$ ;  $n = 1$ , red – irreversible ( $\beta = 0.3$ ,  $n=1$ )) Electrode Area =  $0.071 \text{ cm}^2$ ; C) oxidation peak potentials of process III of OLZP as a function of pH; D) oxidation peak potentials of process III of QTP as a function of pH.

Figure 8: Comparison between the experimental  $\beta$  values of the processes III from OLZP and QTP obtained in the Tafel plots presented in figures S5 and S6.

Scheme 3: Electrochemical oxidation mechanism proposed to OLZP processes I/ II with the follow up chemical processes, III and IV. B) Electrochemical oxidation mechanism proposed to QTP processes III and IV.

**Appendix 5 - Olanzapine and quetiapine oxidation mechanism in glassy carbon electrode at physiological pH – Supplementary material.**

Figure S1: Cronoamperogram at GCE of a solution 1.0mM of OLZP in PBS 0.1M, pH = 7.4,  $E_{app} = 0.25$  V. Insert: Current as a function of the inverse of the square root of the time, in minutes.

Figure S2: Cronoamperogram at GCE of a solution 1.0mM of QTP in PBS 0.1M, pH = 7.4,  $E_{app} = 1.25$  V. Insert: Current as a function of the inverse of the square root of the time, in seconds.

Figure S3: CV presented in figure 3A with the respective Tafel plots as inset. The red parts of the voltammograms show the part of the curve sub-plotted to the Tafel analysis as in the insets. The parameters used in the simulations are presented in table 1.

Figure S4: Simulated CVs presented in figure 9 with the respective Tafel plots as inset. The red parts of the voltammograms show the part of the curve sub-plotted to the Tafel analysis as in the insets.

Figure S5: CV presented in figure 2A with the respective Tafel plots as inset. The red parts of the voltammograms show the part of the curve sub-plotted to the Tafel analysis as in the insets.

Figure S6: CV presented in figure 2B with the respective Tafel plots as inset. The red parts of the voltammograms show the part of the curve sub-plotted to the Tafel analysis as in the insets.

Figure S7: Peak potentials of process IV of QTP as a function of pH.

## **Chapter 6 - Dopamine oxidation at gold electrodes: mechanism and kinetics near neutral pH**

Scheme 1: Schematic representation of the literature dopamine electrochemical oxidation mechanism. <sup>1</sup>

Scheme 2: Schematic representation of the oxidized dopamine cyclization reaction at pH = 7.4. <sup>6</sup>

Figure 1. CVs of DA solutions in PBS 0.1 M, pH = 7.4 at different scan rates: A = 0.02 V s<sup>-1</sup>; B = 0.1 V s<sup>-1</sup>; C = 0.20 V s<sup>-1</sup> and D = 1.00 V s<sup>-1</sup>.

Figure 2. Plot of the dopamine oxidative peak currents as a function of the square root of the scan rates, compared to the theoretical peak currents predicted by the Randles-Sevcik equations for a single step two-electron reversible transfer (-), for a multi-step irreversible (n' = 0; n = 2; β = 0.5) process (-), and for a multi-step irreversible (n' = 1; n = 2; β = 0.5) (-), together with experimental results (▪). Electrode Area = 0.0314 cm<sup>2</sup>, C = 10<sup>-3</sup> mol L<sup>-1</sup>.

Figure 3: Dimensionless parameter λ parameter versus the inverse of the voltage scan rate. Linear regression: λ = 0.0063 ± 0.0008 v<sup>-1</sup> - 0.00873. R<sup>2</sup> = 0.897

Figure 4: CV presented in figure 1 with the respective Tafel plots as inset. The red parts of the voltammograms show the part of the curve sub-plotted to the Tafel analysis as in the inserts.

Figure 5: (-) Simulated CV voltammograms; (-) of DA solutions in PBS 0.1 M, pH = 7.4 at different scan rates: A = 0.02 V s<sup>-1</sup>; B = 0.05 V s<sup>-1</sup>; C = 0.10 V s<sup>-1</sup>; D = 0.20 V s<sup>-1</sup>; E = 0.05 V s<sup>-1</sup> and F = 1.00 V s<sup>-1</sup>.

Figure 6: Peak current ratios (anodic/ cathodic) of the experimental and simulated voltammograms as a function of the scan rate, presented in a logarithm scale.

Figure 7. β values for the A/C processes versus the scan rate.

Scheme 3: Proposed electrochemical oxidation mechanism for dopamine in near-neutral pH.

**Chapter 7 - New insights on the electrochemical mechanism of epinephrine on glassy carbon electrode.**

Scheme 1: Most accepted oxidation mechanism of Epi. [6]

Figure 1: Typical CVs of Epi solutions in 0.1M PBS, pH = 7.4 at different scan rates, from 0.01 to 10.0 V s<sup>-1</sup>.

Figure 2: Typical SWV of Epi solutions in 0.1M PBS, pH = 7.4. A) Swept from -0.6 V to 1.0 V. B) Swept from 1.0 V to -0.6 V.

Figure 3: Plot of the Epi oxidation peak current as a function of the square root of the scan rates, compared to the theoretical plots of Randles-Sevcik equations (Black square – Epi experimental peak current values; blue – reversible,  $n=2$ ; dark gray – Multi-step irreversible  $n'=1$ ,  $n=2$ ,  $\beta=0.5$ ; red – Multi-step irreversible  $n'=0$ ,  $n=2$ ,  $\beta=0.5$ ), Electrode Area =  $0.071 \text{ cm}^2$ ,  $D = 1.03 \times 10^{-5} \text{ cm}^2 \text{ s}^{-1}$ .

Figure 4: Dimensionless parameter ( $\lambda$ ) as a function of the inverse of the scan rate.

Figure 5: Pourbaix diagram (Peak potential values as a function of pH) of Epi at different scan rates A) Process I, B) Process II, C) Process III, D) Process IV.

Scheme 2: Schematic representation of the Epi oxidation behaviour as a function of pH.

Figure 6: Experimental and simulated CVs of Epi. The simulations were obtained with the parameters presented in Tables 1 and 2.

Figure 7: Comparison between the experimental and simulated  $\beta$  values.

Figure 8: A) Diagram of Gibbs energy as a function of the reaction coordinate of the oxidation of Epi. B) Schematic representation of the Gibbs energy as function of the reaction coordinate, illustrating each product and intermediate formed.

Scheme 3: A proposed electrochemical mechanism to Epi's processes I, II, III and IV with the follow-up cyclization.

**Appendix 7 - New insights on the electrochemical mechanism of epinephrine on glassy carbon electrode – Supplementary material**

Figure S1: Cronoamperogram of 1.0 mM of Epi in 0.1 PBS, pH=7.4 and its respective linearization (insert)

Figure S2: Experimental working curve that correlates the apparent number of electrons and the dimensionless parameter  $\lambda$ .

Figure S3: CVs of Epi solutions in 0.1M PBS, pHs = 1.0, 3.0, 4.0, 5.0, 6.0, 7,4 at different scan rates, from 0.01 to 10.0 V s<sup>-1</sup>.

Figure S4: Pourbaix diagrams (Peak potential x pH) of processes A) I; B) II, C) III and D) IV.

## **Chapter 8 - The chemical interaction between the neurotransmitter dopamine and the antipsychotic drugs olanzapine and quetiapine.**

Scheme 1: Chemical structures of Olanzapine (OLZP) and Quetiapine (QTP).

Scheme 2: Schematic representation of the electrochemical redox mechanism of dopamine (DA), leading to neuromelanin. [38,42]

Figure 1: CV obtained using GCE in a solution containing: A) 1.0 mM DA solution (grey); 1.0 mM OLZP solution (blue); 1.0 mM DA and OLZP (red), in 0.1 M PBS,

pH = 7.4, at the scan rate of  $100 \text{ mV s}^{-1}$ . B) 1.0 mM DA solution (grey); 1.0 mM QTP solution (blue); and 1.0 mM DA and QTP (red), in 0.1 M PBS, pH = 7.4, at the scan rate of  $100 \text{ mV s}^{-1}$ .

Figure 2: CV obtained using GCE in a solution containing: A) 1.0 mM DA solution; B) 1.0 mM OLZP solution; C) and D) 1.0 mM DA and OLZP, in 0.1 M PBS, pH = 7.4, at different scan rates.

Figure 3: CV obtained using GCE in a solution containing: A) 1.0 mM DA; B) 1.0 mM QTP; C) and D) 1.0 mM DA and QTP, in 0.1 M PBS, pH = 7.4, at different scan rates.

Figure 4: A) Peak potential of processes I and II of DA (dark grey and red, respectively), DA in the presence of OLZP (blue and green, respectively), and DA in the presence of QTP (purple and dark yellow, respectively) as a function of the scan rate. B) Charge transfer coefficient ( $\ln // dE$ ) as a function of the potential obtained from respective CVs at  $20 \text{ mV s}^{-1}$ ; C) UV-Vis spectra of a 90 nM of DA, 90 nM of OLZP, OLZP in the presence of DA, 90 nM (1:1) after 6 hours and overnight; D) 90 nM of DA, 90 nM of QTP, QTP in the presence of DA, 90 nM (1:1) after 6 hours and overnight; Photo of E) a 10 mM (1:1) DA + PIPES solution after 6 hrs, F) 10 mM solution of DA used as control, G) a 10 mM (1:1) DA + OLZP solution after 6 hours, H) a 10 mM (1:1) DA + QTP solution after 6 hours.

Scheme 3: Mechanism proposition of the chemical reaction between dopamine and the antipsychotic drugs.

Figure 5: A) DPV obtained for the individual solutions of 1.0 mM DA (black line) and 1.0 mM of OLZP (red line) in 0.1 M PBS, pH = 7.4, and for the mixture of 1.0 mM of OLZP and DA solutions, along the time of reaction, with DPV data obtained every 15 min; B) Peak current extracted from DPV data for different time of

reaction; C) Logarithm of the DA oxidation peak current versus time in minutes ( $\ln I_{DA} = -1.5 \cdot 10^{-2} t + 2.2$ ,  $R^2 = 0.99$ )

Figure 6: A) DPVs obtained for individual solutions of 1.0 mM QTP (red line) and 1.0 mM DA (black line) and for the mixture of 1.0 mM QTP+DA along the time of reaction, recording the DPV data every 15 min. B); Peak current extracted from DPV data presented in A along the time of reaction. C) logarithm of DA's oxidation peak current versus time in minutes ( $\ln I_{DA} = -9.0 \cdot 10^{-3} t + 2.07$ ,  $R^2 = 0.99$ )

Figure 7: A) DPVs obtained for the mixture of CAT and PIPES solutions, 1.0 mM, each along the time of reaction, recording the DPV data every 15 min. B); Peak current extracted from DPV data presented in A along the time of reaction. C) logarithm of the DA oxidation peak current versus time in minutes ( $\ln I_{CAT} = -1.7 \cdot 10^{-2} t + 1.3$ ,  $R^2 = 0.87$ )

## **Appendix 8 - The chemical interaction between the neurotransmitter dopamine and the anti-psychotic drugs olanzapine and quetiapine Supplementary material.**

Figure S1:  $^1\text{H}$  NMR (DMSO- $d_6$ , 300 MHz) of OLZP samples obtained after the extraction procedure.

Figure S2:  $^1\text{H}$  NMR ( $\text{CDCl}_3$ , 300 MHz) of QTP samples obtained after the extraction procedure.

Figure S3: EPR spectra of A) DA, PPZ, OLZP and QTP samples; B) DA+ PPZ, DA+OLZP, DA+QTP and PDA samples.



Figure S4: A) DPVs obtained using GCE in a solution containing a mixture of DA solutions, 1.0 mM along the time of reaction, recording the DPV data every 15 min. B); Peak current extracted from DPV data presented in A along the time of reaction. CV

Figure S5: A) DPVs obtained using GCE in a solution containing a mixture of DA and PIPES solutions, 1.0 mM, each along the time of reaction, recording the DPV data every 15 min. B); Peak current extracted from DPV data presented in A along the time of reaction. C) logarithm of the DA oxidation peak current versus time in minutes ( $\ln I_{\text{CAT}} = -2.06 \cdot 10^{-2} t + 1.65$ ,  $R^2 = 0.92$ )

## **Chapter 9 - A reaction between neurotransmitter epinephrine and antipsychotics drugs olanzapine and quetiapine at physiological pH.**

Scheme 1: Schematic representation of the oxidation mechanisms of epinephrine, olanzapine and quetiapine.

Figure 1: CV of 1.0 mM solutions in PBS of A) Epi, B) OLZP, and C) QTP at different scan rates.

Figure 2: CV of 1.0 mM solutions of A) Epi with OLZP, B) Epi with QTP at different scan rates.

Figure 3: A) Peak potential values of process E I in the presence of the drugs as a function of the scan rate. B) Plot of the experimental peak current values of process EI in the presence of the drugs as a function of the square root of the scan rate, compared with the theoretical predictions of the multi-step irreversible Randles-Sevcik equation ( $n'=0$ ;  $n=2$ ,  $\beta=0,5$ ), electrode area =  $0.071 \text{ cm}^2$ ,  $C = 1.0 \cdot 10^{-6} \text{ mol cm}^{-3}$ ,  $D_0=2.5 \cdot 10^{-6} \text{ cm}^2 \text{ s}^{-1}$ .

Figure 4: CV of 1.0 mM solutions of A) Epi with OLZP, B) Epi with QTP at  $0.1 \text{ V s}^{-1}$  and different times.

Figure 5: SWV of 1.0 mM solutions of A and B Epi, C and D Epi with OLZP, and E and F Epi with QTP. A, C and E were obtained by sweeping the potential from negative to positive potentials. B, D and F were obtained by sweeping the potential from positive to negative potentials.

Figure 6: Charge transfer coefficient as a function of potential from the CV of A) Epi with OLZP, B) Epi with QTP at a scan rate of  $0.1 \text{ V s}^{-1}$ .

Figure 7: UV-Vis spectra of solutions 1.0 mM of A) Epi, OLZP and QTP, separately. B) Epi with OLZP, C) Epi with QTP.

Scheme 2: Mechanism proposition of the chemical reaction between epinephrine and the antipsychotic drugs olanzapine and quetiapine.

## Papers in collaboration during the Ph.D. program

Journal of The Electrochemical Society

### Insights toward the Electrochemical Behavior of Hematin Using a Hematin Modified Glassy Carbon Electrode

Rafael M. Buoro<sup>1,2</sup>, Othon S. Campos<sup>1</sup>, Raphael P. Bacil<sup>1</sup> and Sílvia H. P. Serrano<sup>3,1</sup>

Published 8 September 2016 • © 2016 The Electrochemical Society

[Journal of The Electrochemical Society, Volume 163, Number 10](#)

Citation Rafael M. Buoro *et al* 2016 *J. Electrochem. Soc.* 163 G178

29 Total downloads



[Turn on MathJax](#)

[Get permission to re-use this article](#)

Share this article



[+ Article information](#)

[Abstract](#)

#### Abstract

The electrochemical behavior of heme-phorphyrin iron (III) centered hematin (Htin) was investigated at a Htin modified glassy carbon electrode with cyclic, differential pulse, square wave voltammetry in different pH values. For all pH values, the electrochemical process attributed to the reduction of hematin follows an EE mechanism, in which the ligand suffers mediated electrochemical reduction by the iron metallic center. At the backward scan, the same mechanism is observed for the oxidation of hematin in pH > 5.5. However, the electrochemical oxidation at backward scan in pH < 5.5 occurs firstly and directly at the ligand with the formation of IS (intermediate specie) that is further oxidized at the metallic center and forms Fe(Htin)<sup>3+</sup>. In acid and neutral media, the oxidation of hematin at the positive potential range is an irreversible and pH-dependent process that follows an ECE mechanism. In the first step, the electrochemical oxidation of hematin involves the transfer of one electron from the pyrrolic nitrogen heteroatom with the formation of a cationic radical that loses its iron (III) center in a subsequent chemical step. The resulting cationic radical suffers further oxidation to produce a structure similar to the protoporphyrin IX.

- [1] R.M. Buoro, O.S. Campos, R.P. Bacil, S.H.P. Serrano, Insights toward the Electrochemical Behavior of Hematin Using a Hematin Modified Glassy Carbon Electrode, *J. Electrochem. Soc.* 163 (2016) G178–G185. <https://doi.org/10.1149/2.0021613jes>.

The student collaborated in this work with data acquiring, and the electrochemical mechanism discussions, especially regarding the loss of the iron after the oxidation of the ligand. Moreover, the student participated in the writing and revision process of the original draft.



## Biomimetic behavior and nanomolar detection of hydrogen peroxide on an electrochemically pre-treated hematin modified glassy carbon electrode

Rafael M. Buoro<sup>a, b</sup>, Raphael P. Bacil<sup>b</sup>, Caroline G. Sanz<sup>b</sup>, Othon S. Campos<sup>b</sup>, Silvia H.P. Serrano<sup>b</sup>

Show more

+ Add to Mendeley Share Cite

<https://doi.org/10.1016/j.snb.2017.03.176>

[Get rights and content](#)

[2] R.M. Buoro, R.P. Bacil, C.G. Sanz, O.S. Campos, S.H.P. Serrano, Biomimetic behavior and nanomolar detection of hydrogen peroxide on an electrochemically pre-treated hematin modified glassy carbon electrode, *Sensors Actuators B Chem.* 250 (2017) 169–178. <https://doi.org/10.1016/j.snb.2017.03.176>.

The student collaborated in this work with data acquiring, especially the obtention of the data to the calibration curves, data curation, the writing and revision process of the original draft.

## Study of Electrochemical Oxidation and Quantification of the Pesticide Pirimicarb Using a Boron-Doped Diamond Electrode

Thiago Matheus Guimarães Selva <sup>a, b</sup>✉, William Reis de Araujo <sup>b</sup>✉, Raphael Prata Bacil <sup>b</sup>, Thiago Regis Longo Cesar Paixão <sup>b</sup>✉

Show more ▾

+ Add to Mendeley   🔗 Share   📄 Cite

<https://doi.org/10.1016/j.electacta.2017.06.051>

[Get rights and content](#)



[3] T.M.G. Selva, W.R. de Araujo, R.P. Bacil, T.R.L.C. Paixão, Study of Electrochemical Oxidation and Quantification of the Pesticide Pirimicarb Using a Boron-Doped Diamond Electrode, *Electrochim. Acta.* 246 (2017) 588–596. <https://doi.org/10.1016/j.electacta.2017.06.051>.

The student collaborated in this work with data acquiring, the molecular (mechanism proposition) and interfacial electrochemistry discussions, the data curation, and both writing and revision of the original draft.

## Forensic electrochemistry: Electrochemical study and quantification of xylazine in pharmaceutical and urine samples

Letícia Francine Mendes <sup>a</sup>, Ângela Rodrigues Souza e Silva <sup>b</sup>, Raphael Prata Bacil <sup>a</sup>, Sílvia Helena Pires Serrano <sup>a</sup>, Lúcio Angnes <sup>a</sup>, Thiago Regis Longo Cesar Paixão <sup>a</sup>, William Reis de Araujo <sup>c</sup>✉

Show more 

+ Add to Mendeley  Share  Cite

<https://doi.org/10.1016/j.electacta.2018.10.120>

[Get rights and content](#)

[4] L.F. Mendes, Â.R. Souza e Silva, R.P. Bacil, S.H.P. Serrano, L. Angnes, T.R.L.C. Paixão, W.R. de Araujo, Forensic electrochemistry: Electrochemical study and quantification of xylazine in pharmaceutical and urine samples, *Electrochim. Acta.* 295 (2019) 726–734.

<https://doi.org/10.1016/j.electacta.2018.10.120>.

The student collaborated in this work with conceptualization, investigation and validation as well as data curation, the writing and revision process of the original draft.



## Electrochemical characterization of *para*- and *meta*-nitro substituents in aqueous media of new antichagasic pharmaceutical leaders

Caroline G. Sanz <sup>a</sup>, Kevin A. Dias <sup>a</sup>, Raphael P. Bacil <sup>a</sup>, Ricardo A.M. Serafim <sup>b</sup>, Leandro H. Andrade <sup>a</sup>, Elizabeth I. Ferreira <sup>b</sup>, Silvia H.P. Serrano <sup>a</sup>✉

Show more

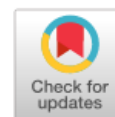
+ Add to Mendeley Share Cite


<https://doi.org/10.1016/j.electacta.2020.137582>

[Get rights and content](#)

[5] C.G. Sanz, K.A. Dias, R.P. Bacil, R.A.M. Serafim, L.H. Andrade, E.I. Ferreira, S.H.P. Serrano, Electrochemical characterization of *para*- and *meta*-nitro substituents in aqueous media of new antichagasic pharmaceutical leaders, *Electrochim. Acta.* 368 (2021) 137582. <https://doi.org/10.1016/j.electacta.2020.137582>.

The student collaborated in this work in the investigation and validation processes as well as data curation, and the writing of the original draft.


[View PDF Version](#)
[Previous Article](#)
[Next Article](#)
 Open Access Article

 This Open Access Article is licensed under a [Creative Commons Attribution-Non Commercial 3.0 Unported Licence](#)

 DOI: [10.1039/D0RA08874A](https://doi.org/10.1039/D0RA08874A) (Paper) *RSC Adv.*, 2021, **11**, 1644–1653

## Enhanced performance of pencil-drawn paper-based electrodes by laser-scribing treatment<sup>†</sup>

 Vanessa N. Ataide<sup>†,a</sup>, Wilson A. Ameku<sup>†,a</sup>, Raphael P. Bacil<sup>†,b</sup>, Lúcio Angnes<sup>†,b</sup>, William R. de Araujo<sup>†,b</sup> and Thiago R. L. C. Paixão<sup>†,a</sup>
<sup>a</sup>Department of Fundamental Chemistry, Institute of Chemistry, São Paulo University-USP, São Paulo, SP 05508-900, Brazil. E-mail: [trlcp@iq.usp.br](mailto:trlcp@iq.usp.br)
<sup>b</sup>Department of Analytical Chemistry, Institute of Chemistry, State University of Campinas-UNICAMP, Campinas, SP 13083-970, Brazil

Received 18th October 2020, Accepted 28th November 2020

First published on 5th January 2021

### Abstract

Electrochemical Paper-based Analytical Devices (ePADs) are an alternative to traditional portable analytical techniques due to features such as low-cost, easy surface modification with different materials, and high sensitivity. A fast and simple method to fabricate enhanced ePADs using pencil-drawing which involves the CO<sub>2</sub> laser treatment of the carbon surface deposited on paper is described. The electrochemical performances of the devices were evaluated using cyclic voltammetry (CV) with different redox probes and electrochemical impedance spectroscopy (EIS). The electrochemical results show that a treated surface presents a lower resistance to charge transfer and changes the approach of the probe and the overlap of its orbitals with the electrode. To investigate the effects of the laser treatment process, chemical and structural characteristics were evaluated using scanning electron microscopy (SEM), X-ray photoelectron spectroscopy (XPS), and Raman spectroscopy. These results indicated that laser treatment promoted the restoration of carbon–carbon double bonds and removed a thin layer of nanodebris present in commercial pencils, resulting in an improvement of the electrochemical kinetics. As a proof-of-concept, the Pencil-Drawing Electrode (PDE) was used for the detection and quantification of furosemide (FUR) in a sample of synthetic urine, exhibiting a limit of detection (LOD) of  $2.4 \times 10^{-7}$  mol L<sup>-1</sup>. The percentages of recovery of the FUR added to the samples A and B were 95% and 110%, respectively. The analysis using CO<sub>2</sub> laser-treated PDE resulted in a fast, simple, and reliable method for this doping agent.

[6] V.N. Ataide, W.A. Ameku, R.P. Bacil, L. Angnes, W.R. de Araujo, T.R.L.C. Paixão, Enhanced performance of pencil-drawn paper-based electrodes by laser-scribing treatment, *RSC Adv.* **11** (2021) 1644–1653. <https://doi.org/10.1039/D0RA08874A>.



The student collaborated in this work in the data acquirement, investigation and validation processes, data treatment and discussions, especially regarding the Tafel analysis in the SI. The student also participated in the writing and revision process.

## Book chapters published in collaboration during the Ph.D. program

### Sensing Materials: Electrochemical Applications of DNA Sensors and Biosensors

**Caroline G Sanz<sup>a</sup>, Rafael M Buoro<sup>b</sup>, Raphael P Bacil<sup>c</sup>, Iranaldo S da Silva<sup>d</sup>, Adriana D Rendelucci<sup>c</sup>, Fernanda P Costa<sup>c</sup>, and Silvia HP Serrano<sup>c</sup>.** <sup>a</sup>National Institute of Materials Physics (NIMP), Măgurele, Romania; <sup>b</sup>Department of Molecular Physics and Chemistry, Institute of Chemistry of São Carlos (IQSC), University of São Paulo, São Carlos, SP, Brazil; <sup>c</sup>Department of Fundamental Chemistry, Institute of Chemistry (IQUSP), University of São Paulo, São Paulo, SP, Brazil; <sup>d</sup>Chemistry Technology Department, Science and Technology Center, Maranhão Federal University, São Luís, MA, Brazil

© 2021 Elsevier Inc. All rights reserved.

<b>Historical aspects</b>	<b>1</b>
<b>General methodology</b>	<b>2</b>
Recognition elements	3
Nucleic acid structures	4
Electrode modification	6
<b>Applications</b>	<b>6</b>
Drug Interactions	6
Cancer biomarkers	8
Proteins/metalloproteinases/cytokines	8
Nucleic acid	9
MicroRNA	9
Exosomes	9
Immunosensors	10
Pathogens	11
Food analysis	13
Environmental	13
<b>Trends and perspectives</b>	<b>15</b>
<b>References</b>	<b>16</b>

- [1] C.G. Sanz, R.M. Buoro, R.P. Bacil, I.S. da Silva, A.D. Rendelucci, F.P. Costa, S.H.P. Serrano, Sensing Materials: Electrochemical Applications of DNA Sensors and Biosensors, in: Ref. Modul. Biomed. Sci., Elsevier, 2021.  
<https://doi.org/10.1016/B978-0-12-822548-6.00039-X>.

The student contributed to this book chapter mainly by organizing and writing the 'drug interaction' section as well as writing and revising the original draft.

## Sensing Materials: Diamond-Based Materials

Thiago Matheus Guimarães Selva<sup>a</sup>, Jéssica Soares Guimarães Selva<sup>b</sup>, and Raphael Bacil Prata<sup>b</sup>, <sup>a</sup>Federal Institute of Education, Science and Technology of Rio de Janeiro, Rio de Janeiro, Brazil; <sup>b</sup>Institute of Chemistry, University of São Paulo, São Paulo, Brazil

© 2021 Elsevier Inc. All rights reserved.

<b>A brief history about diamond</b>	<b>2</b>
<b>General aspects of the most common carbon allotropes</b>	<b>3</b>
<b>Diamond synthesis methods (diamond growth)</b>	<b>5</b>
High pressure-high temperature method	7
Chemical vapor deposition	7
Detonation nanodiamond synthesis	9
Hydrothermal synthesis and the reduction of carbide	9
<b>Characterization techniques</b>	<b>10</b>
Contact angle	10
X-ray photoelectron spectroscopy	10
Secondary ion mass spectrometry	10
Scanning electron microscopy	11
X-ray diffraction	11
Raman spectroscopy	12
Voltammetry	12
Electrochemical impedance spectroscopy	13
<b>Diamond-based sensors: General properties and applications</b>	<b>13</b>
Electrochemical sensors	14
Dopant content	14
Non-diamond carbon content	15
Surface termination	17
Applications	18
Particle and radiation sensors	20
Pressure and gas sensors	22
<b>What is next? (trends and perspectives)</b>	<b>23</b>
<b>Acknowledgments</b>	<b>24</b>
<b>References</b>	<b>24</b>

- [2] T.M.G. Selva, J.S.G. Selva, R.B. Prata, Sensing Materials: Diamond-Based Materials, in: Ref. Modul. Biomed. Sci., Elsevier, 2021: pp. 1–27.  
<https://doi.org/10.1016/B978-0-12-822548-6.00081-9>.

The student contributed to this book chapter mainly by organizing and writing the particle and radiation sensor' section as well as writing and revising the original draft.

## **Summarized CV**

Raphael Bacil Prata

São Paulo – SP, nascido em 10/06/1989

### **Educação**

Bacharel em química – Universidade de São Paulo – Campus capital- SP

2008-2014

Iniciação científica sob orientação da professora Silvia H. P. Serrano

2010 - 2015

Doutorado em ciencias com ênfase em química sob orientação da professora  
Silvia H. P. Serrano

2016-

### **Formação complementar**

Doutoramento sanduíche – Universidade de Oxford, sob orientação do  
professor Richard G. Compton

2018 - 2019

408

## **Ocupação**

Bolsista de iniciação

RUSP 2010 – 2011

CNPq PIBIC 2012 - 2013

Bolsista de doutoramento

CNPq 2016 –

Capes PDSE 2018 - 2019

## **Publicações em periódicos**

[1] R.P. Bacil, R.M. Buoro, R.P. Da-Silva, D.B. Medinas, A.W. Lima, S.H. Serrano, Mechanism of Electro-Oxidation of Metamizole Using Cyclic Voltammetry at a Glassy Carbon Electrode, *ECS Trans.* 43 (2012) 251–258. <https://doi.org/10.1149/1.4704966>.

[2] R.M. Buoro, R.P. Silva, R.P. Bacil, A.W.O. Lima, T. Rabóczkay, L.C. Cides Da Silva, S.H.P. Serrano, Electrochemical characterization and evaluation of the analytical potentialities of glassy carbon electrodes modified with extracted lignin from black (Kraft) liquor, in: *ECS Trans.*, 2012. <https://doi.org/10.1149/1.4704948>.

[3] R.M. Buoro, R.P. Bacil, R.P. da Silva, L.C.C. da Silva, A.W.O. Lima, I.C. Cosentino, S.H.P. Serrano, Lignin-AuNp modified carbon paste electrodes—Preparation, characterization, and applications, *Electrochim. Acta.* 96 (2013) 191–198. <https://doi.org/10.1016/j.electacta.2013.02.081>.

- [4] R.M. Buoro, O.S. Campos, R.P. Bacil, S.H.P. Serrano, Insights toward the Electrochemical Behavior of Hematin Using a Hematin Modified Glassy Carbon Electrode, *J. Electrochem. Soc.* 163 (2016) G178–G185.  
<https://doi.org/10.1149/2.0021613jes>.
- [5] R.M. Buoro, R.P. Bacil, C.G. Sanz, O.S. Campos, S.H.P. Serrano, Biomimetic behavior and nanomolar detection of hydrogen peroxide on an electrochemically pre-treated hematin modified glassy carbon electrode, *Sensors Actuators B Chem.* 250 (2017) 169–178.  
<https://doi.org/10.1016/j.snb.2017.03.176>.
- [6] T.M.G. Selva, W.R. de Araujo, R.P. Bacil, T.R.L.C. Paixão, Study of Electrochemical Oxidation and Quantification of the Pesticide Pirimicarb Using a Boron-Doped Diamond Electrode, *Electrochim. Acta.* 246 (2017) 588–596.  
<https://doi.org/10.1016/j.electacta.2017.06.051>.
- [7] R.P. Bacil, R.M. Buoro, O.S. Campos, M.A. Ramos, C.G. Sanz, S.H.P. Serrano, Electrochemical behaviour of dipyrone (metamizole) and others pyrazolones, *Electrochim. Acta.* 273 (2018) 358–366.  
<https://doi.org/10.1016/j.electacta.2018.04.082>.
- [8] L.F. Mendes, Â.R. Souza e Silva, R.P. Bacil, S.H.P. Serrano, L. Angnes, T.R.L.C. Paixão, W.R. de Araujo, Forensic electrochemistry: Electrochemical study and quantification of xylazine in pharmaceutical and urine samples, *Electrochim. Acta.* 295 (2019) 726–734.  
<https://doi.org/10.1016/j.electacta.2018.10.120>.
- [9] R.P. Bacil, L. Chen, S.H.P. Serrano, R.G. Compton, Dopamine oxidation at gold electrodes: Mechanism and kinetics near neutral pH, *Phys. Chem. Chem. Phys.* 22 (2020) 607–614. <https://doi.org/10.1039/c9cp05527d>.

- [10] R.P. Bacil, P.H.M. Garcia, S.H.H.P. Pires Serrano, New Insights on the Electrochemical Mechanism of Epinephrine on Glassy Carbon Electrode, SSRN Electron. J. (2021). <https://doi.org/10.2139/ssrn.3948392>.
- [11] C.G. Sanz, K.A. Dias, R.P. Bacil, R.A.M. Serafim, L.H. Andrade, E.I. Ferreira, S.H.P. Serrano, Electrochemical characterization of para- and meta-nitro substituents in aqueous media of new antichagasic pharmaceutical leaders, *Electrochim. Acta.* 368 (2021) 137582. <https://doi.org/10.1016/j.electacta.2020.137582>.
- [12] R.P. Bacil, P.H.M. Garcia, W.R. de Araujo, S.H.P. Serrano, Mechanism and kinetics of olanzapine and quetiapine oxidations at glassy carbon electrode, *Electrochim. Acta.* 368 (2021) 137683. <https://doi.org/10.1016/j.electacta.2020.137683>.
- [13] R.P. Bacil, E.A. de O. Marcondes Filho, K. de A. Dias, M.C. Portes, W.R. de Araujo, D. Oliveira-Silva, A.A. dos Santos, S.H.P. Serrano, The chemical interaction between the neurotransmitter dopamine and the antipsychotic drugs olanzapine and quetiapine, *J. Electroanal. Chem.* 881 (2021) 114946. <https://doi.org/10.1016/j.jelechem.2020.114946>.
- [14] V.N. Ataíde, W.A. Ameku, R.P. Bacil, L. Angnes, W.R. de Araujo, T.R.L.C. Paixão, Enhanced performance of pencil-drawn paper-based electrodes by laser-scribing treatment, *RSC Adv.* 11 (2021) 1644–1653. <https://doi.org/10.1039/D0RA08874A>.

### **Publicações de capítulos de livro**

- [1] C.G. Sanz, R.M. Buoro, R.P. Bacil, I.S. da Silva, A.D. Rendelucci, F.P. Costa, S.H.P. Serrano, Sensing Materials: Electrochemical Applications of DNA Sensors and Biosensors, in: Ref. Modul. Biomed. Sci., Elsevier, 2021.  
<https://doi.org/10.1016/B978-0-12-822548-6.00039-X>.
- [2] T.M.G. Selva, J.S.G. Selva, R.B. Prata, Sensing Materials: Diamond-Based Materials, in: Ref. Modul. Biomed. Sci., Elsevier, 2021: pp. 1–27.  
<https://doi.org/10.1016/B978-0-12-822548-6.00081-9>.